



The behavior of composite deep deck ComFlor210 under concentrated load

Olga Bushunova

in partial fulfillment of the requirements for the degree of

Master of Science
in Civil Engineering

at the Delft University of Technology,
Faculty of Civil Engineering and Geosciences,

Supervisor: Prof. Dr. Ir. M. Veljkovic

Thesis committee:

Dr. Ir. R. Abspoel, TU Delft

Ir. P. Lagendijk, TU Delft

Dr. ir.M. A. N. Hendriks, TU Delft

Ir. M. Feijen, FMAX-ISAAC.

Contents

SUMMARY	7
List of Tables	8
List of Figures	10
List of Symbols	15
1 INTRODUCTION	17
1.1 General information	17
1.2 Composite deep deck ComFlor 210	18
1.3 Thesis objective	19
1.4 Outline of the report	20
2 LITERATURE REVIEW	21
2.1 Distribution of concentrated load according to Eurocode	21
2.2 Review of scientific works on the distribution of point load in a composite slab	22
2.3 Review of finite element methods available for composite slab	23
2.4 Plate theory in the application for composite slab	23
3 Modeling object	25
3.1 Geometry	25
3.2 The effective area of a steel deck	26
3.3 Boundary conditions, applied load and possible failure modes	27
4 Engineering model	30
4.1 Initial model and assumptions	30
4.2 Model description	31
4.2.1 Engineering model in the longitudinal direction	31
4.2.1.1 Beam model with a load in the center.	31
4.2.1.2 Beam model with load at a quarter of the span.	33
4.2.2 Engineering model transversal	34
4.3 Model parameters	36
4.3.1 Bending stiffness and cracking moment of the rib	36
4.3.2 Bending stiffness and cracking moment of the top deck	40
4.3.2.1 Cracking moment and bending stiffness of the uncracked section	40
4.3.2.2 Bending stiffness of the cracked section	41
4.4 Influence of different parameters in the engineering model	43
4.4.1 Spring stiffness	43
4.4.2 Top deck positive bending stiffness	45
4.4.3 Length of the top deck between ribs	46
4.5 Engineering model results and conclusion	48
4.5.1 Load at the middle of the span	48

4.5.2	Load at the quarter of the span	49
4.5.3	Conclusion on the engineering model	51
5	FINITE ELEMENT MODEL	53
5.1	Introduction	53
5.2	Simulation environment of Abaqus/CAE	53
5.3	Material properties	54
5.3.1	Concrete models	54
5.3.2	Concrete compressive and tensile behavior	54
5.3.3	Concrete properties	56
5.3.4	Steel model	57
5.3.5	Steel properties	58
5.4	The composition of the finite element model	59
5.4.1	Boundary conditions	59
5.4.2	Geometry, meshing, and finite elements	59
5.4.3	Concrete-steel interaction	63
5.4.4	Primary verification of the model composition	64
5.5	Effect of different parameters in finite element model on the load-deflection response of composite slab	67
5.5.1	Mesh sensitivity	67
5.5.2	Dilation angle effect	69
5.5.3	Influence of contact definition	70
5.5.4	Conclusion regarding the influence of the finite element model parameters	71
5.6	Load control finite element analysis	72
5.6.1	Model description	72
5.6.2	Load control analysis results	73
5.6.2.1	Deformed shape and displacements	73
5.6.2.2	Stresses and strains	75
5.6.2.3	Reaction force distribution in one mesh composite slab	78
5.7	The displacement control finite element analysis	81
5.7.1	Model description	81
5.7.2	Displacement control analysis results	82
5.7.2.1	Deformed shape and displacements	82
5.7.2.2	Stresses	83
5.7.2.3	Reaction force distribution in one mesh composite slab	86
5.8	Conclusion on the finite element model and comparison with the engineering model	88
6	PARAMETRIC STUDY ON COMPOSITE SLAB COMFLOR210	89

6.1	Introduction	89
6.2	Composite slab ComFlor210: span 3.6m	91
6.2.1	Concentrated load at $L_{\text{span}}/2$	91
6.2.2	Concentrated load at $L_{\text{span}}/4$	92
6.2.3	Concentrated load at $L_{\text{span}}/6$	95
6.3	Composite slab ComFlor210: span 5.4m	99
6.3.1	Concentrated load at $L_{\text{span}}/2$	99
6.3.2	Concentrated load at $L_{\text{span}}/4$	101
6.3.3	Concentrated load at $L_{\text{span}}/6$	103
6.4	Composite slab ComFlor210: span 7.2m	107
6.4.1	Concentrated load at $L_{\text{span}}/2$	107
6.4.2	Concentrated load at $L_{\text{span}}/4$	110
6.4.3	Concentrated load at $L_{\text{span}}/6$	112
6.5	Composite slab ComFlor210: change in cross-section properties	116
6.5.1	Variation of profile steel sheeting thickness	116
6.5.2	Variation of rib reinforcement	116
6.5.3	Variation of the effective section of the steel sheeting	117
6.6	Conclusion on the parametric study of composite slab ComFlor210 with finite element analysis	119
7	Conclusions and recommendations	122
7.1	Conclusions	122
7.2	Recommendations	124
8	References	125
	A The effective area of profiled steel sheeting ComFlor210	127
	B Engineering model parameters	128
	C Damage parameters in concrete damaged plasticity model	139
	D Engineering model results	142
	E Finite element model results	151
	F Rib bending resistance verification	164
	G Distribution of the point load relative to the distance to the applied load	170

PREFACE

This thesis is a final work as partial fulfillment for the degree of Master of Science in Civil Engineering. The report consists of five main parts: a literature research on the topic, an engineering modeling of the composite slab, finite element analysis and parts with parametric study and results evaluation. The numerical modeling was done in the simulation environment Abaqus/CAE.

I would gladly thank all members of the graduation committee whose guidance during the work was of significant importance in thesis completion.

Finally, I thank my husband for being on my side all this time.

*Olga S. Bushunova,
Tricht, 2018*

SUMMARY

The research concentrated on studying a behavior of the deep composite deck ComFlor210 under a concentrated force placed on a rib at different locations. The research is essential because the procedure to establish the effective width, over which the concentrated force is distributed, in a case of the deep composite deck is out the scope of Eurocode 4. In Eurocode 4 the procedure to calculate the effective width is applicable for slabs with narrowly spaced webs only (the ratio of rib width to the rib spacing does not exceed 0.6). The distribution of a concentrated force in a composite slab ComFlor210 was studied numerically and analytically.

The finite element analysis of the composite slab in the simulation environment Abaqus/CAE was performed using the material properties and geometry of a tested specimen at TU Delft – composite slab ComFlor210 with one reinforcement in the top deck. In order to conduct a parametric study on a composite slab with varying load positions and geometry properties, the finite element model included the entire slab length and all reinforcement present in a slab in reality.

The created finite element model was verified by making a comparison with results of a conducted test at TU Delft performed by M. Dracht. The finite element model of a composite slab with 5.4m span and one reinforcement mesh in the top deck showed good agreement with test results in the elastic stage.

The parametric study of composite slab ComFlor210 loaded with concentrated force 60kN revealed that in a slab with spans 3.2m and 5.4m the load was distributed over three middle ribs, as the contribution of two outer ribs was less than 10%. However, in a slab with 7.2m span, the load was spread over all five ribs (contribution of two external ribs accounted for 20%). The finite element analysis showed that the failure criterion – exceeding the bending resistance of the rib – was reached for slab with 7.2m span under design load combination of dead, live and concentrated load 60kN applied halfway the span on the middle rib. Additionally, for slabs with span longer 5.4m under a combination of dead load and concentrated force, the serviceability requirement (maximum deflection $L_{\text{span}}/250$) can be violated at a load lower 60kN.

The parametric study on a composite slab ComFlor210 loaded with concentrated force 145kN showed that with increasing the area of rib reinforcement and the thickness of steel sheeting the composite slab displays stiffer behavior in the plastic zone of the load-deflection curve. For the elastic part of the load-deflection curve, the variation in cross-sectional parameters causes a minor change in a slab response.

The proposed engineering model was unable to predict the deflection of the composite slab under concentrated load in a loading range 10-40kN with the desired accuracy. The assumptions that the modulus of elasticity of cracked concrete equals one-third of not cracked material, probably, lead to an underestimation of rib bending stiffness at low load level.

List of Tables

Table 3.1 Concentrated load magnitude	28
Table 4.1 Boundary and intermediate conditions for rib loaded centrally	32
Table 4.2 Boundary and intermediate conditions for rib loaded at a quarter of the span	33
Table 4.3 Boundary and intermediate conditions for slab model	34
Table 4.4 Rib stiffness values for composite slab under point load applied halfway the span derived from test and FEA	35
Table 4.5 Rib stiffness values for composite slab under point load applied at the quarter of the span derived from test and FEA	35
Table 4.6 Properties used in bending capacity calculation	38
Table 4.7 Bending stiffnesses of the rib	38
Table 4.8 Properties used in bending stiffness calculation of top deck	41
Table 4.9 Bending stiffnesses of top deck (per 200mm length)	42
Table 4.10 Deflection per rib with changed rib stiffness values	43
Table 4.11 Deflection per rib with a changed positive bending stiffness of the top deck	45
Table 4.12 Deflection per rib with the changed internal length of the top deck	47
Table 4.13 Comparison between engineering model results ($b_{rib}=600\text{mm}$) and test for a slab with two reinforcement meshes	48
Table 4.14 Comparison between engineering model results ($b_{rib}=600\text{mm}$) and test for a slab with one reinforcement mesh	49
Table 4.15 Comparison between engineering model results ($b_{rib}=600\text{mm}$) and test for a slab with no reinforcement mesh	49
Table 4.16 Comparison between engineering model results ($b_{rib}=600\text{mm}$) and test for a slab with two reinforcement meshes	50
Table 4.17 Comparison between engineering model results ($b_{rib}=600\text{mm}$) and test for a slab with one reinforcement mesh	50
Table 4.18 Comparison between engineering model results ($b_{rib}=600\text{mm}$) and test for a slab with no reinforcement mesh	50
Table 5.1 Concrete models in Abaqus	54
Table 5.2 Concrete material properties	56
Table 5.3 Finite element characteristics of concrete	57
Table 5.4 Steel material properties	58
Table 5.5 Finite element characteristics of steel components	58
Table 5.6 Total gravity load in the experiment, the finite element model and hand calculation	65
Table 5.7 General characteristics of finite element models in mesh sensitivity study	68
Table 5.8 Ultimate reaction forces reached in FEA of one mesh slab with different dilation angle and the experiment	70
Table 5.9 Concrete input parameters for damaged plasticity model	72
Table 5.10 Steel input parameters for plasticity domain	73
Table 5.11 Maximum rib displacements in FEM, engineering model and test at 60kN load	88
Table 6.1 Possible geometry configuration for ComFlor210 slab	90
Table 6.2 Steel sheeting sections (per 600mm width)	118
Table 6.3 Maximum deflection of composite slab 7.2m in FEA with a load on Rib 3	121
Table 6.4 Maximum deflection of composite slab 7.2m in FEA with a load on Rib 2	121

Table 6.5 Bending moment resistance check for load combination dead load+live load+point load with point load placed halfway the span on Rib3

121

List of Figures

Figure 1.1 Chapter I overview	17
Figure 1.2 Composite slab (<i>Gholamhoseini et al. 2014</i>)	17
Figure 1.3 Types of interlocks in the composite slab (<i>Eurocode 4</i>)	18
Figure 1.4 Section ComFlor 210	19
Figure 2.1 Chapter II overview	21
Figure 2.2 Distribution of concentrated load (<i>Eurocode 4</i>)	21
Figure 3.1 Cross-sections of the composite slab, from top to bottom: no mesh, 1 mesh, 2 meshes	25
Figure 3.2 Detailed cross-sections of the rib, from left to right: no mesh, 1 mesh, 2 meshes	26
Figure 3.3 Effective steel area (<i>M. Dracht, 2015</i>)	26
Figure 3.4 The effective area ComFlor210	27
Figure 3.5 Composite slab: boundary conditions	27
Figure 3.6 Composite slab: load application	28
Figure 3.7 Failure modes: I – rib failure due to bending or vertical shear, II – interface failure due to vertical shear, III – longitudinal shear failure	29
Figure 4.1 Chapter overview	30
Figure 4.2 Sketch of the initial model	30
Figure 4.3 Beam geometry: a) load and varied bending stiffness along the beam; b) beam cross-section with 600mm width; c) beam cross-section with 175mm width; d) crack formation in a rib during testing (<i>M. Dracht, 2015</i>)	32
Figure 4.4 Discrete elements of a beam	32
Figure 4.5 Beam geometry: a) load and bending stiffness; b) beam cross-section with 600mm width; c) beam discrete elements; d) beam cross-section with 175mm width;	33
Figure 4.6 Slab model transversely	34
Figure 4.7 Ordinary clamped beam with prescribed support settlement and resulting moment diagram	35
Figure 4.8 Strain distribution and forces in the rib cross-section: a) rib with 600mm width; b) rib with 175mm width.	37
Figure 4.9 Linear variation of rib bending stiffness with $b_{rib}=600\text{mm}$	39
Figure 4.10 Linear variation of rib bending stiffness with $b_{rib}=175\text{mm}$	39
Figure 4.11 Top deck cross-section	40
Figure 4.12 Illustration of the distributive length L_{dis} of the composite slab	40
Figure 4.13 Stress and strain diagrams of the top deck: a) top deck with one reinforcement mesh under positive bending moment; b) top deck with two reinforcement meshes under positive bending moment; c) top deck with one reinforcement mesh under negative bending moment; d) top deck with two reinforcement meshes under negative bending moment.	42
Figure 4.14 Deflection of one mesh slab in the default case	43
Figure 4.15 Deflection of one mesh slab with 500% rib stiffness	44
Figure 4.16 Deflection of one mesh slab with 20% rib stiffness	44
Figure 4.17 Deflection of one mesh slab with 75% and 125% rib stiffness	44
Figure 4.18 Deflection of one mesh slab with 20% positive bending stiffness of the top deck	45
Figure 4.19 Deflection of one mesh slab with 500% positive bending stiffness of the top deck	46
Figure 4.20 Deflection of one mesh slab with 75% and 125% positive bending stiffness of the top deck	46

Figure 4.21 Deflection of two mesh slab with the decreased internal length of the top deck	47
Figure 4.22 Deflection of two mesh slab with the increased internal length of the top deck	47
Figure 5.1 Chapter overview	53
Figure 5.2 Tensile concrete behavior under uniaxial loading in Abaqus (Dassault Systèmes Simulia Corp. 2012)	55
Figure 5.3 Compressive concrete behavior under uniaxial loading in Abaqus (Dassault Systèmes Simulia Corp. 2012)	55
Figure 5.4 Uniaxial compression stress-strain response of concrete C20/25 with damaged plasticity	56
Figure 5.5 Uniaxial tension stress-strain response of concrete C20/25 with damaged plasticity	56
Figure 5.6 Engineering stress-strain and true stress-strain curves of profiled steel sheeting ComFlor210	57
Figure 5.7 Engineering stress-strain and true stress-strain curves of steel rod 8mm	58
Figure 5.8 Engineering stress-strain and true stress-strain curves of steel rod 20mm	58
Figure 5.9 Boundary conditions and load application of composite slab in finite element model	59
Figure 5.10 Geometry of finite element model of composite slab (top figure);	60
Figure 5.11 Concrete mesh	61
Figure 5.12 Steel sheeting mesh	61
Figure 5.13 Solid element C3D8R: node ordering and face numbering (left figure), the numbering of integration points for output (right figure) in stress-displacement analysis	62
Figure 5.14 Shell element S4R: node ordering and face numbering (left figure), the numbering of integration points for output (right figure) in stress-displacement analysis	62
Figure 5.15 Beam element B31: node ordering (left figure), the numbering of integration points for output (right figure) in stress-displacement analysis	62
Figure 5.16 Truss element T3D2: node ordering (left figure), the numbering of integration points for output (right figure) in stress-displacement analysis	62
Figure 5.17 Reaction force distribution per rib in the composite slab with 1 reinforcement mesh due to dead load	64
Figure 5.18 Development of total energy ETOTAL, strain energy ALLSE and internal energy ALLIE during finite element analysis in Abaqus	65
Figure 5.19 Energy development during FEA: kinetic energy ALLKE and internal energy ALLIE of the whole model (left figure); the energy of constraint and contact (right figure)	66
Figure 5.20 Load-deflection response of composite slab in the experiment and finite element load control analysis with mesh element size 100mm, 50mm, and 25mm	67
Figure 5.21 Load-deflection response of composite slab in a range 0-60kN in the experiment and finite element load control analysis with mesh element size 100mm, 50mm, and 25mm	68
Figure 5.22 Von Mises stress sensitivity to mesh density in displacement control FEA	69
Figure 5.23 Dilation angle effect on the load-deflection response of composite slab in load control FEA	70
Figure 5.24 Contact effect on the load-deflection response of composite slab in load control FEA	71
Figure 5.25 Displacement field U2 in one-mesh slab under concentrated force 145kN in load-control FEA	73
Figure 5.26 Total load vs. maximum deflection of the middle rib of the composite slab in load control FEA and test	74

Figure 5.27 Total load vs. maximum deflection of rib 2 (left figure) and rib 1 (right figure) of the composite slab in load control FEA and test	74
Figure 5.28 Von Mises stress distribution in concrete in load control FEA at the end of the analysis	75
Figure 5.29 Normal stresses (MPa) in X, Y and Z direction for concrete in load control FEA at the end of the analysis	76
Figure 5.30 Von Mises stress distribution in steel sheeting in load control FEA at the end of the analysis	77
Figure 5.31 Normal stress distribution in reinforcement mesh 8mm (left figure) and steel bars 20mm (right figure) in load control FEA at the end of the analysis	77
Figure 5.32 Strain distribution in Rib 3 bottom flange of steel sheeting	78
Figure 5.33 Load-deflection curves of each rib in experiment and load control FEA	79
Figure 5.34 Distribution of 10kN concentrated force in load control FEA and experiment	79
Figure 5.35 Distribution of 60kN concentrated force in load control FEA and experiment	80
Figure 5.36 Distribution of 145kN concentrated force in load control FEA and experiment	80
Figure 5.37 Kinetic and internal energy of the finite element model in displacement control analysis	81
Figure 5.38 Displacement field U2 in the one-mesh slab in displacement-control FEA	82
Figure 5.39 Total load vs. maximum deflection of the middle rib of the composite slab in displacement control FEA and test	82
Figure 5.40 Total load vs. maximum deflection of rib 2 (left figure) and rib 1 (right figure) of the composite slab in displacement control FEA and test	83
Figure 5.41 Von Mises stress distribution in concrete part in displacement control FEA at the end of analysis	83
Figure 5.42 Normal stresses (MPa) in X, Y and Z direction for concrete in displacement control FEA at the end of the analysis	84
Figure 5.43 Von Mises stress distribution in steel sheeting in displacement control FEA at the end of the analysis	84
Figure 5.44 Normal stress distribution in reinforcement mesh 8mm (left figure) and steel bars 20mm (right figure) in load control FEA at the end of the analysis	85
Figure 5.45 Load-deflection curves of each rib in experiment and displacement control FEA	86
Figure 5.46 Distribution of 10kN concentrated force in displacement control FEA and experiment	86
Figure 5.47 Distribution of 60kN concentrated force in displacement control FEA and experiment	87
Figure 5.48 Distribution of 145kN concentrated force in load control FEA and experiment	87
Figure 5.49 Average deviation between FEM, engineering model (max. rib deflections) and test	88
Figure 6.1 Distribution of concentrated load per rib (top figure) and reaction forces (bottom figure) in the composite slab L=3600mm with force on Rib 3 at L/2	91
Figure 6.2 Distribution of concentrated load per rib (top figure) and reaction forces (bottom figure) in the composite slab L=3600mm with force on Rib 2 at L/2	92
Figure 6.3 Distribution of concentrated load per rib (top figure) and reaction forces (bottom figure) in the composite slab L=3600mm with force on Rib 3 at L/4	93
Figure 6.4 Distribution of concentrated load in right and left support of each rib (L=3600mm with force on Rib 3 at L/4)	93

Figure 6.5 Distribution of concentrated load per rib (top figure) and reaction forces (bottom figure) in the composite slab L=3600mm with force on Rib 2 at L/4	94
Figure 6.6 Distribution of concentrated load in the right support of each rib (L=3600mm with force on Rib 2 at L/4)	94
Figure 6.7 Distribution of concentrated load per rib (top figure) and reaction forces (bottom figure) in the composite slab L=3600mm with force on Rib 3 at L/6	96
Figure 6.8 Distribution of concentrated load in right and left support of each rib (L=3600mm with force on Rib 3 at L/6)	96
Figure 6.9 Distribution of concentrated load per rib (top figure) and reaction forces (bottom figure) in the composite slab L=3600mm with force on Rib 2 at L/6	97
Figure 6.10 Distribution of concentrated load in the right support of each rib (L=3600mm with force on Rib 2 at L/6)	97
Figure 6.11 Distribution of concentrated load per rib (top figure) and reaction forces (bottom figure) in the composite slab L=5400mm with force on Rib 3 at L/2	99
Figure 6.12 Distribution of concentrated load per rib (top figure) and reaction forces (bottom figure) in the composite slab L=5400mm with force on Rib 2 at L/2	100
Figure 6.13 Distribution of concentrated load per rib (top figure) and reaction forces (bottom figure) in the composite slab L=5400mm with force on Rib 3 at L/4	101
Figure 6.14 Distribution of concentrated load in right and left support of each rib (L=5400mm with force on Rib 3 at L/4)	102
Figure 6.15 Distribution of concentrated load per rib (top figure) and reaction forces (bottom figure) in the composite slab L=5400mm with force on Rib 2 at L/4	102
Figure 6.16 Distribution of concentrated load in the right support of each rib (L=5400mm with force on Rib 2 at L/4)	103
Figure 6.17 Distribution of concentrated load per rib (top figure) and reaction forces (bottom figure) in the composite slab L=5400mm with force on Rib 3 at L/6	104
Figure 6.18 Distribution of concentrated load in right and left support of each rib (L=5400mm with force on Rib 3 at L/6)	104
Figure 6.19 Distribution of concentrated load per rib (top figure) and reaction forces (bottom figure) in the composite slab (L=5400mm with force on Rib 2 at L/6)	105
Figure 6.20 Distribution of concentrated load in the right support of each rib (L=5400mm with force on Rib 2 at L/6)	105
Figure 6.21 Distribution of concentrated load per rib (top figure) and reaction forces (bottom figure) in the composite slab L=7200mm with force on Rib 3 at L/2	107
Figure 6.22 Distribution of concentrated load per rib (top figure) and reaction forces (bottom figure) in the composite slab L=7200mm with force on Rib 2 at L/2	108
Figure 6.23 Stress distribution S33 in concrete at 30kN (top figure); concrete tension damage DAMAGET at 30kN (bottom figure)	109
Figure 6.24 Distribution of concentrated load per rib (top figure) and reaction forces (bottom figure) in the composite slab L=7200mm with force on Rib 3 at L/4	110
Figure 6.25 Distribution of concentrated load in right and left support of each rib (L=7200mm with force on Rib 3 at L/4)	111
Figure 6.26 Distribution of concentrated load per rib (top figure) and reaction forces (bottom figure) in the composite slab L=7200mm with force on Rib 2 at L/4	111
Figure 6.27 Distribution of concentrated load in the right support of each rib (L=7200mm with force on Rib 2 at L/4)	112
Figure 6.28 Distribution of concentrated load per rib (top figure) and reaction forces (bottom figure) in the composite slab L=7200mm with force on Rib 3 at L/6	113
Figure 6.29 Distribution of concentrated load in right and left support of each rib (L=7200mm with force on Rib 3 at L/6)	113

Figure 6.30 Distribution of concentrated load per rib (top figure) and reaction forces (bottom figure) in the composite slab $L=7200\text{mm}$ with force on Rib 2 at $L/6$	114
Figure 6.31 Distribution of concentrated load in the right support of each rib ($L=7200\text{mm}$ with force on Rib 2 at $L/6$)	114
Figure 6.32 Load-deflection response of Rib 3 in composite slab ComFlor210 with steel sheeting thickness $t=1.25\text{mm}$ and $t=1.0\text{mm}$	116
Figure 6.33 Load-deflection response of Rib 3 in composite slab ComFlor210 with a diameter of rib reinforcement 12mm, 20mm, and 25mm	117
Figure 6.34 Load-deflection response of Rib3 with different sections of the steel sheeting	118
Figure 6.35 Reaction force distribution in the loaded Rib 3 in the composite slab with length 3.6m and different load location: at $L/2$, $L/4$, and $L/6$	119
Figure 6.36 Reaction force distribution in the external Rib 1 in the composite slab with length 3.6m and different load location: at $L/2$, $L/4$, and $L/6$	120
Figure 6.37 Reaction force distribution in the loaded Rib 3 in the composite slab with length 3.6m, 5.4m, 7.2m and load position at $L_{\text{span}}/2$	120

List of Symbols

Latin uppercase letters

A_b	Area of the bottom flange of steel sheeting ComFlor210
A_c	Area of concrete in the top deck
$A_{c,rib}$	Area of concrete in a rib
A_{bar}	Area of steel bar $\varnothing 20$
A_{eff}	The effective area of steel sheeting ComFlor210
A_p	Area of steel sheeting ComFlor210
A_{s1}	Area of steel wire $\varnothing 8$ (top reinforcement mesh)
A_{s2}	Area of steel wire $\varnothing 8$ (bottom reinforcement mesh)
A_t	Area of the top flange of steel sheeting ComFlor210
B_{slab}	The width of the composite slab
E_c	Young's Modulus of uncracked concrete
E_{cm}	Secant modulus of elasticity of concrete
E_{CF}	Young's Modulus of steel sheeting ComFlor210
E_{rib}	Young's Modulus of cracked concrete in rib
E_s	Young's Modulus of reinforcement mesh
EI_{cr}	Bending stiffness of a rib with cracked concrete
EI_{deck}	Bending stiffness of top deck with uncracked concrete
$EI_{neg,cr}$	Bending stiffness of top deck with cracked concrete under negative bending moment
$EI_{pos,cr}$	Bending stiffness of top deck with cracked concrete under positive bending moment
EI_{un}	Bending stiffness of a rib with uncracked concrete
F_{rib}	The concentrated force acting on a rib
K_c	The ratio of the second stress invariant on the tensile meridian to that on the compressive meridian
L_{cr}	Length of a rib with cracked bending stiffness
L_{dis}	Distributive length of the top deck
L_{int}	Length of the top deck between the ribs
L_{span}	The total length of the composite slab
$M_{cr,deck}$	Cracking moment of the top deck
$M_{cr,rib}$	Cracking moment of a rib
$M_{k,rib}$	Bending resistance of a rib
N_c	Compressive force in the cross-section
N_s	Tensile force in the cross-section
Q_k	Characteristic variable action
W_c	Elastic section modulus

Latin lower case letters

b_{rib}	The width of the rib
d_c	Damage parameter for concrete in compression in damaged plasticity model
d_t	Damage parameter for concrete in tension in damaged plasticity model
f_{cm}	The compressive strength of concrete
f_{ctm}	The tensile strength of concrete
f_y	The yield stress of reinforcement
$f_{y,CF}$	The yield stress of steel sheeting ComFlor210
h_b	Height to the bottom flange of steel effective area ComFlor210
h_{bar}	Height to the steel bar $\varnothing 20$
h_c	The total height of the top deck
h_{s1}	Height to the top mesh $\varnothing 8$ from the top surface of the composite slab
h_{s2}	Height to the bottom mesh $\varnothing 8$ from the top surface of the composite slab
h_t	Height to the top flange of steel effective area ComFlor210
h_{tot}	The total height of the cross-section
k_{rib}	Spring stiffness
q	Distributed load
ν_c	Poisson's ratio for the concrete
ν_s	Poisson's ratio for steel
w_{rib}	Deflection of a rib
x_e	Concrete compression zone

Greek lower case letters

ε	Eccentricity parameter in concrete damaged plasticity model
ε_{bar}	Yielding strain of steel bar $\varnothing 20$
ε_{bottom}	Strain at a bottom flange of the effective area of steel sheeting
ε_{top}	Strain at a top flange of the effective area of steel sheeting
ε_{cu}	Ultimate compressive strain in the concrete
ε_{s1}	Tensile strain in the top reinforcement mesh
ε_{s2}	Tensile strain in the bottom reinforcement mesh
ρ_c	The density of the concrete
ρ_s	The density of the steel
σ_{b0}	The initial equibiaxial compressive yield stress of the concrete
σ_c	Compressive stress in the concrete
σ_{c0}	Initial uniaxial compressive yield stress
σ_t	Tensile stress in the concrete
ψ	Dilation angle of concrete

1 INTRODUCTION

The chapter I is presented in the following order, see Figure 1.1.



Figure 1.1 Chapter I overview

1.1 General information

Composite deck spanning in one direction consists of profiled steel sheeting, cast in-situ concrete and reinforcement meshes, and bars (Figure 1.2, [1]). In practice, the composite construction prevails in the non-residential multi-story sector like industrial and commercial buildings due to the labor and material efficiency it combines together with good structural performance. The application of composite decks in the building industry has many advantages, the e.g. low-self weight of the floor, adjustable floor height and faster construction procedure. Another benefit of using a composite element in construction is that steel sheeting can function as permanent formwork supporting the concrete layer. From the structural point of view, the profiled steel sheeting acts as external reinforcement helping to resist the tension forces arisen from the positive bending moment in the slab. The resistance of a composite slab is affected by different factors, such as the compressive strength of concrete, the thickness of the steel sheeting and overall geometry of the slab.

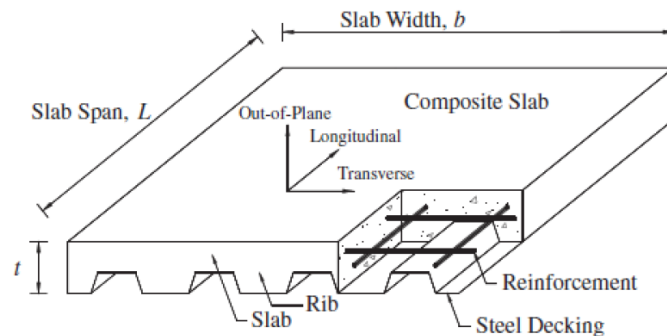


Figure 1.2 Composite slab (Gholamhoseini et al. 2014)

The transmission of the horizontal forces occurs at the concrete-steel interface; therefore, the adequate interaction between these two layers is of significant importance in order to guarantee the sufficient composite behavior. The composite action between concrete and profiled sheeting can be installed in different ways (Figure 1.3), for example, by mechanical or frictional interlock, end anchorage provided by rib deformation or welded studs.

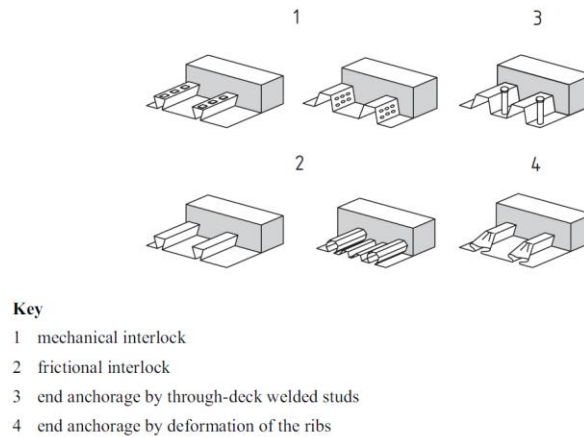


Figure 1.3 Types of interlocks in the composite slab (*Eurocode 4*)

Analysis of internal forces and moments of the composite slab is performed for two design situations:

- Design of profiled steel sheeting as shuttering.
- Ultimate limit state design.

Two design methods of the composite slab are proposed in Eurocode 4: shear-bond method, also known as the m-k method, and the partial connection method. Both methods are semi-empirical and require extensive test program in order to verify the resistance of composite slab under service and ultimate loads.

If the concentrated load is acting on the slab, the concept of the effective width is implemented. The basic principles for effective width determination are provided in Eurocode 4 [2]. For the deep slab, i.e. height of the slab is more than 200mm, the given principles are not elaborated; thus, the additional analysis is necessary, especially when high concentrated loads resulting in high internal shear forces act on the structure. Because of the ribbed geometry and comparatively thin top concrete layer, only limited distribution of the local loads is possible. The horizontal distribution of the point load over the ribs in the composite deck has been studied before in the works of M.S. Dracht [3] and M.Michalaki [4]. However, the final results of the analytical model proposed by M. Dracht diverged from the results of laboratory tests and finite element analysis. It was stated that further research is needed to achieve better accuracy of the analytical model and finite element model.

1.2 Composite deep deck ComFlor 210

The composite deck, in which the height of the rib accounts for more than 60% of the total deck height, is regarded as a deep deck. The main advantage of the deep slab is that it can span over a larger distance. Different types of deep decks are present on the market; the particular interest of this study is the behavior of composite deep deck ComFlor 210 under concentrated load.

The geometry of ComFlor 210 is shown below (Figure 1.4 [5]).

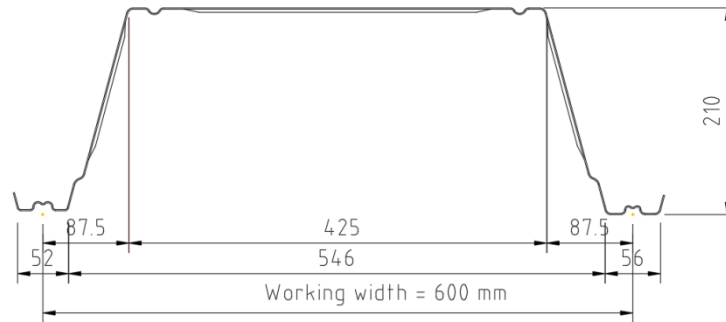


Figure 1.4 Section ComFlor 210

The utilization of deep profile generates an efficient metal deck due to less concrete and to steel mass used when compared to the solid concrete floor. The embedded steel profile helps reduce transport and installation costs. The application of the section allows spanning up to 5.3m in case if no shear studs are used [5]; consequently, with shear connectors, the possible spanning is even larger. Temporary propping is not needed for spans circa up to 5m; for large spans, propping becomes necessary during construction. Galvanized steel FeE280G with a guaranteed minimum yield strength of 280 N/mm² is utilized for profiled sheeting [5]. The thickness of the sheeting can be 1.0mm and 1.25mm. The minimal floor thickness with ComFlor210 (S350) profile is to be 280mm; this height of the slab is considered for the finite element analysis in the study.

1.3 Thesis objective

The scope of the work is to study the behavior of an orthotropic composite deck ComFlor210 under concentrated load placed on a rib at various locations.

The main objectives of the study are:

- Creation of engineering model of the composite slab in order to estimate the behavior of composite slab under concentrated load and to provide the mathematical tool for engineers.
- Development of three-dimensional finite element model (FEM) of the composite slab ComFlor210 using Abaqus/CAE based on existing experimental data.
- Validation of the proposed finite element model by making a comparison of the existing experimental results and those of finite element analysis.
- Conduction a parametric study in order to estimate the impact of the changing different parameters, e.g. mesh sensitivity, concrete-steel interaction properties, concrete properties, etc., on the finite element model created in Abaqus/CAE.
- Conduction a parametric study on composite slab ComFlor210 with different length and geometry properties.

1.4 Outline of the report

The thesis consists of seven chapters:

Chapter 1 gives a brief introduction into the composite slabs and characteristics of ComFlor210, followed by objectives of the study.

Chapter 2 presents a literature review on the subject, including the review of scientific works and finite element methods available for composite slabs.

Chapter 3 provides a detailed description of the modeling subject.

Chapter 4 introduces an engineering model.

Chapter 5 deals with numerical modeling of the composite slab in Abaqus/CAE.

Chapter 6 includes the parametric study on composite slab ComFlor210 of different length and various load positioning.

Chapter 7 presents the evaluation of the results followed by the recommendations for further research.

2 LITERATURE REVIEW

In this chapter, the development and recent investigations in the field of composite slab behavior under concentrated load are described. Additionally, a brief introduction into the finite element modeling of the composite slab is presented. Literature study is based on the works M. Dracht [3], M. Michalaki [4] and others.

The chapter is given in the following order, see Figure 2.1.

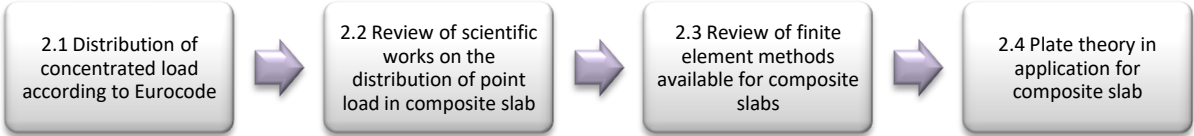


Figure 2.1 Chapter II overview

2.1 Distribution of concentrated load according to Eurocode

Eurocode 1 [6] provides values of the concentrated force Q_k acting on the building element in according with its function. These values vary from 2.0kN to 7kN depending on the category of the loaded area. The dimensions of the loaded area may be assumed as a square with a side length of 50mm for concentrated loads up to 7kN and as a square with a side length of 200mm for greater load values. On a roof with a profiled surface, the concentrated force is distributed over the effective width, and the procedure to determine the effective width in a case of a shallow composite deck is given in Eurocode 4 [2] (Figure 2.2).

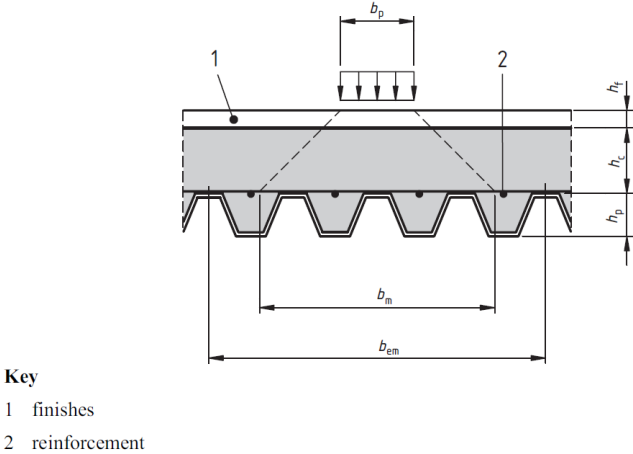


Figure 2.2 Distribution of concentrated load (Eurocode 4)

As mentioned the effective width concept is applicable to the composite slabs with narrowly spaced webs for which the ratio of rib width to the rib spacing does not exceed 0.6; the procedure to establish the effective width for the deep composite deck is out of scope Eurocode 4 [2]. It means that the distribution of the bending moment caused by point load acting on the slab should be assessed individually in each situation. Therefore, the distribution of a point load over the slab width is an open question nowadays. Some research has been done on this subject, information about which is to be presented in this chapter.

2.2 Review of scientific works on the distribution of point load in a composite slab

Research on the distribution of point loads in deep decks ComFlor210 had been conducted by Bode et al. [7], from which it became known that a concentrated load, placed between the ribs of the composite slab with a concrete height of 75 mm and a concrete strength of C20/25, is not critical for the punching shear verification. On the contrary, it was concluded that the vertical shear capacity often became decisive for ComFlor210 resistance. Additionally, it was found that the shear capacity of the steel sheeting could be summed up with that of the concrete in order to reflect actual value of the total shear capacity of the slab.

In the work of Stark et al. [8] regarding the structural behavior of shallow composite slab ComFlor60 under concentrated load, it was stated that half of the point load was carried by the central rib, in the meantime the quarter of the applied load has been transferred to the adjacent ribs on each side. It can be expected that in a case with deep composite slab ComFlor210 the distribution of concentrated force will follow the tendency observed in the shallow deck: the loaded rib will carry most of the load and adjacent ribs will bear the rest of the load; naturally, in different proportionally than in shallow composite slab.

More information about the horizontal distribution of concentrated load in the composite deep deck can be found in the work of M. Dracht [3]. He studied the behavior of ComFlor210 with different section arrangement under point load both analytically and numerically. An analytical model was a two-dimensional model of the slab strip over its width. The ribs were assumed to act as translation springs supporting the top part modeled as a continuous beam. The three-dimensional behavior of the composite slab was included in the model by adding the parameters such as the translation spring stiffness, the rib rotation resistance, the bending stiffness of the top slab and the distributive length. Meanwhile, the problem with the concept of the ribs acting as separate beams was discovered during the laboratory testing. The values of translation stiffness of the ribs in the analytical model were different from experimental results. Therefore, the model cannot be used in the present state.

The conducted laboratory testing on composite slab ComFlor210 [3] at TU Delft gave sufficient information about the composite slab behavior under concentrated load when the slab is simply supported and the load is applied at the middle of the slab. It was shown that the presence of reinforcement mesh in the slab influences the horizontal load distribution, and the effect becomes more pronounced when load increases. Additionally, the effective width length, over which the point load is spread, is influenced by the number of reinforcement meshes included. It was found from the testing that the load spreads over all five ribs in the width direction with two meshes; yet, with one mesh or no mesh at all the concentrated load is carried by three middle ribs.

2.3 Review of finite element methods available for composite slab

Different models have been offered for finite element analysis of a composite slab; most of these models took in consideration the shallow composite decks.

Veljkovic [9] made a three-dimensional non-linear analysis of composite slab in DIANA to study the behavior of interface between concrete and steel sheeting. One of the characteristics of this model was the modeling shear interaction between two materials with nodal elements, properties for which were derived from the push and pull-push tests, i.e. small-scale tests. Based on the FEM results, the partial connection strength method was introduced as a design method in which the mechanical interlocking parameter can be adjusted for any sheeting profile. This model showed good results for shallow composite slabs.

Michalaki [4] created a finite element model of composite slab ComFlor210 in DIANA in which the concept of the weak concrete zone was implemented for non-linear analysis together with the effective area of profiled steel sheeting. The weak zone model suggested dividing concrete into three parts with each part having different elastic modulus; this way the cracking of concrete had been taken into account. The results up to elastic limit showed good agreement with experimental findings; however, the results up to the slab failure were conservative. Additionally, the created model displayed only a quarter of the composite slab, which means it only can be used under symmetrical boundary and loading conditions.

Attarde [10] made a nonlinear finite element model of the shallow composite deck in Abaqus/CAE in order to study the effect of implementation of different concrete type, namely engineered cementations composites and self-consolidating concrete. His study proved that the displacement control analysis in Abaqus is a better option for simulation the behavior of composite slab than load control analysis. Additionally, the concrete damaged plasticity model is a favorable choice among all concrete models available in the program to define concrete behavior.

Considering the finite element models above, an initial decision on the development of the finite element model in Abaqus can be made. Implementation of displacement control analysis, modeling of the whole composite slab together with all reinforcement present in the slab and usage of concrete damage plasticity model might be the possible starting points to create a finite element model.

2.4 Plate theory in the application for composite slab

The slab is a general term for a concrete plate that subjected to a load perpendicular to its plane. The plate theory, therefore, is applicable for slabs. In plate theory [11] the distinction is made between thick plates and thin plates; the main difference between the two plate types is that in a case of thin plates loaded perpendicularly to their plane the shear deformations can be neglected while for thick plates both bending and shear deformations have to be taken into account. The composite slab ComFlor210 can be regarded as a thin plate because its depth much smaller than the length.

The analysis of thin plates is based on the assumptions:

- No membrane forces occur due to support constraints and the mid-plane of the slab remains stainless after load application.
- The straight line normal to the mid-plane of the slab in unloaded situation remains straight but not necessarily normal to the mid-plane of the slab after load application.
- Stress in the direction normal to the mid-plane of the slab is assumed to be zero.
- Shear deformations due to applied load are negligible.

Plate theory formulation for the isotropic and homogeneous structure is straightforward and composed of kinematic, constitutive and equilibrium equations that relate degrees of freedom, deformations, stress resultants and loads to each other. The displacement w of the plate under point load F can be found by solving the differential biharmonic plate equation (2.1) with respect to the governing boundary conditions [11].

$$D\nabla^2\nabla^2w = F \quad (2.1)$$

In equation (2.1) D is a stiffness term for the isotropic plate and ∇^2 is the Laplace operator.

The composite slab is an example of non-homogeneous and non-isotropic plate, thus, the stiffness of the orthotropic plate cannot be expressed in one term. Now for the two-dimensional orthotropic plate in commonly used x-y coordinate system four stiffnesses should be determined D_{xx} , D_{xy} , D_{yx} , and D_{yy} . These different stiffnesses should be taken into account in corresponding kinematic and constitutive equations; for example, bending moment m_{xx} becomes then a product of plate stiffness D_{xx} and curvature k_{xx} .

The boundary conditions for two-dimensional simply supported in length direction orthotropic plate will be:

- At supported edge: $w=0$ and $\partial^2w/\partial x^2 = 0$ (displacement and second derivative are zero).
- At free not loaded edge: $m_{xx}=0$ and $v_x + \partial m_{xy}/\partial y = 0$ (moment and shear force are zero).

When the section properties of the plate are established, the displacement of the plate can be found by solving the differential equation (2.1) with prescribed boundary conditions. However, finding the initial expression for plate displacement by hand can be difficult and of limited accuracy, especially in a case when orthotropic plate does not have a symmetrical mid-plane. In that case, the plate should be divided into multiple elements of relatively small size in order to gain the desired accuracy, and each such element will have own displacement expression. Solving all these expressions simultaneously will require an enormous effort from a user; therefore, in practice, these equations are solved with the help of numerical software. Many finite element programs include the theory of plate in the code in order to make it feasible for a user to analyze the structural behavior of a plate with complicated geometry and different cross-sectional properties. Because one of the objectives of this work is assessing the performance of the composite slab with a numerical model, the manual application of plate theory for orthotropic slab will not be elaborated further.

3 Modeling object

3.1 Geometry

The object of the modeling is a composite slab ComFlor210, which consists of four main elements; i. e. profiled steel sheeting ComFlor, concrete C20/25, reinforcement mesh in the top deck with main and cross wires 8mm and mesh size 150mmx150mm, and steel bars $\varnothing 20$ in the ribs. The composite slab is modeled with five ribs, and three arrangements of reinforcement meshes installed in the top concrete deck are distinguished: no mesh, 1 mesh and two meshes. The corresponding cross-sections of the composite slab are shown on Figure 3.1.

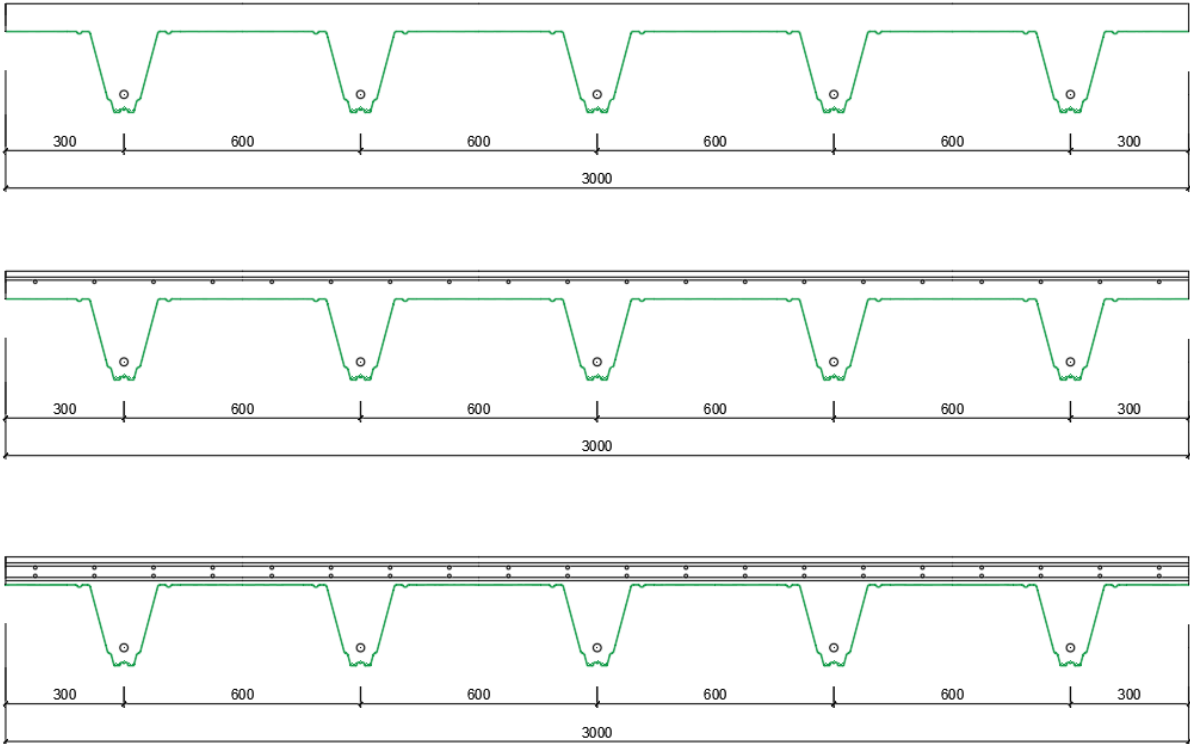


Figure 3.1 Cross-sections of the composite slab, from top to bottom: no mesh, 1 mesh, 2 meshes

The thickness of the concrete top deck is 70mm, while the whole thickness of the slab is 280mm. The steel bar $\varnothing 20$ is placed in the rib center at a height of 56mm from the bottom of the slab. The position of the top and bottom mesh wires starting from the top of the slab is at a height of 19mm, 27mm and 48mm, 56mm respectively, and given in Figure 3.2.

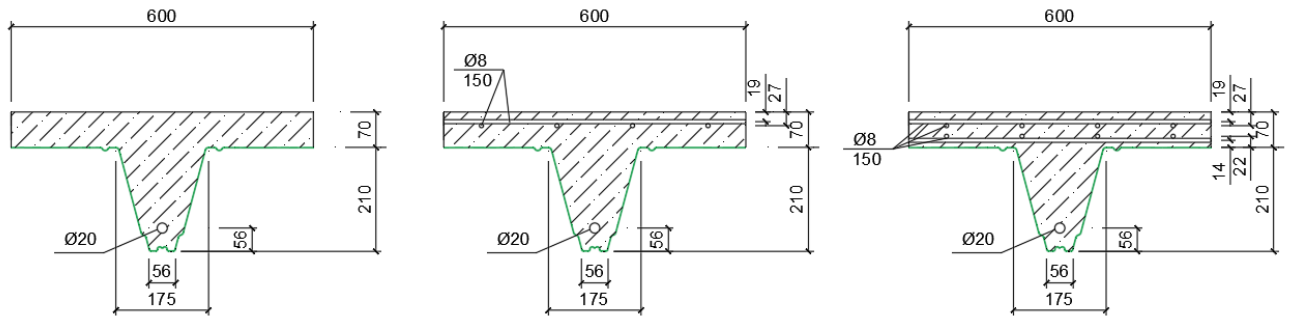


Figure 3.2 Detailed cross-sections of the rib, from left to right: no mesh, 1 mesh, 2 meshes

Generally, the slab width is a variable parameter; it can be formed by adding different numbers of the rib to each other. With the center-to-center distance between ribs being 600mm, the slab with two ribs will have a width 1200mm, slab with three ribs – 1800mm, etc. In this study, the starting point is to consider five ribs, which gives the slab width 3000mm utmost. The slab length is 5400mm.

3.2 The effective area of a steel deck

The steel sheeting has a complex shape due to embossments in a longitudinal direction. Although the presence of sunken and risen relief on a plain steel sheeting is a functional improvement of this element because it introduces additional composite action between concrete and steel deck; yet, the area with embossments does not contribute to the bending slab resistance in the longitudinal direction when the slab is mainly subjected to bending. Thus, instead of whole profile, the effective area of profiled steel sheeting should be used in calculations of the bending moment capacity. And this raises a question which part of a steel deck can be considered effective.

M. Dracht [3] used for his analytical model the effective deck area of 572.1mm². This area is shown in Figure 3.3.

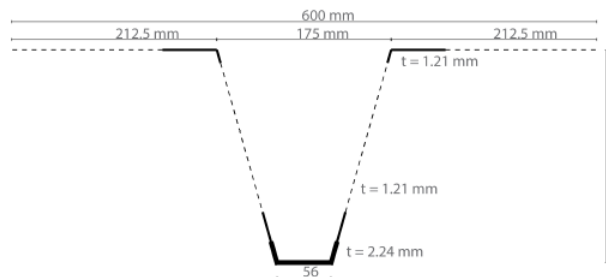


Figure 3.3 Effective steel area (M. Dracht, 2015)

Van Erp [12] in his work conducted several full-scale experiments in order to determine the longitudinal shear resistance of ComFlor210, and one of the objectives was to measure the effective area of steel deck using a large number of strain gauges during testing. Even though it was stated that more tests are necessary to establish an effective area more accurately, it is decided to use Van Erp value of effective steel area in this study rather than making an assumption. Therefore, the effective steel area is an average value when effective areas of all specimens are summarized and then divided by a number of specimens. This value equals 559.25mm² which is slightly lower than the value of M. Dracht. The detailed information about the effective area of ComFlor210 is given in Appendix A.

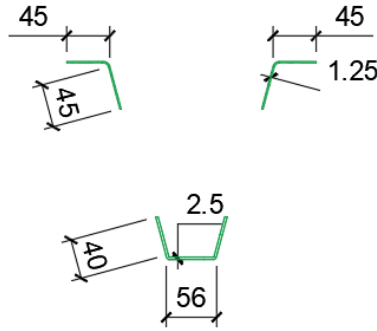


Figure 3.4 The effective area ComFlor210

3.3 Boundary conditions, applied load and possible failure modes

The composite slab is simply supported on the short sides; the other two sides are free. The supports are positioned 100mm away from the slab edges. This is depicted in Figure 3.5 where the top of the slab is shown together with rib positions, which are indicated by horizontal dashed lines, and support locations, which are indicated by vertical dashed lines.

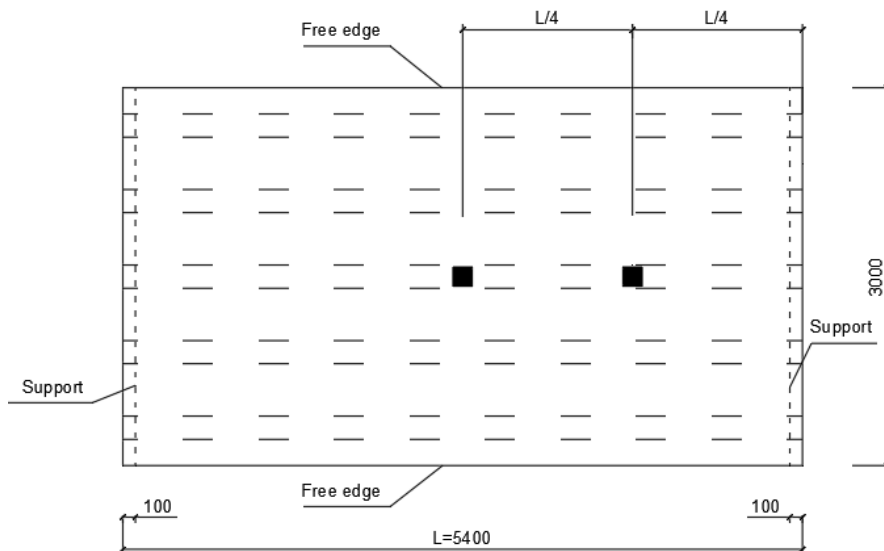


Figure 3.5 Composite slab: boundary conditions

The concentrated load F is applied on top of the slab. The position of the load can vary, however, for setting the engineering model it has been chosen to place the point load above the center of the middle rib at a half span length and at a quarter of the span. Hence, two locations of the point load are considered (Figure 3.6):

- at a half span length, which is 2700mm;
- at a quarter of the span, i.e. 1350mm.

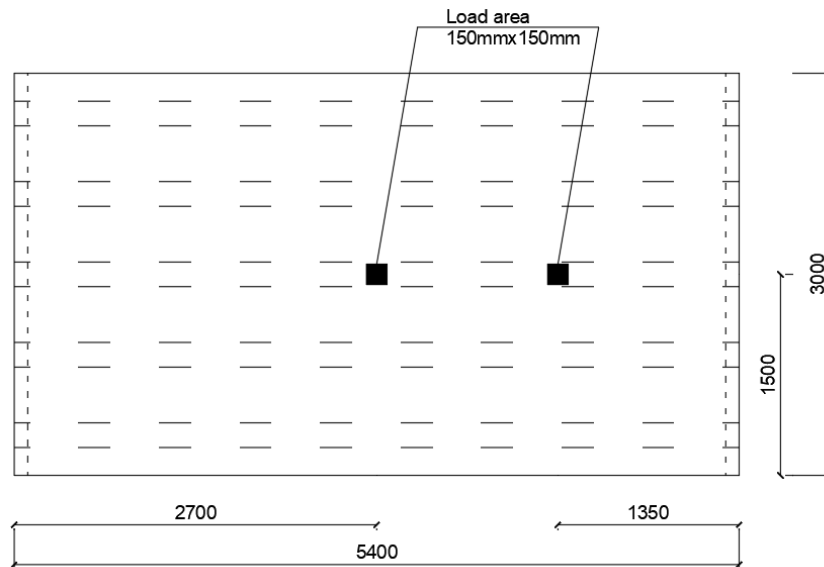


Figure 3.6 Composite slab: load application

The area of concentrated force application is 150mmx150mm. This area is smaller than 200mmx200mm mentioned in Eurocode 1 [6] in a case when loads higher 10kN are specified; however, for the consistency with experiments the same loaded area as in Dracht [3] work is considered in this thesis.

The concentrated load F has different magnitudes for each slab type that is modeled. These magnitudes of concentrated load are given in Table 3.1. The maximum concentrated load does not exceed 60kN; this is because the engineering model is based on elastic analysis of slab cross-section and because during the testing slab behavior was elastic approximately up to 60kN. For load applied at the quarter of the span the highest magnitude is different – 50kN instead of 60kN; this is because the slab with load application in the quarter of the span was loaded up to 50kN during a laboratory experiment.

Table 3.1 Concentrated load magnitude

Slab type	Magnitude F	Unit
	$L_{span}/2$ ($L_{span}/4$)	
no mesh	10 (10)	kN
1 mesh	60 (50)	
2 meshes		

When the load is positioned on the composite slab as it is shown in Figure 3.6, three possible failure modes can be distinguished:

- Failure of the rib due to exceeding bending moment capacity or vertical shear resistance (I).
- Failure of the interface between the rib and top deck due to vertical shear (II).
- Longitudinal shear failure (III).

The locations where such failure might occur are shown in Figure 3.7.

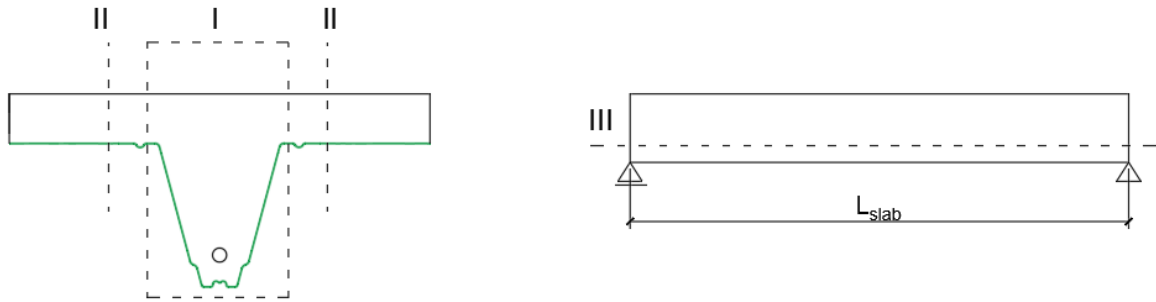


Figure 3.7 Failure modes: I – rib failure due to bending or vertical shear, II – interface failure due to vertical shear, III – longitudinal shear failure

Flexural failure occurs when the plastic bending capacity of the composite slab has been reached. For this failure mode to take place the excessive yielding of steel sheeting and sufficient rotational capacity in the cross-section are necessary to develop. Longitudinal shear failure is accompanied by concrete slipping over the steel sheeting; the maximum load reached in this failure mode can be of less magnitude than in a case with flexural failure [9]. Vertical shear failure is associated with vertical shear resistance of the composite slab. This failure mode usually occurs at a location with the largest shear force. Origin of failure mechanism depends on many parameters; one of them is a slab length. Usually, short slabs are likely to fail in vertical shear; while long slabs are prone to flexural failure. It is worth to mention that when point load is moved to another location, for instance, between the ribs, the possible failure mode can be punching shear of the concrete top deck.

4 Engineering model

This chapter deals with setting the engineering model of the composite slab and evaluation of the results. The overview of the chapter is given in Figure 4.1.

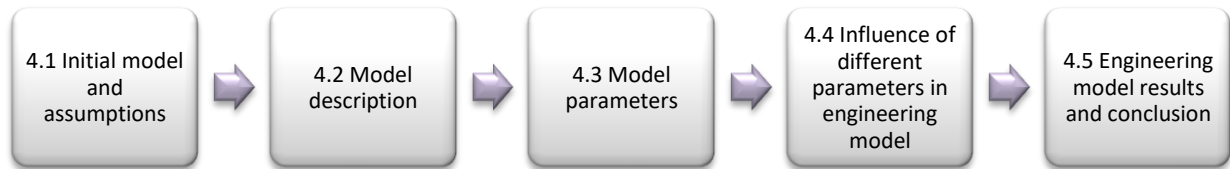


Figure 4.1 Chapter overview

4.1 Initial model and assumptions

The initial model of the composite slab is a model of a slab strip over five ribs. The composite slab in width direction is modeled as follows: the top deck is substituted with a continuous beam that is supported by five translation springs; in this way, the springs represent the five ribs. In the center of the top deck the concentrated force F is applied, thus, the center spring is also loaded directly with a concentrated load. The applied action causes the deflection of the top deck and central spring; as a result, the other springs begin to deflect as well. In the longitudinal direction, the slab is modeled as a simply supported beam. Both models are shown in Figure 4.2.

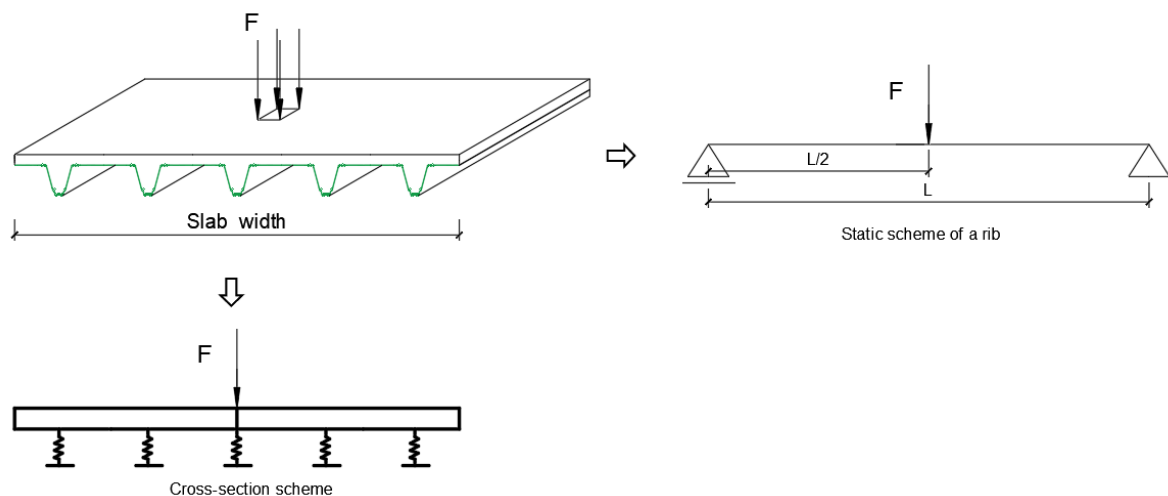


Figure 4.2 Sketch of the initial model

The initial assumptions for the model are:

- Concrete has no tensile resistance.
- There is no slip on concrete-steel sheeting interface.
- For the bending stiffness determination of composite steel sheeting, only the effective area of ComFlor210 is used (see 3.2 [The effective area of a steel deck](#)).
- The self-weight of the composite slab is not included in the model.
- Elastic analysis of cross-section is applied.

In the longitudinal direction, the bending capacity of a slab is determined by the bending resistance of the ribs. The transverse bending capacity is associated with the bending resistance of the top deck.

4.2 Model description

4.2.1 Engineering model in the longitudinal direction

The composite slab is modeled longitudinally as a simply supported beam. The behavior of such beam can be described with Euler-Bernoulli beam theory. According to this theory, the deflection of the beam can be found by solving a fourth-order linear ordinary differential equation (4.1).

$$EI \frac{d^4 w}{dx^4} = q \quad (4.1)$$

The general solution to this differential equation is obtained by integrating both parts of the expression in order to acquire expressions for bending moment, shear force, rotation, and deflection. The deflection is, then, given by equation (4.2).

$$w(x) = \frac{1}{EI} \left(\frac{1}{24} qx^4 + \frac{1}{6} C_1 x^3 + \frac{1}{2} C_2 x^2 + C_3 x + C_4 \right) \quad (4.2)$$

In Eq. (4.2) $w(x)$ is a deflection of a beam at location x , q is a distributed load, EI is bending stiffness of the beam, $C_1..C_4$ are integration constants, values for which are found by solving the differential equation simultaneously with appropriate boundary and interface conditions. In a case when distributed load q is not present, the corresponding part in the equation, that contains q , becomes zero. Additionally, the expression (4.2) holds true for a beam with constant bending stiffness. If the bending stiffness of the beam varies along its length, the beam must be divided into several discrete parts, and for each discrete part the corresponding expression of deflection must be set.

As it mentioned before the rib is loaded by concentrated force in its middle and a quarter of the span. Because of the loading concrete starts to crack when the bending moment due to applied force exceeds the cracking moment of concrete. The Young's modulus of concrete decreases, as a result, the bending stiffness of the rib decreases as well. Therefore, in both loading cases, the rib must be divided into several discrete elements in order to take into account the difference in bending stiffness due to cracking of concrete. In the next subsections, the detailed information regarding the deflection calculation of a beam with two load arrangements is provided.

4.2.1.1 Beam model with a load in the center.

The sketch of a beam and its cross-section is given in Figure 4.3. In this figure L_{cr} is a length of the beam part where concrete is cracked, a is a length of the beam with uncracked concrete, EI_{cr} is bending stiffness of cracked part, and EI_{un} is bending stiffness of uncracked part. Bending stiffness of the beam is dependent on the number of reinforcement meshes used in the cross-section, and, thus, it changes its value.

The width of the beam, that is taken into account to calculate EI_{cr} and EI_{un} , equals 600mm or 175mm. The 600mm width of the beam corresponds to the spacing between the ribs, and 175mm width of the rib is set in accordance with an observation during the laboratory testing of the slab regarding the crack propagation in the rib (see Figure 4.3, d). The appeared cracks separated the rib from the top deck across the top width of a rib; therefore, it was decided to check whether the model with a smaller cross-section of a rib will deliver more accurate results.

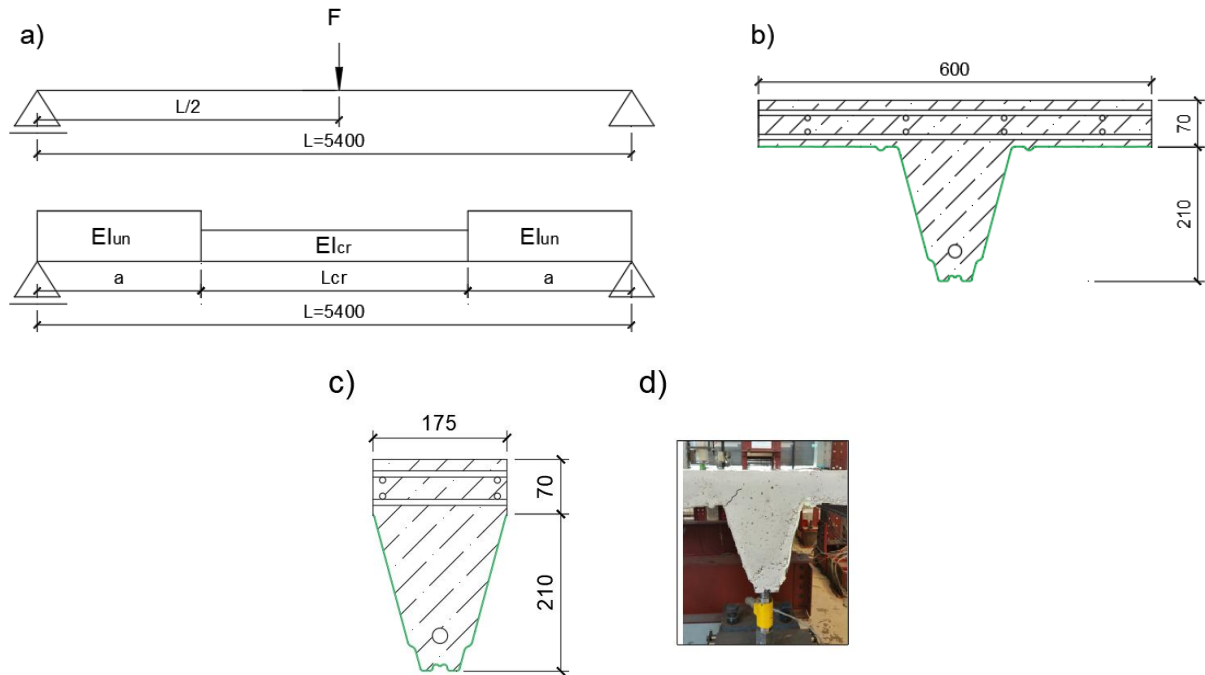


Figure 4.3 Beam geometry: a) load and varied bending stiffness along the beam; b) beam cross-section with 600mm width; c) beam cross-section with 175mm width; d) crack formation in a rib during testing (M. Dracht, 2015)

The beam is divided into four discrete parts, see Figure 4.4; and for each part the deflection expression (4.2) holds, thus, resulting in a system of four differential equations. This system of equations can be solved when appropriate boundary and interface conditions are established. Those conditions are given in Table 4.1.

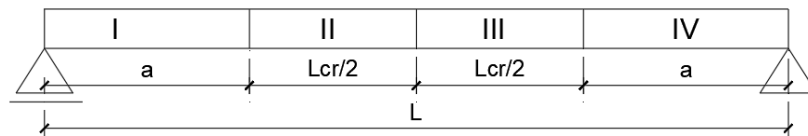


Figure 4.4 Discrete elements of a beam

As it can be seen in Table 4.1 the bending moment and deflection equal to zero at the supports and for discrete elements between the supports the continuity of bending moment, shear force, rotation and deflection retains. That means that on interface those parameters must be identical. Together boundary and intermediate conditions account for sixteen differential equations, and the total amount of integration constants is of the same order. Hence, the total amount of equations, that necessary to be solved to get deflection at any point along the beam, is sixteen.

Table 4.1 Boundary and intermediate conditions for rib loaded centrally

Boundary conditions		Intermediate conditions		
$x=0$	$x=L$	$x=a$	$x=L-a$	$x=a+Lcr/2$
$M_I=0$	$M_{IV}=0$	$M_I = M_{II}$	$M_{III} = M_{IV}$	$M_{II} = M_{III}$
$w_I=0$	$w_{IV}=0$	$V_I = V_{II}$	$V_{III} = V_{IV}$	$V_{II} = F + V_{III}$
		$\phi_I = \phi_{II}$	$\phi_{III} = \phi_{IV}$	$\phi_{II} = \phi_{III}$
		$w_I = w_{II}$	$w_{III} = w_{IV}$	$w_{II} = w_{III}$

This resulting system of equations is presented in matrix notation in Appendix B. (see Eq. (B. 1)). This system of equations can be easily resolved with the help of mathematical software like Maple or Mathcad.

4.2.1.2 Beam model with load at a quarter of the span.

The sketch of a beam and its cross-section can be seen in Figure 4.5, where L_{cr} is a length of the beam part where concrete is cracked, a and b represent the length of the beam with uncracked concrete, of which b has the smallest value. The width of the beam that is taken into account to calculate bending stiffness's EI_{cr} and EI_{un} equals 600mm or, in the second case, 175mm.

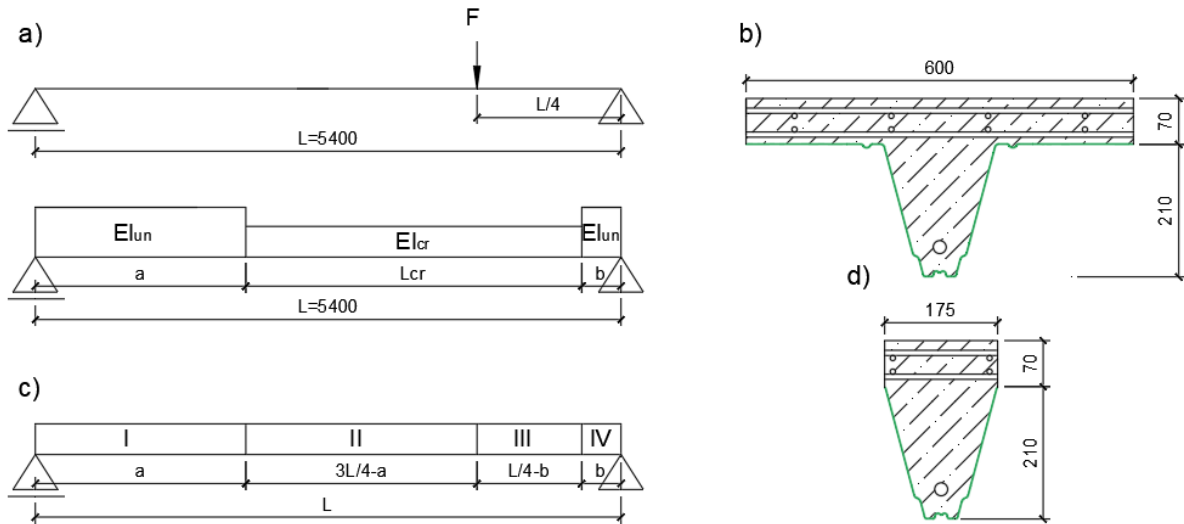


Figure 4.5 Beam geometry: a) load and bending stiffness; b) beam cross-section with 600mm width; c) beam discrete elements; d) beam cross-section with 175mm width;

Once again the beam can be divided into four discrete parts. The deflection of the beam can be obtained by solving equation (4.2) of each part together with boundary and intermediate conditions; these conditions are shown in Table 4.2. The resulting system of equations is presented in matrix notation in Appendix B. (see Eq. (B. 2)).

Table 4.2 Boundary and intermediate conditions for rib loaded at a quarter of the span

Boundary conditions		Intermediate conditions		
$x=0$	$x=L$	$x=a$	$x=L-b$	$x=L-L/4$
$M_I=0$	$M_{IV}=0$	$M_I= M_{II}$	$M_{III}= M_{IV}$	$M_{II}= M_{III}$
$w_I=0$	$w_{IV}=0$	$V_I= V_{II}$	$V_{III}= V_{IV}$	$V_{II}= F+V_{III}$
		$\varphi_I= \varphi_{II}$	$\varphi_{III}= \varphi_{IV}$	$\varphi_{II}= \varphi_{III}$
		$w_I= w_{II}$	$w_{III}= w_{IV}$	$w_{II}= w_{III}$

4.2.2 Engineering model transversal

The engineering model in width direction (transversal) consists of five springs, that represent ribs, and top deck which acts as a beam. The beam element of the top deck is divided into multiple discrete parts in order to take into account change in moment direction (negative and positive bending moments when top deck is seen as a clamped beam between ribs) and cracking of concrete. This is shown in Figure 4.6.

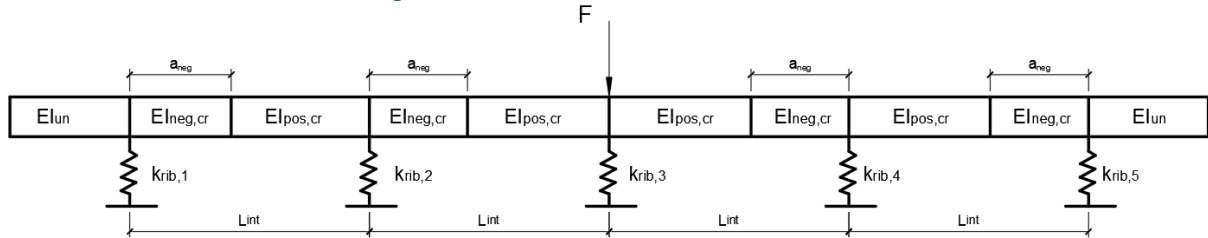


Figure 4.6 Slab model transversely

The amount of discrete elements is ten. The deflection of the structure can be obtained by solving equation (4.2) of each discrete element together with boundary and intermediate conditions: the bending moment and shear force equal to zero at the free edges, and for discrete elements at interface the continuity of bending moment, shear force, rotation, and deflection retains, as it can be seen in Table 4.3. The nine intermediate locations, of which five are support positions and four are interface locations at top deck where bending moment changes sign, together with two boundary locations at slab edges produce in the total set of forty equations.

Table 4.3 Boundary and intermediate conditions for slab model

Boundary conditions		Intermediate conditions at spring support	Intermediate conditions at the interface with bending moment change
$x=0$	$x=B_{slab}$	$x=L_{support}$	$x=L_{interface}$
$M_l=0$	$M_x=0$	$M_{Left}=M_{Right}$	$M_{Left}=M_{Right}$
$V_l=0$	$V_x=0$	$F_{rib}+k_{rib}w_{Left}+V_{Left}=V_{Right}$	$V_{Left}=V_{Right}$
		$\phi_{Left}=\phi_{Right}$	$\phi_{Left}=\phi_{Right}$
		$w_{Left}=w_{Right}$	$w_{Left}=w_{Right}$

The equation for the shear force at each spring support contains spring stiffness k_{rib} . The value of spring stiffness is described by the force-deflection ratio of the rib, see eq. (4.3). The force-deflection ratio can be derived directly from rib model in the longitudinal direction when force and deflection in the position of interest are known.

$$k_{rib} = F_{rib}/w_{rib} \quad (4.3)$$

The rib stiffness can be also obtained from the rib load-deflection diagram derived from testing [3] or finite element analysis. The values of rib stiffnesses derived from test and FEA are given in Table 4.4 and Table 4.5.

Table 4.4 Rib stiffness values for composite slab under point load applied halfway the span derived from test and FEA

Load, kN	Rib	Rib stiffness k_{rib} , kN/mm					
		2 mesh		1 mesh		no mesh	
$L_{span}/2$	#	Test	FEA	Test	FEA	Test	FEA
10	1	4.00	2.83	3.50	2.48	1.20	0.85
	2	5.30	6.02	5.30	6.03	2.00	2.79
	3	5.30	5.20	5.30	5.30	2.80	2.79
	4	5.30	6.02	5.30	6.03	2.80	2.79
	5	4.00	2.83	3.50	2.48	0.80	0.85
60	1	0.60	0.83	0.00	0.33	-	-
	2	1.60	2.92	1.80	3.29	4.30	6.20
	3	2.60	2.17	2.70	2.25	5.00	4.17
	4	1.60	2.92	1.80	3.29	4.30	6.20
	5	0.50	0.83	0.00	0.33	-	-

Table 4.5 Rib stiffness values for composite slab under point load applied at the quarter of the span derived from test and FEA

Load, kN	Rib	Rib stiffness k_{rib} , kN/mm					
		2 mesh		1 mesh		no mesh	
$L_{span}/4$	#	Test	FEA	Test	FEA	Test	FEA
10	1	2.50	2.20	2.70	2.37	1.70	1.50
	2	7.50	7.30	8.75	7.26	11.25	9.30
	3	8.75	8.09	8.75	8.04	8.33	7.66
	4	7.50	7.30	7.50	7.26	13.30	9.30
	5	2.50	2.20	3.50	2.37	1.60	1.50

The location at which the bending moment changes sign can be found by assessing ordinary clamped beam with prescribed unit settlement at one of the support, see Figure 4.7. The assessment yields the expression (4.4) for a length of the top deck under a negative bending moment [3]. Seeing the top deck as clamped between the ribs is an assumption; in reality, the top deck will not be fully clamped due to the small torsional stiffness of the ribs and because the ribs are simply supported.

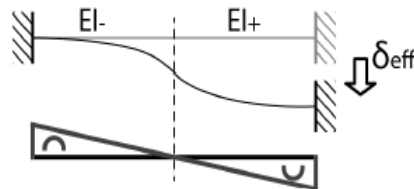


Figure 4.7 Ordinary clamped beam with prescribed support settlement and resulting moment diagram

$$l = \frac{-L_{int} + \sqrt{\frac{EI_+}{EI_-} * L_{int}^2}}{EI_+/EI_- - 1} \quad (4.4)$$

In the expression (4.4) L_{int} is a length of the clamped part of the top deck between the ribs, EI_+ and EI_- are the positive and negative bending stiffnesses of the top deck, and l is a length of the clamped beam that has negative bending stiffness.

The resulting system of equations for the transversal model of the composite slab with five ribs is presented in matrix notation in Appendix B. (see Eq. (B. 2)).

4.3 Model parameters

In this subchapter the main parameters of engineering model are determined. These parameters are:

- Bending stiffness of the rib and bending stiffness of the top slab;
- Cracking bending moment of the rib and cracking bending moment of the top slab;
- Bending resistance of the rib.

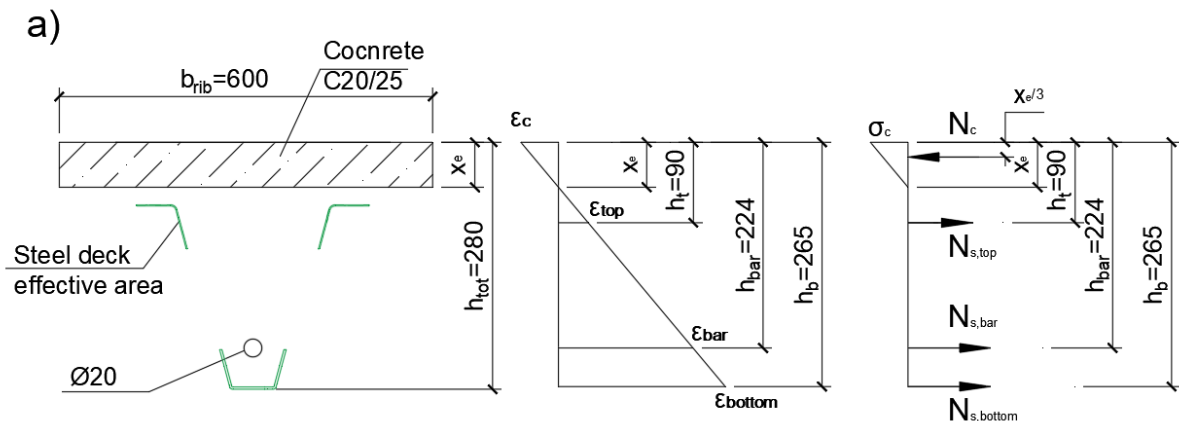
4.3.1 Bending stiffness and cracking moment of the rib

The bending resistance of the rib with width 600mm and 175mm is defined in accordance with Eurocode 4 [2]. First of all, the cracking moment of the rib is computed by making an assumption that steel parts of the cross-section are not activated so far and only concrete is acting. The cracking moment can be calculated as the product of concrete mean tensile strength and the elastic section modulus (see Eq. (4.5) and (4.6)).

$$M_{cr,rib,600} = f_{ctm} W_{c,bot} = \frac{f_{ctm} * I_{c,rib}}{h_{bot}} = \frac{2.2 * 4.82 * 10^8}{187} = 5.67 * 10^6 Nmm. \quad (4.5)$$

$$M_{cr,rib,175} = f_{ctm} W_{c,bot} = \frac{f_{ctm} * I_{c,rib,175}}{h_{bot}} = \frac{2.2 * 6.37 * 10^7}{163} = 8.59 * 10^5 Nmm. \quad (4.6)$$

In the second place, the bending resistance of the rib is calculated. The initial step is to assume that the neutral axis position is situated above the steel sheeting. The rib cross-section includes several parts: concrete in compression, the reinforcement $\varnothing 20$ in the rib, the top flange and the bottom flange of the steel sheeting. The cross-section and elastic strain distribution in the cross-section after cracking of concrete is shown in Figure 4.8.



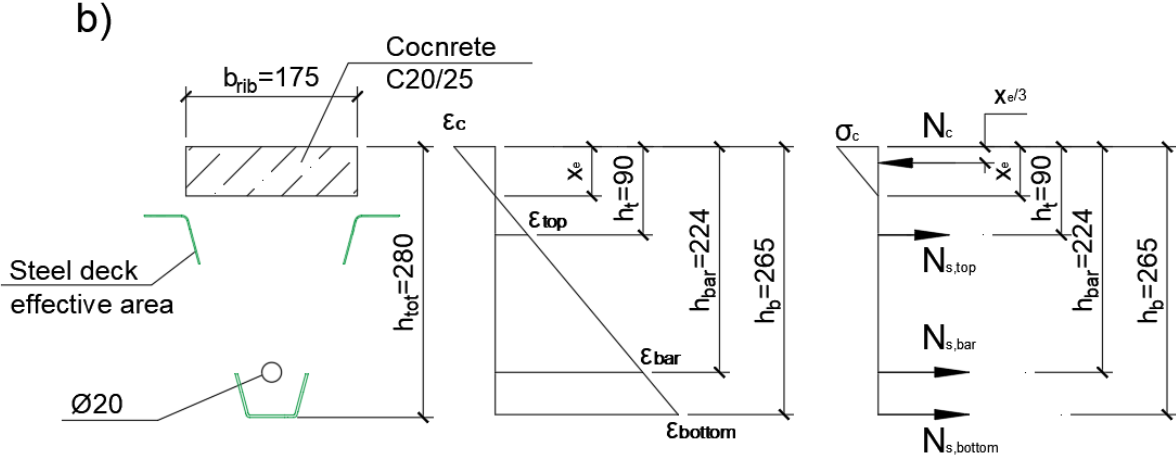


Figure 4.8 Strain distribution and forces in the rib cross-section: a) rib with 600mm width; b) rib with 175mm width.

The height of the concrete compressive zone can be determined by solving a set of equilibrium equations obtained from strain distribution and forces in the cross-section. Thus, the height of the concrete compressive zone just after it cracks follows from proportion (4.7) and equations (4.8), (4.9).

$$\frac{\varepsilon_c}{x_e} = \frac{\varepsilon_{top}}{h_t - x_e} = \frac{\varepsilon_{bottom}}{h_b - x_e} = \frac{\varepsilon_{bar}}{h_{bar} - x_e}, \quad (4.7)$$

$$\frac{1}{2} b_{rib} \varepsilon_c x_e E_{cm} = \varepsilon_{top} E_{CF} A_t + \varepsilon_{bottom} E_{CF} A_b + \varepsilon_{bar} E_s A_{bar} \quad (4.8)$$

$$M_{cr,rib} = \varepsilon_{top} E_{CF} A_t h_t + \varepsilon_{bottom} E_{CF} A_b h_b + \varepsilon_{bar} E_s A_{bar} h_{bar} - \frac{1}{6} b_{rib} \varepsilon_c x_e^2 E_{cm} \quad (4.9)$$

Solving simultaneously Eq. (4.7), (4.8) and (4.9), the value of concrete compressive zone can be found to be $x_e = 54.6\text{mm}$ (when $b_{rib} = 600\text{mm}$) and $x_e = 88.7\text{mm}$ (when $b_{rib} = 175\text{mm}$). Assuming that steel bar is yielding at a strain $\varepsilon_{bar} = 2 \cdot 10^{-3}$, the strain at a top flange of the effective area of steel sheeting becomes $\varepsilon_{top} = 8.04 \cdot 10^{-4}$ (Eq. (4.10)) and $\varepsilon_{top,175} = 1.92 \cdot 10^{-5}$.

$$\frac{\varepsilon_{bar}}{h_{bar}} = \frac{\varepsilon_{top}}{h_t} \quad (4.10)$$

Now the compressive force in concrete and the total tensile force of steel in the cross-section can be determined with equations (4.11) and (4.12).

$$\begin{aligned} N_s &= f_{y,CF} A_t + f_{y,CF} A_b + f_y A_{bar} = \\ &= 400 \cdot 231.75 + 400 \cdot 327.5 + 540 \cdot 314 = 393\text{kN} \end{aligned} \quad (4.11)$$

$$\begin{aligned} N_{s,175} &= \varepsilon_{top} E_{CF} A_t + f_{y,CF} A_b + f_y A_{bar} = \\ &= 1.92 \cdot 10^{-5} \cdot 210000 \cdot 231.75 + 400 \cdot 327.5 + 540 \cdot 314 = 301\text{kN} \end{aligned}$$

$$N_c = 0.75 b_{rib} x_e f_{cm} = 0.75 \cdot 600 \cdot 54.6 \cdot 28 = 688\text{kN} \quad (4.12)$$

$$N_{c,175} = 0.75 b_{rib} x_e f_{cm} = 0.75 \cdot 175 \cdot 88.7 \cdot 28 = 326\text{kN}$$

Finally, the bending resistance of the rib is calculated as it can be seen in equation (4.13). The influence of rib self-weight is excluded from the calculation.

$$\begin{aligned}
M_{k,rib} &= \varepsilon_{top} E_{CF} A_t h_t + f_{y,CF} A_b h_b + f_y A_{bar} h_{bar} - \frac{1}{3} N_s x_e \\
&= 8.04 \cdot 10^{-4} \cdot 210000 \cdot 231.75 \cdot 90 + 400 \cdot 327.5 \cdot 265 \\
&\quad + 540 \cdot 314 \cdot 224 - \frac{1}{3} \cdot 393.26 \cdot 10^3 \cdot 54.6 = 69.1 kNm \\
M_{k,rib,175} &= \varepsilon_{top} E_{CF} A_t h_t + f_{y,CF} A_b h_b + f_y A_{bar} h_{bar} - \frac{1}{3} N_s x_e \\
&= 1.92 \cdot 10^{-5} \cdot 210000 \cdot 231.75 \cdot 90 + 400 \cdot 327.5 \cdot 265 \\
&\quad + 540 \cdot 314 \cdot 224 - \frac{1}{3} \cdot 301.5 \cdot 10^3 \cdot 88.7 = 63.8 kNm
\end{aligned} \tag{4.13}$$

The properties, that are used to calculate the bending capacity of the rib, are given in Table 4.6.

Table 4.6 Properties used in bending capacity calculation

Property		Value	Unit
Young's Modulus concrete	E_{cm}	30000	N/mm^2
Young's Modulus ComFlor210	E_{CF}	210000	N/mm^2
Young's Modulus steel bar	E_s	200000	N/mm^2
Compressive strength concrete	f_{cm}	28	N/mm^2
Tensile strength concrete	f_{ctm}	2.2	N/mm^2
Yield stress ComFlor210	$f_{y,CF}$	400	N/mm^2
Yield stress reinforcement	f_y	540	N/mm^2
Total height of the cross-section	h_{tot}	280	mm
Height to the top flange of steel effective area ComFlor210	h_t	90	mm
Height to the bottom flange of steel effective area ComFlor210	h_b	265	mm
Height to the steel bar Ø20	h_{bar}	224	mm
Area of top flange ComFlor210	A_t	231.75	mm^2
Area of bottom flange ComFlor210	A_b	327.5	mm^2
Area of steel bar Ø20	A_{bar}	314	mm^2
Width of the rib	b_{rib}	600 175	mm

Determination of bending stiffness of the rib is given in detail in Appendix B.

The resulting values of bending stiffness of the rib with different amount reinforcement meshes are displayed in Table 4.7.

Table 4.7 Bending stiffnesses of the rib

Section type	Value for $b_{rib}=600mm$, E+12	Value for $b_{rib}=175mm$, E+12	Unit
Cracked section and no mesh	7.73	5.23	Nmm^2
Cracked section and one mesh	7.87	5.49	
Cracked section and two meshes	8.01	5.60	
Uncracked section and no mesh	12.3	7.63	
Uncracked section and one mesh	12.6	8.03	
Uncracked section and two meshes	12.8	8.19	

It is necessary to mention that the bending stiffness of the ribs might be higher at small loads than calculated values for cracked section shown in Table 4.7. The bending stiffness of a rib depends on how much concrete is cracked in a cross-section, and no distinction is made in engineering model so far between the load level and amount of cracked concrete in a section. The assumptions that only concrete in a rib is cracked and modulus of elasticity of cracked concrete equals one-third of not cracked material can lead to an underestimation of rib bending stiffness at low load level. In order to mitigate the effect of this assumption on engineering model results, a linear dependence between rib bending stiffness and applied load is adopted. In Figure 4.9 and Figure 4.10 the linear dependencies are presented for rib of width 600mm and 175mm with 2 meshes, 1 mesh and no mesh in the cross-section: the cracked bending stiffness values from Table 4.7 correspond to the total load 60kN, and the uncracked bending stiffness values from Table 4.7 correspond to the total load 0kN. The values in between can be used in engineering model with 10kN, 20kN load, and so forth.

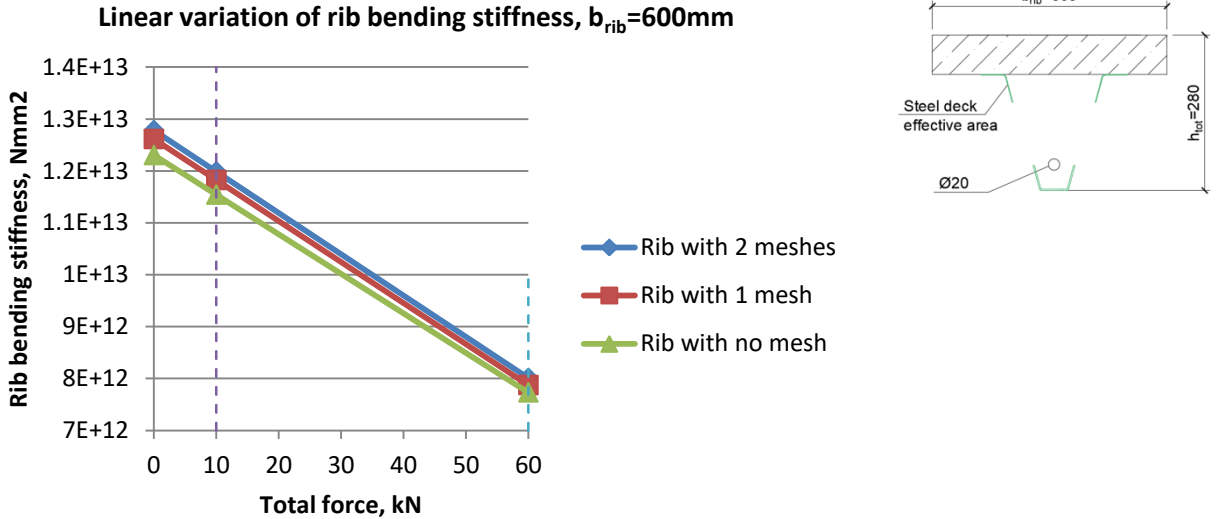


Figure 4.9 Linear variation of rib bending stiffness with $b_{rib}=600\text{mm}$

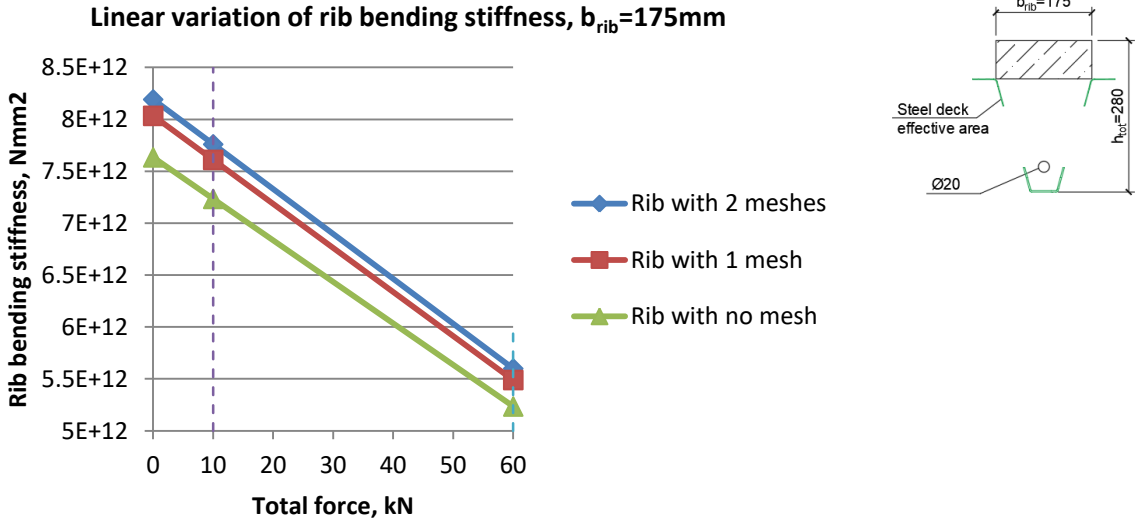


Figure 4.10 Linear variation of rib bending stiffness with $b_{rib}=175\text{mm}$

4.3.2 Bending stiffness and cracking moment of the top deck

4.3.2.1 Cracking moment and bending stiffness of the uncracked section

The bending resistance of the top deck is defined in accordance with Eurocode 4 [2]. It has been assumed to exclude the steel sheeting from the calculation of bending resistance and bending stiffness of the top slab. The steel sheeting is not consolidated sufficiently in top deck to suppose that it will contribute much to the bending stiffness. Therefore, the parts which are taken into account in calculation onwards are:

- Concrete C20/25;
- Reinforcement mesh $\varnothing 8\text{mm}$ -150mm.

Once again, the cracking moment of the top deck is computed first by making an assumption that steel elements of the cross-section are not acting and only concrete is activated. The cracking moment follows from the product of concrete mean tensile strength and the elastic section modulus of the corresponding cross-section (see eq.(4.14)). This cross-section is shown in Figure 4.11.

$$M_{cr,deck} = f_{ctm} W_c = f_{ctm} \frac{1}{6} L_{dis} h_c^2 = 2.2 \cdot \frac{1}{6} \cdot 200 \cdot 70^2 = 3.59 \cdot 10^5 \text{ Nmm}. \quad (4.14)$$

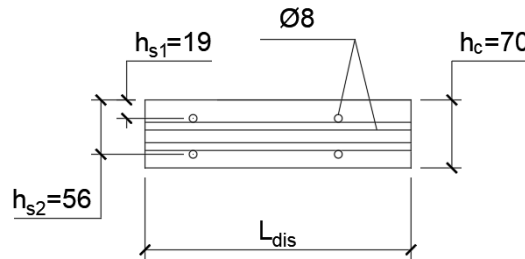


Figure 4.11 Top deck cross-section

The distributive length L_{dis} initially equals 200mm. The value of 200mm is chosen because this is the minimum width on which the concentrated load should be applied according to Eurocode 1 [6]. This parameter shows how the top deck distributes the applied load in the transversal direction and, thus, what part of it needs to be taken into account to calculate the bending stiffness of the top deck, see Figure 4.12.

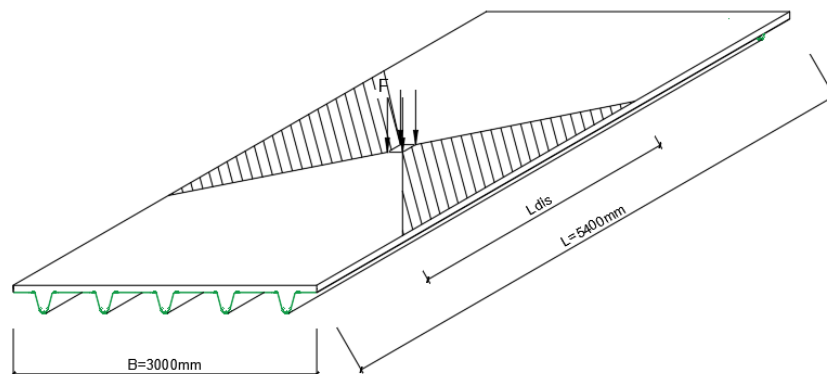


Figure 4.12 Illustration of the distributive length L_{dis} of the composite slab

The bending stiffness of the top deck when concrete is not cracked can be easily computed because the influence of reinforcement meshes is not present yet. Thus, the resulting value is the same for the top deck with no reinforcement mesh, one mesh or two meshes. The bending stiffness of the top deck with uncracked concrete is calculated according to Eq. (4.15).

$$EI_{deck} = E_{cm}I_{deck} = E_{cm} \frac{1}{12} L_{dis} h_c^3 = 30000 \cdot \frac{1}{12} \cdot 200 \cdot 70^3 = 1.71 * 10^{11} mm^4. \quad (4.15)$$

The properties, which are utilized to calculate cracking moment and bending stiffness of the top deck (with cracked and uncracked concrete), are shown in Table 4.8.

Table 4.8 Properties used in bending stiffness calculation of top deck

Property		Value	Unit
Young's Modulus concrete	E_{cm}	30000	N/mm^2
Young's Modulus cracked concrete	E_c	10000	N/mm^2
Young's Modulus reinforcement	E_s	200000	N/mm^2
Compressive strength concrete	f_{cm}	28	N/mm^2
Tensile strength concrete	f_{ctm}	2.2	N/mm^2
Yield stress reinforcement	f_y	540	N/mm^2
Distributive length	L_{dis}	200	mm
Area of steel wire Ø8	A_{s1}	50.3	mm^2
Height to the top mesh Ø8 from the top surface	h_{s1}	19	mm
Height to the bottom mesh Ø8 from the top surface	h_{s2}	56	mm
The total height of the top deck	h_c	70	mm

4.3.2.2 Bending stiffness of the cracked section

Bending stiffness of cracked top deck is influenced by the presence and quantity of reinforcement meshes in cross-section and type of bending moment acting on the top deck, i.e. positive or negative bending moment. When positive bending moment acts on the top deck with one reinforcement mesh, the compressive zone of concrete becomes smaller than in a case with the negative bending moment; this is due to the position of one reinforcement mesh in the cross-section which is only 19mm away from the top surface, see Figure 4.13.

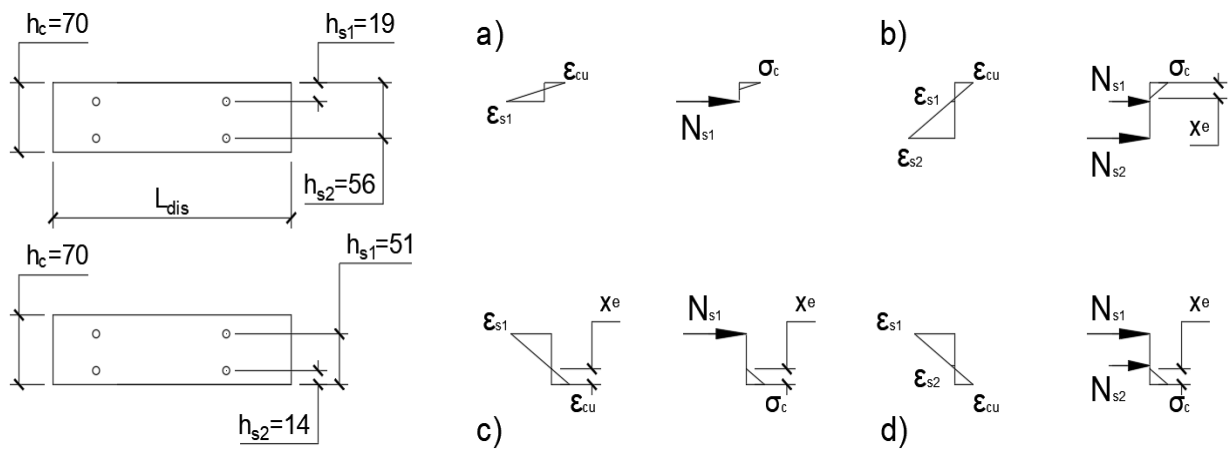


Figure 4.13 Stress and strain diagrams of the top deck: a) top deck with one reinforcement mesh under positive bending moment; b) top deck with two reinforcement meshes under positive bending moment; c) top deck with one reinforcement mesh under negative bending moment; d) top deck with two reinforcement meshes under negative bending moment.

Determination of bending stiffness of top deck is given in Appendix B. The resulting values of bending stiffness of top deck with different amount reinforcement meshes are displayed in Table 4.9.

Table 4.9 Bending stiffnesses of top deck (per 200mm length)

Section type	Value for positive bending moment, E+10	Value for negative bending moment, E+10	Unit
Cracked section and no mesh	8.12	8.11	Nmm^2
Cracked section and one mesh	8.28	8.81	
Cracked section and two meshes	9.28	9.18	

4.4 Influence of different parameters in the engineering model

4.4.1 Spring stiffness

Spring stiffness k_{rib} plays a prominent role in defining the final deflection form in the engineering model. The spring stiffness is defined as force deflection ratio of the rib. The stiffness of the rib can be changed due to variation in rib geometry or material, i.e. concrete grade or type of reinforcement.

One can predict that when this parameter increases, while other parameters are kept unchanged, the deflections become smaller. And when the stiffness of the spring decreases, the whole model becomes less stiff and, thus, the deflections are increasing. Four cases are examined of which two are associated with small changes in rib stiffness and two cases display what might happen with a slab when the variation in rib stiffness is high:

- Increasing spring stiffness in 5 and 1.25 times to its default value;
- Decreasing spring stiffness in 5 and 0.75 times to its default value.

The default case: composite slab with 1 reinforcement mesh and concentrated load in the center rib 60kN. Of course, different layout of reinforcement meshes in top deck might affect the deflection shape, but the effect is small and, therefore, can be considered insignificant; $k_{rib,def.} = 2250N/mm$. The deflection of the slab in the default case is shown in Figure 4.14.

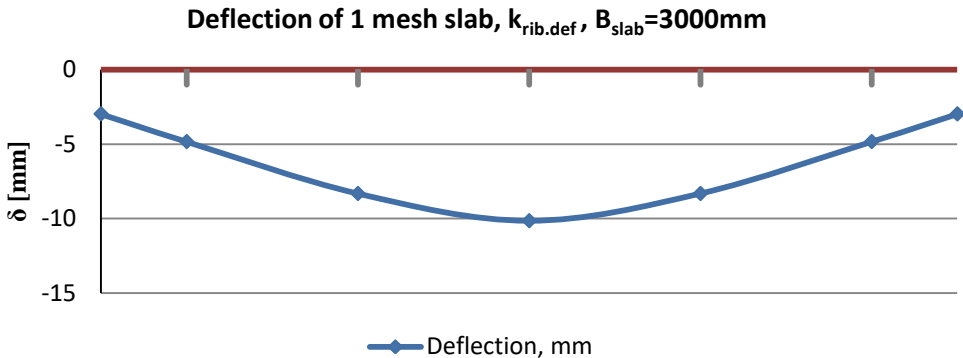


Figure 4.14 Deflection of one mesh slab in the default case

The comparison is made in Table 4.10 for a slab with $k_{rib,500\%} = 11250N/mm$, $k_{rib,20\%} = 420N/mm$, $k_{rib,75\%} = 1687.5N/mm$, $k_{rib,125\%} = 2812.5N/mm$ and $k_{rib,def} = 2250N/mm$.

Table 4.10 Deflection per rib with changed rib stiffness values

Rib number	Deflections, mm				
	$k_{rib,def}$	$k_{rib,500\%}$	$k_{rib,20\%}$	$k_{rib,125\%}$	$k_{rib,75\%}$
1	4.83	0.12	42.54	3.33	7.55
2	8.32	1.3	48.0	6.45	11.49
3	10.15	2.03	50.79	8.12	13.54
4	8.32	1.3	48.0	6.45	11.49
5	4.83	0.12	42.54	3.33	7.55

Figure 4.15 and Figure 4.16 display the resulting deflection forms in two cases: increased and decreased spring stiffness in 5 times. Figure 4.17 presents a comparison between the deflection of one mesh slab in default case and deflection of the composite slab with a small change in rib stiffness, namely, 125% and 75%.

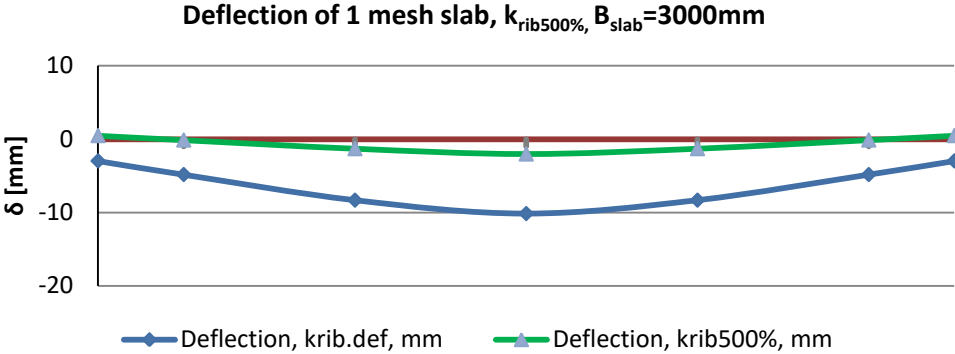


Figure 4.15 Deflection of one mesh slab with 500% rib stiffness

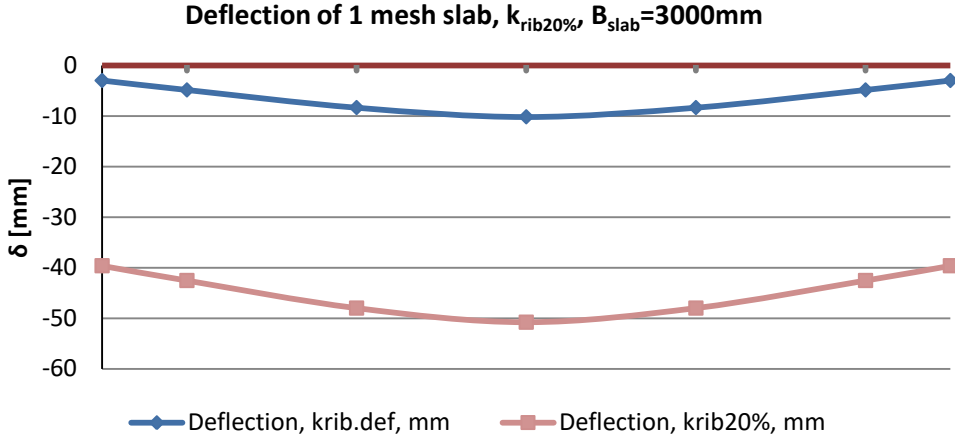


Figure 4.16 Deflection of one mesh slab with 20% rib stiffness

In a case when rib stiffness equals 20% of the default value, the deflection of each rib is drastically increased. The top deck, then, behaves more likely as the continuous stiff beam and distributes the load more evenly. When rib stiffness is increased 5 times to its default value, the load spreading is minimized and the load is mostly concentrated at the middle three ribs; the deflections obtain small values due to very stiff ribs.

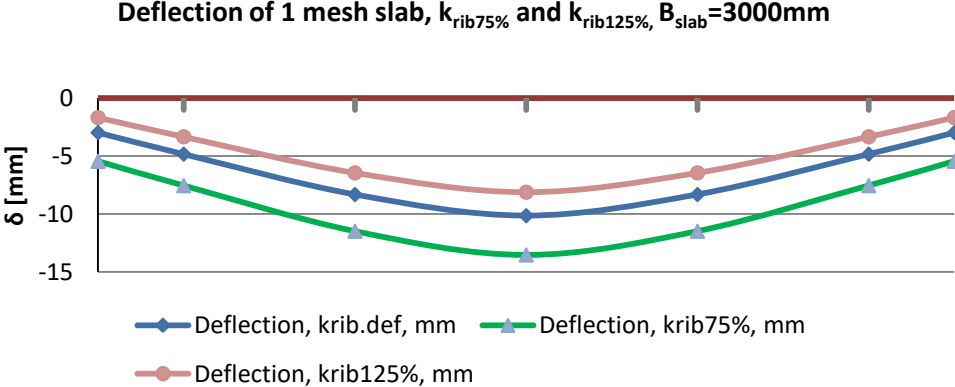


Figure 4.17 Deflection of one mesh slab with 75% and 125% rib stiffness

In a case when rib stiffness is changed to a small degree relatively its default value, i. e. 75% and 125%, the deflection of the composite slab is also changed but this change remains minor. The deflection curves resemble the same shape as in a case when rib stiffness equals 100%; although, the relative change is more prominent in a slab with 75% rib stiffness.

4.4.2 Top deck positive bending stiffness

The influence of the bending stiffness of the top deck is analyzed in this subchapter. The bending stiffness of the top deck might vary due to geometry and material modification. For example, with increasing thickness of the top deck, the bending stiffness increases as well. The position and quantity of reinforcement in the top deck also influence the bending stiffness.

Four cases are examined:

- Increasing positive bending stiffness of top deck in 5 and 1.25 times to its default value;
- Decreasing positive bending stiffness of top deck in 5 and 0.75 times to its default value.

The default case is a slab with one reinforcement mesh under 60kN concentrated load. The comparison of results is presented in Table 4.11 for a slab with $EI_{pos,cr} = 8.2871 \cdot 10^{10} Nmm^2$, $EI_{pos,cr,500\%} = 4.143 \cdot 10^{11} Nmm^2$, $EI_{pos,cr,20\%} = 1.6574 \cdot 10^{10} Nmm^2$, $EI_{pos,cr,125\%} = 1.035 \cdot 10^{11} Nmm^2$ and $EI_{pos,cr,75\%} = 6.215 \cdot 10^{10} Nmm^2$ (values per 200mm).

Table 4.11 Deflection per rib with a changed positive bending stiffness of the top deck

Rib number	Deflections, mm				
	$EI_{pos,cr}$	$EI_{pos,cr,500\%}$	$EI_{pos,cr,20\%}$	$EI_{pos,cr,125\%}$	$EI_{pos,cr,75\%}$
1	4.83	7.78	1.68	5.3	4.21
2	8.32	9.51	6.69	8.52	8.03
3	10.15	10.14	10.16	10.16	10.16
4	8.32	9.51	6.69	8.52	8.03
5	4.83	7.78	1.68	5.3	4.21

Figure 4.18 and Figure 4.19 display the resulting deflection forms from two cases: increased and decreased positive bending stiffness of top deck in 5 times.

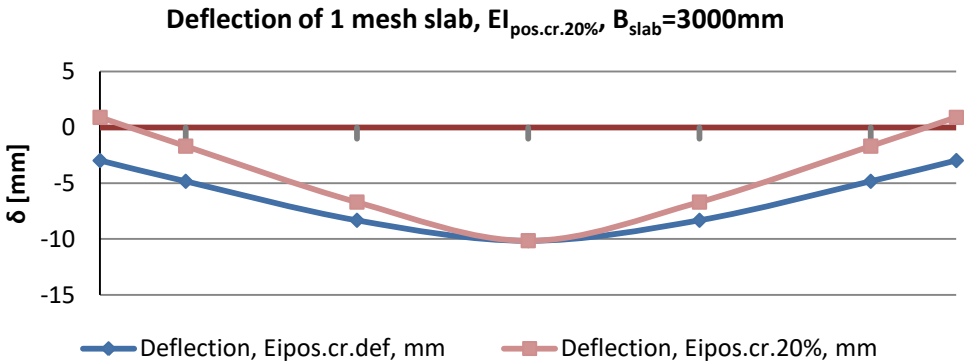


Figure 4.18 Deflection of one mesh slab with 20% positive bending stiffness of the top deck

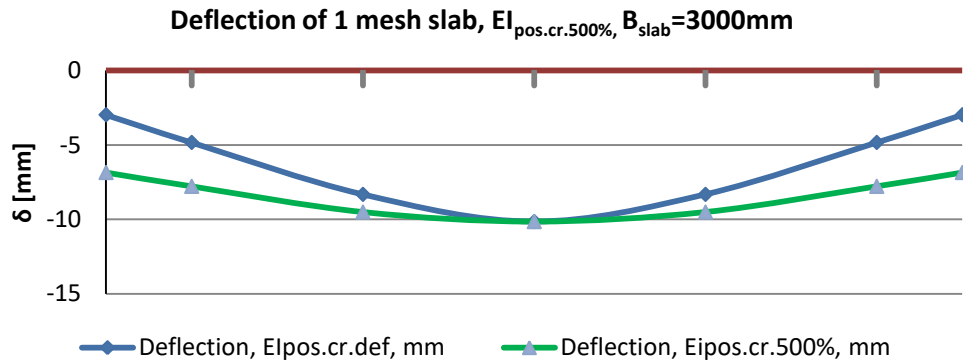


Figure 4.19 Deflection of one mesh slab with 500% positive bending stiffness of the top deck

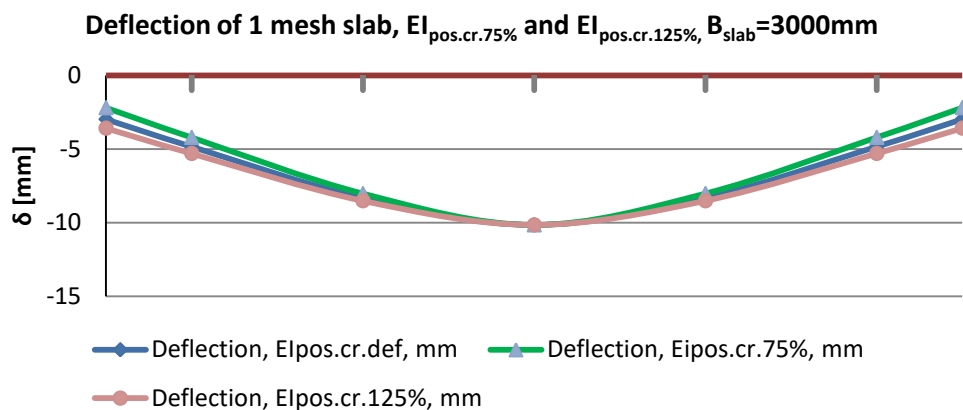


Figure 4.20 Deflection of one mesh slab with 75% and 125% positive bending stiffness of the top deck

From figures above it can be observed that a change in positive bending stiffness of top deck has a minor impact on a maximal deflection of the central rib on which the load is applied. In all cases, most of the load is carried by the center rib. However, with bending stiffness increased by 5 times the load spreads more evenly among all five ribs.

It can be noticed that in figures above the deflection of the middle rib is about 10mm. The load is positioned precisely on rib 3, and the deflection of the point under the load is mainly determined by the bending stiffness of rib 3. The bending stiffness of this rib is kept unchanged, and only the top deck stiffness is varied (increased 125% or decreased by 75%). The change in the top deck stiffness influences the deflections of other ribs in the model, but it does not influence the deflection of loaded rib due to the unchanged stiffness of the middle rib. Therefore, the deflection of this rib is about 10mm in all cases.

4.4.3 Length of the top deck between ribs

The length of the top deck between ribs is the next parameter to analyze. This parameter follows from the global dimension of the composite slab, namely, the spacing of the ribs. When the spacing between of the ribs decreases drastically, the deflection shape of the slab should be found using another approach: theory of continuous beam on elastic foundation. Therefore, it is decided to decrease the length between ribs slightly in order to use the existing differential equations.

Two cases are examined:

- Increasing the top deck length in 5 times to its default value;
- Decreasing the length of the top deck in 2 times to its default value.

The default case is a slab with one reinforcement mesh under 60kN concentrated load and internal top deck length 425mm. The comparison of results is presented in Table 4.12 for a slab with $L_{deck.def.} = 425mm$, $L_{deck,500\%} = 2125mm$ and $L_{deck,50\%} = 212.5mm$.

Table 4.12 Deflection per rib with the changed internal length of the top deck

Rib number	Deflections, mm		
	$L_{deck.def.}$	$L_{deck,500\%}$	$L_{deck,50\%}$
1	4.83	-0.5	9.07
2	8.32	1.97	9.79
3	10.15	10.15	10.15
4	8.32	1.97	9.79
5	4.83	-0.5	9.07

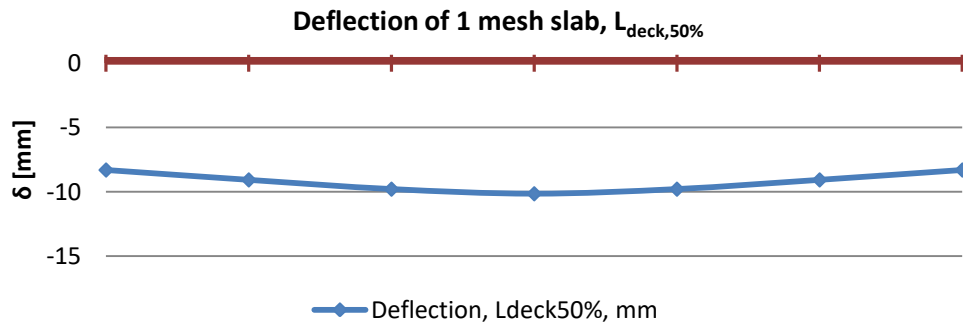


Figure 4.21 Deflection of two mesh slab with the decreased internal length of the top deck

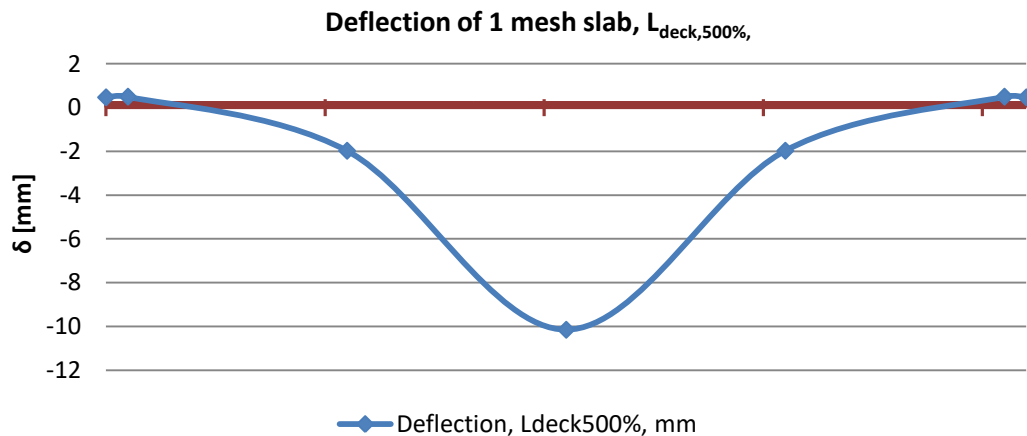


Figure 4.22 Deflection of two mesh slab with the increased internal length of the top deck

The change in deflection curve when the length of the top deck increased by 500% is quite noticeable. First of all, most of the load goes directly to the rib on which load is placed; the middle rib is, then, deflects excessively, while other ribs show a small response. Secondly, the change of curvature is observed for the top deck between two outer ribs, which means that upon

these parts negative bending moment is acting. This effect was not registered before when other parameters in engineering model were changed. In this way, the slab acts similarly to the multi-span beam.

When the length of the top deck between ribs is decreased slightly, the slab becomes shorter and, therefore, spreads the load more evenly.

4.5 Engineering model results and conclusion

The outcome of a comparison between the engineering model and the test is given in this subchapter. The results of the engineering model are computed in mathematical environment Maple, and the test results are obtained from laboratory experiment made by Dracht [3]. The deflections of ribs are computed with spring stiffness values derived from load-deflection diagram of each rib of finite element analysis. First, the results for a composite slab with the load applied at the center of the middle rib will be presented; and then the results for a composite slab with the load applied at the quarter of middle rib will be given.

4.5.1 Load at the middle of the span

In Table 4.13, Table 4.14 and Table 4.15 comparison between the engineering model results with a width of the rib $b_{rib}=600\text{mm}$ and test results are made for a composite slab with two, one and no reinforcement mesh in the top deck and concentrated load at the span middle. Additionally, the deflection and bending moment diagrams resulting from engineering model with different rib width $b_{rib}=600\text{mm}$ and $b_{rib}=175\text{mm}$ are presented in Appendix D.

Table 4.13 Comparison between engineering model results ($b_{rib}=600\text{mm}$) and test for a slab with two reinforcement meshes

2 mesh		Deflection, mm			Ldis, mm	Loading scheme
Load at $L_{span}/2$	Rib	Engineer.	Test	Ratio		
10 kN	1	1.21	0.5	2.42	5400	
	2	1.65	0.5	3.3		
	3	1.88	0.5	3.76		
	4	1.65	0.5	3.3		
	5	1.21	0.5	2.42		
60 kN	1	4.96	4.3	1.15	4000	
	2	8.26	4.8	1.72		
	3	9.98	5.6	1.78		
	4	8.26	4.8	1.72		
	5	4.96	4.3	1.15		

Table 4.14 Comparison between engineering model results ($b_{rib}=600\text{mm}$) and test for a slab with one reinforcement mesh

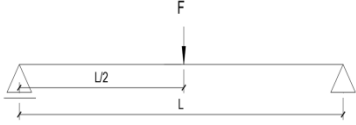

<i>1 mesh</i>		<i>Deflection, mm</i>			<i>Ldis, mm</i>	<i>Loading scheme</i>
<i>Load at $L_{span}/2$</i>	<i>Rib</i>	<i>Engineer.</i>	<i>Test</i>	<i>Ratio</i>		
10 kN	1	1.18	0.32	3.69	5400	
	2	1.64	0.36	4.56		
	3	1.89	0.52	3.63		
	4	1.64	0.36	4.56		
	5	1.18	0.32	3.69		
60 kN	1	4.83	4.5	1.07	4000	
	2	8.32	5.5	1.51		
	3	10.15	6.5	1.56		
	4	8.32	5.5	1.51		
	5	4.83	4.5	1.07		

Table 4.15 Comparison between engineering model results ($b_{rib}=600\text{mm}$) and test for a slab with no reinforcement mesh

<i>no mesh</i>		<i>Deflection, mm</i>			<i>Ldis, mm</i>	<i>Loading scheme</i>
<i>Load at $L_{span}/2$</i>	<i>Rib</i>	<i>Engineer.</i>	<i>Test</i>	<i>Ratio</i>		
10 kN	1	1.64	0.33	4.97	5400	
	2	2.2	0.34	6.47		
	3	2.49	0.51	4.88		
	4	2.2	0.34	6.47		
	5	1.64	0.33	4.97		
60 kN	1	3.34	5	0.67	4000	
	2	6.53	5.8	1.13		
	3	8.22	6.5	1.26		
	4	6.53	5.8	1.13		
	5	3.34	5	0.67		

4.5.2 Load at the quarter of the span

In Table 4.16, Table 4.17 and Table 4.18 comparison between the engineering model results and test results are made for a composite slab with two, one and no reinforcement mesh in top deck and concentrated load at the quarter of the span.

Table 4.16 Comparison between engineering model results ($b_{rib}=600\text{mm}$) and test for a slab with two reinforcement meshes

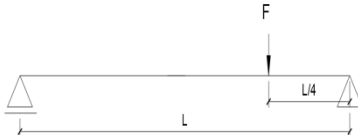
2 mesh		Deflection, mm			Ldis, mm	Loading scheme
Load at $L_{span}/4$	Rib	Engineer.	Test	Ratio		
10 kN	1	0.65	0.18	3.61	2500	
	2	1.03	0.25	4.12		
	3	1.23	0.45	2.73		
	4	1.03	0.25	4.12		
	5	0.65	0.18	3.61		
50 kN	1	-0.08	1.3	0.06	1500	
	2	0.79	1.75	0.45		
	3	1.49	2.25	0.66		
	4	0.79	1.75	0.45		
	5	-0.08	1.3	0.06		

Table 4.17 Comparison between engineering model results ($b_{rib}=600\text{mm}$) and test for a slab with one reinforcement mesh

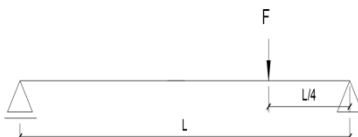

1 mesh		Deflection, mm			Ldis, mm	Loading scheme
Load at $L_{span}/4$	Rib	Engineer.	Test	Ratio		
10 kN	1	0.86	0.2	4.30	2500	
	2	1.1	0.45	2.44		
	3	1.25	0.55	2.27		
	4	1.1	0.45	2.44		
	5	0.86	0.2	4.30		
50 kN	1	-0.10	1.6	0.06	1500	
	2	0.76	2.25	0.34		
	3	1.53	2.7	0.57		
	4	0.76	2.25	0.34		
	5	-0.10	1.6	0.06		

Table 4.18 Comparison between engineering model results ($b_{rib}=600\text{mm}$) and test for a slab with no reinforcement mesh

no mesh		Deflection, mm			Ldis, mm	Loading scheme
Load at $L_{span}/4$	Rib	Engineer.	Test	Ratio		
10 kN	1	0.87	0.22	3.95	2500	
	2	1.14	0.25	4.56		
	3	1.3	0.37	3.51		
	4	1.14	0.25	4.56		
	5	0.87	0.22	3.95		

4.5.3 Conclusion on the engineering model

Based on results comparison made in chapters 4.5.1 and 4.5.2 it can be stated that the engineering model with an implemented width of the rib $b_{rib}=600\text{mm}$ can predict the deflection of the composite slab under concentrated load with limited accuracy only if rib spring stiffness is determined from load-deflection diagram extracted from finite element analysis. The results of the engineering model with a width of the rib $b_{rib}=175\text{mm}$ differ even more from test results (see Appendix D). Therefore, only the results from the engineering model with a width of the rib $b_{rib}=600\text{mm}$ are discussed below.

In a range 10-40kN load, the results obtained with the engineering model are somewhat different from experimental ones. With increasing the load the difference in deflections of middle three ribs becomes smaller: the difference in results for a slab with no reinforcement mesh in the top deck becomes 26% at 60kN. However, the desired accuracy with the engineering model for a slab with two and one mesh in the top deck is yet not reached at 60kN: difference in center rib deflections are 78% and 56% respectively.

The behavior of two outer ribs for all load level is dissimilar to test outcomes. A possible explanation of this might be the fact that stiffness of outer ribs is not the same as the stiffness of middle ribs: unlike the middle rib, each external rib has an unsupported edge along its length which might result in less stiff behavior in the loaded state. Additionally, the bending stiffness of all five ribs might be higher at small loads than calculated value because the bending stiffness of a rib depends on how much concrete is cracked in a cross-section. The assumptions that modulus of elasticity of cracked concrete equals one-third of not cracked material can lead to an underestimation of rib bending stiffness at low load level. The stiffness of the cross-section with cracked concrete can be established in another way, for example, the mean stiffness can be used instead of one-third of not cracked concrete. The procedure to determine the mean stiffness of the cracked reinforced structure is described in a paper written by Li [13].

The implemented in the model linear dependence between rib bending stiffness and applied load that is described in §4.3.1 did not lead to accurate results as it was thought.

Another difficulty with the engineering model is a precise determination of distributive length. The distributive length is a varied parameter that depends on the load level and shows how load spreads over the slab length. When the load is small, the load is spreading almost all over the entire slab length; with increasing the load the distributive length decreases. This parameter has an influence on the bending stiffness of the top deck: the higher the distributive length, the higher the bending stiffness of the top deck. The determination of this parameter requires numerous iterations, which is a drawback of the current model. When no experimental data or literature reference exists for the composite slab, this iterative procedure turns into a tedious work.

Composite slab with two, one and no reinforcement mesh in top deck under 10kN load applied in the quarter of the span shows more or less the same behavior: all five ribs deflect and, thus, participate in spreading the load. Composite slab under 50kN behaves differently: the middle three ribs are affected the most with applied concentrated force; additionally, the uplift of free edges is observed when the load applied at the quarter of span. Whether the uplift of free slab edges reflects the reality is not known as no measurement had been done on this matter in laboratory testing.

Composite slab with two, one and no reinforcement mesh in top deck under 10kN load applied in the middle of the span behaves similarly in all cases: all five ribs deflect more or less evenly while spreading the load. Composite slabs under 60kN show that middle three ribs are most influenced by concentrated force; the deflection of the middle rib is increased a lot compared to a slab under 10kN load. The uplift of free edges does not occur here unlike in a case when the load was applied at the quarter of the span. Additionally, the resulting bending moment is positive in all cases; this is a contradiction to the proposed model of top deck that is assumed to be clamped between the ribs. The possible explanation can be that the top deck behaves in reality not as a clamped element between the ribs but more like a continuous beam supported by ribs. The comparison with experiment (see § 4.5.1) shows that the difference in rib deflection between engineering model and test results are reasonable but only for high load, i.e. 60kN.

Parametric study on engineering model showed that the rib stiffness is the most influential parameter on slab behavior. Therefore, if one is in need to change the structural performance of the composite slab, it is advisable to influence the rib stiffness at first. The rib stiffness can be influenced by changing the area of rib reinforcement and overall geometry of the rib.

5 FINITE ELEMENT MODEL

5.1 Introduction

The finite element model (FEM) of the composite slab ComFlor210 is conducted in the program Abaqus/CAE in order to simulate the behavior of the slab under concentrated force. The developed numerical model is based on test results made by M. Dracht [3] in TU Delft. The main purpose of the modeling is to set a reliable three-dimensional model of the composite slab that can be used later on to verify the engineering model and conduct a parametric study on composite slab ComFlor210 with varied geometry and load applications.

The chapter is given in the following order (Figure 5.1).

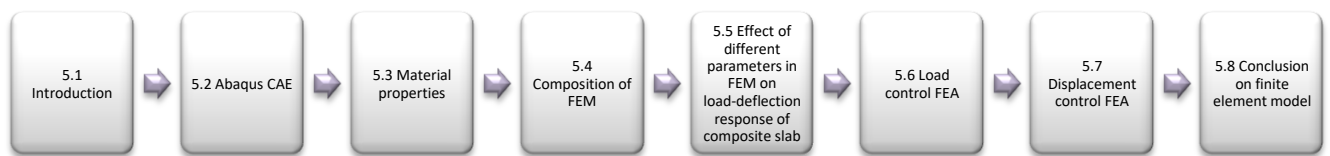


Figure 5.1 Chapter overview

5.2 Simulation environment of Abaqus/CAE

Abaqus/CAE serves as a comprehensive simulation environment for the modeling of different elements with complex geometry under various conditions. The parameters such as material properties, loads, boundary conditions and interactive properties can be individually assigned to the elements. The software includes two analysis products: Abaqus/Standard and Abaqus/Explicit. The former is applied for general analysis, likewise static, dynamic and thermal analyses of elements. The latter provides an exclusive analysis module based on explicit dynamic integration.

In this study finite element analysis is done with Abaqus/Explicit package in order to improve several performance features:

- avoiding convergence problem during analysis that often occurs in Abaqus/Standard (implicit) solver due to excessive distortion of finite elements and concrete degradation;
- Abaqus/Explicit is efficient in solving non-linear problems involving difficult contact formulation;
- Abaqus/Explicit requires less computational time to obtain a convergent solution for a three-dimensional object like a composite slab.

However, it is important to check whether the obtained results from Abaqus/Explicit solver truly represent the quasi-static solution. This can be done by monitoring the energy balance of the modeling object: the kinetic energy of the object should not exceed a small fraction (5-10%) of its internal energy throughout the whole quasi-static analysis, such that the inertia effect in the dynamic analysis is negligible.

5.3 Material properties

5.3.1 Concrete models

Abaqus/CAE has three different models to simulate concrete structural behavior:

- Smearred cracking model;
- Brittle cracking model;
- Concrete damaged plasticity model.

All three concrete models have their pro and cons in a direct application dependent on the structural and loading conditions necessary to simulate.

The smearred cracking model defines concrete behavior under monotonic loading with special attention to cracking representation. During the analysis, the post-cracking behavior of concrete dominates the modeling.

The brittle cracking model allows modeling concrete which behavior is dominated by tensile cracking. This model is applicable for concrete modeling not only of typical structural elements, e.g. trusses, beams, solids, shells but also of ceramics and brittle rocks.

The concrete damaged plasticity (CDP) model is considered to be the most advanced model of concrete in Abaqus. This model is based on two failure mechanisms of concrete: compressive crushing and tensile cracking; and model is applicable for different types of structures under monotonic, cyclic or dynamic loading.

A short comparison of concrete models used in Abaqus [14] is given in Table 5.1.

Table 5.1 Concrete models in Abaqus

Characteristic	Smearred cracking	Brittle cracking	Damaged plasticity
<i>Application</i>	reinforced and plain concrete	concrete, ceramics, brittle rocks	concrete and quasi-brittle materials
<i>Loading</i>	monotonic loadings under low confining pressures	monotonic loadings under low confining pressures	monotonic, cyclic, and/or dynamic loading under low confining pressures
<i>Elastic behavior</i>	linear elastic material	linear elastic material	isotropic and linear material
<i>Inelastic behavior</i>	oriented damaged elasticity concepts (smearred cracking)	cracking anisotropy and brittle failure criterion	isotropic damaged elasticity together with isotropic tensile and compressive plasticity
<i>Failure mechanism</i>	fails by cracking	tensile cracking	tensile cracking and compressive crushing
<i>Special features</i>	tension stiffening	elastic behavior in compression always	control of stiffness recovery effects during cyclic load; effect of the rate of straining;

As mentioned earlier the CDP model is the most comprehensive model among all three concrete models in Abaqus, therefore the concrete damaged plasticity (CDP) model is utilized in the analysis.

5.3.2 Concrete compressive and tensile behavior

In a case of uniaxial loading the tensile behavior of concrete is generally characterized by linear elastic zone until the failure stress is reached; after that point, the material endlessly experiences the softening which is clear can be observed on the strain-stress curve below (Figure 5.2).

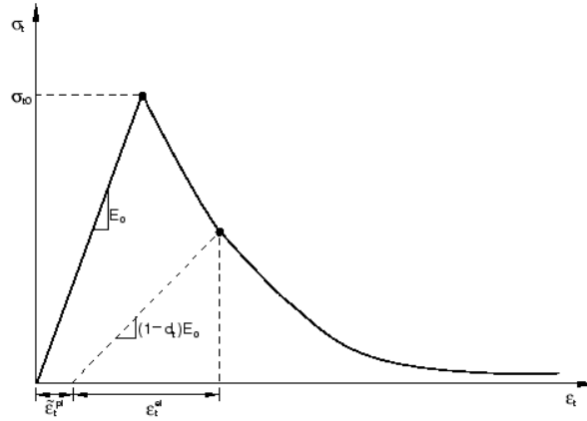


Figure 5.2 Tensile concrete behavior under uniaxial loading in Abaqus
(Dassault Systèmes Simulia Corp. 2012)

From the graph, it follows that the elastic stiffness of the concrete is damaged when the specimen is unloaded from any point in the strain softening region. The degradation effect of the elastic stiffness is taken into consideration by two parameters, d_c and d_t , which are depended on the plastic strains, temperature, and field variables. The damage variables can vary from zero, when no deterioration occurs, and to one, when total loss of strength happens [14]. Determination of damage parameters for concrete class C20/25 is given in Appendix C.

The compressive behavior of concrete under uniaxial loading is defined by linear elastic relation until the initial yield stress is reached, followed by stress hardening and later on by strain softening (Figure 5.3).

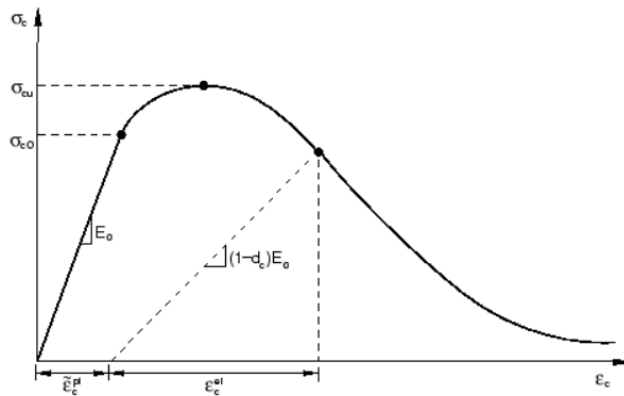


Figure 5.3 Compressive concrete behavior under uniaxial loading in Abaqus
(Dassault Systèmes Simulia Corp. 2012)

Numerically the stress-strain relations of concrete in tension and compression are defined by formulas 5.1 and 5.2.

$$\sigma_t = (1 - d_t)E_0(\varepsilon_t - \tilde{\varepsilon}_t^{pl}) \quad (5.1)$$

$$\sigma_c = (1 - d_c)E_0(\varepsilon_c - \tilde{\varepsilon}_c^{pl}) \quad (5.2)$$

where E_0 is undamaged elastic stiffness of material; $\tilde{\varepsilon}_c^{pl}$, $\tilde{\varepsilon}_t^{pl}$ are equivalent plastic strains.

The conversion of stress-strain curves into the stress versus plastic strain curves is done automatically by Abaqus using the initial strain data entered by the user.

Concrete class C20/25 is applied in the composite slab. The initial stress-strain response of concrete C20/25 in tension and compression is determined in accordance with Eurocode 2 [15].

The uniaxial compression and tension stress responses of concrete C20/25 with damaged

plasticity are given in Figure 5.4 and Figure 5.5. The detailed information regarding the concrete stress response in compression and tension and influence of degradation effect on it is provided in Appendix C.

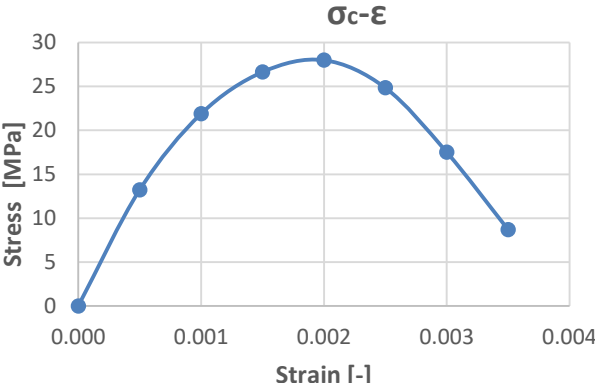


Figure 5.4 Uniaxial compression stress-strain response of concrete C20/25 with damaged plasticity

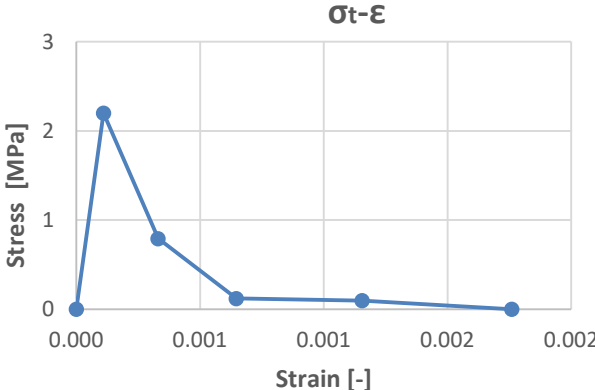


Figure 5.5 Uniaxial tension stress-strain response of concrete C20/25 with damaged plasticity

5.3.3 Concrete properties

The material characteristics of concrete C20/25 can be seen in Table 5.2.

Table 5.2 Concrete material properties

Property		Value	Unit
Young's Modulus	E_c	30000	N/mm^2
Compressive strength	f_{cm}	28	N/mm^2
Tensile strength	f_{ctm}	2.2	N/mm^2
Poisson's ratio	ν_c	0.15	–
Density	ρ_c	2.4E-9	N/mm^3

The characteristic of concrete as finite element applied in Abaqus is shown in Table 5.3.

Table 5.3 Finite element characteristics of concrete

Finite element property	Concrete C20/25
Modeling space	3D
Type	Deformable
Shape	Solid, homogenous
Element name	C3D8R, secondary accuracy
Geometry	Extrusion

5.3.4 Steel model

The finite element analysis of steel element in Abaqus/CAE [14] requires using true stresses and logarithmic strains. The true stresses and strains are related to the engineering stresses and strains by analytical equations (5.3) and (5.4). The engineering values of stress and strain can be obtained from the tensile test results.

$$\sigma_{true} = (1 + \varepsilon_{engineer})\sigma_{engineer} \quad (5.3)$$

$$\varepsilon_{true} = \ln(1 + \varepsilon_{engineer}) \quad (5.4)$$

These relations are valid until the ultimate tensile strength point, which distinguishes between work hardening region and necking region on the stress-strain curve. After this point the following equation (5.5) holds that defines logarithmic plastic strain as the difference between the total true strain and elastic strain.

$$\varepsilon_{true}^{pl} = \ln(1 + \varepsilon_{engineer}) - \frac{\sigma_{true}}{E} \quad (5.5)$$

The engineering values of stresses and strains for profiled steel sheeting ComFlor210 (S350) and reinforcement bars $\varnothing 8, \varnothing 20$ are obtained from the tensile test results made by M. Dracht [3]. The engineering stress-strain curve and the true stress-strain curve are shown in Figure 5.6, Figure 5.7, Figure 5.8.

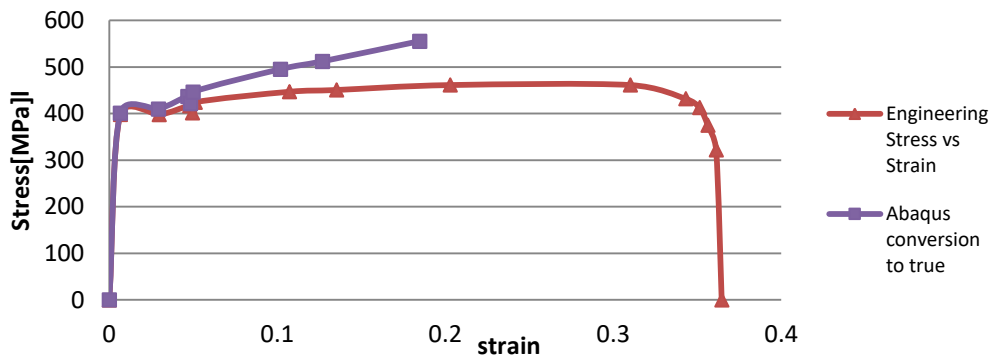


Figure 5.6 Engineering stress-strain and true stress-strain curves of profiled steel sheeting ComFlor210

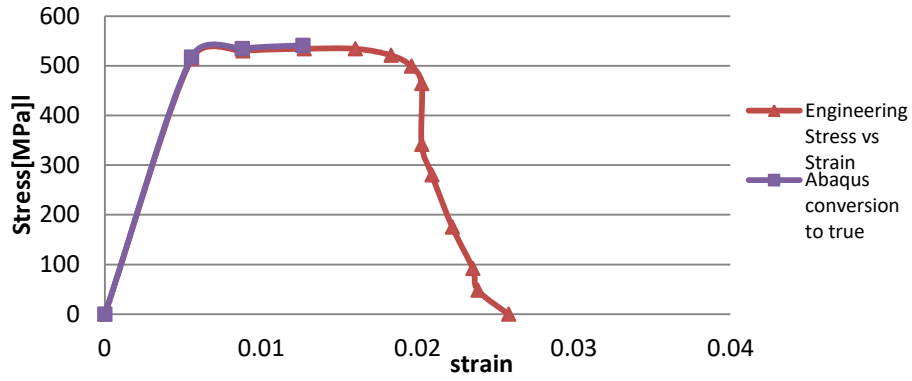


Figure 5.7 Engineering stress-strain and true stress-strain curves of steel rod 8mm

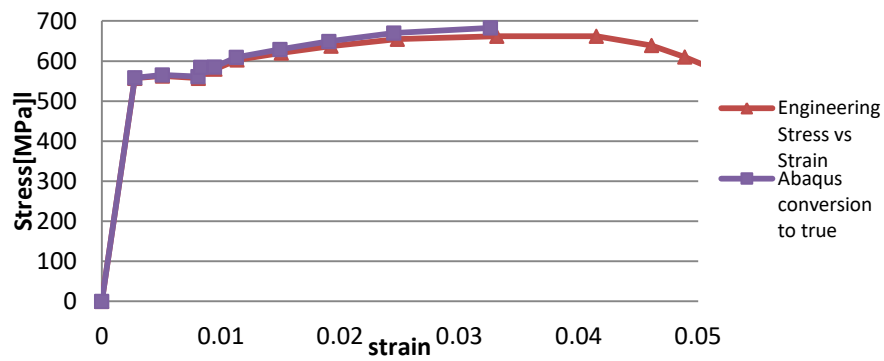


Figure 5.8 Engineering stress-strain and true stress-strain curves of steel rod 20mm

5.3.5 Steel properties

The material properties of steel deck and reinforcement are given in Table 5.4

Table 5.4 Steel material properties

Property		Value	Unit
Young's Modulus ComFlor210	E_{CF}	210000	N/mm^2
Yield stress ComFlor210	$f_{y,CF}$	400	N/mm^2
Steel Poisson's ratio	ν_s	0.3	–
Reinforcement Yield stress	f_y	540	N/mm^2
Reinforcement Young's Modulus	E_s	200000	N/mm^2
Density	ρ_s	7.8E-9	N/mm^3

The defined properties of steel as a finite element defined in Abaqus are given in Table 5.5.

Table 5.5 Finite element characteristics of steel components

Finite element property	Reinforcement $\varnothing 8, \varnothing 20$ mm	Sheeting ComFlor210
Modeling space	3D	
Type	Deformable	
Shape	Beam/Truss, homogenous	Shell, homogenous
Element name	T3D2	S4R, secondary accuracy
Geometry	Planar	Extrusion

5.4 The composition of the finite element model

5.4.1 Boundary conditions

It is essential to define boundary conditions properly in order to obtain a reliable finite element model of the composite slab. Therefore, the applied boundary conditions in a model were set in accordance with conducted laboratory tests in which the slab was simply supported. On the bottom of profiled steel sheeting, the two displacement degrees of freedom (DOF) U_1 and U_2 were restrained on the right, and on the left the DOF U_1 , U_2 and U_3 were restrained. The displacement degrees of freedom U_1 , U_2 and U_3 correspond to translation constraint in X, Y, and Z-direction respectively. Additionally, the supports were placed 100mm away from the slab edges. The boundary conditions are displayed in Figure 5.9.

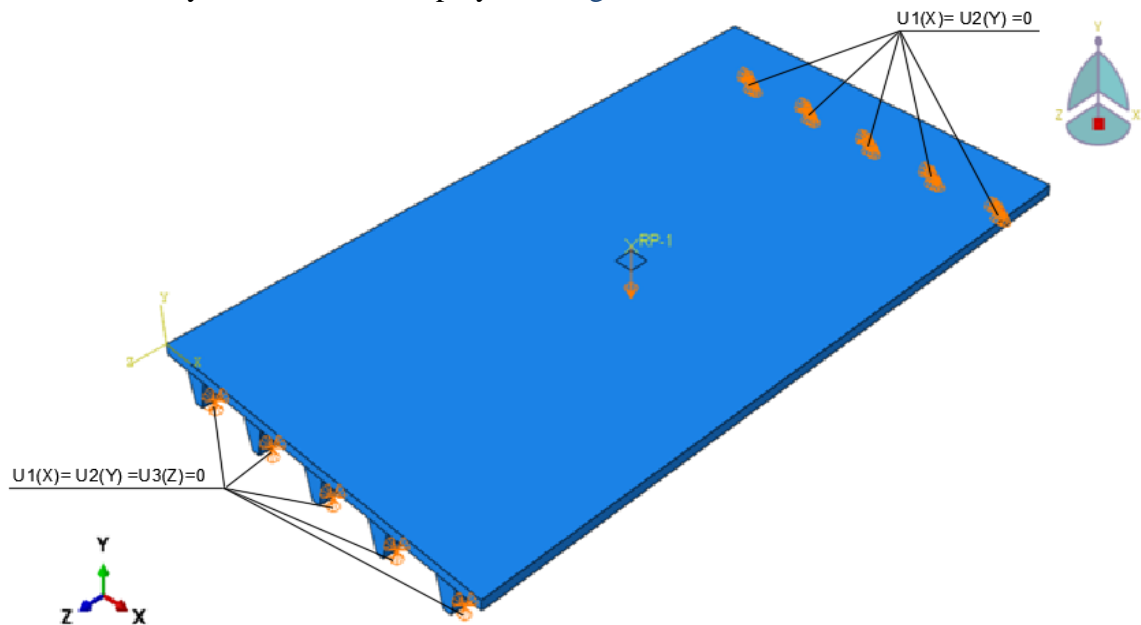


Figure 5.9 Boundary conditions and load application of composite slab in finite element model

5.4.2 Geometry, meshing, and finite elements

Geometry.

Four parts were created for the finite element model of the composite slab in “Part” module:

- Concrete C20/25 part;
- Reinforcement mesh (bar $\varnothing 8\text{mm}$ -150mm);
- Steel reinforcement in ribs (bar $\varnothing 20\text{mm}$);
- Steel sheeting ComFlor210.

The geometry of the composite slab (see Figure 5.10) corresponds to the specimen that was tested in the laboratory and had length 5400mm and width 3000mm. The thickness of the concrete top deck is 70mm; the whole thickness of the slab is 280mm. The steel bar $\varnothing 20$ is placed in the rib center at a height of 56mm from the bottom of the slab. The position of the top and bottom mesh wires starting from the top of the slab is at a height of 19mm, 27mm, and 48mm, 56mm respectively. Bar $\varnothing 8\text{mm}$ has a length of 5330mm in the longitudinal direction and 2930mm in the transversal direction. Steel rod $\varnothing 20\text{mm}$ has 5330mm length. The thickness of profiled steel sheeting is 1.25mm. The steel sheeting in the FEM has plain geometry, and no embossments are modeled. There is complete steel sheeting in the model.

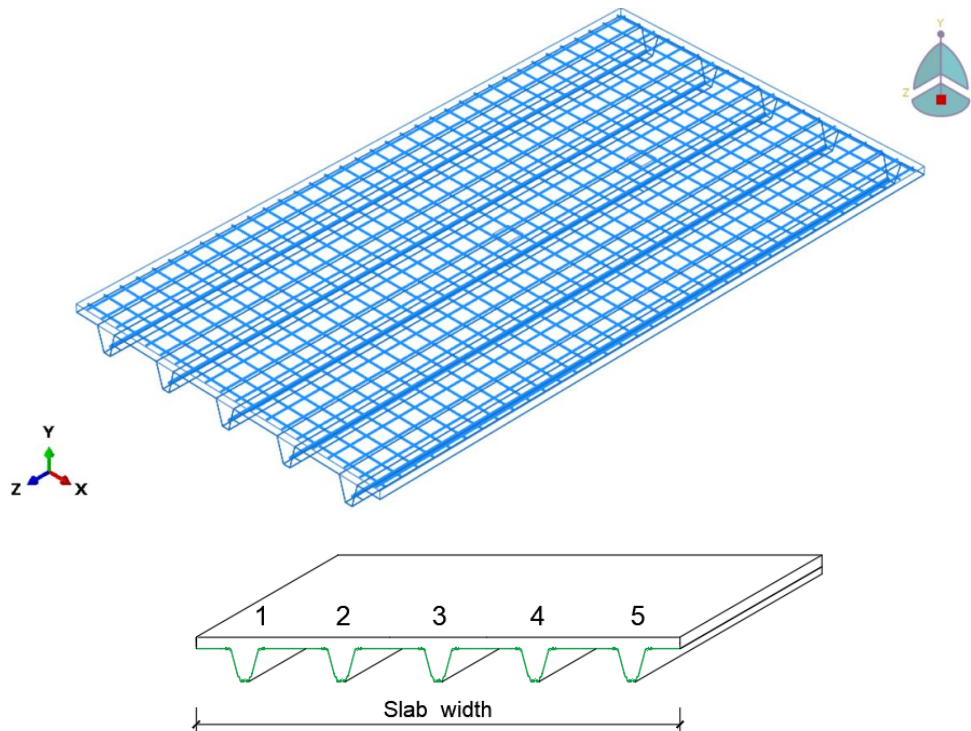


**Figure 5.10 Geometry of finite element model of composite slab (top figure);
Rib numbering (bottom figure)**

Meshing.

Different techniques were used to mesh parts of the composite slab. Steel elements, i. e. reinforcement mesh, steel bar in a rib and steel sheeting, were meshed using automatic native meshing tool within Abaqus. Automatic meshing is an easy and fast way to create a good quality mesh on elements with simple geometry. The complex ribbed geometry of concrete part did not allow for using this technique, therefore, another technique has been used to create a concrete mesh. Each rib and top deck were meshed individually by dividing the initial continuous concrete instance into independent regions of simple geometry. The mesh size for most elements was 50mmx50mm; however, the concrete top deck had two elements through its thickness resulting in 35mm height of the finite element. Mesh of profiled steel sheeting and concrete is shown in Figure 5.11 and Figure 5.12.



Figure 5.11 Concrete mesh

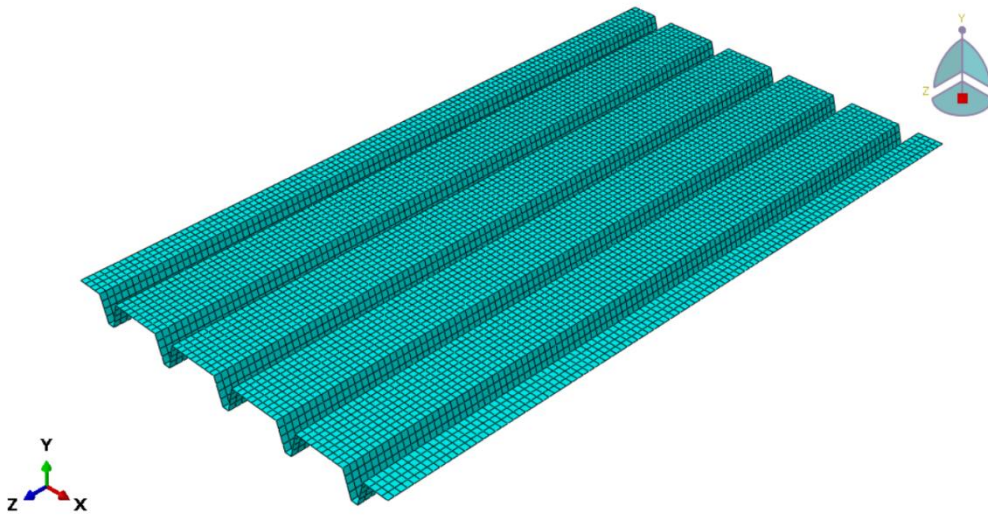


Figure 5.12 Steel sheeting mesh

Finite elements.

Concrete is assigned with 8-node linear brick, reduced integration with the hourglass control C3D8R element. The characteristic of this element is shown in Figure 5.13 [14].

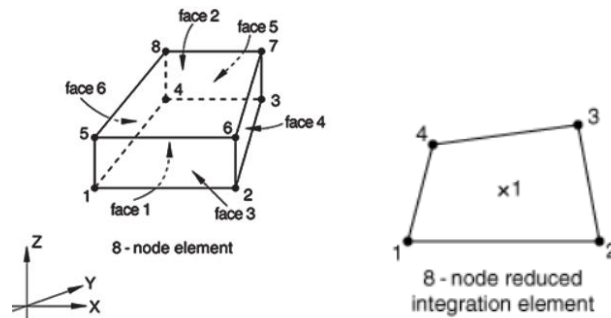


Figure 5.13 Solid element C3D8R: node ordering and face numbering (left figure), the numbering of integration points for output (right figure) in stress-displacement analysis

For steel sheeting, the 4-node general-purpose shell, reduced integration with hourglass control, finite membrane strains S4R is used. The configuration of this element is given in Figure 5.14 [14].

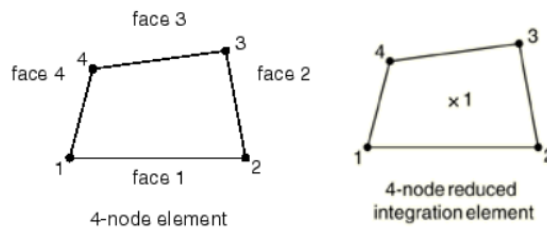


Figure 5.14 Shell element S4R: node ordering and face numbering (left figure), the numbering of integration points for output (right figure) in stress-displacement analysis

The steel reinforcement can be defined either met beam elements or truss elements. The main difference between these elements is that beam element, a one-dimensional line element in three-dimensional space, includes axial deformation, deformations from bending and from torsion. The truss element is a one-dimensional line element that has only axial stiffness. The integration of truss elements requires less computational time during analysis than that of beam elements. The descriptions of the 2-node linear B31 beam element and 2-node linear displacement T3D2 truss element are shown in Figure 5.15 and Figure 5.16 [14].

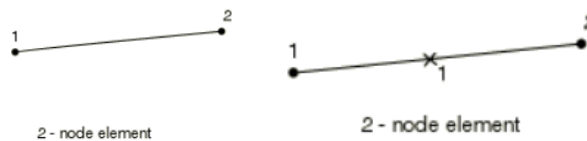


Figure 5.15 Beam element B31: node ordering (left figure), the numbering of integration points for output (right figure) in stress-displacement analysis

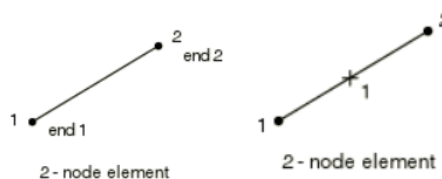


Figure 5.16 Truss element T3D2: node ordering (left figure), the numbering of integration points for output (right figure) in stress-displacement analysis

In the study, the reinforcement is assigned with truss element T3D2 in order to reduce computational time of analysis.

Both solid and shell elements are coupled with reduced integration, which is characterized by lower-order Gaussian integration in order to form the element stiffness. The reduced integration provides reasonably optimal accuracy and yet spares the computational time of analysis. “Hourglass control” is included in reduced-integration elements to limit the development of zero-energy modes that lead to inaccurate results during analysis. In this procedure, an artificial stiffness is allocated to the zero-energy deformation modes; and consequently, it allows obtaining reliable results for reduced integration elements with fine mesh size [14]. However, one needs to keep in mind that hourglass control produces additional artificial energy and with this the total internal energy of the model increases. High level of artificial energy can result in improper results of finite element analysis, therefore, it is important to check the level of this energy and keep it low in relation to internal energy.

5.4.3 Concrete-steel interaction

Steel bars and concrete.

The interaction between top reinforcement mesh $\varnothing 8\text{mm}$ -150 and concrete was assigned with an embedded region option, where the reinforcement mesh serves as an embedded region, and concrete serves as a host region. The same holds for reinforcement $\varnothing 20\text{mm}$: steel bar is defined as an embedded region, and concrete is defined as a host region.

Steel profiled sheeting and concrete.

The interaction between sheeting and concrete is far more complicated, a variety of possibilities to define such interaction exists within Abaqus. A good starting point for modeling this interaction is first to determine what forces act on the concrete-steel interface. When concrete and profiled steel sheeting are connected, the normal force is acting on contacting surfaces that allow transmission of forces between steel sheeting and concrete. The friction between concrete and steel sheeting gives rise to a shear force that prevents sliding between two parts. The important aspects of defining steel-concrete interaction are as follows:

- Allow force transmission between steel and concrete surfaces;
- Failure due to slipping under the external load is minimized.

In Abaqus, the friction behavior that prevents slip on two surfaces can be specified with “tangential behavior” for the contact surfaces in combination with “penalty behavior” [14] which allows small relative motion between surfaces. The friction coefficients can be established in accordance with experiments where the slip rate is measured. But for the simplicity of a finite element model, a uniform friction coefficient of 0.57 [16] is specified in the model. Additionally, “kinematic contact method” was selected to run the penalty contact algorithm, and “finite sliding” was activated in order to allow motion of two surfaces after the slip failure. Thus, both normal and tangential behavior has been specified in the interaction property module that is allocated to the surface-to-surface contact formulation between two surfaces. In surface-to-surface contact, the bottom part of the concrete slab was defined as “master” surface, and the top surface of steel sheeting was defined as “slave” surface. Additionally, the effect of different contact formulation has been studied in subchapter §5.5.3 with the main followed conclusion that surface-to-surface contact formulation in Abaqus is preferred over general contact formulation and that friction coefficient plays a prominent role in defining composite slab interaction behavior.

5.4.4 Primary verification of the model composition

Setting the finite element model requires careful estimation of its accuracy even when output is consistent with expectations of a user. In order to verify model composition several things can be controlled:

- The unit consistency of input parameters (dimensions, density, forces) and output results (reaction force, deflection, stresses).
- Gravity and resulting reaction forces when only gravity load is activated.
- Energy balance in the model during finite element analysis.
- Load arrangement the effect of which can be checked easily with simple calculations; for example, line load acting on slab transversely.

Unit consistency.

In this work the SI unit system is implemented, thus, the dimensions are inputted in millimeters, forces are given in Newton, and stresses are in Newton per unit area. The results are expected to match the dimension of input parameters, for example, if the input load is 145kN, then the resulting reaction forces must be of the same order.

Gravity and resulting reaction forces.

The gravity check was performed just after material properties and boundary conditions were defined in the model. The resulting reaction force distribution per each rib due to initial gravity force is shown in Figure 5.17. The comparison is made between reaction forces from the finite element model under only gravity load and initial reaction forces due to slab weight from experiments.

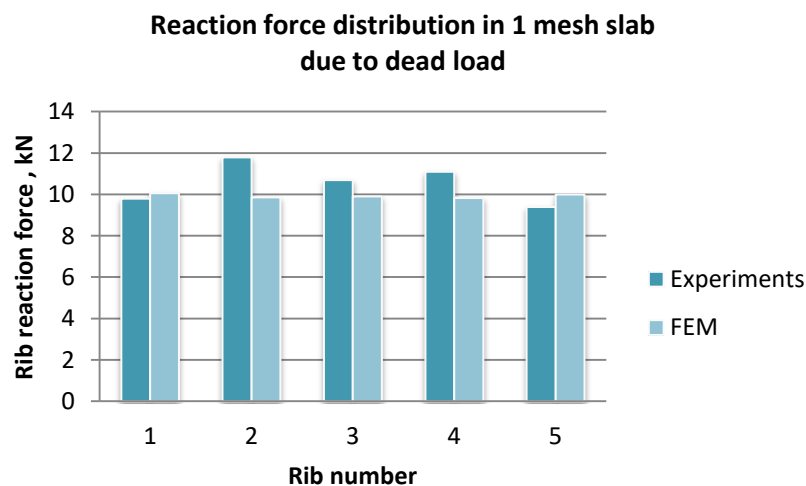


Figure 5.17 Reaction force distribution per rib in the composite slab with 1 reinforcement mesh due to dead load

It can be noticed that there is more variation present in reaction force distribution from testing than from the finite element model. The possible explanation for this is the measurement accuracy in testing and inhomogeneous concrete density in reality. The total dead loads from experiment, calculation and finite element model are compared in Table 5.6; the “hand” calculation value is obtained as the product of average dead load of composite slab 3.05kN/m² (*Dutch Engineering*) and total area of the slab 16.2m².

Table 5.6 Total gravity load in the experiment, the finite element model and hand calculation

Load type	Experiment	FEM	Calculated	Ratio (Exp/FEM)	Ratio (Calc./FEM)
Total gravity load, kN	52.8	49.65	49.41	1.06	0.99

It is confirmed that the geometry of the composite slab and material density were established correctly in the finite element model.

Energy balance.

The energy balance check is “sanity check” of the finite element model and intended to examine the model validity, i.e. whether obtained results from dynamic analysis really display the quasi-static solution. The first requirement is that the kinetic energy of the object must not exceed a small fraction (5-10%) of its internal energy throughout the entire quasi-static analysis [14]. Thus, the inertia forces in the analysis become insignificant. If this requirement is not fulfilled, the dynamic analysis cannot be used for the quasi-static problem at hand.

The second requirement that should be satisfied is that the total energy of the entire model is kept constant and approximately zero through the whole analysis. This condition ensures the energy neutrality of the system meaning that there is no supplementary energy generated during the analysis and just transformation of one form of energy to another occurs. When total energy of the model suddenly rises, the clear indication of “energy leakage” in the system is, then, in evidence. The user should carefully examine the model in order to find the cause of energy change; otherwise, the results from the model cannot be trusted.

The third requirement concerns the contact and constraints: the work of these two should be nearly zero because no work is done by connectivity or constraint process. If the work of constrains is large, the definition of connections in the model should be reviewed and changed.

The last condition in energy check is a limit of artificial strain energy that comes from reduced integration process. It is recommended to keep the ratio of artificial strain energy to actual strain energy below 5% [14]. Otherwise one needs to think about what is possibly causing the energy excess and how the ratio can be decreased to improve the results.

All requirements described in this subchapter were examined after every run of finite element analysis. The example of the resulting energy check for the default finite element model with 50mm mesh size is shown in Figure 5.18 and Figure 5.19.

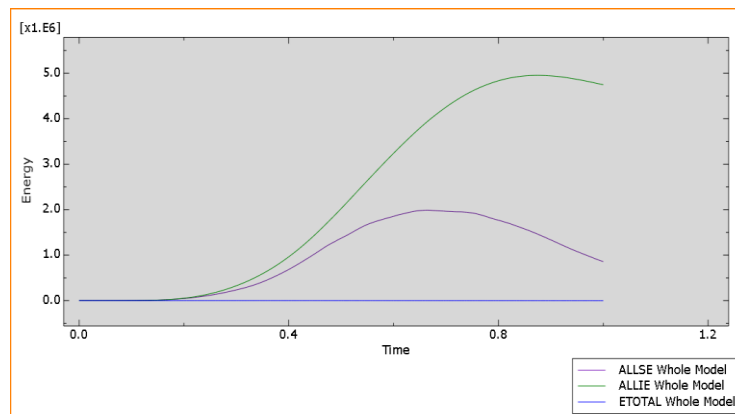


Figure 5.18 Development of total energy ETOTAL, strain energy ALLSE and internal energy ALLIE during finite element analysis in Abaqus

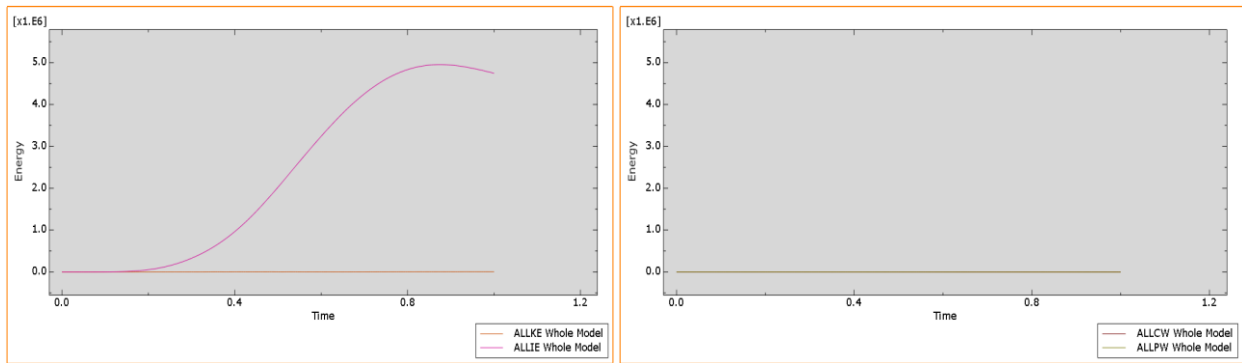


Figure 5.19 Energy development during FEA: kinetic energy ALLKE and internal energy ALLIE of the whole model (left figure); the energy of constraint and contact (right figure)

The evaluation of energy development during analysis leads to several conclusions regarding the finite element model configuration. First of all, the kinetic energy stayed very low relatively internal energy in all cases, as well as the energy of constraints stayed nearly zero in every run of the model. That proves that dynamic analysis represents the quasi-static problem and that no work is done by constraints implemented in the model. Secondly, in several cases, the total energy of the whole model was increasing at the end of the analysis, which is, as it was stated before, a sign of “energy leakage” in the model. This increase was accompanied by the growth of artificial strain energy that reached a level beyond the recommended limit. The development of artificial strain energy is bound to the controlling process of “hourglassing” deformation of finite elements with reduced integration. It is probable that a large number of finite elements with reduced integration might cause the excess of artificial strain energy and, later, the surplus in the total energy of the whole model. The possible remedy for this problem is to use finite elements with full integration or reduced integration elements with secondary accuracy. Both options will increase the computational cost of analysis, however, implementation of elements with secondary accuracy requires less time to complete the analysis when compared to full integration time-cost. Therefore, it is advised to employ in the finite element model reduced integration elements with secondary accuracy.

5.5 Effect of different parameters in finite element model on the load-deflection response of composite slab

The effect of different model parameters on finite element load control analysis results is presented in this subchapter. Several parameters are examined:

- Mesh sensitivity.
- Dilation angle.
- Contact definition.

5.5.1 Mesh sensitivity

In order to obtain reliable results from finite element analysis, it is important to establish a good mesh, i. e. mesh that generates results with satisfactory quality and a reasonable level of accuracy, assuming that input parameters for the model are correct. Mesh accuracy can be controlled by different ways; the straightforward option is to compare the finite element analysis results with experimental data or theoretical value. In a case when such data is not available, the quality of mesh can be controlled by examining mesh density and result discontinuities [17]. A comparison of experimental load-deflection result and load-deflection response of composite slab in displacement control analysis with mesh element size 100mm, 50mm and 25mm is presented in Figure 5.20.

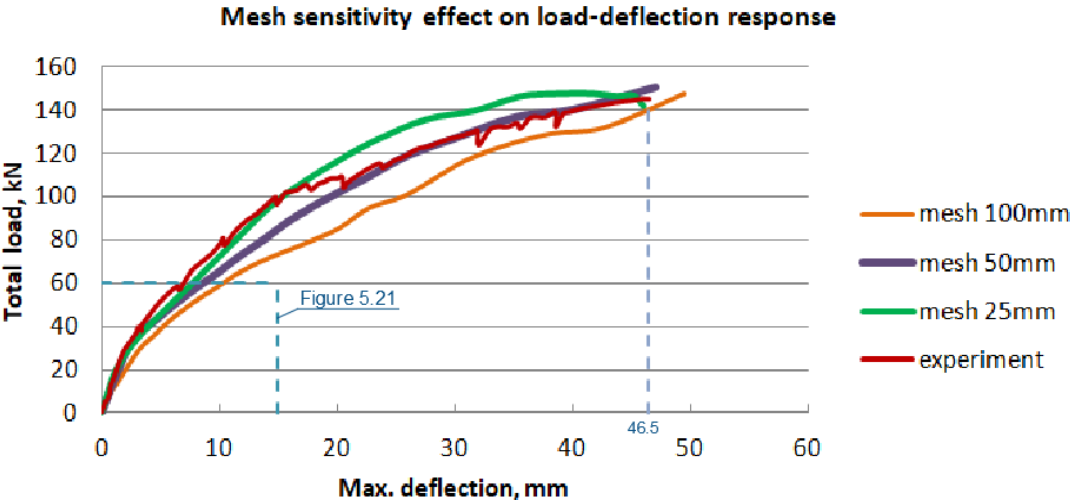


Figure 5.20 Load-deflection response of composite slab in the experiment and finite element load control analysis with mesh element size 100mm, 50mm, and 25mm

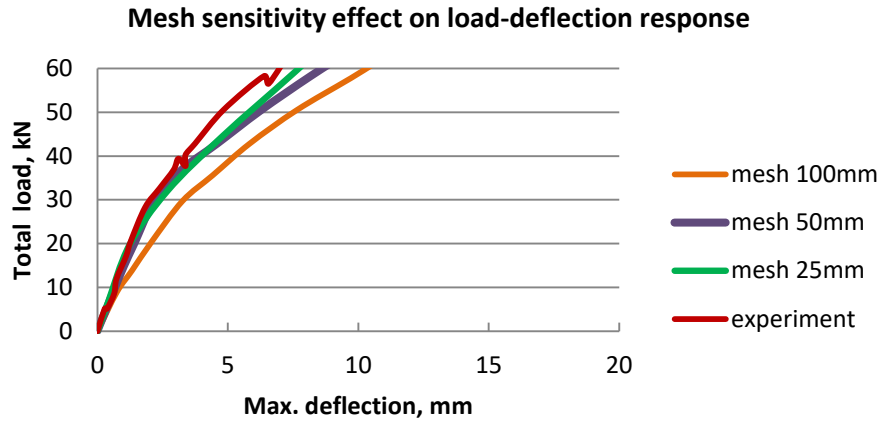


Figure 5.21 Load-deflection response of composite slab in a range 0-60kN in the experiment and finite element load control analysis with mesh element size 100mm, 50mm, and 25mm

Figure 5.20 makes it clear that load-deflection response from finite element model with different mesh size shows mesh dependency as the curves are diverging from each other. It can be noticed that the substantial divergence occurs between the load-deflection curve of finite element model with 100mm element size and other three curves. The difference between mesh 50mm and 25mm on interval 0-60kN is small, as shown in Figure 5.21. The finite element model with element size 25mm seems more accurate; however, running the parametric study with finite element model having fine mesh can be very time-consuming. Table 5.7 gives an overview of time cost required to perform finite element dynamic analysis in Abaqus for models with different finite element size.

Table 5.7 General characteristics of finite element models in mesh sensitivity study

Mesh size	Total number of elements	Total number of nodes	Amount of increments in FEA	Time to complete FEA (hour)
100mm	7446	9966	87547	0.25
50mm	36976	47012	217021	2.73
25mm	152532	187324	409055	9.16

With each mesh refinement, the amount of finite elements in the model increases approximately 5 times compared to the previous step, while time to finish the finite element analysis increases in circa 6 times. Running the analysis of model with 50mm element mesh size requires less than 3 hours, and analysis of model with 25mm element size demands more than 9 hours, which is rather laborious for parametric study with multiple models runs. Additionally, in practice, the concentrated force on composite slab ComFlor210 does not exceed 50kN, and up to this load the load-deflection responses of FEM with 50mm and 25mm mesh size are almost identical. Therefore, it is decided to conduct a parametric study with a model having 50mm element size.

Although the experimental results are available to make a comparison with finite element analysis results (see Figure 5.20), the other two options to verify mesh quality are also briefly discussed.

Another option to check mesh accuracy is an examination of stress discontinuities between adjacent elements in the crucial region. Commonly, the finite element method deducts stresses at interior locations of the element, i.e. Gauss integration points, and then extrapolates stresses to the nodes on the element boundaries, resulting in each element computing inequable stresses at

shared nodes. The level of stress discontinuity lessens with mesh refinement, thus, this property can be also used to evaluate mesh accuracy.

Mesh density is another alternative to monitor mesh precision; in general, a high-density mesh will yield results of high accuracy. An application of mesh density metric implies multiple mesh refinements until a critical result converges, for example, the maximum stress in a certain location does not change drastically with each mesh refinement. In Figure 5.22 the maximum Von Mises stress of steel reinforcement in the middle of the composite slab is plotted against mesh density (number of elements in the model over model volume).

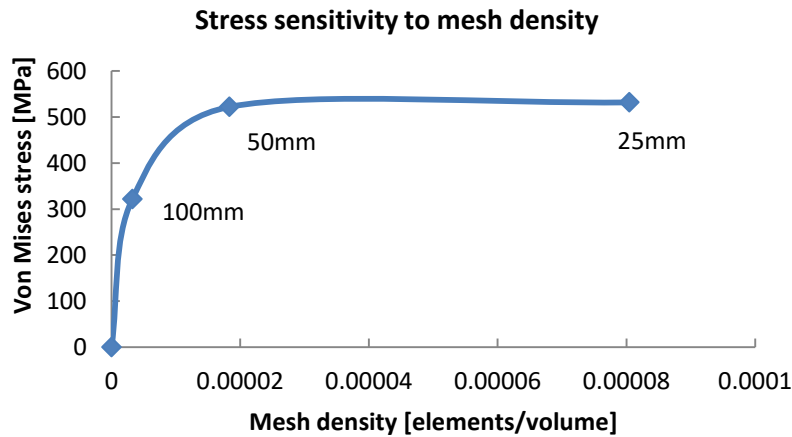


Figure 5.22 Von Mises stress sensitivity to mesh density in displacement control FEA

The curve in Figure 5.22 shows that the Von Mises stress of reinforcement grows as mesh density increases. Eventually, increasing the mesh density further induces small stress growth: an increase from 36976 elements per unit volume to 152532 elements per unit volume generates only a 1.8% increase in stress. This again proves the point that mesh composed of 50mm element size is efficient and advisable to use in order to obtain reliable results from finite element analysis.

Considering all that was mentioned above, it becomes clear that the finite element analysis performed with the dynamic explicit procedure in Abaqus is mesh dependent, meaning that the results of such analysis are influenced by the mesh size and mesh refinement in the critical location. Additionally, the mesh with element size 50mm produces results close to experimental ones, and, therefore, can be utilized in the further parametric study of composite slab.

5.5.2 Dilation angle effect

Dilation angle is input parameter in concrete damaged plasticity model that defines the three-dimensional surface of damaged concrete compression and tension behavior relatively to principal stresses axes. Dilation angle obtains values in a range 15-55 degrees [14]. In most cases, the large value of dilation angle results in stiffer concrete behavior in plastic stage. Dilation angle can be determined from concrete test data, however, the specific tests should be performed, and because the results of these tests are not available, it is crucial to conduct a parametric study on dilation angle variation in order to establish the plastic concrete behavior similar to laboratory test results. The load control finite element analysis of composite slab was executed with three different values of dilation angle: 20°, 30°, and 40°.

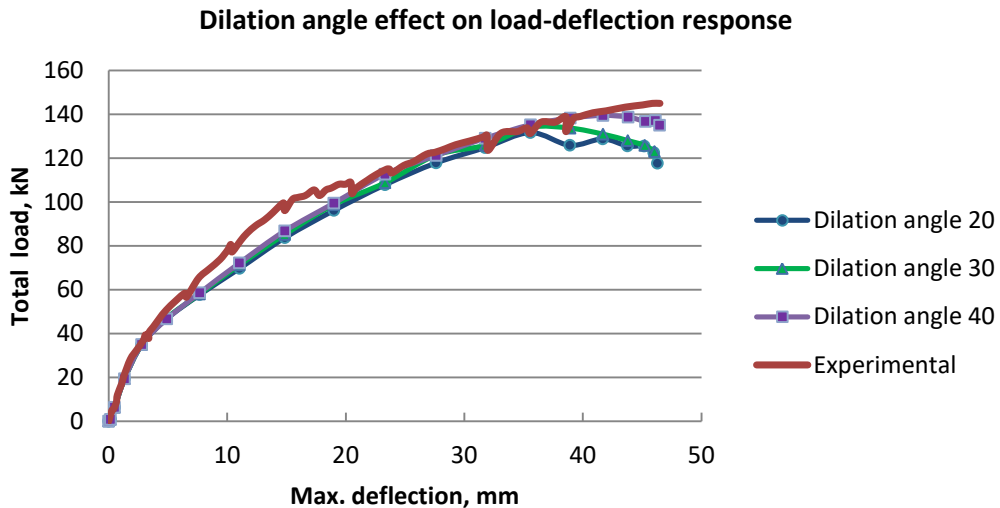


Figure 5.23 Dilation angle effect on the load-deflection response of composite slab in load control FEA

Figure 5.23 shows that, indeed, the variation in dilation angle caused the difference in load-deflection behavior of composite slab, and this effect is most pronounced in the inelastic part of the curves. As dilation angle increases, the eventual total load reached in finite element analysis increases as well. Additionally, the response of the composite slab becomes stiffer. Based on Figure 5.23 it was decided that implementation of 40° dilation angle in concrete damaged plasticity model produces results similar to experimental findings.

Table 5.8 Ultimate reaction forces reached in FEA of one mesh slab with different dilation angle and the experiment

Dilation angle	Maximum force, kN	Force ratio (FEA/Exp)
20°	117.72	0.81
30°	123.02	0.85
40°	135.06	0.93
Experiment	145	-

5.5.3 Influence of contact definition

Abaqus/Explicit provides two types of contact definition: general contact and contact pairs. General contact allows setting contact between all regions and bodies in the model with one single interaction; the contact pairs define contact between two specific surfaces with individual interaction [14]. In general contact just penalty method can be used for mechanical constraint, while contact pairs include penalty and kinematic methods as constraint type. Abaqus offers two possibilities to define the relative motion of the surfaces in contact, namely finite sliding, in which general arbitrary motion of two surfaces is allowed, and small sliding that enables little sliding of one surface along the other.

In Figure 5.24 a comparison is made between load-deflection responses of the composite slab in FEA with a different type of prescribed contact on a concrete-sheeting interface: general contact with penalty mechanical constraint, surface-to-surface contact with kinematic mechanical constraint with small sliding and finite sliding.

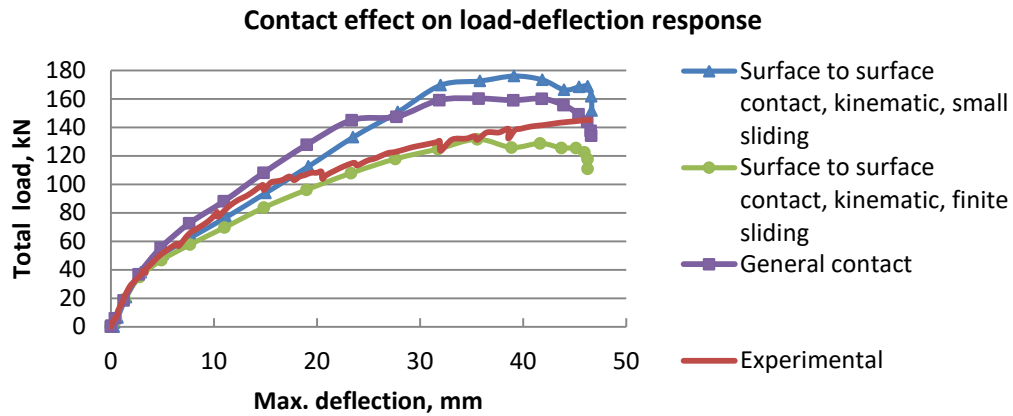


Figure 5.24 Contact effect on the load-deflection response of composite slab in load control FEA

There is not much difference in load-deflection response of composite slab with a different type of interaction up to 60kN, i.e. where the slab is in the elastic stage. Above 60kN the curves diverge from each other significantly. From Figure 5.24 it follows that surface-to-surface contact with kinematic mechanical constraint and finite sliding generates a load-deflection response of composite slab in a plastic stage close to the experimental results.

5.5.4 Conclusion regarding the influence of the finite element model parameters

The study on the influence of different parameters in finite element model on the load-deflection response of composite slab reveals that the plastic behavior of the slab is highly influenced by mesh size, chosen concrete properties and contact definition on the concrete-sheeting interface. The most accurate finite element results in comparison to experiments in the plastic stage are obtained with mesh size 25mm, dilation angle 40° and surface-to-surface contact interaction with finite sliding.

There is not much difference in load-deflection response of composite slab in the elastic stage when mentioned parameters in finite element model are changed besides the mesh size. The mesh size effects the elastic response of composite slab significantly: mesh size 100mm is coarse and is not recommended for finite element analysis, while 50mm and 25mm element size show the almost identical elastic response of composite slab.

5.6 Load control finite element analysis

5.6.1 Model description

In the load control analysis, the load (in a form of concentrated force, pressure, and stress) changes with increments while the displacement follows from the stiffness of the structure. The applied load is 145kN which is connected through the reference point, located 100mm above the slab center, to the load surface 150mmx150mm by coupling (see Figure 5.9). In order to compare the experimental and finite element results, the load of 145kN was chosen to be employed in finite element load control analysis, because 145kN is the maximum load reached during laboratory testing of the one-mesh slab.

The load-deflection response in experiments was determined at a half span. Thus, the load-deflection response in finite element model subjected to load control analysis is taken from the same location which is 2700mm away from slab edges.

The material properties are used as in §5.3. The loads and boundary conditions are described in §5.4.1. The input parameters for concrete damaged plasticity model are presented in Table 5.9, where ψ is the dilation angle, K_c is the ratio of the second stress invariant on the tensile meridian to that on the compressive meridian, σ_{b0}/σ_{c0} is the ratio of initial equibiaxial compressive yield stress to initial uniaxial compressive yield stress, and ϵ is an eccentricity parameter. The default values (values recommended by Abaqus user guide, [14]) are used for these parameters. Determination of damage parameters for concrete in tension and compression is explained in Appendix C.

Table 5.9 Concrete input parameters for damaged plasticity model

Damaged plasticity parameters			
ψ	K_c	σ_{b0}/σ_{c0}	ϵ
40	0.667	1.16	0.1
Concrete compression behavior		Concrete compression damage	
<i>Yield stress, MPa</i>	<i>Inelastic strain, mm/mm</i>	<i>Damage parameter</i>	<i>Inelastic strain, mm/mm</i>
13.21	0.0	0.0	0.0
21.89	0.00027	0.0	0.00027
26.64	0.000612	0.0	0.000612
28	0.001067	0.0	0.001067
26.37	0.001621	0.057861	0.001621
22.14	0.002262	0.209030	0.002262
15.60	0.0035	0.442641	0.0035
Concrete tensile behavior		Concrete tension damage	
<i>Yield stress, MPa</i>	<i>Cracking strain, mm/mm</i>	<i>Damage parameter</i>	<i>Cracking strain, mm/mm</i>
2.20	0.0	0.0	0.0
1.467	0.000281	0.333182	0.000281
0.825	0.000619	0.625000	0.000619
0.367	0.001143	0.833182	0.001143
0.0	0.001760	1.0	0.001760

The input parameters for steel reinforcement and steel sheeting are shown in Table 5.10.

Table 5.10 Steel input parameters for plasticity domain

Steel reinforcement Ø8mm		Steel reinforcement Ø20mm		Steel sheeting ComFlor210	
Yield stress, Mpa	Plastic strain, mm/mm	Yield stress, Mpa	Plastic strain, mm/mm	Yield stress, Mpa	Plastic strain, mm/mm
517.33	0	558.44	0	400.71	0
534.6	0.00878	565.5	0.005083708	409.54	0.02927
540.99	0.01266	561.41	0.008075623	436.61	0.04675
		584.7	0.0083054	421.39	0.04832
		585.37	0.009453493	445.94	0.04989
		609.67	0.011287691	494.91	0.10189
		629.38	0.014946082	511.75	0.12691
		649.52	0.019045719	555.02	0.18479
		670.72	0.02448603		
		683.9	0.032591331		

5.6.2 Load control analysis results

This subchapter divided into several parts in order to give an overview on analysis output, namely deformed shape and displacements, stresses and strains, and rib reaction forces.

5.6.2.1 Deformed shape and displacements

The deformation of the composite slab, subjected to a concentrated force in the middle, is characterized by the slightly concave shape of the top surface with a maximum deviation from the undeformed surface in a point under applied load. The maximum deformation occurs under loading surface, and then deformations are spreading over the slab to its edges as it can be seen in Figure 5.25.

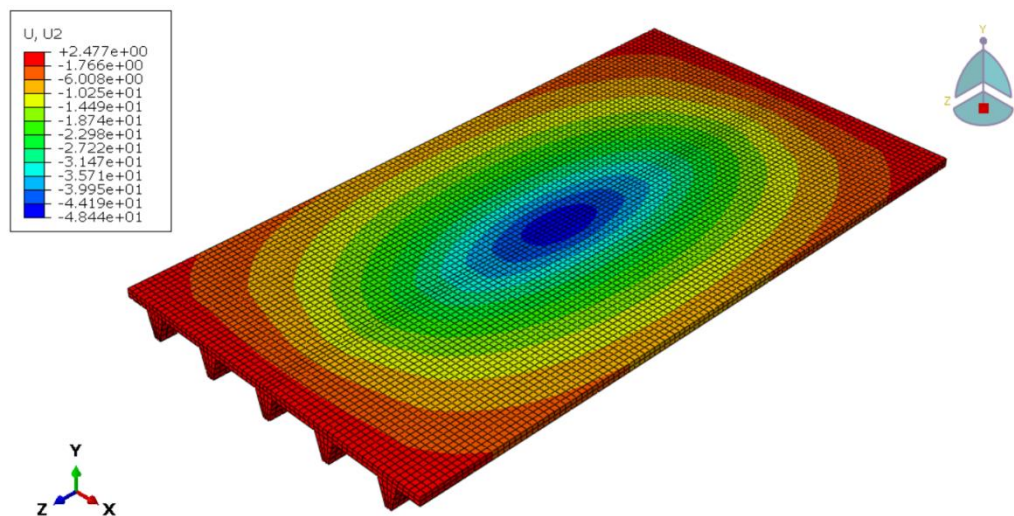


Figure 5.25 Displacement field U2 in one-mesh slab under concentrated force 145kN in load-control FEA

A comparison is made between load-control finite element analysis and experiment presented in Figure 5.26 and Figure 5.27 for total load vs. deflection response of middle rib (Rib 3), adjacent rib (Rib 2) and outer rib (Rib 1) of composite slab. Naturally, the response of other two ribs Rib 4 and Rib 5 will be similar to that of Rib 2 and Rib 1 due to the symmetry of slab geometry and load application (for rib numbering see Figure 5.10).

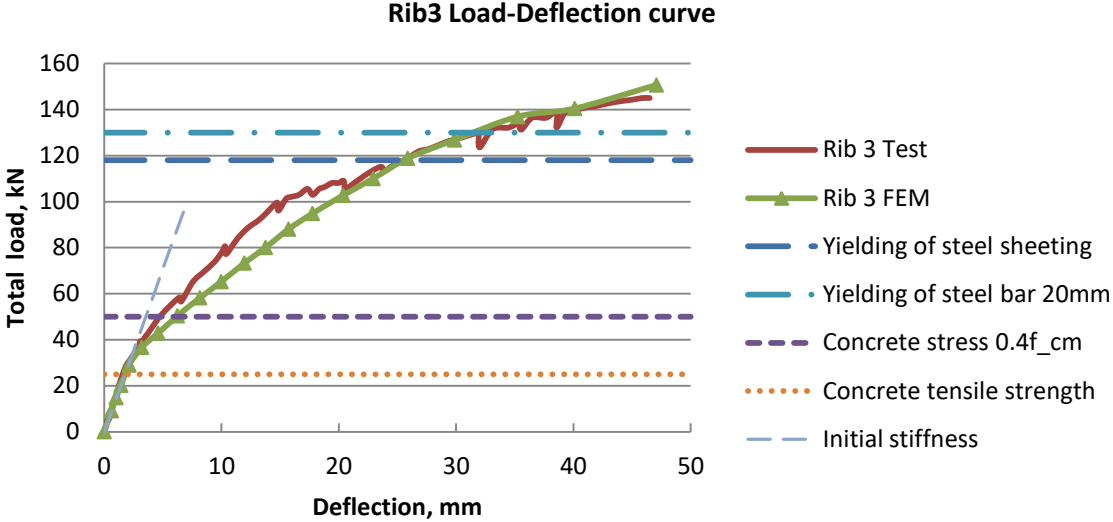


Figure 5.26 Total load vs. maximum deflection of the middle rib of the composite slab in load control FEA and test

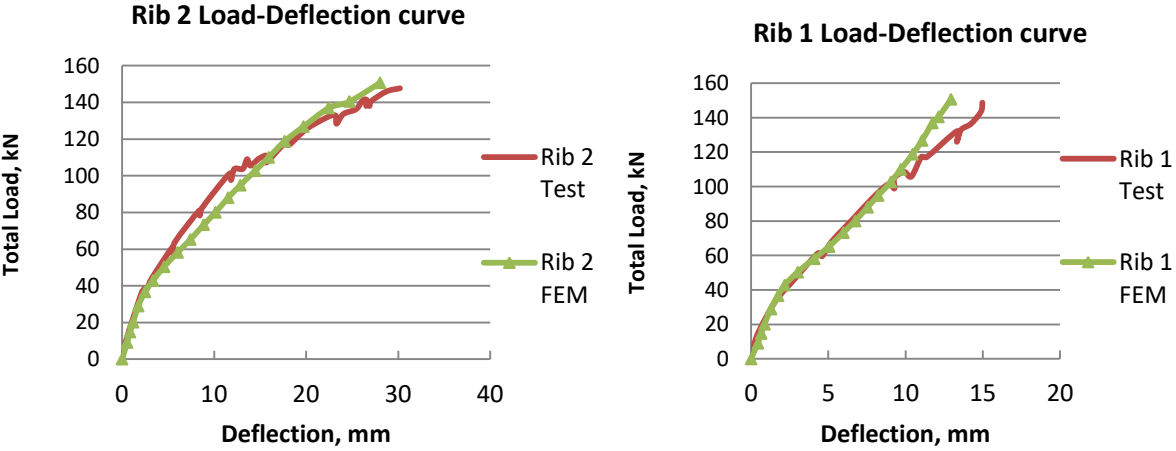


Figure 5.27 Total load vs. maximum deflection of rib 2 (left figure) and rib 1 (right figure) of the composite slab in load control FEA and test

The maximum reachable displacement of 48.44mm in load-control FEA is slightly higher than the maximum displacement of 46.5mm from testing. This can be explained by the fact that in reality the test was displacement driven and was stopped manually just after reaction force reached 145kN; apparently, if the applied displacement was maintained a little longer, the final displacement of the slab will be also higher in a test.

The load-deflection responses of ribs from load control FEA show good agreement with the test results for most of the load-deflection curves beside the part between 50kN and 100kN where small divergence in results occurs. From an examination of analysis output follows that at about 50kN the Von Mises stress of concrete part exceeds $0.4f_{cm}$ (i.e. 11.2MPa) compressive concrete strength, which indicates the beginning of non-linear concrete behavior. The non-linear behavior

of concrete is difficult to capture accurately within the finite element analysis because such behavior is dependent on many factors, namely tensile cracking of concrete and nonlinearity introduced by reinforcement. This can explain the deviation of load-deflection FEA response from test results (see Figure 5.26).

5.6.2.2 Stresses and strains

The Von Mises stress, also known as Huber stress that accounts for all six components of general 3D stress state, is used to present stresses from finite element analysis since the safety of materials with elasto-plastic properties can be evaluated using Von Mises stresses. The Von Mises stress is, therefore, accepted as failure criterion to assess stress formation in the composite slab.

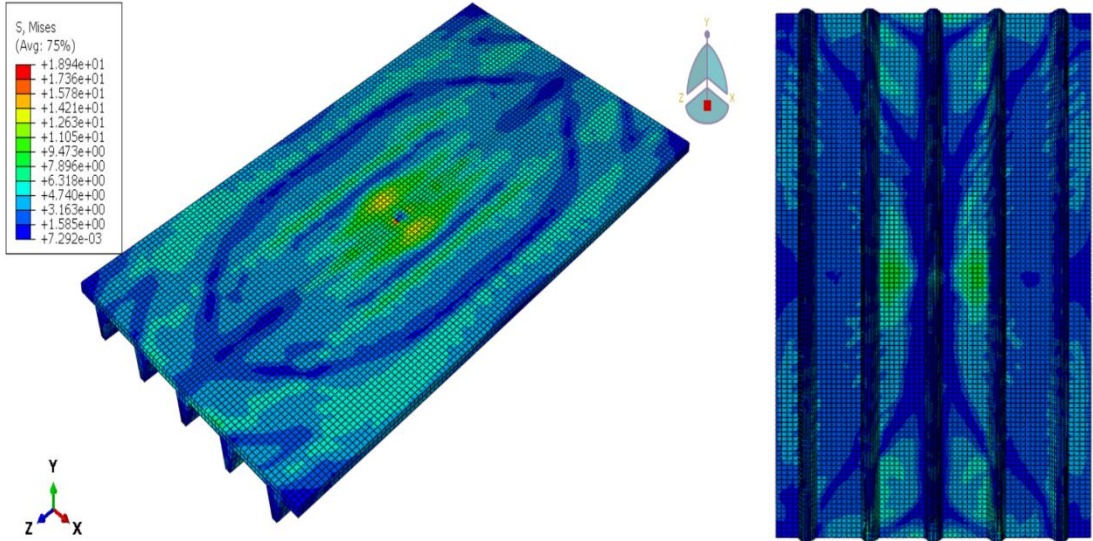
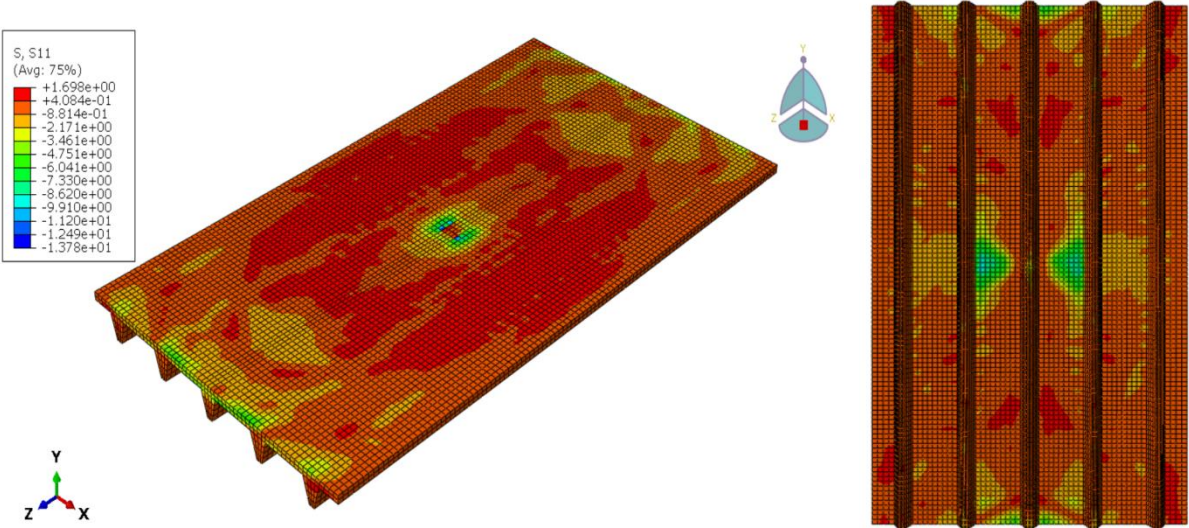


Figure 5.28 Von Mises stress distribution in concrete in load control FEA at the end of the analysis



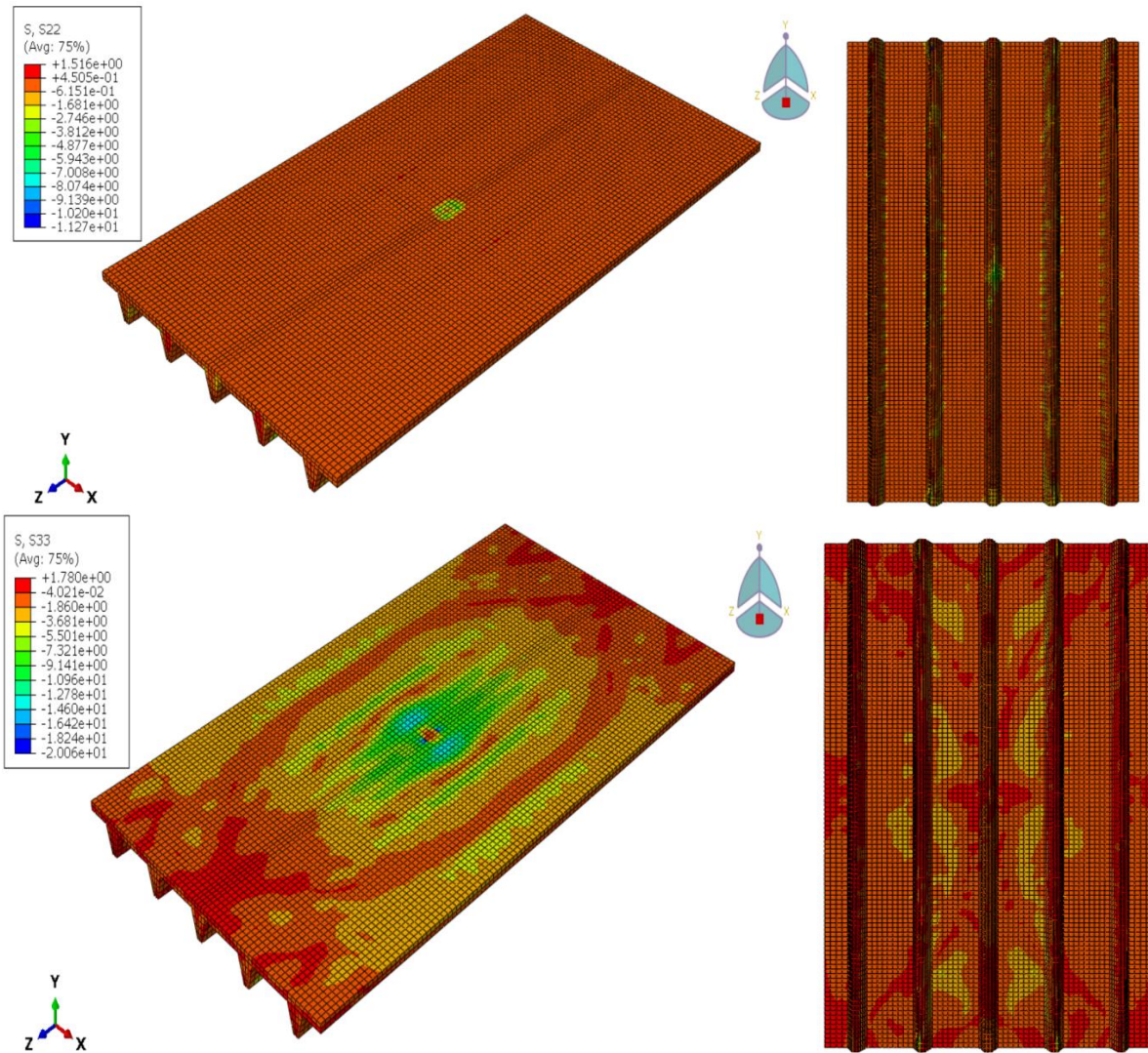


Figure 5.29 Normal stresses (MPa) in X, Y and Z direction for concrete in load control FEA at the end of the analysis

The contour plots of Von Mises stress and three principal stresses in X (S11), Y (S22) and Z (S33) direction for concrete part of composite slab ComFlor210 are illustrated in Figure 5.28 and Figure 5.29. As shown on the pictures, the highest concentration of three principal stresses occurs at the center of the slab close to the load application surface where concrete is obviously in compression. Besides the load application zone, the compression in concrete is also developed at supports; while most of the concrete in ribs stays in tension during analysis. The principal stress σ_{zz} reached -20.06MPa at the end of analysis, which is lower the concrete compression strength; the conclusion can be drawn that concrete behaviour in compression is characterized by stress hardening at the last stage of analysis. Regarding tensile concrete capacity, it can be said that the maximum tensile stress σ_{zz} originates at the bottom of the middle rib at approximately 25kN load, indicating that concrete gains its tensile resistance capacity at this load level and flexure cracks are starting to evolve from rib bottom. As a result of concrete cracking and further load increase, the tensile stress in concrete is decreasing hereafter, reaching $\sigma_{zz} = +1.78\text{MPa}$ at the end of the analysis.

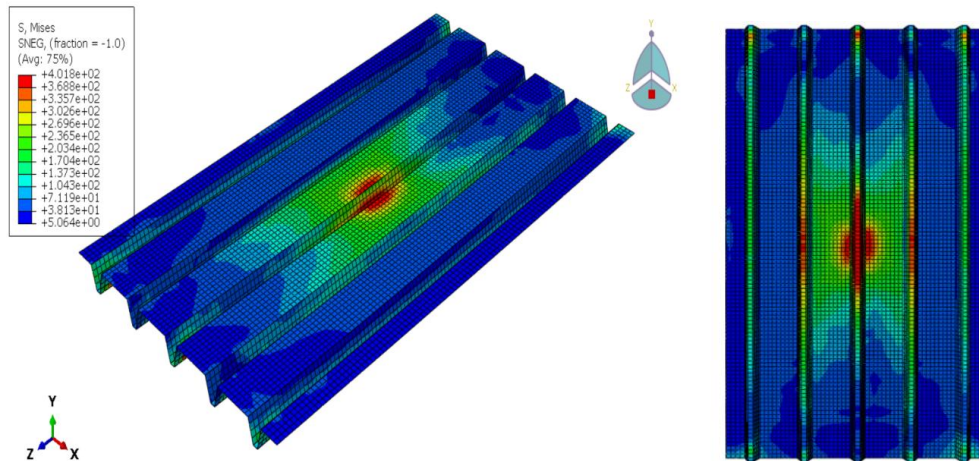


Figure 5.30 Von Mises stress distribution in steel sheeting in load control FEA at the end of the analysis

The steel sheeting starts yielding at a bottom flange of the center rib at about 118kN, which is expected because the bottom flange is the furthest part of steel sheeting from the neutral line in the cross-section, and it is clear that the yielding should occur there first. Hereafter the adjacent sides reach the yielding stress and then the connected top flange of steel sheeting begins to yield. At the end of the analysis, the Von Mises stress in steel sheeting reaches 401.8MPa with the highest concentration at the middle rib of steel sheeting, which is shown in Figure 5.30. At the same time, the stress at the two outer ribs of steel sheeting does not exceed the yielding limit.

The stress in transverse reinforcement $\varnothing 8mm$ obtains a maximum value of 459.5MPa, while the maximum stress in longitudinal wires $\varnothing 8mm$ is less and equals 177.1MPa at the end of analysis, indicating that the reinforcement mesh did not yield so far. The highest stress in reinforcement mesh concentrates again at the location where the load is applied on a slab, while the stress in the wires close to slab edges does not exceed 100MPa.

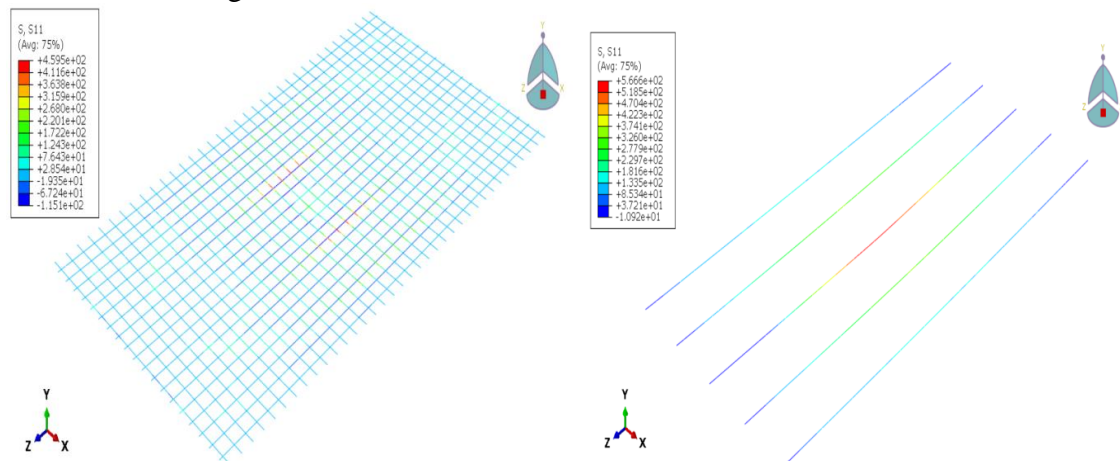


Figure 5.31 Normal stress distribution in reinforcement mesh 8mm (left figure) and steel bars 20mm (right figure) in load control FEA at the end of the analysis

The maximum stress in reinforcement $\varnothing 20mm$ occurs in a bar placed in the central rib and equals 566.6MPa. The yielding stress of reinforcement steel is $f_y = 540MPa$, meaning the centre bar is yielding at approximately 130kN, while other bars in ribs are not even when the applied load is at the maximum. The contour plots of Von Mises stress for reinforcement $\varnothing 8mm$ and $\varnothing 20mm$ are presented in Figure 5.31.

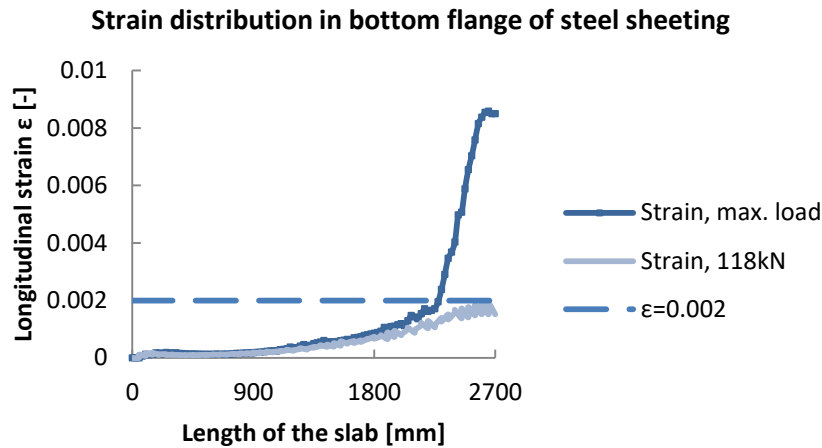


Figure 5.32 Strain distribution in Rib 3 bottom flange of steel sheeting

Figure 5.32 shows the strain distribution over the slab length in the bottom flange of steel sheeting at the middle rib. It is clear that the strain in steel sheeting is just about to reach the yielding strain of steel 0.002 at 118kN. At the end of analysis when the load is at maximum the intersection of strain curve with yielding strain occurs at 2275mm from slab supported edge. Thus, the total length of the yielded section of bottom flange is 850mm.

Now with the stress distributions in concrete and steel elements of the composite slab are analyzed, the conclusion on the failure mode of the composite slab under concentrated force in load control FEA can be inferred. The concrete reached its tensile capacity at approximately 25kN followed by crack development in concrete that is typical for flexure. From that moment the reinforcement and steel sheeting started contributing to slab bending resistance with steel sheeting reaching the yielding limit at approximately 118kN; meanwhile, the separation of steel sheeting from concrete was observed in finite element model. Concluding, the composite slab ComFlor210 fails by flexure.

5.6.2.3 Reaction force distribution in one mesh composite slab

A comparison is made in Figure 5.33 between reaction force distribution in finite element load control analysis and experiment. Firstly, the distributions of loads 10kN, 60kN and 145kN resulting from finite element load control analysis will be analyzed. At 10kN the concentrated force spreads over all five ribs with the slightly higher contribution of center rib: center rib carries 28% of the load, while the contribution of each adjacent rib accounts for 27% of the load at this stage, and the rest of the load goes to the outer ribs. This distribution of 10kN load obtained from load control FEA is almost similar to the experimental results; this is presented in Figure 5.34.

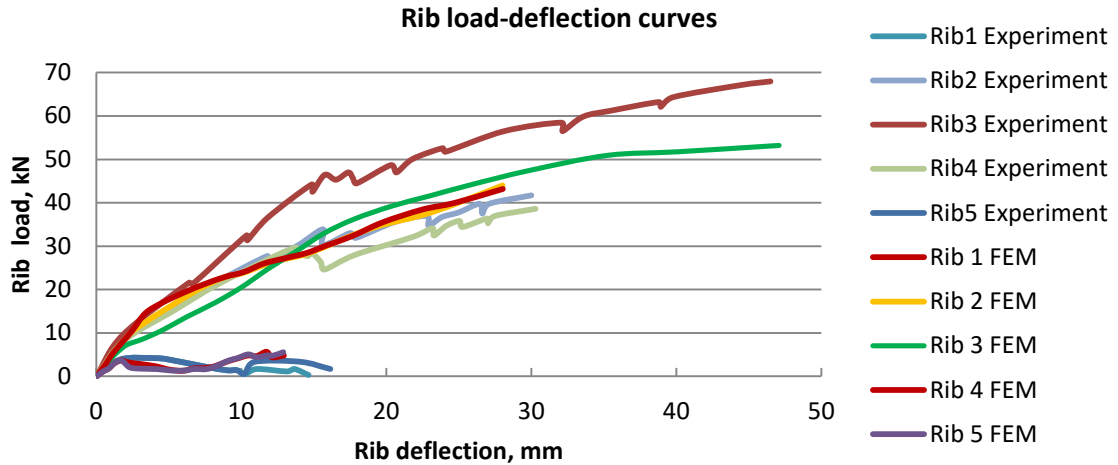


Figure 5.33 Load-deflection curves of each rib in experiment and load control FEA

When total load rises up to 60kN, the distribution of the force in load control FEA is barely changed compared to 10kN load distribution: all five ribs of composite slab participate in spreading the point load. The main difference can be seen in the decreased contribution of outer ribs: dropping to 2%. Nevertheless, the deviation from the experiment is observed at this loading stage, namely the center rib in a test carries 36% of the load, while the center rib in FEA accounts for 30% of total load (see Figure 5.35).

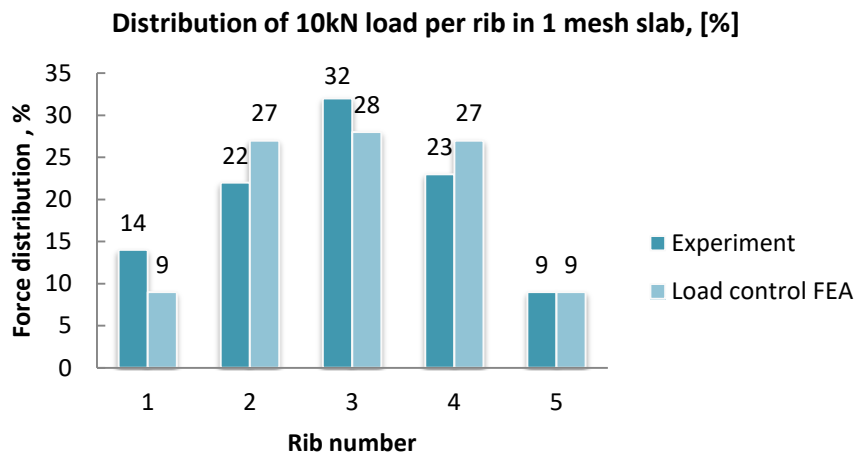


Figure 5.34 Distribution of 10kN concentrated force in load control FEA and experiment

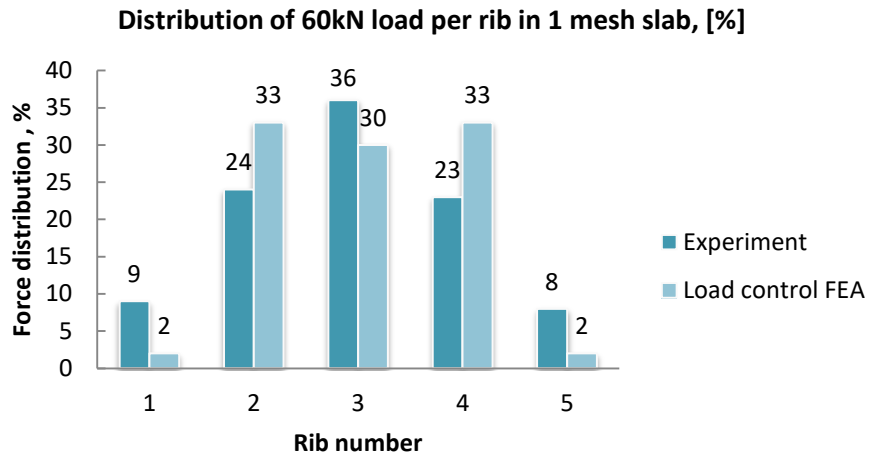


Figure 5.35 Distribution of 60kN concentrated force in load control FEA and experiment

At 145kN the concentrated force distribution is drastically changed. The two outer ribs contribute almost no more to spreading the load, and most of the load passes to the center rib which carries 38% of the total load at this stage. The contribution of adjacent ribs is also decreased to 28% each. The final distribution of the maximum load from FEA in percentage is somewhat similar to that of the experiment, see Figure 5.36.

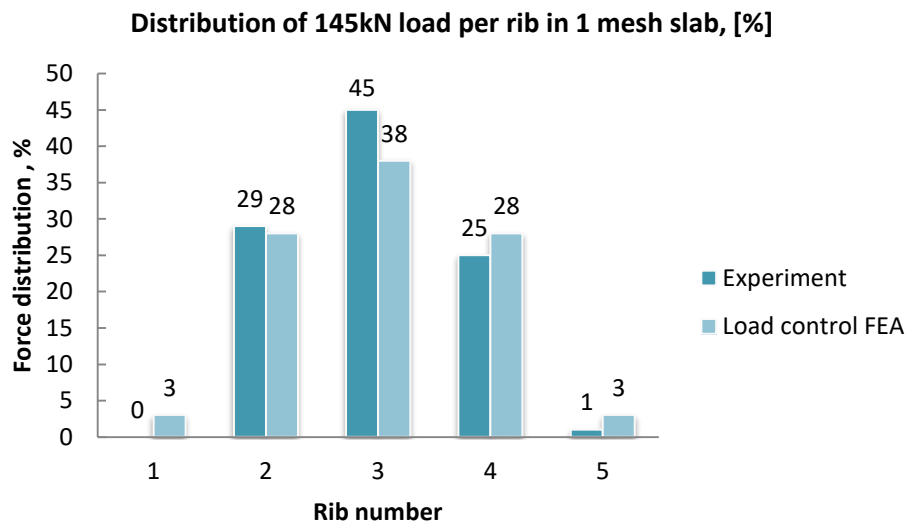


Figure 5.36 Distribution of 145kN concentrated force in load control FEA and experiment

5.7 The displacement control finite element analysis

5.7.1 Model description

In the displacement control analysis, the load is applied in a form of prescribed displacement to a specific point. Specifically, the displacement is attached to a reference point (RP) that is connected through coupling to the surface 150mmx150mm at the center of top slab surface. The prescribed displacement was specified with smooth step amplitude function and uniform distribution in the boundary condition module.

The prescribed displacement for the slab loaded centrally equals 46.5mm, and for the slab loaded at the quarter of the span equals 2.7mm.

The material properties are used as described in §5.3. Boundary conditions of the composite slab are presented in §5.4.1. The input parameters for concrete damaged plasticity model are given in Table 5.9. The input parameters for steel elements are defined in Table 5.10. These parameters are the same as in load-control analysis.

The analysis was executed in Abaqus/Explicit module with Dynamic, Explicit step. As mentioned before, it is necessary to check whether the obtained results really represent the quasi-static solution: the kinetic energy of the object should not exceed a small fraction (5-10%) of its internal energy throughout the whole quasi-static analysis. The main energy balance requirement is fulfilled, as it can be seen in Figure 5.37, where kinetic energy (ALLKE) and internal energy (ALLIE) are plotted against step time.

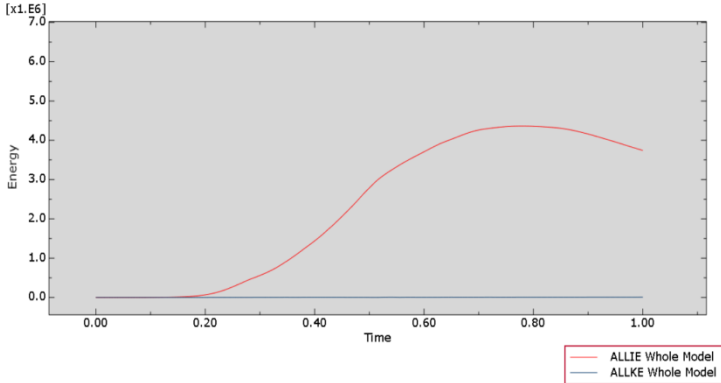


Figure 5.37 Kinetic and internal energy of the finite element model in displacement control analysis

Indeed, the kinetic energy stays almost on the same level, while the internal energy of the whole model is constantly increasing on 0.2-0.8 step interval.

5.7.2 Displacement control analysis results

This subchapter divided into several parts in order to give an overview on analysis output, namely deformed shape and displacements, stresses and rib reaction forces.

5.7.2.1 Deformed shape and displacements

The deformation of the composite slab under concentrated load is characterized by the concave shape of the top surface. The maximum deformation of 47.07mm occurs under loading surface, and then deformations evolve over the slab to its edges, see Figure 5.38.

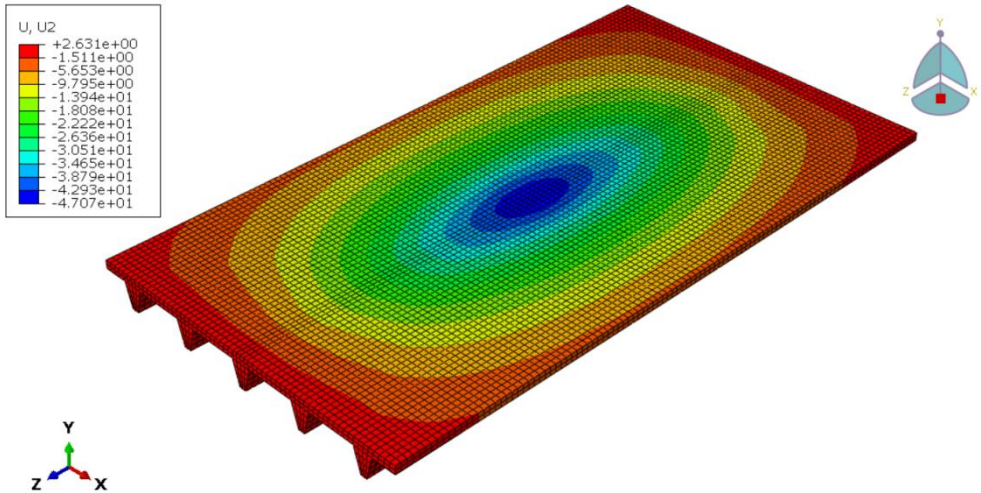


Figure 5.38 Displacement field U2 in the one-mesh slab in displacement-control FEA

A comparison is made between displacement-control finite element analysis and experiment presented in Figure 5.39 and Figure 5.40 for total load vs. deflection response of middle rib (Rib 3), adjacent rib (Rib 2) and outer rib (Rib 1) of composite slab. Once again, the response of the other two ribs Rib 4 and Rib 5 will be similar to that of Rib 2 and Rib 1 due to the symmetry of slab geometry and load application.

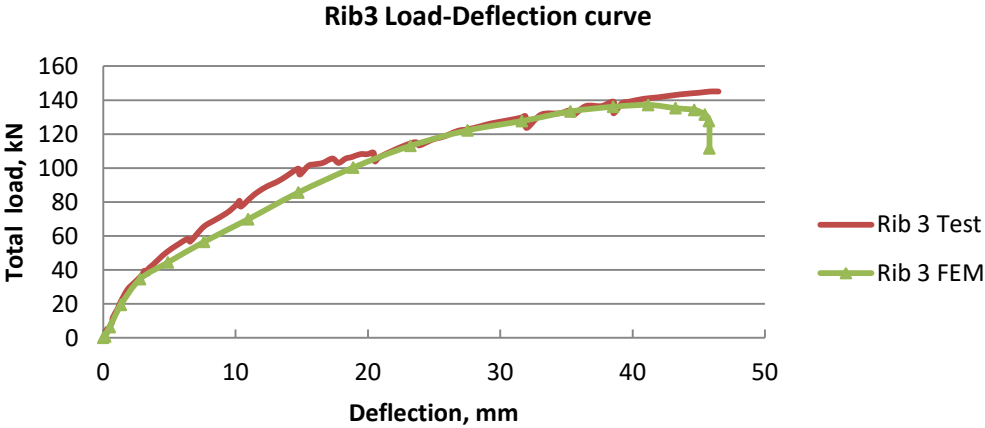


Figure 5.39 Total load vs. maximum deflection of the middle rib of the composite slab in displacement control FEA and test

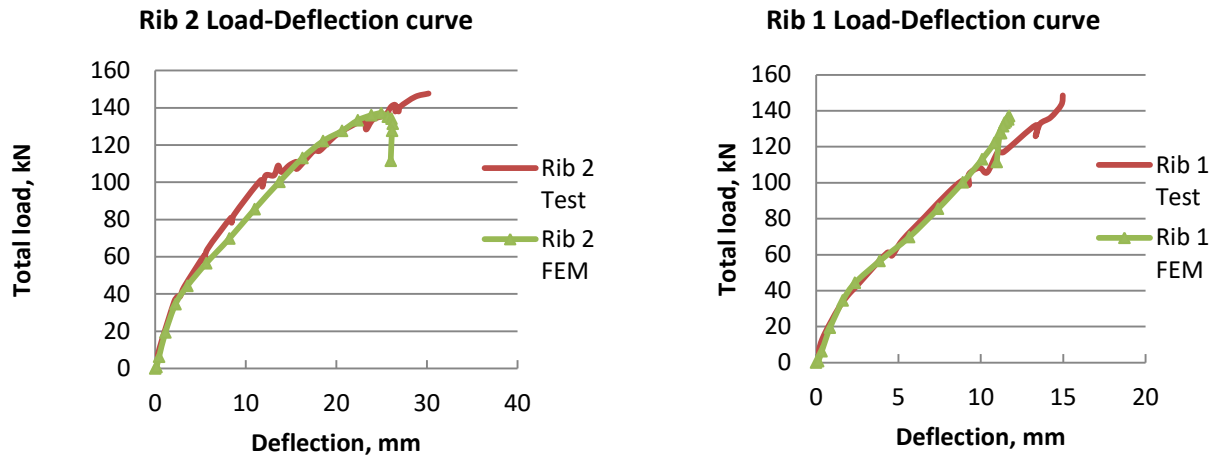


Figure 5.40 Total load vs. maximum deflection of rib 2 (left figure) and rib 1 (right figure) of the composite slab in displacement control FEA and test

5.7.2.2 Stresses

The contour plots of Von Mises stress and three principal stresses in X (S11), Y (S22) and Z (S33) direction for a concrete part in composite slab ComFlor210 are given in Figure 5.41 and Figure 5.29, Figure 5.42. The highest concentration of three principal stresses occurs at the load application surface where concrete is under compression; meantime, concrete in ribs experiences mainly tensile stress. The principal stress σ_{zz} reached -16.28MPa at the end of analysis, which is lower the yielding stress of concrete in compression; from that the conclusion can be drawn that concrete behaviour in compression is characterized by strain softening at the last stage of analysis. The maximum tensile stress σ_{zz} originates from middle rib bottom at approximately 28kN total load, meaning that concrete obtains tensile resistance capacity and flexure cracks appear at rib bottom. With continuing concrete cracking and load increase, the tensile resistance of concrete is decreasing furthermore, reaching $\sigma_{zz} = +1.656\text{MPa}$ at the end of analysis.

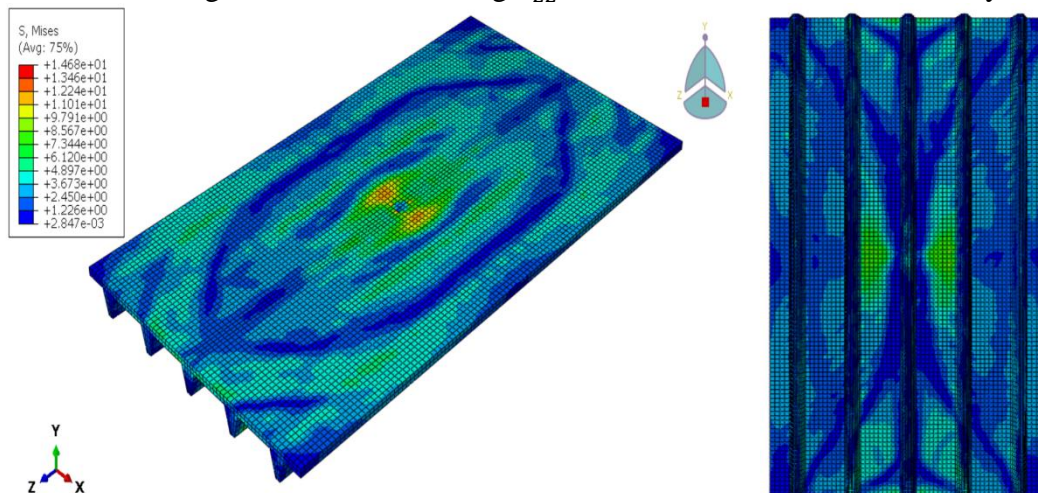


Figure 5.41 Von Mises stress distribution in concrete part in displacement control FEA at the end of analysis

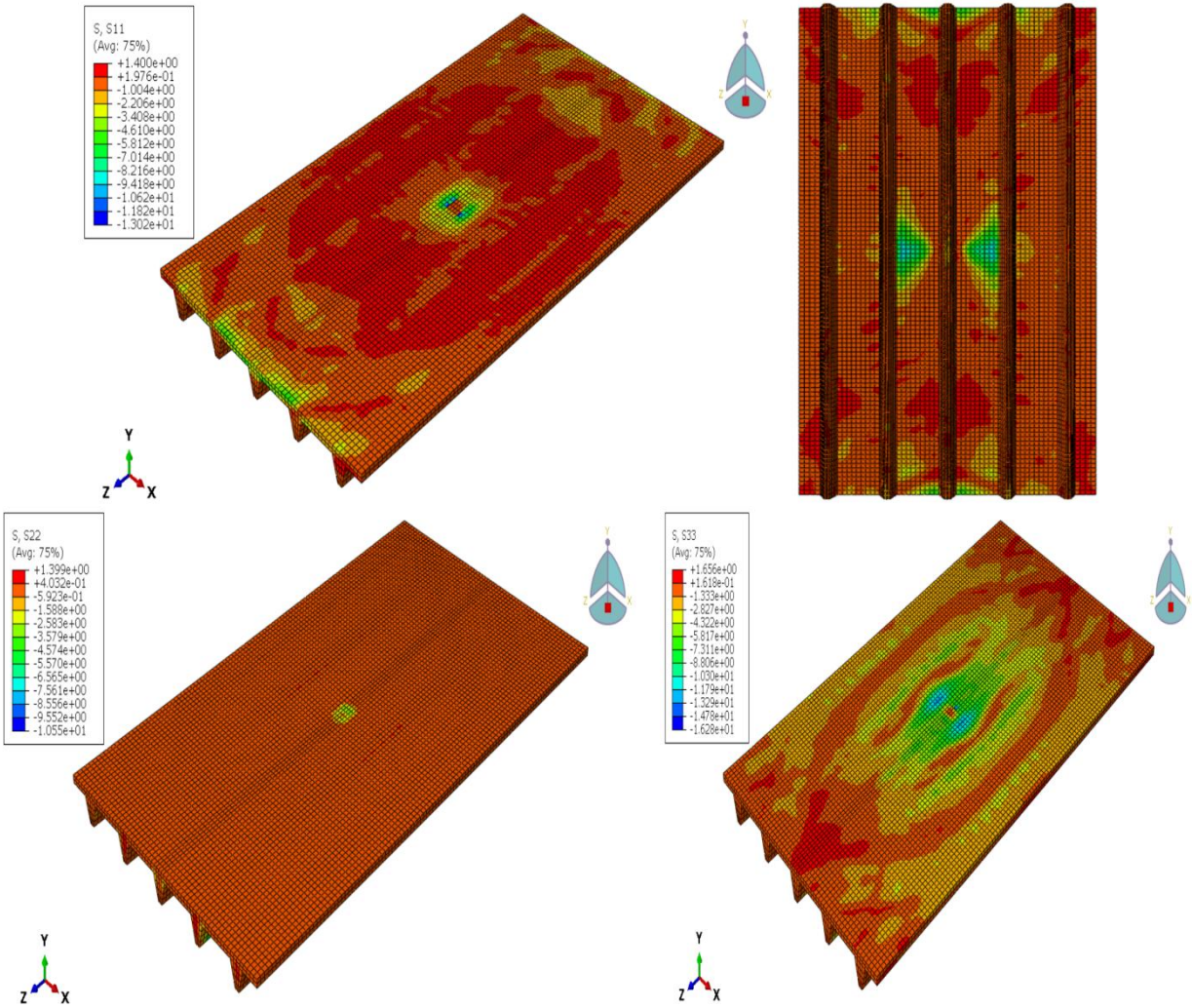


Figure 5.42 Normal stresses (MPa) in X, Y and Z direction for concrete in displacement control FEA at the end of the analysis

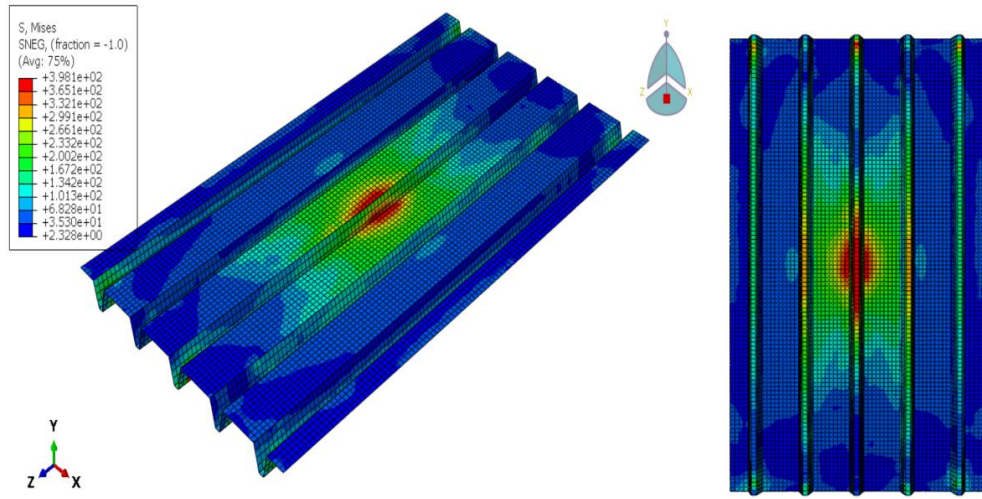


Figure 5.43 Von Mises stress distribution in steel sheeting in displacement control FEA at the end of the analysis

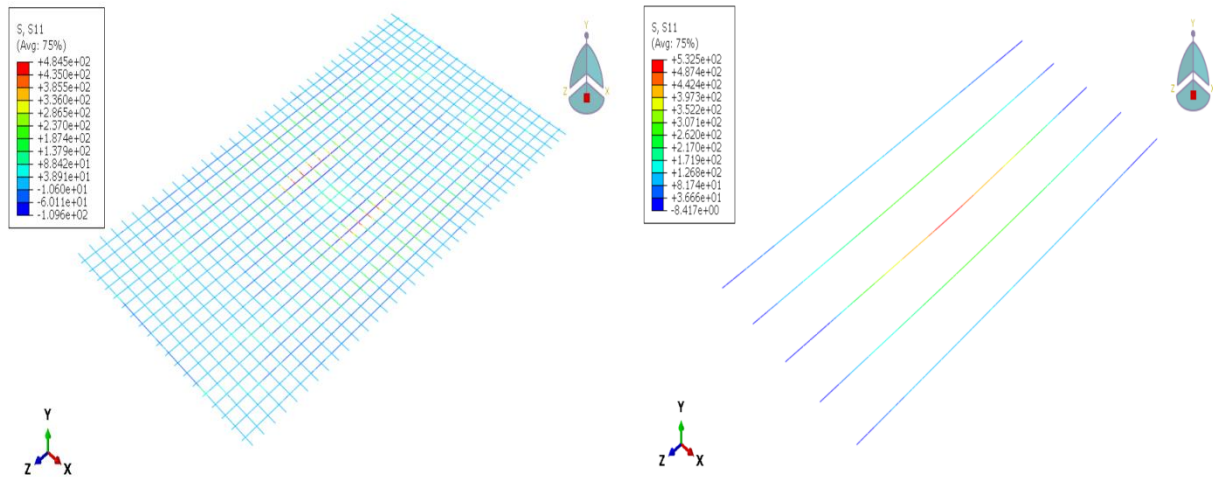


Figure 5.44 Normal stress distribution in reinforcement mesh 8mm (left figure) and steel bars 20mm (right figure) in load control FEA at the end of the analysis

The steel sheeting starts yielding at a bottom flange of the center rib at about 120kN. Over time the adjacent sides reach the yielding stress, and then the top flange of steel sheeting begins to yield. At the end of the analysis, the Von Mises stress in steel sheeting reaches 398.1MPa with the highest concentration at the middle rib of steel sheeting, which is shown in Figure 5.43. The stress at the two outer ribs of steel sheeting does not exceed the yielding limit.

The maximum stress in transverse reinforcement $\varnothing 8mm$ is 484.5MPa; the maximum stress in longitudinal wires $\varnothing 8mm$ is less and equals 130MPa at the end of analysis, indicating that the reinforcement mesh did not yet yield.

The maximum stress in reinforcement $\varnothing 20mm$ occurs in a bar placed in the centre rib and equals 558.1MPa. The yielding stress of reinforcement steel is $f_y = 540MPa$, which means that only the centre bar is yielding while other bars in ribs are not. The contour plots of principal stress for reinforcement $\varnothing 8mm$ and $\varnothing 20mm$ are shown in Figure 5.44.

After analyzing the stress distributions in concrete and steel elements of the composite slab, the conclusion on the failure mode of the composite slab under concentrated force in displacement control FEA can be drawn. First of all, concrete gained tensile resistance at approximately 28kN followed by flexural crack development in ribs. Secondly, the reinforcement and steel sheeting started contributing to slab bending resistance with steel sheeting reaching the yielding limit at approximately 120kN. The composite slab ComFlor210 fails by flexure.

5.7.2.3 Reaction force distribution in one mesh composite slab

A comparison is made in Figure 5.45 between reaction force distribution in finite element displacement control analysis and experiment. Again, the distributions of loads 10kN, 60kN and 135kN will be studied. At 10kN the concentrated force spreads over all five ribs with higher contribution of three middle ribs: center rib carries 28% of the load, the contribution of each adjacent rib accounts for 27% and each outer rib takes 9% of the load. This distribution of 10kN load from displacement control FEA is in some measure similar to the experimental results; this is shown in Figure 5.46.

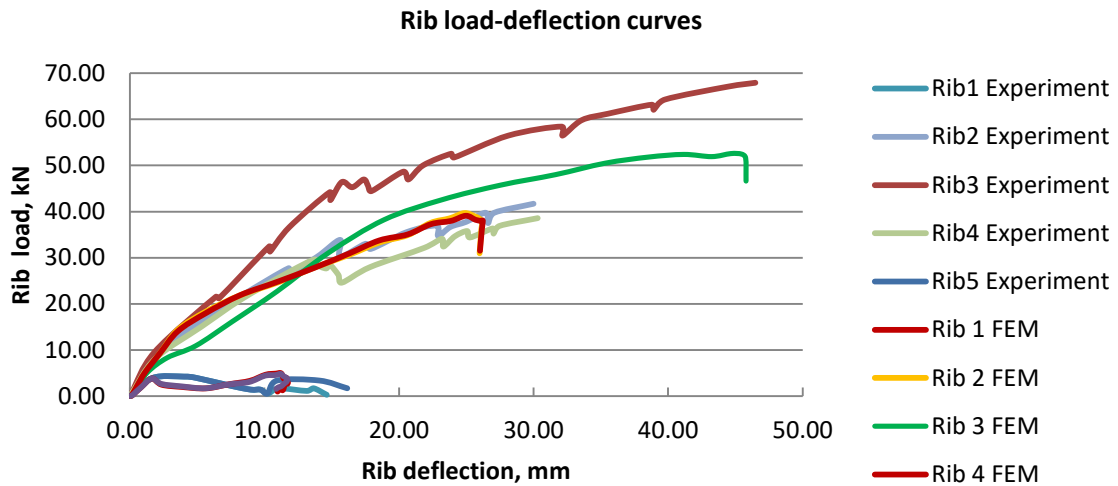


Figure 5.45 Load-deflection curves of each rib in experiment and displacement control FEA

When total load rises up to 60kN, the distribution of the force is slightly changed compared to 10kN load distribution: all five ribs spread the load. The main difference can be seen in the decreased contribution of outer ribs resulting in 3%. Additionally, the deviation from the experiment is observed at this loading stage, namely the center rib in a test carries 36% of the load, while the center rib in FEA accounts only for 30% of the total load; the contribution of adjacent ribs is increased as well (see Figure 5.47).

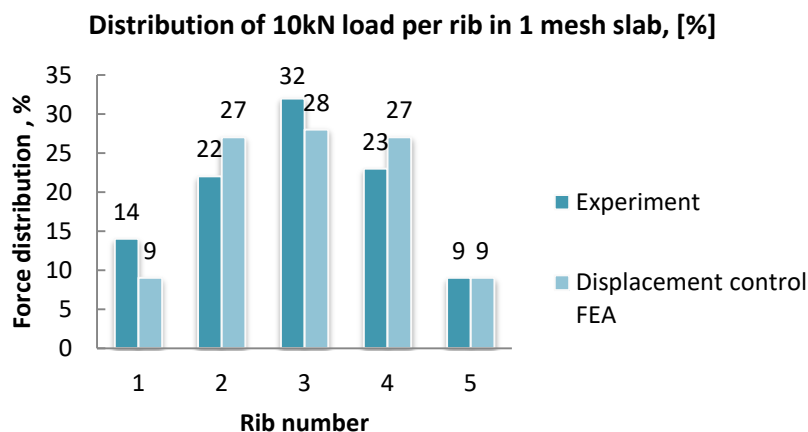


Figure 5.46 Distribution of 10kN concentrated force in displacement control FEA and experiment

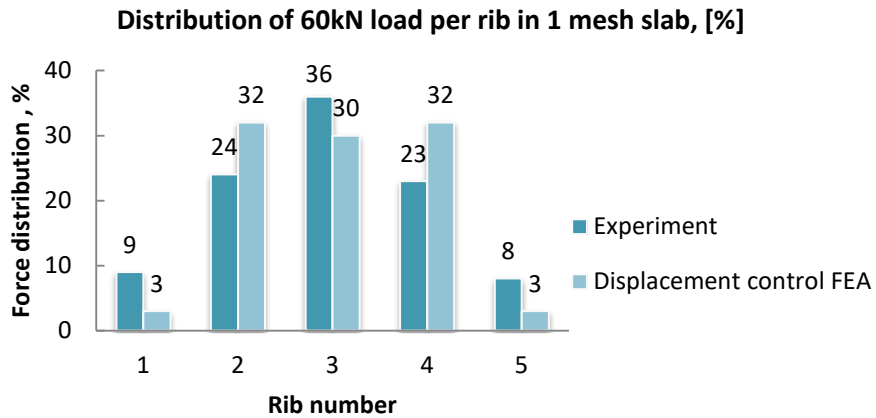


Figure 5.47 Distribution of 60kN concentrated force in displacement control FEA and experiment

At 135kN the concentrated force distribution is changed a lot. The two outer ribs contribute almost no more to spreading the load, and nearly half of the load passes to the center rib which carries 40% of the total load. The contribution of adjacent ribs is decreased to 28%. The final distribution of the maximum load from FEA in percentage is presented in Figure 5.48.

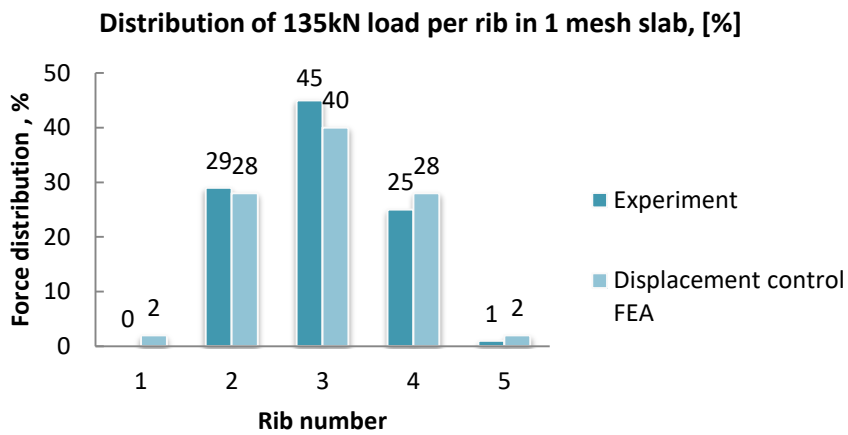


Figure 5.48 Distribution of 145kN concentrated force in load control FEA and experiment

5.8 Conclusion on the finite element model and comparison with the engineering model

The finite element model (FEM) of composite slab ComFlor210 is described in detail in chapter 4. The input parameters for FEM are based not only on test results (e.g. material properties, geometry) but also on the assumptions and several recommendations. For instance, the parameters of concrete in damaged plasticity model are recommended from Abaqus guide [14]; they are used in various studies and proven to be accurate enough, but it is always better to obtain those parameters from specific concrete tests. In the determination of the damage coefficients for concrete in tension and compression (described in Appendix C) the simplified approach is used. Additionally, the friction coefficient between concrete and steel sheeting for setting interaction in FEM was assumed, because no test was performed in order to determine that coefficient for composite slab ComFlor210.

The results from load control and displacement control finite element analyses of the composite slab were compared in chapter 5 to laboratory test results made by M. Dracht in TU Delft. It was found that there is no much difference observed between the results from displacement control and load control FEA with regard to stress distributions in different elements of the composite slab. Therefore, both types of finite element analyses can be used for assessing slab response under point load in loading range 0-145kN.

The finite element model of a composite slab shows good agreement with test results. The ratio of maximum deflections in FEM and test is 1.24 at a load 60kN and 1.01 at 145kN. The average deviation of the finite element model results from test is given in Figure 5.49.

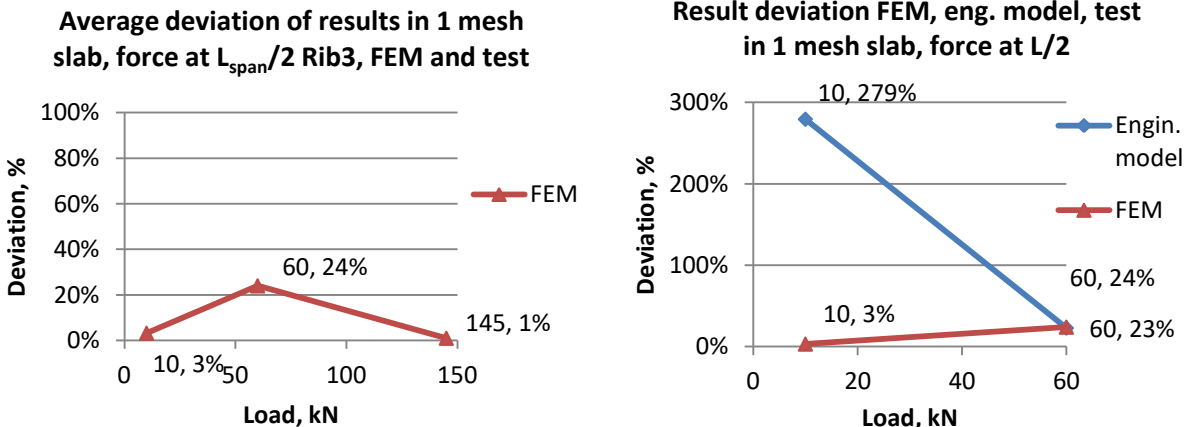


Figure 5.49 Average deviation between FEM, engineering model (max. rib deflections) and test

The comparison is made between the engineering model and finite element model results in Table 5.11. The difference between FEM and engineering model rib displacements is about 20% at 60kN.

Table 5.11 Maximum rib displacements in FEM, engineering model and test at 60kN load

Force, kN	FEM	Engineering model	Test	Ratio		
				Eng./Test	FEM/Test	FEM/Eng.
Displacement Rib3, mm	8.15	10.15	6.5	1.56	1.25	0.80
Displacement Rib2,4 mm	6.04	8.32	5.5	1.51	1.10	0.73
Displacement Rib1,5 mm	4.09	4.83	4.5	1.07	0.91	0.85

6 PARAMETRIC STUDY ON COMPOSITE SLAB COMFLOR210

6.1 Introduction

The finite element model (FEM) of composite slab ComFlor210 has been created in the program Abaqus/CAE and described in detail in chapter 4. The results from load control and displacement control finite element analyses of the composite slab were compared to laboratory test results made by M. Dracht in TU Delft. It was illustrated that the finite element model can predict quite well the load-deflection response of composite slab subjected to a concentrated force placed on the middle rib at the half of the span. However, in practice, it is of main interest to be able to get a vision on slab behavior when concentrated force is moved to another location, and when the length of the slab is changed. Firstly, the desired load positions are to be elaborated, and, then, the wishful geometry characteristics will be discussed.

The load can be moved in width and in longitudinal directions. The composite slab in question has by default five ribs; therefore, in width direction, the point load can be placed on adjacent and outer ribs – rib 1 and rib 2, or rib 4 and rib 5 (for rib numbering see [Figure 5.10](#)). Additionally, the situation with unsupported outer rib does not occur in practice: the composite slab is usually supported at all four edges; thus, the positioning of the load on the outer rib is not of practical interest. Hence, only one adjacent rib together with middle rib needs to be examined due to the geometrical symmetry of the composite slab. In longitudinal direction the load was placed at slab middle; it is wishful to place the load at slab quarter and at one-sixth of the length in order to oversee the evolution in the distribution of concentrated load when load travels towards the slab edges.

The composite slab ComFlor210 can be produced with different geometry: length, concrete grade, slab height, type of reinforcement can vary per slab in order to meet the construction needs. [Table 6.1](#) presents the possible configurations of composite slab ComFlor210 (*Dutch Engineering*).

Table 6.1 Possible geometry configuration for ComFlor210 slab

Slab length, mm	Slab Height, mm	Rib reinforcement, mm	Cover, mm	Concrete class	The thickness of steel sheeting, mm	
3600	280	12	40	C20/25	1	
4200	300	16	30	C30/37	1.25	
4800	320	20			Load variation per slab	
5400		25			rib 2, 3 center	
6000					2 at 1/2L	2 at 1/4L
6600						2 at 1/6L
7200						
Total number of possible configurations				$7*3*4*2*$ $2*6$		2016
Reduced configurations:						
Slab length, mm	Slab Height, mm	Rib reinforcement, mm	Cover, mm	Concrete class	Thickness of steel sheeting,mm	
3600	280	20	40	C20/25	1.25	
5400						
7200					Load variation per slab	
					rib 2 and rib 3	
					2 at 1/2L	2 at 1/4L
						2 at 1/6L
Number of reduced configurations				$3*1*1*1*$ $1*6$		18
Effect of parameters below studied on default case only: L=5400mm, load at Rib 3 at 1/2L						
<i>rib reinforcement</i>		<i>the thickness of steel sheeting</i>				
12		1				
20		1.25				
25						
Total number of analyzed configurations				18+3		21

6.2 Composite slab ComFlor210: span 3.6m

6.2.1 Concentrated load at $L_{span}/2$

The concentrated load of 60kN is positioned at the half span length, which equals 1.8m, on the middle Rib 3 and adjacent Rib 2 alternately. The resulting distribution of total reaction force in each rib in relation to the total applied load that increases from 0 to 60kN is given in Figure 6.1 and Figure 6.2. Due to the symmetrical load application at $L_{span}/2$ Rib3, the reaction forces in Rib 2 and Rib 4, Rib 1 and Rib 5 are identical.

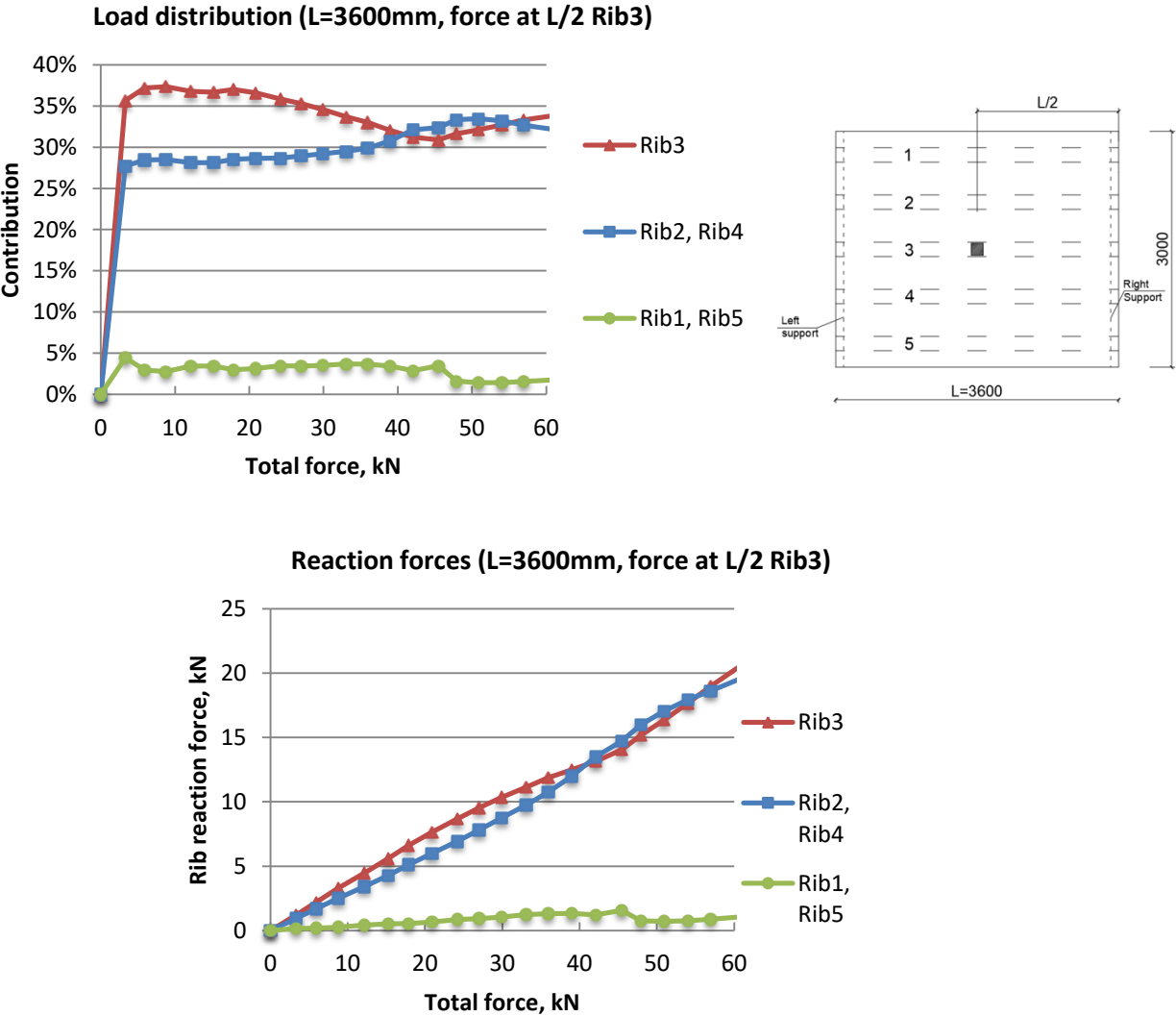


Figure 6.1 Distribution of concentrated load per rib (top figure) and reaction forces (bottom figure) in the composite slab L=3600mm with force on Rib 3 at L/2

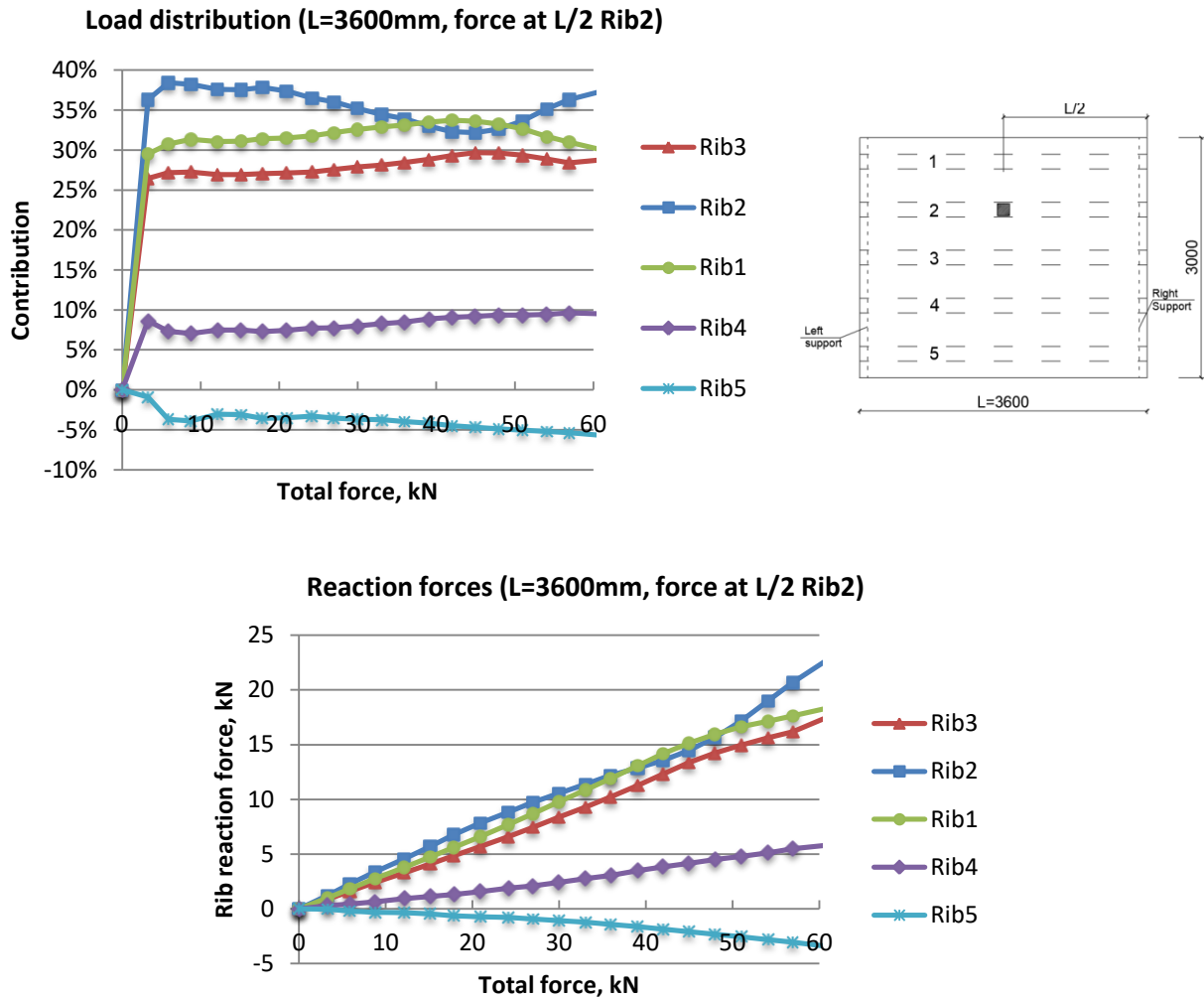


Figure 6.2 Distribution of concentrated load per rib (top figure) and reaction forces (bottom figure) in the composite slab L=3600mm with force on Rib 2 at L/2

Figure 6.1 shows that Rib 3 carries most of the load up to 40kN total load, after that contribution of Rib 3 decreases to almost 30% while the contribution of Rib 2 increases to the same level. The contribution of external Rib 1 is less than 5% for the entire load range.

Figure 6.2 displays that contribution of Rib 1, Rib 3 and Rib 4 is approximately constant in a load range 5-60kN. Reaction force in Rib 3 amounts to 25-30% of total load, the reaction force of Rib 1 adsorbs 30-34% of total load and reaction force in loaded Rib 2 decreases from 38% at the beginning of loading to 32% at 45kN total load and then increases again up to 37%. The load on Rib 2 results in uplift of the farthest corner of the slab and tensile reaction force in Rib 5; this explains why the contribution of Rib 5 has opposite sign, unlike other four ribs.

6.2.2 Concentrated load at $L_{span}/4$

The concentrated load of 60kN magnitude is placed at the quarter of a span on the middle Rib 3 and adjacent Rib 2. The resulting distribution of total reaction force in each rib in relation to the total applied load is displayed in Figure 6.3 and Figure 6.5. Due to unsymmetrical load application, the reaction forces in right and left supports of the composite slab are not equal. Therefore, distribution in the right support closest to the applied load is also given in Figure 6.4 and Figure 6.6.

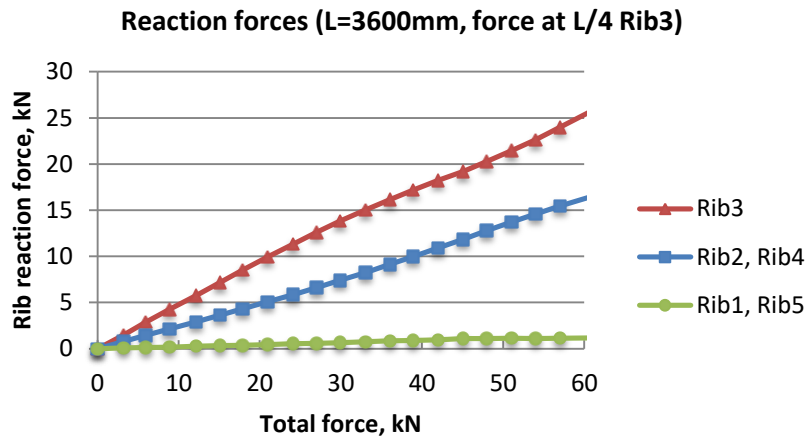
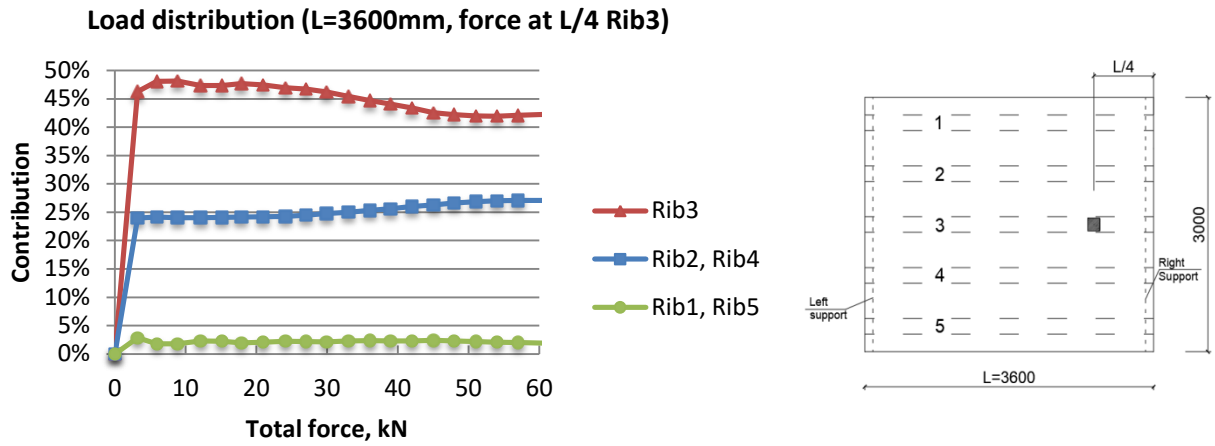


Figure 6.3 Distribution of concentrated load per rib (top figure) and reaction forces (bottom figure) in the composite slab L=3600mm with force on Rib 3 at L/4

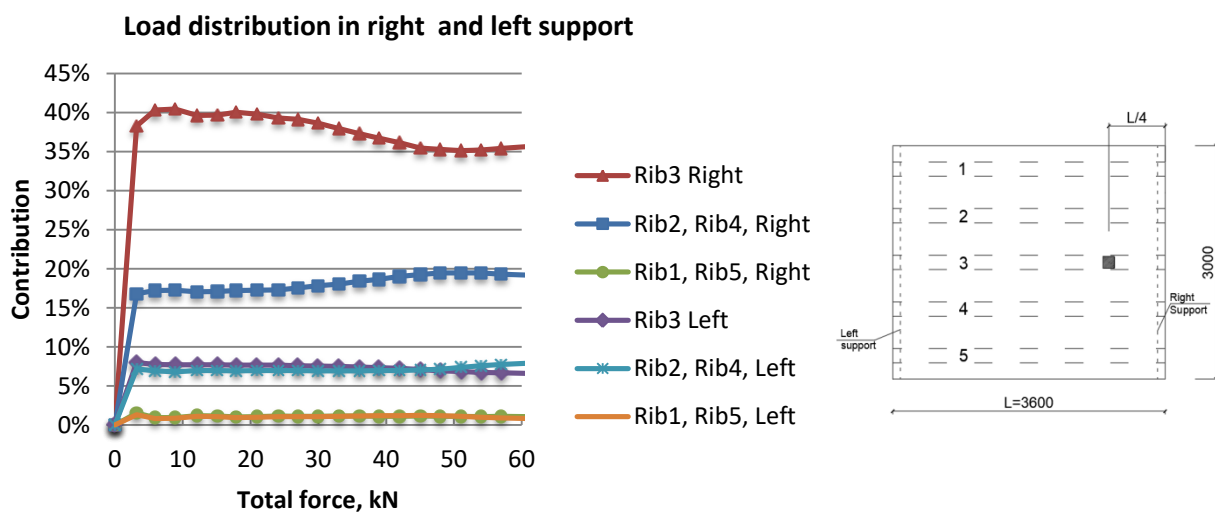


Figure 6.4 Distribution of concentrated load in right and left support of each rib (L=3600mm with force on Rib 3 at L/4)

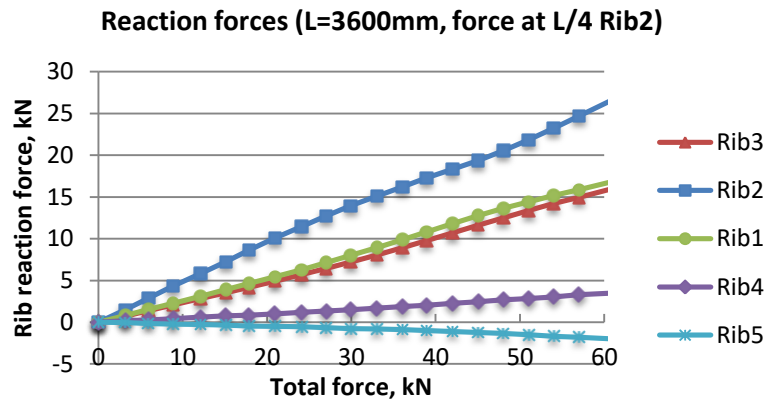
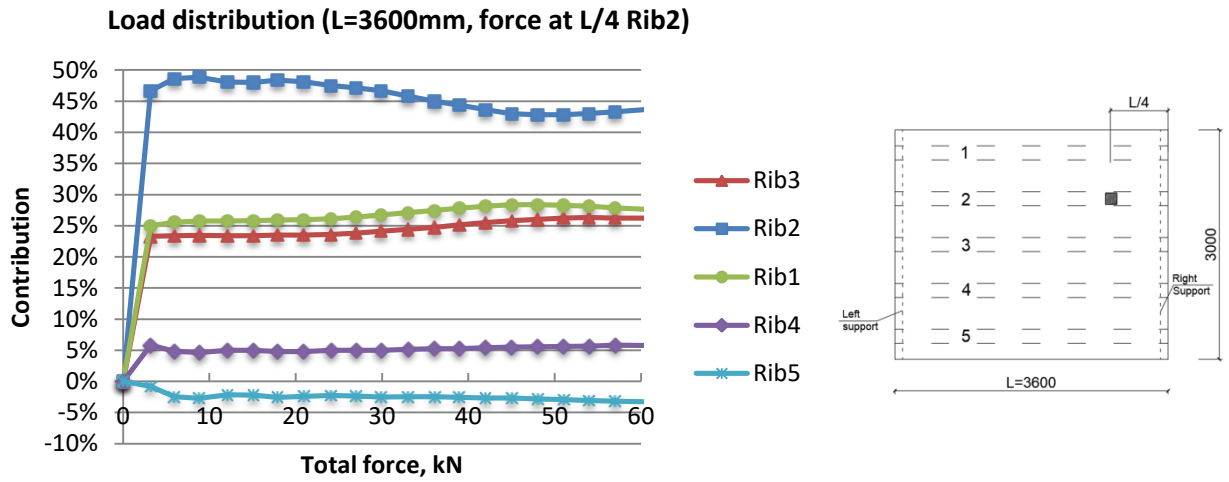


Figure 6.5 Distribution of concentrated load per rib (top figure) and reaction forces (bottom figure) in the composite slab L=3600mm with force on Rib 2 at L/4

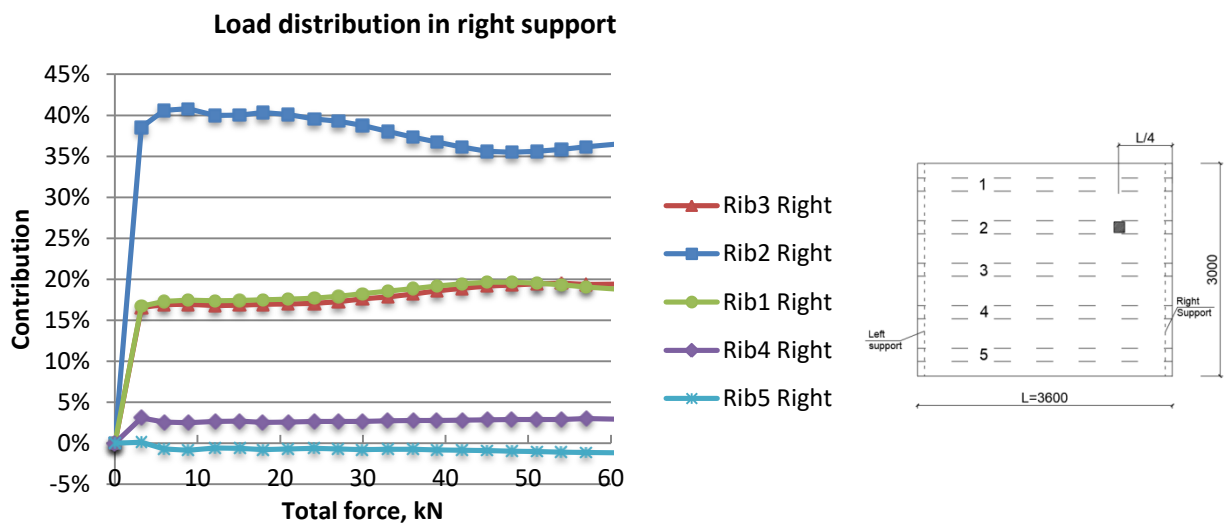


Figure 6.6 Distribution of concentrated load in the right support of each rib (L=3600mm with force on Rib 2 at L/4)

When the load is placed on Rib 3 at the quarter of a span, the contribution of Rib 3 is the highest among other ribs resulting in more than 45% of total force up to 30kN and in 42% in range 30-60kN. The contribution of Rib 2 is about 25%; the contribution of Rib 1 is constant and equals 2%. It is clear that most of the load is carried by Rib 3 and Rib 2 (Figure 6.3). The reaction forces in right support that is in proximity to load application account for 76% of total load and the left support carries 24% of total load. The proportion of 76%-24% of support reaction force distribution holds unchanged through the whole analysis.

In a case with the load placed on Rib 2 at the quarter of a span the contribution of Rib 1 – Rib 5 stays unaltered in a range 5-30kN with Rib 2 being loaded the most with 48% of total load. After that contribution of Rib 2 drops to 43% while contributions of Rib 3 and Rib 1 increase amounting for 26% and 28% respectively at the end of loading. The contribution of Rib 4 equals 5% in a range 5-60kN total load. Again the concentrated load on Rib 2 leads to an uplift of the farthest corner of the slab and tensile reaction force in Rib 5; this is why the Rib 5 contribution has reverse sign unlike other four ribs in Figure 6.5. The distribution of reaction force in right support of each rib, in general, follows the pattern of total reaction force distribution in ribs; the proportion 76%-24% with 76% being the total reaction force in right support of composite slab can be seen (Figure 6.6).

6.2.3 Concentrated load at $L_{span}/6$

The concentrated load of 60kN is positioned at the one-sixth of the span on the Rib 3 and Rib 2. The resulting distributions of total reaction force in each rib in relation to the total applied force are presented in Figure 6.7 and Figure 6.9. Because the position of the concentrated force is unsymmetrical in relation to the span length, the reaction forces in right and left supports of the composite slab are not the same. Thus, distributions in the right support closest to the applied load are also presented in Figure 6.8 and Figure 6.10.

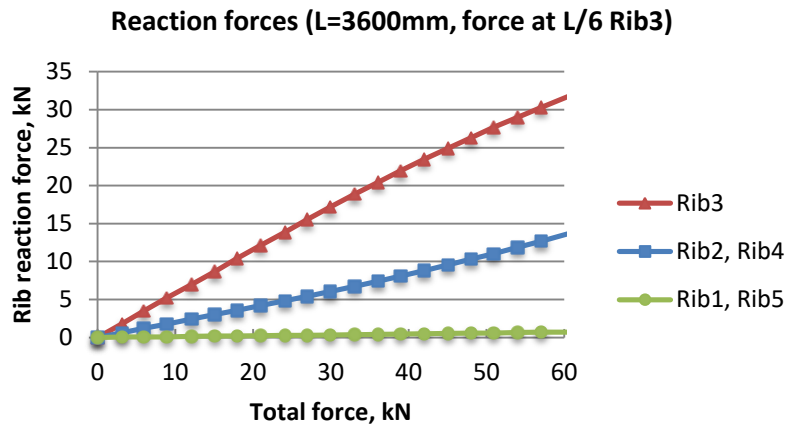
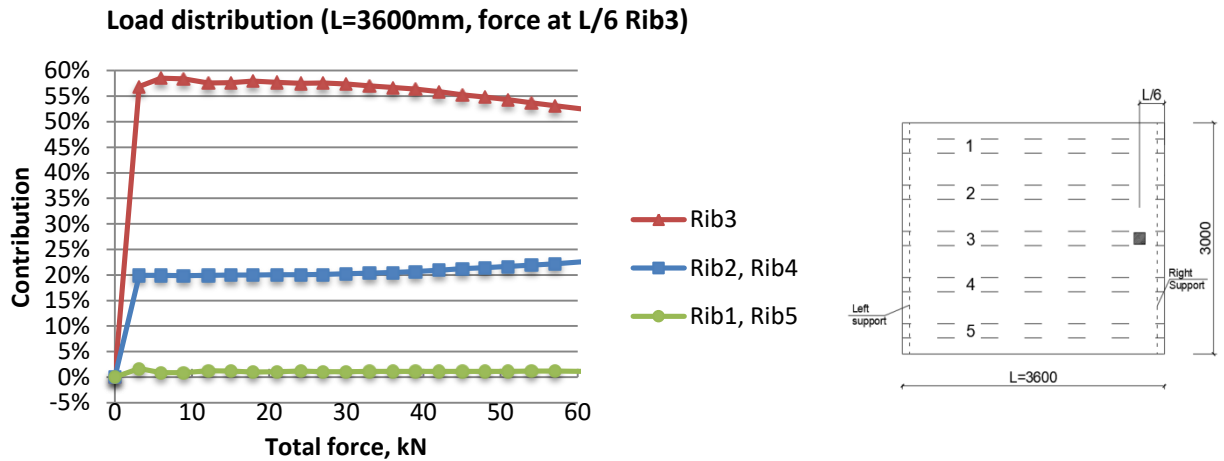


Figure 6.7 Distribution of concentrated load per rib (top figure) and reaction forces (bottom figure) in the composite slab L=3600mm with force on Rib 3 at L/6

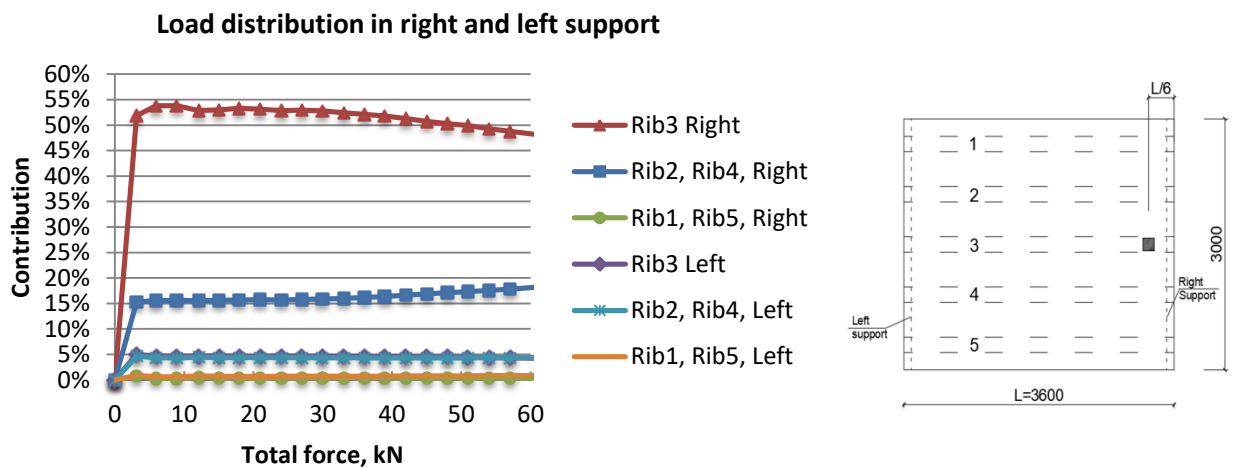


Figure 6.8 Distribution of concentrated load in right and left support of each rib (L=3600mm with force on Rib 3 at L/6)

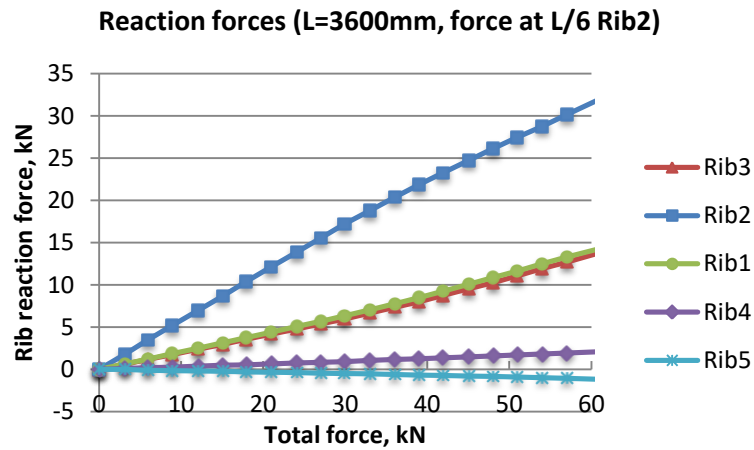
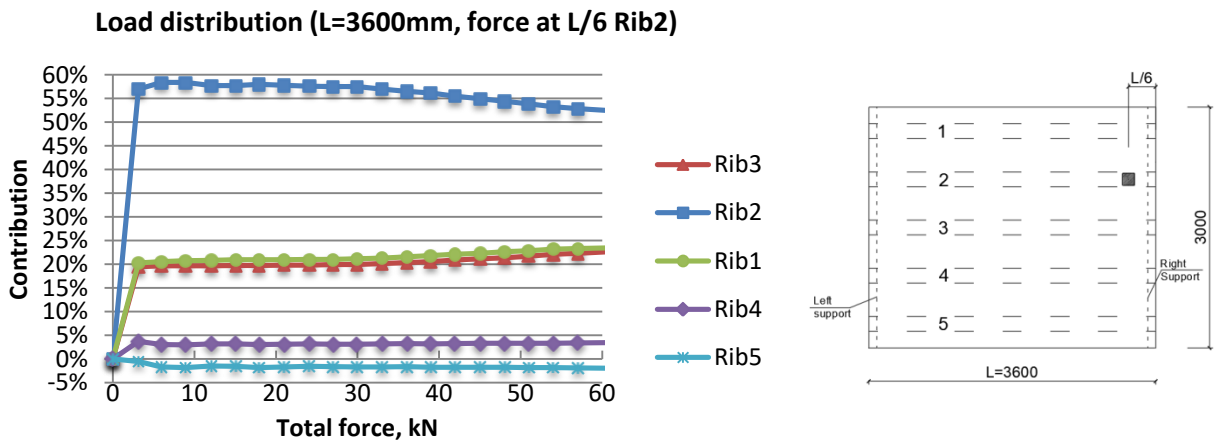


Figure 6.9 Distribution of concentrated load per rib (top figure) and reaction forces (bottom figure) in the composite slab L=3600mm with force on Rib 2 at L/6

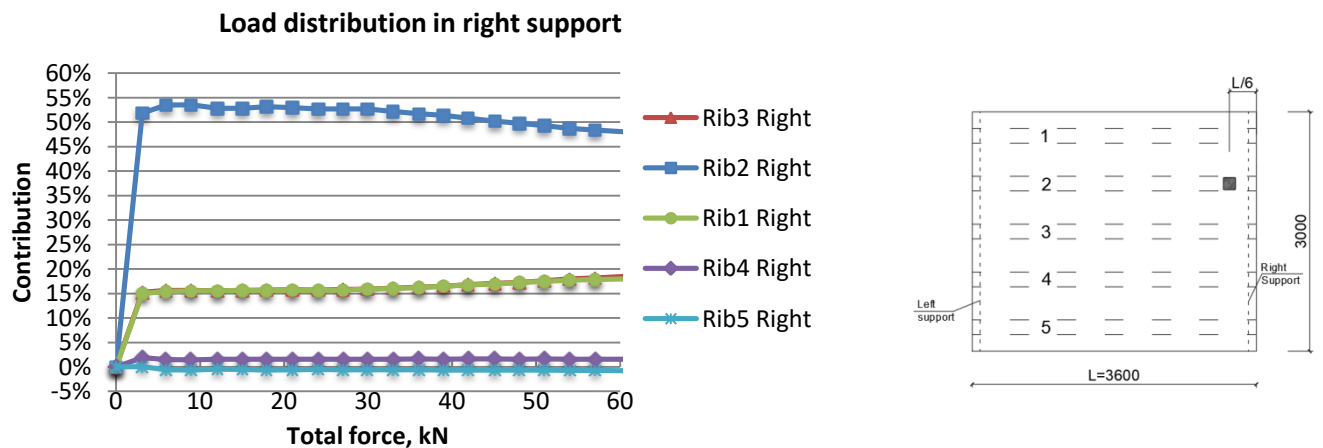


Figure 6.10 Distribution of concentrated load in the right support of each rib (L=3600mm with force on Rib 2 at L/6)

When the load is placed on Rib 3 at the one-sixth of the span, the contribution of Rib 3 varies from 58% to 52% in a range 5-60kN of total load and is distinctly higher compared to reaction forces in other ribs. The contribution of Rib 2 remains almost constant and equals 21%. The reaction force in Rib 1 is 1%; Rib 1 hardly participates in spreading the concentrated load, and, therefore, its contribution can be neglected. The reaction forces in right support that is close to the applied load account for 85% of the total load, and the left support carries 15% of the total load. This proportion 85%-15% holds unchanged.

When the load is placed on Rib 2 at the one-sixth of the span, the contribution of Rib 1 – Rib 5 stays more or less the same in a range 5-30kN with Rib 2 is loaded with 58% of total load. In a range 30-60kN reaction force in Rib 2 gradually decreases from 58% to 52%, while reaction forces in Rib 1 and Rib 3 are equal, slowly increasing from 21% to 23%. The reaction force in Rib 1 equals 3% of the total load in a range 5-60kN. The concentrated load on Rib 2 results in tensile reaction force in Rib 5 which amounts for 2%. The distribution of reaction force in right support of a rib tracks the form of total reaction force distribution in ribs; the proportion 85%-15% can be again noticed.

6.3 Composite slab ComFlor210: span 5.4m

6.3.1 Concentrated load at $L_{span}/2$

The concentrated load of 60kN magnitude is placed at the half span length, which equals 2.7m, on the middle Rib 3 and adjacent Rib 2 alternately. The resulting distribution of total reaction force in each rib in relation to the total applied load that increases from 0 to 60kN is presented in Figure 6.11 and Figure 6.12.

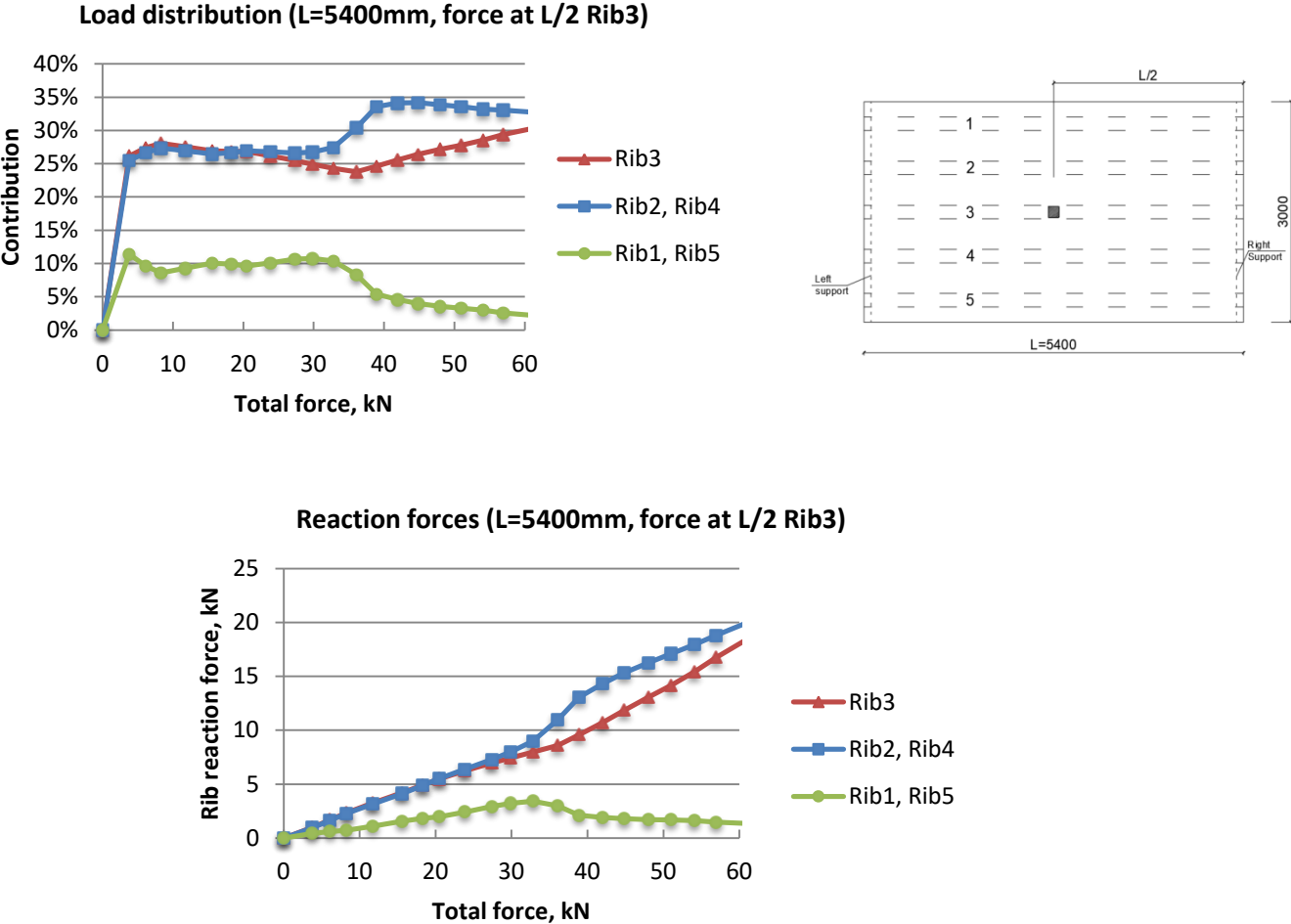


Figure 6.11 Distribution of concentrated load per rib (top figure) and reaction forces (bottom figure) in the composite slab L=5400mm with force on Rib 3 at L/2

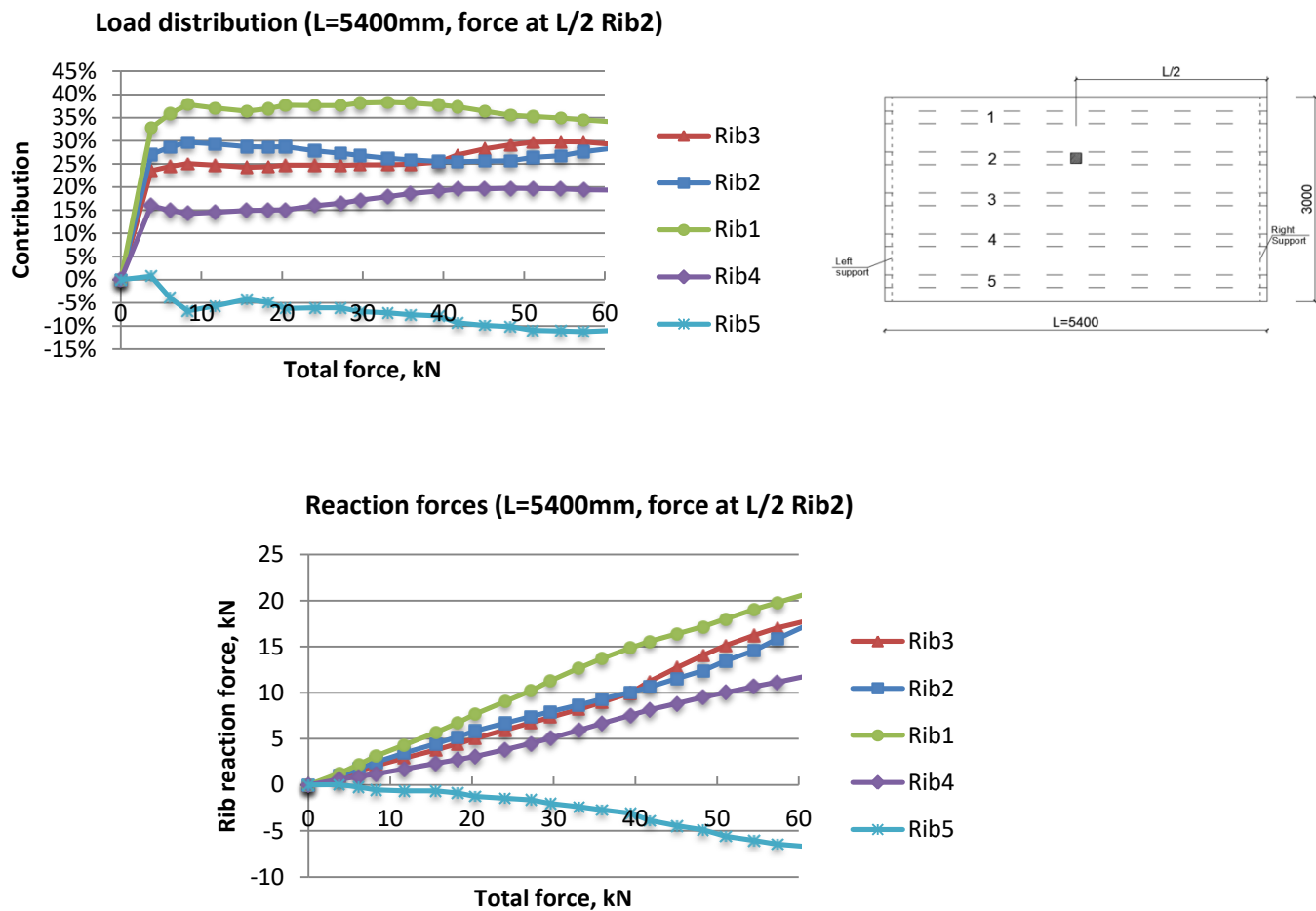


Figure 6.12 Distribution of concentrated load per rib (top figure) and reaction forces (bottom figure) in the composite slab L=5400mm with force on Rib 2 at L/2

Figure 6.11 displays that contribution of Rib 3 and Rib 2 is the same up to 30kN total load, after that contribution of Rib 2 increases when compared to Rib 3; though, both ribs show the tendency to resist more force when applied load grows. The contribution of outer Rib 1 is about 10% up to 30kN total load, and then the contribution of Rib 1 drops rapidly to 2% at 60kN total load.

Figure 6.12 shows that contribution of all five ribs stays more or less constant in a range 5-60kN total load. Reaction forces in Rib 2 and Rib 3 are almost identical; while reaction force in Rib 1 is higher because Rib 1 is unsupported along its long edge and less stiff, and, therefore, it deforms noticeably and adsorbs more load. The load on Rib 2 results in uplift of the farthest corner of the slab and tensile reaction force in Rib 5; this explains why the contribution of Rib 5 has opposite sign, unlike other four ribs.

6.3.2 Concentrated load at $L_{span}/4$

The concentrated load of 60kN magnitude is placed at the quarter of a span on the middle Rib 3 and adjacent Rib 2. The resulting distribution of total reaction force in each rib in relation to the total applied load is displayed in Figure 6.13 and Figure 6.15. Due to unsymmetrical load application, the reaction forces in right and left supports of the composite slab are not equal. Therefore, distribution in the right support closest to the applied load is also given in Figure 6.14 and Figure 6.16.

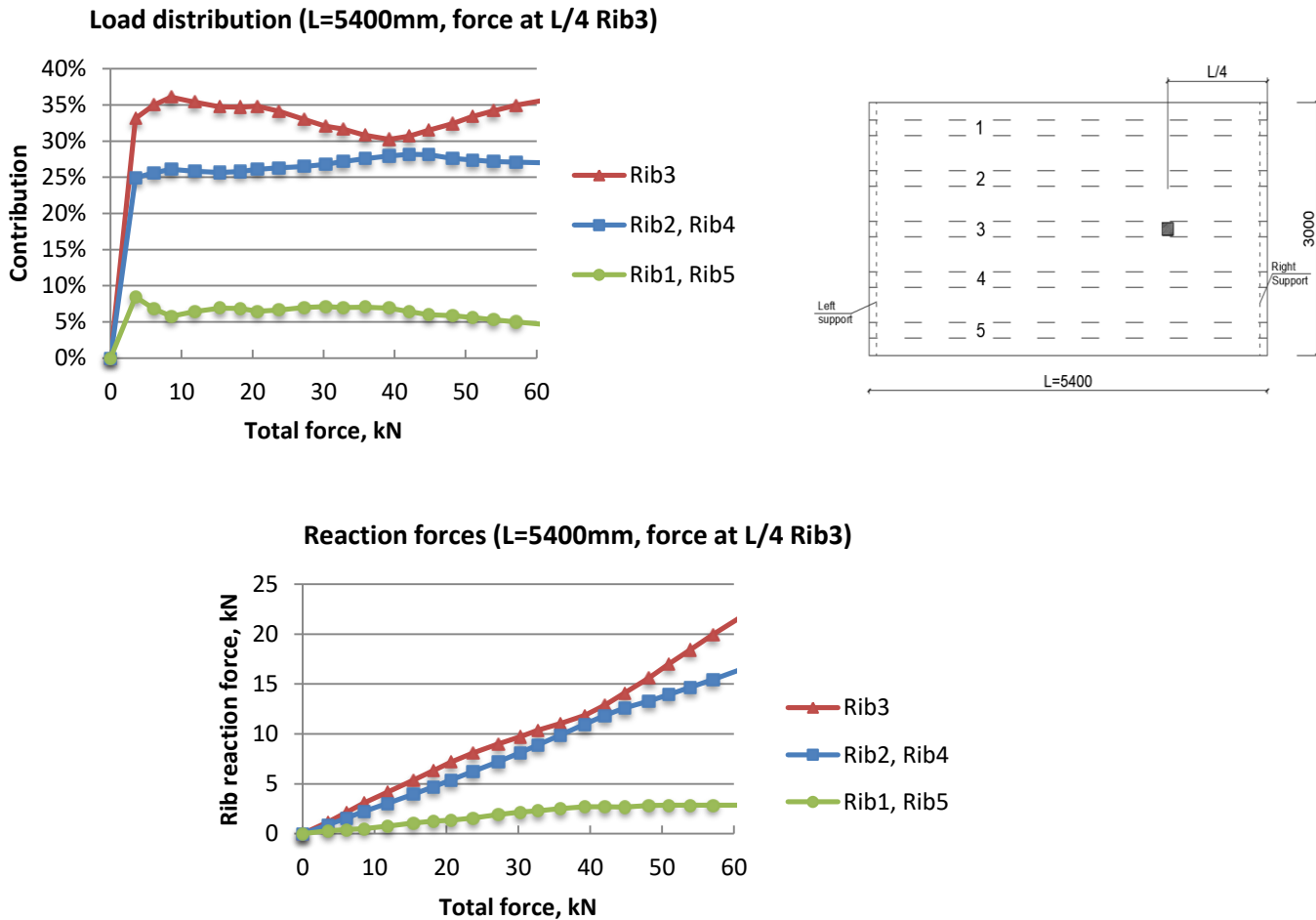


Figure 6.13 Distribution of concentrated load per rib (top figure) and reaction forces (bottom figure) in the composite slab L=5400mm with force on Rib 3 at L/4

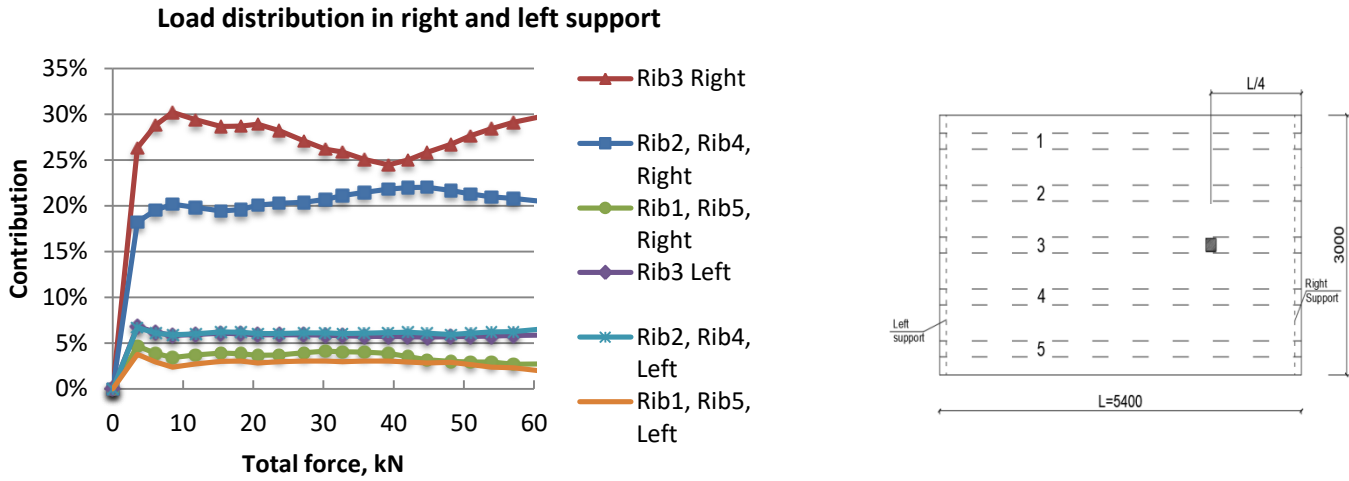


Figure 6.14 Distribution of concentrated load in right and left support of each rib (L=5400mm with force on Rib 3 at L/4)

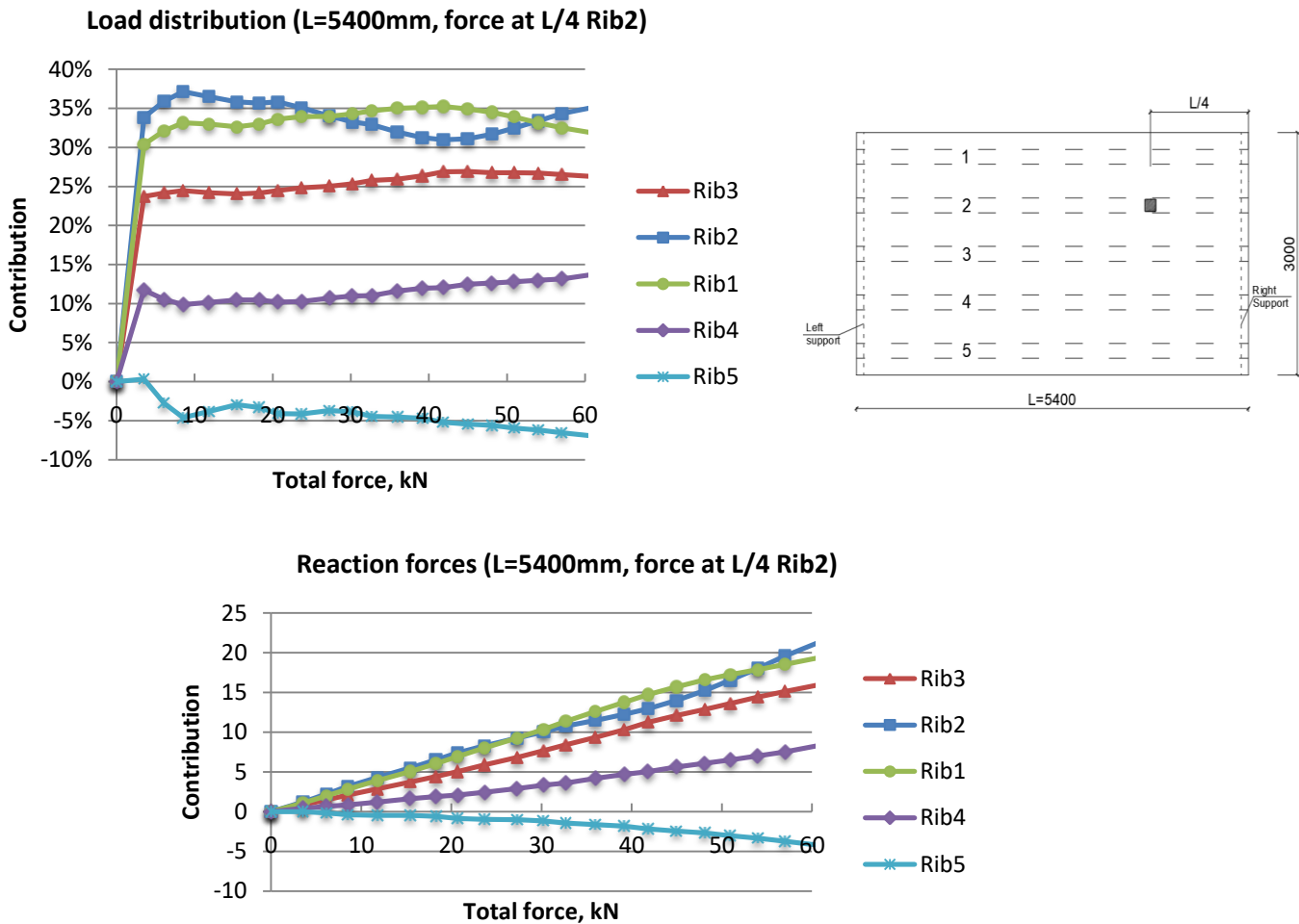


Figure 6.15 Distribution of concentrated load per rib (top figure) and reaction forces (bottom figure) in the composite slab L=5400mm with force on Rib 2 at L/4

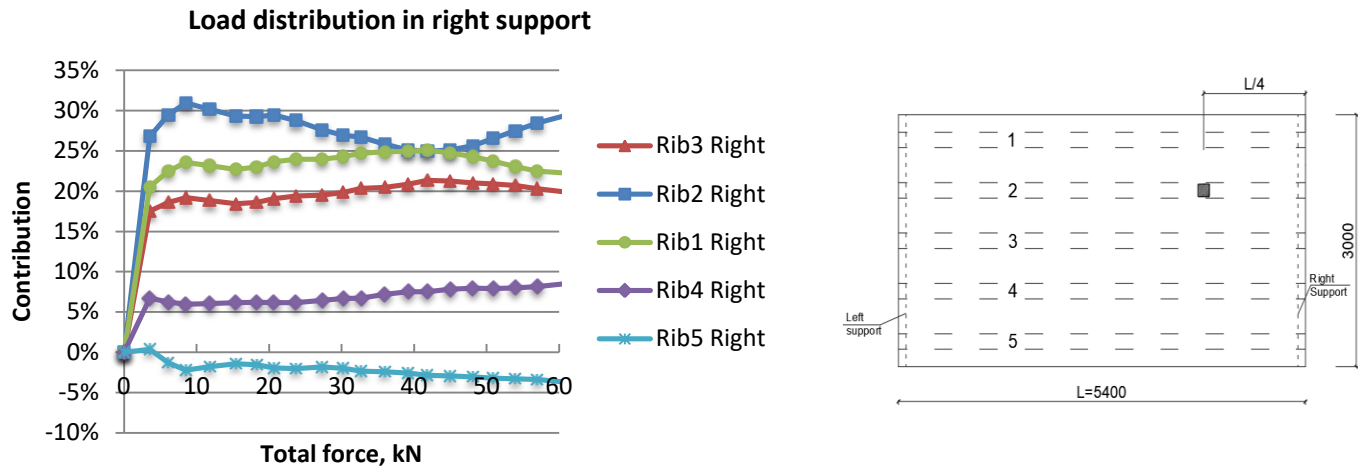


Figure 6.16 Distribution of concentrated load in the right support of each rib (L=5400mm with force on Rib 2 at L/4)

When the load is placed on Rib 3 at the quarter of a span, the contribution of Rib 3 is the highest among other ribs resulting in 35% of total force; the contribution of Rib 1 is about 5%. Most of the load is, then, carried by Rib 3 and Rib 2 (Figure 6.13). The reaction forces in right support that is near to load application account for 76% of the total load and the left support carries 24% of the total load. Additionally, this proportion 76%-24% of support reaction force distribution holds unchanged through the whole analysis.

In a case with the load placed on Rib 2 at the quarter of a span the contribution of Rib 1 – Rib 4 stays more or less unaltered in a range 5-60kN with Rib 1 and Rib 2 being loaded the most with 35% of total load each; while the contribution of Rib 4 is below 10%. The concentrated load on Rib 2 leads to an uplift of the farthest corner of the slab and tensile reaction force in Rib 5; this is why the Rib 5 contribution has reverse sign unlike other four ribs in Figure 6.15. The distribution of reaction force in right support of each rib follows the pattern of total reaction force distribution in ribs; the proportion 76%-24% with 76% being the total reaction force in right support of composite slab once again can be noticed (Figure 6.16).

6.3.3 Concentrated load at $L_{span}/6$

The concentrated load of 60kN is positioned at the one-sixth of the span on the Rib 3 and Rib 2. The resulting distributions of total reaction force in each rib in relation to the total applied force are shown in Figure 6.17 and Figure 6.19. Due to the unsymmetrical position of the concentrated force in relation to the span length the reaction forces in right and left supports of the composite slab are not equal. Therefore, distributions in the right support closest to the applied load are also presented in Figure 6.18 and Figure 6.20.

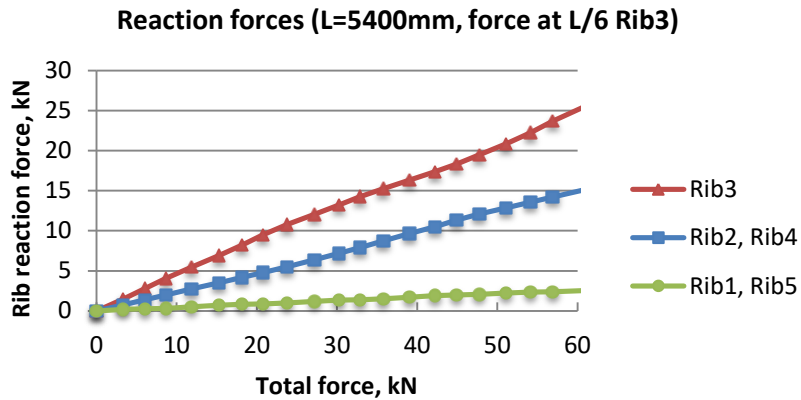
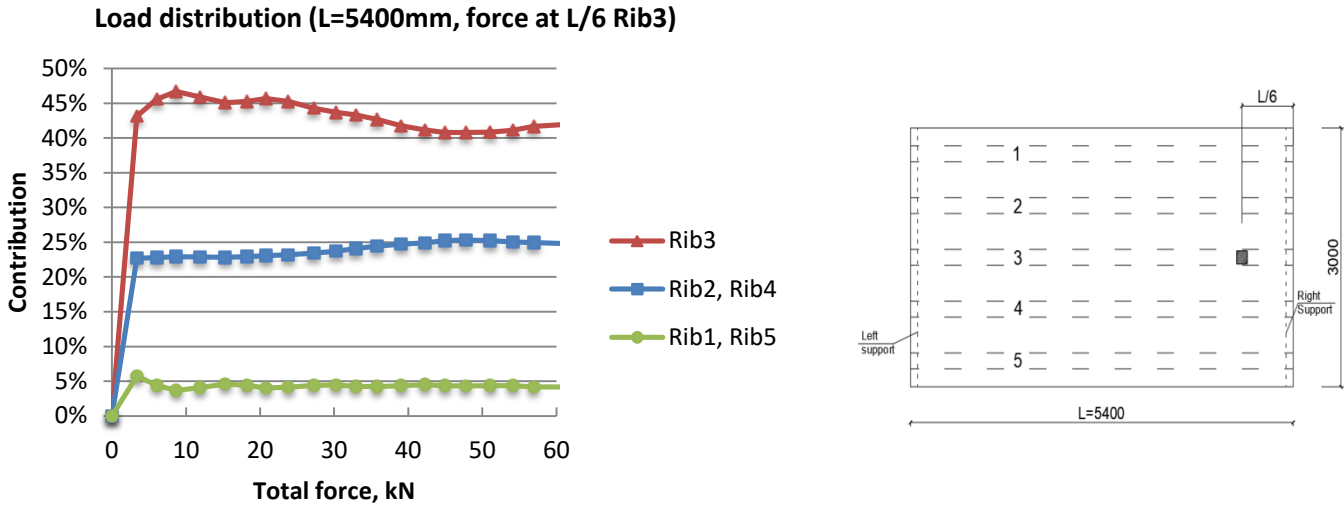


Figure 6.17 Distribution of concentrated load per rib (top figure) and reaction forces (bottom figure) in the composite slab L=5400mm with force on Rib 3 at L/6

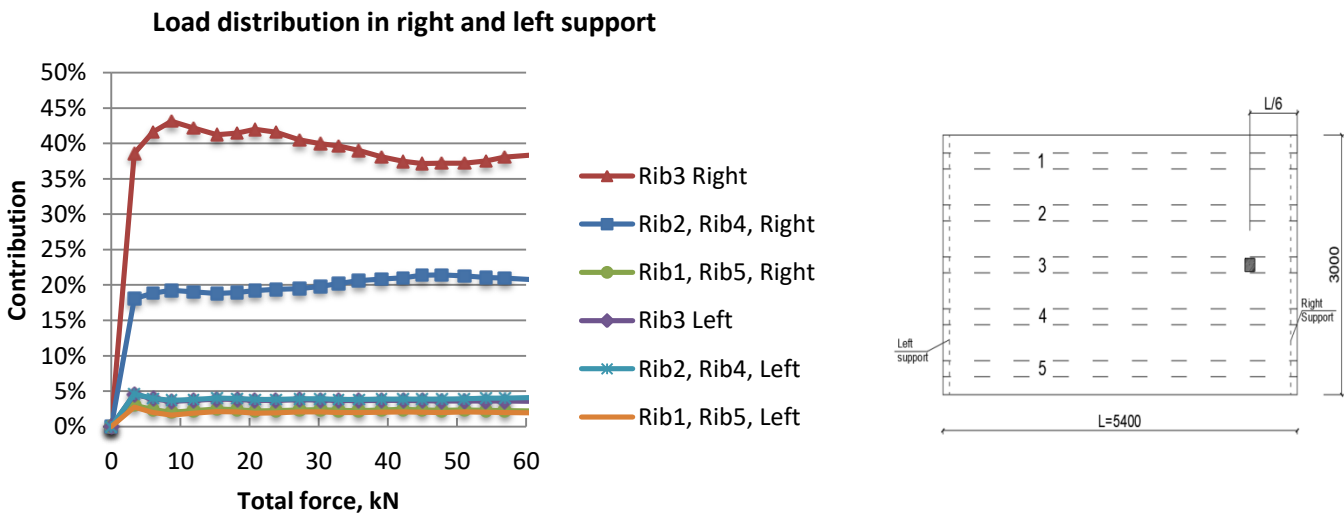


Figure 6.18 Distribution of concentrated load in right and left support of each rib (L=5400mm with force on Rib 3 at L/6)

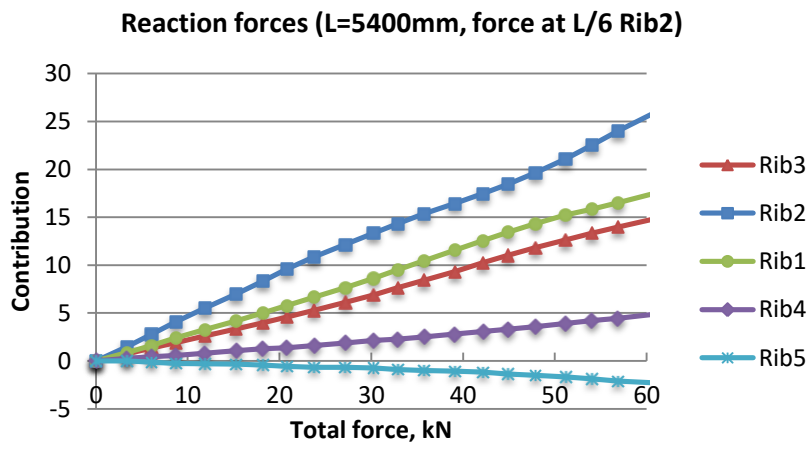
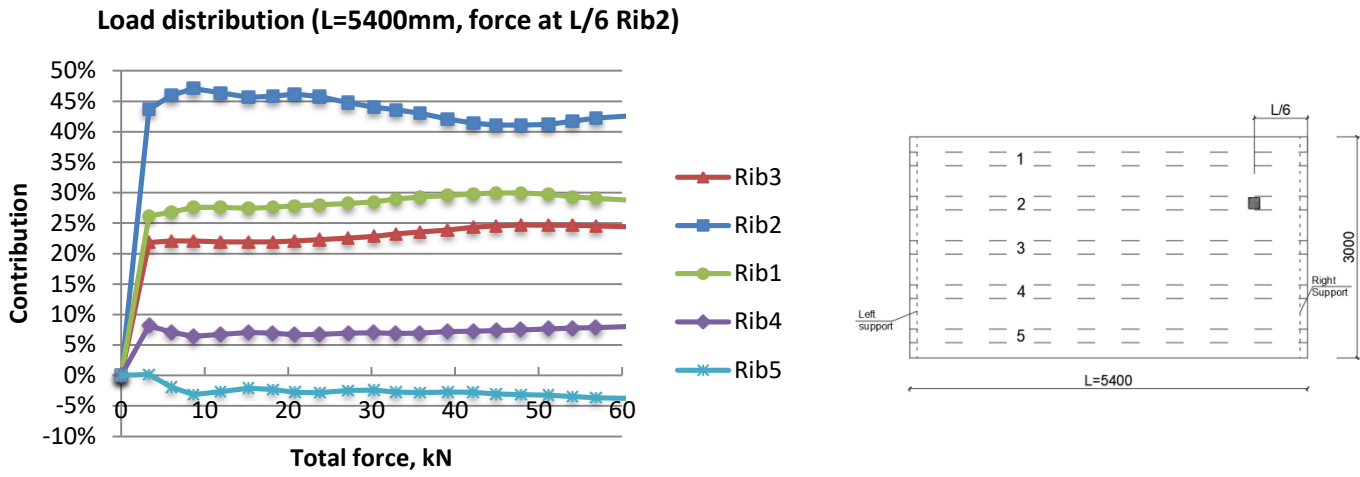


Figure 6.19 Distribution of concentrated load per rib (top figure) and reaction forces (bottom figure) in the composite slab (L=5400mm with force on Rib 2 at L/6)

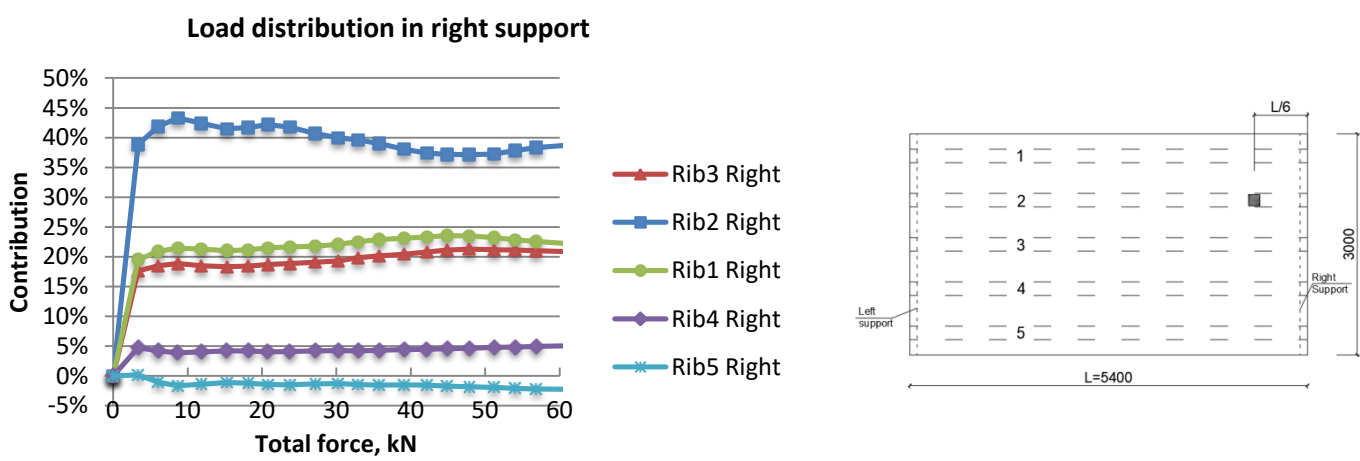


Figure 6.20 Distribution of concentrated load in the right support of each rib (L=5400mm with force on Rib 2 at L/6)

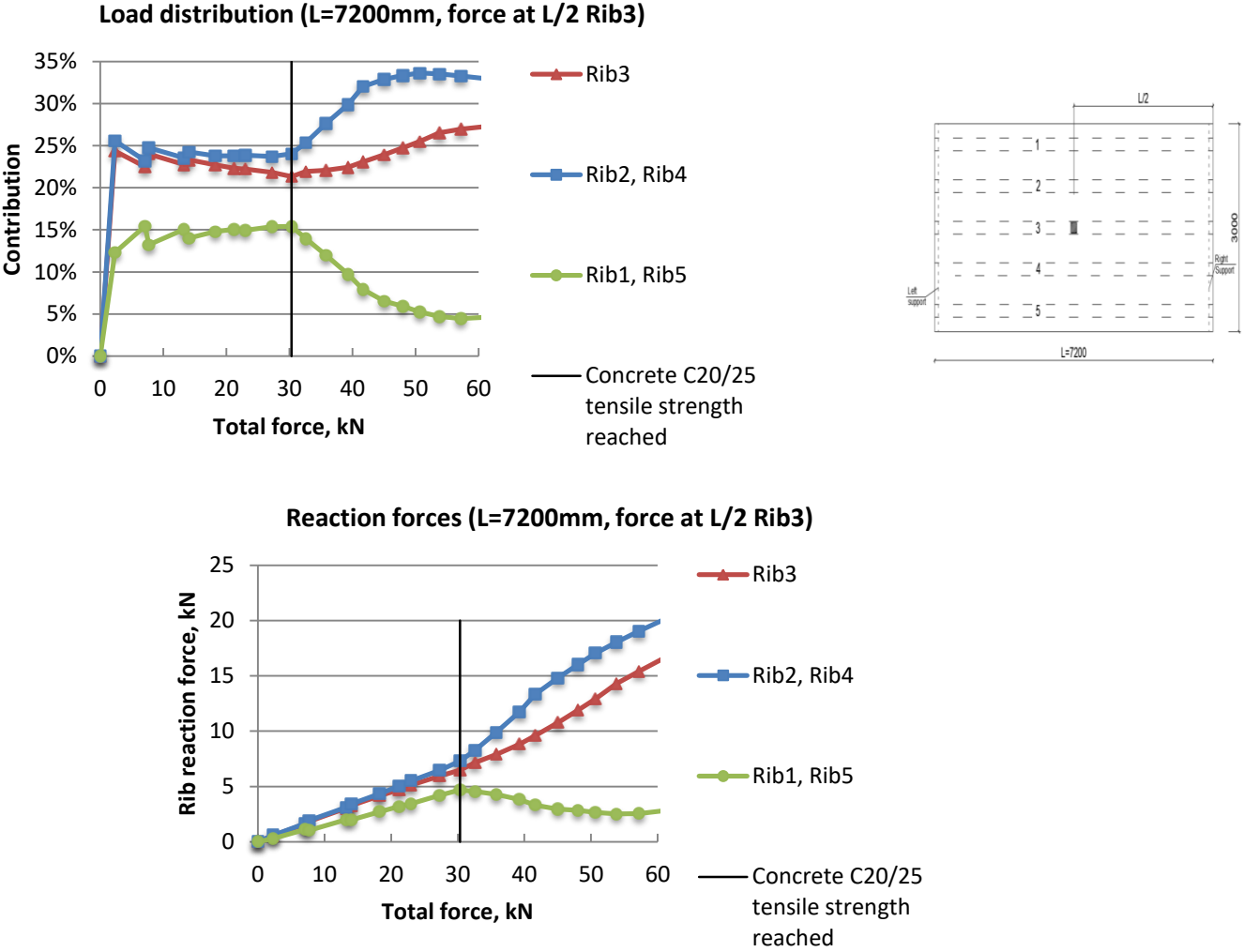
When the load is located on Rib 3 at the one-sixth of the span, the contribution of Rib 3 varies from 45% to 40% in a range 5-60kN of the total load and is noticeably higher compared to reaction forces in other ribs. Contributions of Rib 2 and Rib 1 remain nearly constant through the whole analysis and equal 25% and 5% respectively (Figure 6.17). The reaction forces in right support that is close to the applied load account for 85% of the total load, and the left support carries 15% of the total load. This proportion 85%-15% has remained unchanged for the whole analysis.

In a case when the load is placed on Rib 2 at the one-sixth of the span the contribution of Rib 1 – Rib 4 stays somewhat constant in a range 5-60kN. Loaded Rib 2 carries more than 40% of the total load; contributions of Rib 3 and Rib 1 are about 23% and 29% respectively, and Rib 1 amounts for 7% of total load (Figure 6.19). Once again the asymmetric position of the concentrated load causes uplift of the farthest corner of the slab and tensile reaction force in Rib 5. The sum of reaction forces in right supports of composite slab equals 85% of the total load; the proportion 85%-15% holds constant during the finite element analysis.

6.4 Composite slab ComFlor210: span 7.2m

6.4.1 Concentrated load at $L_{span}/2$

The concentrated load of 60kN magnitude is placed at the half span length, which equals 2.7m, on the middle Rib 3 and adjacent Rib 2 alternately. The resulting distribution of total reaction force in each rib in relation to the total applied load that increases from 0 to 60kN is presented in Figure 6.21 and Figure 6.22. The



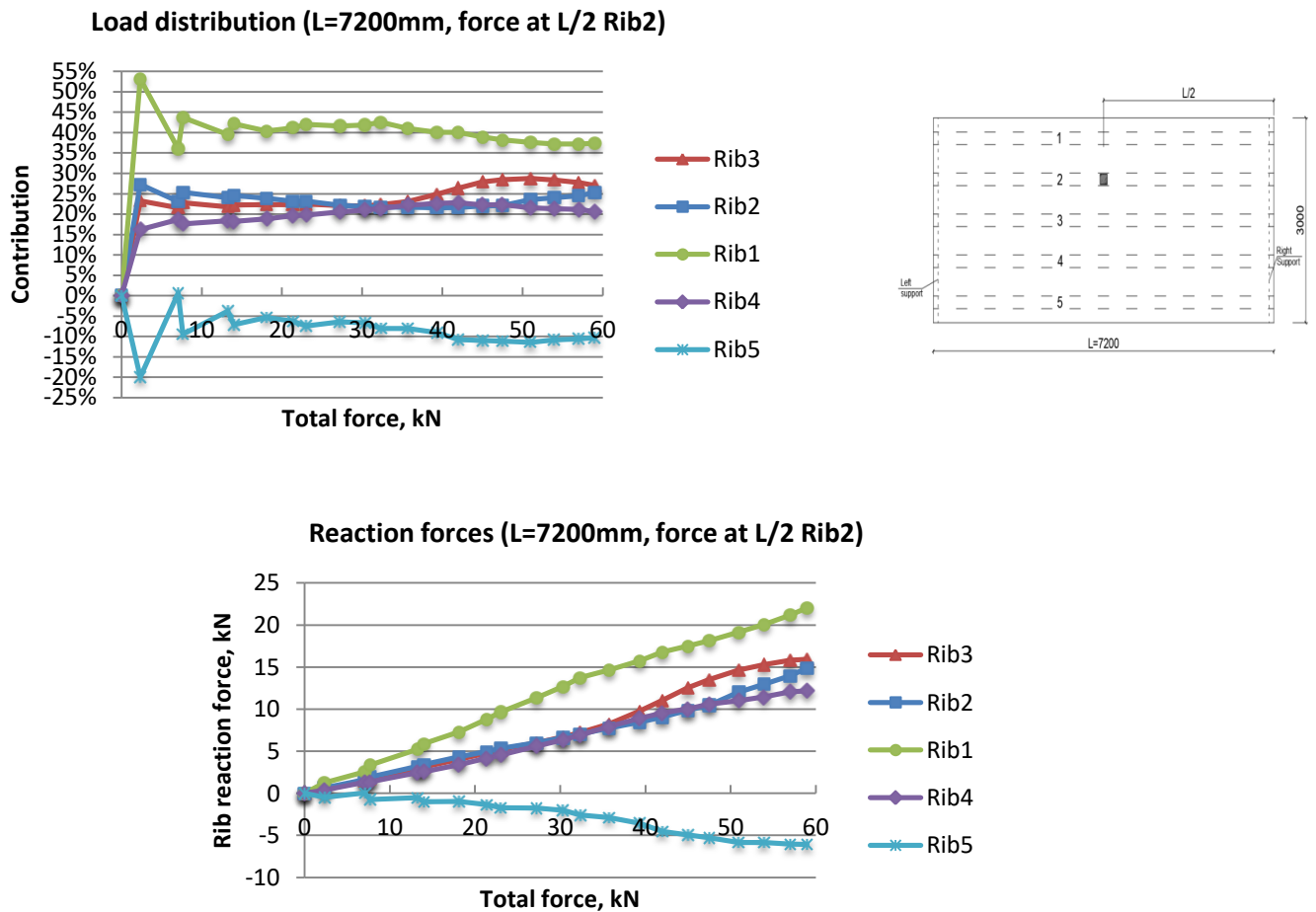


Figure 6.22 Distribution of concentrated load per rib (top figure) and reaction forces (bottom figure) in the composite slab L=7200mm with force on Rib 2 at L/2

Figure 6.21 shows that the load distribution in the slab with length 7200mm is different from a slab with 3600mm and 5400mm length. First, the zigzag peaks in reaction force distribution of Rib 1 – Rib 3 can be seen in a range 2-15kN; this did not happen in other slabs. Second, the drastic change in reaction force distribution occurs just after concrete reaches tensile strength at 30kN. This change can be possibly induced by the crack formation in a slab that causes significant redistribution of concentrated force. This explanation followed from the examination of strain and stress distributions in different parts of the composite slab at 30kN: no yielding of steel elements was observed; concrete reached its tensile capacity which is 2.2MPa. The first figure below shows the stress distribution S33 in the concrete part resulting from FEA at approximately 30kN (Figure 6.23). It can be noticed that while the stresses in other ribs are just about to reach 2.2MPa the stress contour in the bottom of the middle rib has yellow spots with stress below 2.2MPa, indicating that the concrete in this locations reached already the failure stress and then experiences softening; and when concrete stress passed f_{ctm} , it is a sign of crack formation. Another figure shows the contour plot of DAMAGET (tensile damage) parameter at 30kN; this parameter visualizes the damage of concrete in tension when concrete is modeled with concrete damaged plasticity model in Abaqus. The DAMAGET parameter is a simplified way to represent the crack pattern in concrete under loading. In the figure, the most damage (red lines) can be seen at the middle of rib 3; this pattern resembles the flexural cracks which are typical for a structure in bending. All this made me think that the cracking of rib 3 causes the abrupt change in reaction force distribution in all ribs visible in Figure 6.21.

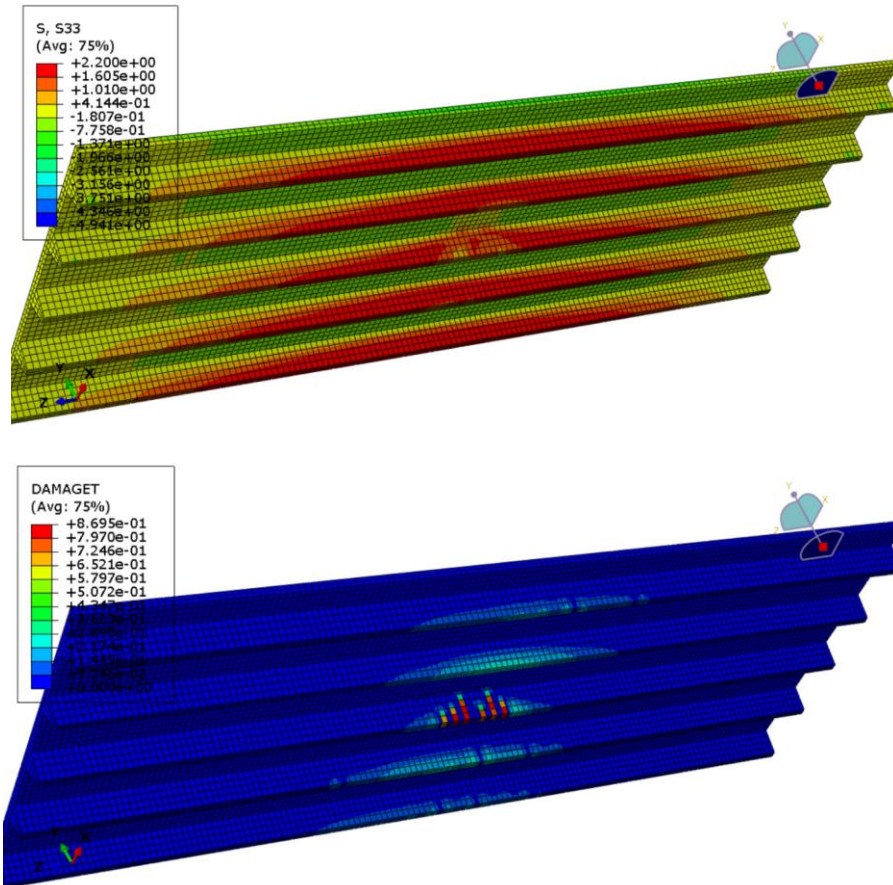


Figure 6.23 Stress distribution S33 in concrete at 30kN (top figure); concrete tension damage DAMAGET at 30kN (bottom figure)

The contribution of Rib 2 is 24% in a range 15-30kN and then increases up to 33%. The contribution of Rib 3 equals 22% in a range 15-30kN and after that goes up to 27%. Meanwhile reaction force in Rib 1 drops from 15% at 30kN total load to 5% at the end of loading.

Figure 6.22 displays that contribution of all five ribs varies little in a range 15-60kN total load. The contribution of Rib 1 in this range is about 40%, while contributions of Rib 2 – Rib 4 are less than 30% each. In a range 2-15kN the zigzag peaks in reaction force in Rib 1 and Rib 5 are visible; especially the first peak is of interest because the force in Rib 1 decreases from 53% to 36% and, in the meantime, the force in Rib 5 changes from -20% to 1%. Additionally, reaction force in Rib 1 is higher because Rib 1 is unsupported along its long edge and, apparently, less stiff, and, therefore, it deforms noticeably adsorbing more load. The load on Rib 2 causes uplift of the farthest corner of the slab and tensile reaction force in Rib 5; this explains why the contribution of Rib 5 has opposite sign, unlike other four ribs.

6.4.2 Concentrated load at $L_{span}/4$

The concentrated load of 60kN magnitude is placed at the quarter of a span on the middle Rib 3 and adjacent Rib 2. The resulting distribution of total reaction force in each rib in relation to the total applied load is displayed in Figure 6.24 and Figure 6.26. Due to unsymmetrical load application, the reaction forces in right and left supports of the composite slab are not equal. Therefore, distribution in the right support closest to the applied load is also given in Figure 6.25 and Figure 6.27.

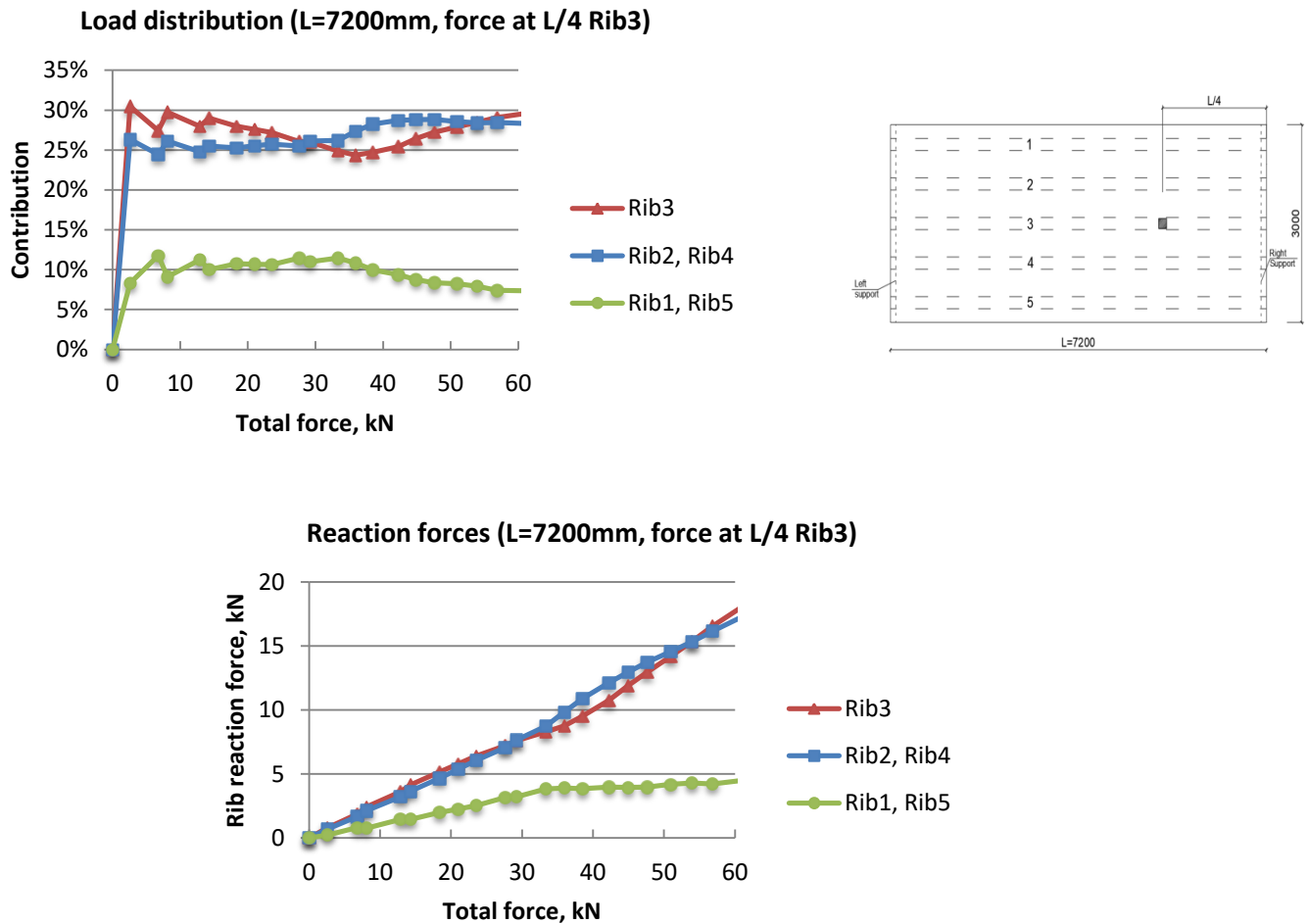


Figure 6.24 Distribution of concentrated load per rib (top figure) and reaction forces (bottom figure) in the composite slab $L=7200$ mm with force on Rib 3 at $L/4$

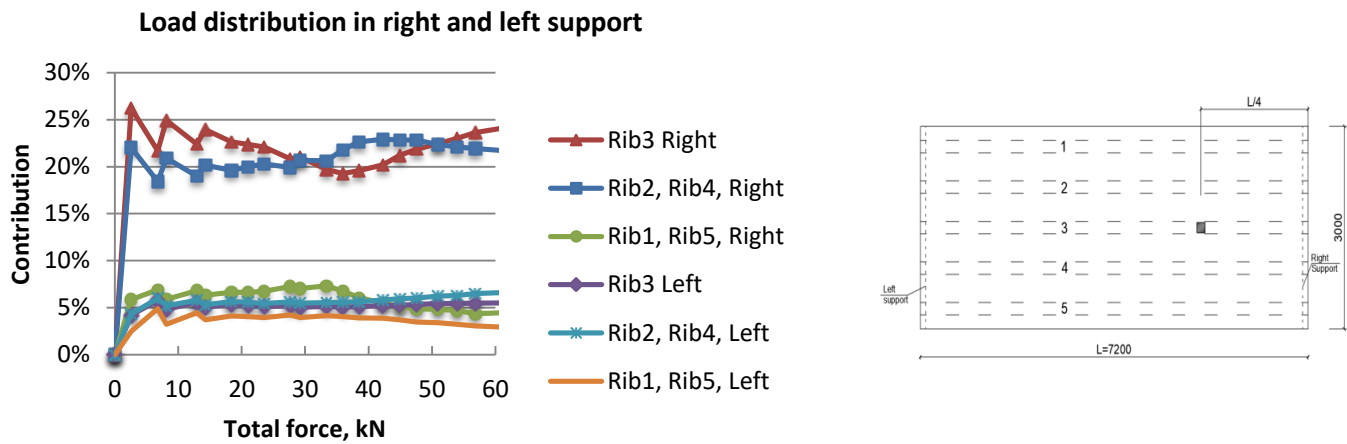


Figure 6.25 Distribution of concentrated load in right and left support of each rib (L=7200mm with force on Rib 3 at L/4)

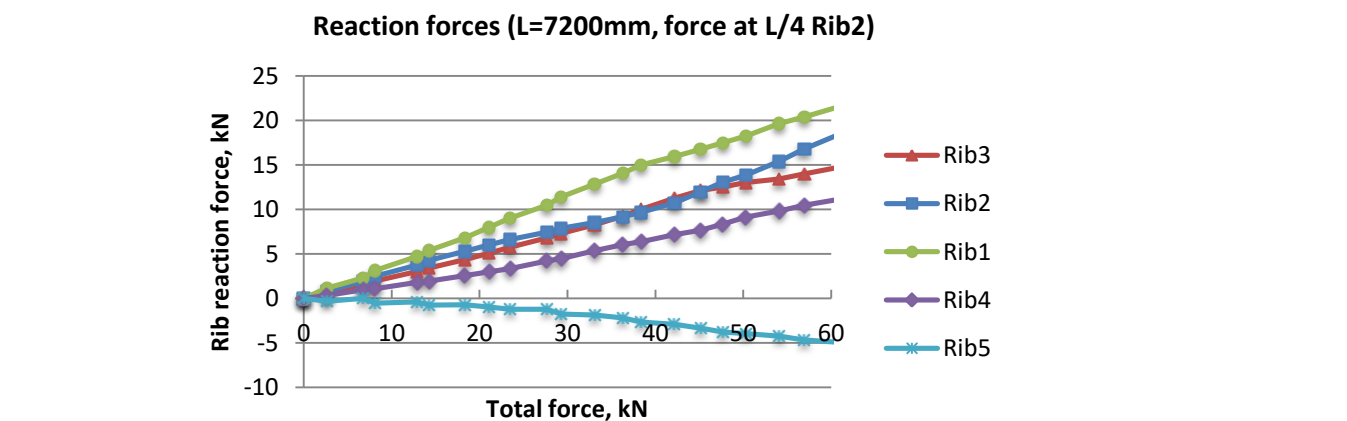
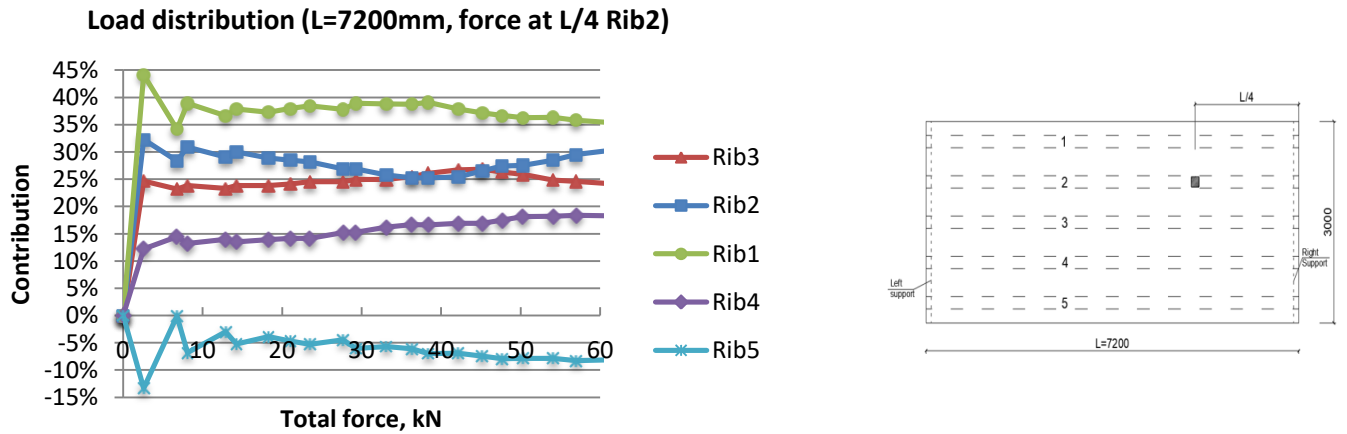


Figure 6.26 Distribution of concentrated load per rib (top figure) and reaction forces (bottom figure) in the composite slab L=7200mm with force on Rib 2 at L/4

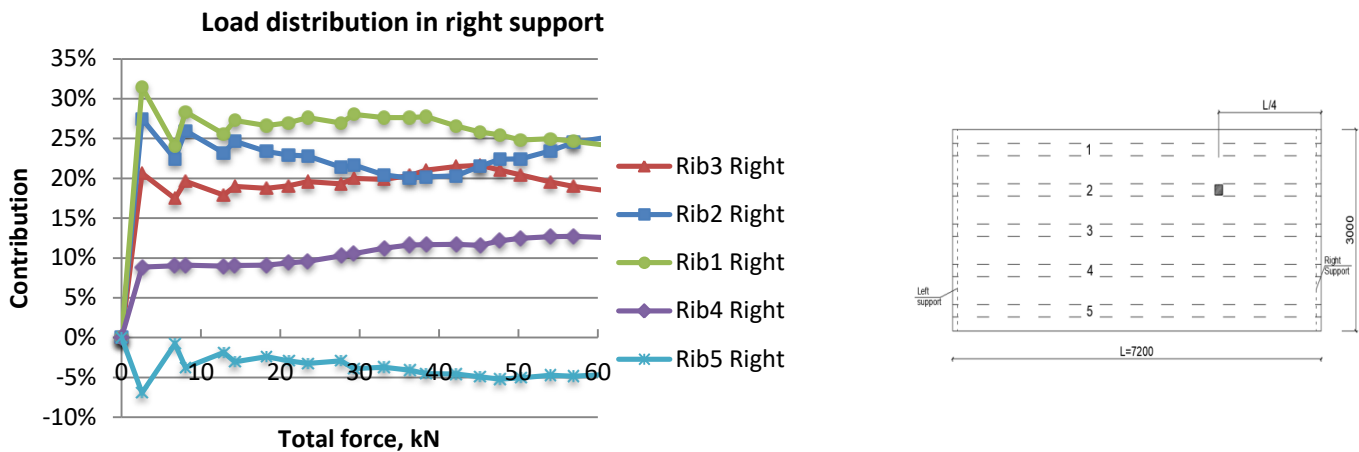


Figure 6.27 Distribution of concentrated load in the right support of each rib (L=7200mm with force on Rib 2 at L/4)

When the load is placed on Rib 3 at the quarter of a span, the zigzag peaks in reaction force distribution of Rib 1 – Rib 3 once again occur in a range 2-15kN total load. However, the change in reaction force distribution at 30kN is not as prominent as in a case when the load was placed on the middle rib at the half span length. The contribution of Rib 2 is 26% in a range 15-30kN and after that becomes 28%. The contribution of Rib 3 equals 25% in a range 15-30kN and then rises to 30%. Reaction force in Rib 1 changes from 11% at 30kN total load to 7% at the end of loading. Therefore, all five ribs participate in spreading the load.

The reaction forces in right support that is near to load application account for 76% of the total load and the left support carries 24% of the total load. The proportion of 76%-24% of support reaction force distribution holds unchanged (Figure 6.25).

In a case with the load placed on Rib 2 at the quarter of a span the contribution of Rib 1 – Rib 5 stays somewhat unaltered in a range 15-60kN with Rib 1 being loaded the most with average 38% of total load. Contributions of Rib 2 – Rib 4 stay less than 30%. In a range 2-15kN the zigzag peaks in reaction force in Rib 1 and Rib 5 are present; the first peak is where the force in Rib 1 decreases from 44% to 34% and the force in Rib 5 varies from -13% to 0%. The position of concentrated load on Rib 2 results in uplift of the farthest corner of the slab and tensile reaction force in Rib 5; this is a reason why the contribution of Rib 5 has reverse sign unlike other four ribs in Figure 6.26. The distribution of reaction force in right support generally abides the pattern of total reaction force distribution in ribs but with smaller percentages; the proportion 76%-24% keeps unchanged.

6.4.3 Concentrated load at $L_{span}/6$

The concentrated load of 60kN is positioned at the one-sixth of the span on the Rib 3 and Rib 2. The resulting distributions of total reaction force in each rib in relation to the total applied force are shown in Figure 6.28 and Figure 6.30. Because of unsymmetrical load application, the reaction forces in right and left supports of the composite slab are not equal. Thus, distributions in the right support closest to the applied load are also given in Figure 6.29 and Figure 6.31.

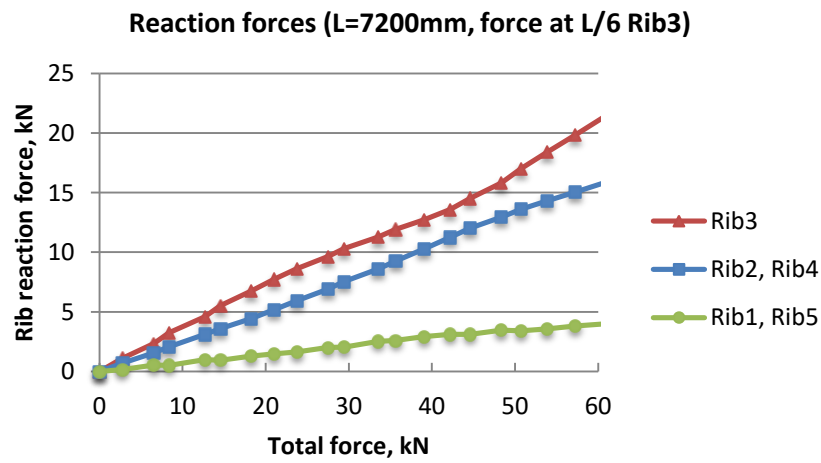
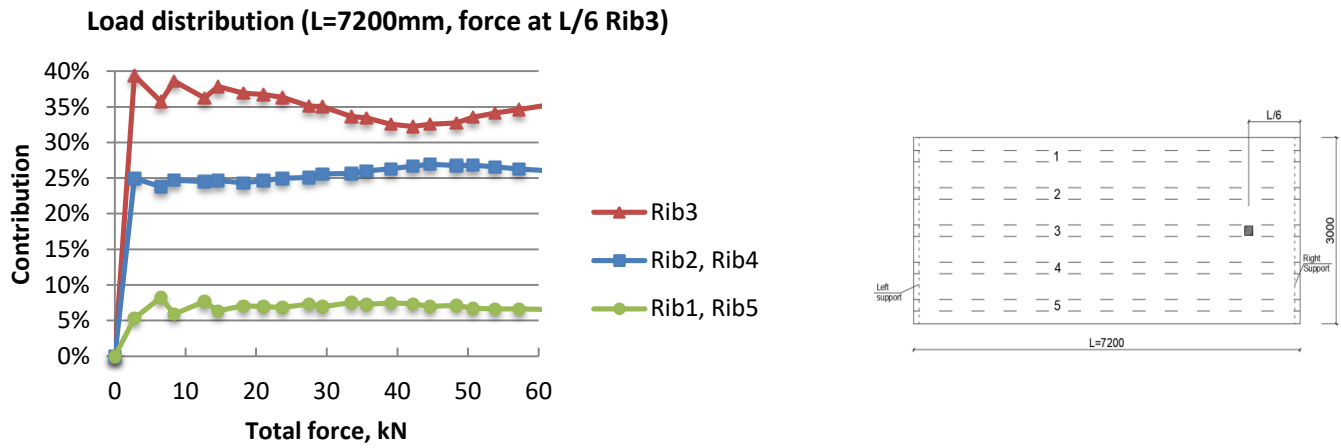


Figure 6.28 Distribution of concentrated load per rib (top figure) and reaction forces (bottom figure) in the composite slab L=7200mm with force on Rib 3 at L/6

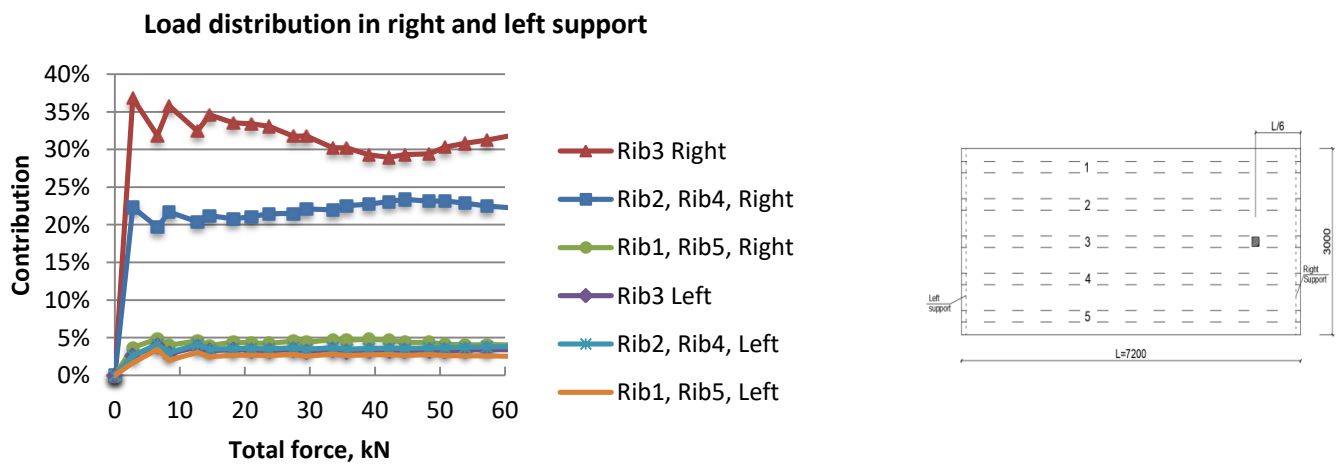


Figure 6.29 Distribution of concentrated load in right and left support of each rib (L=7200mm with force on Rib 3 at L/6)

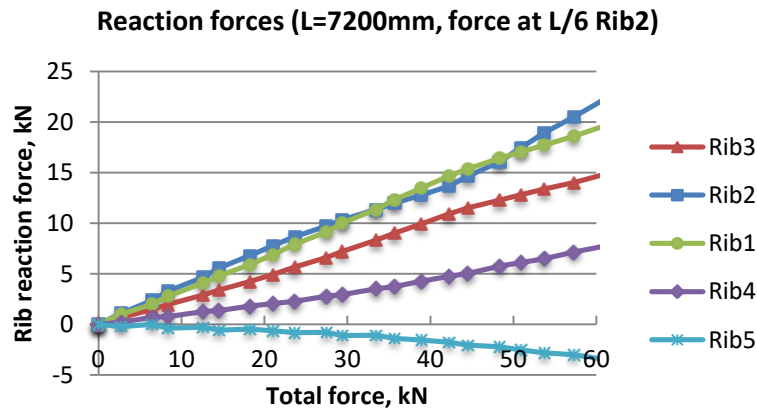
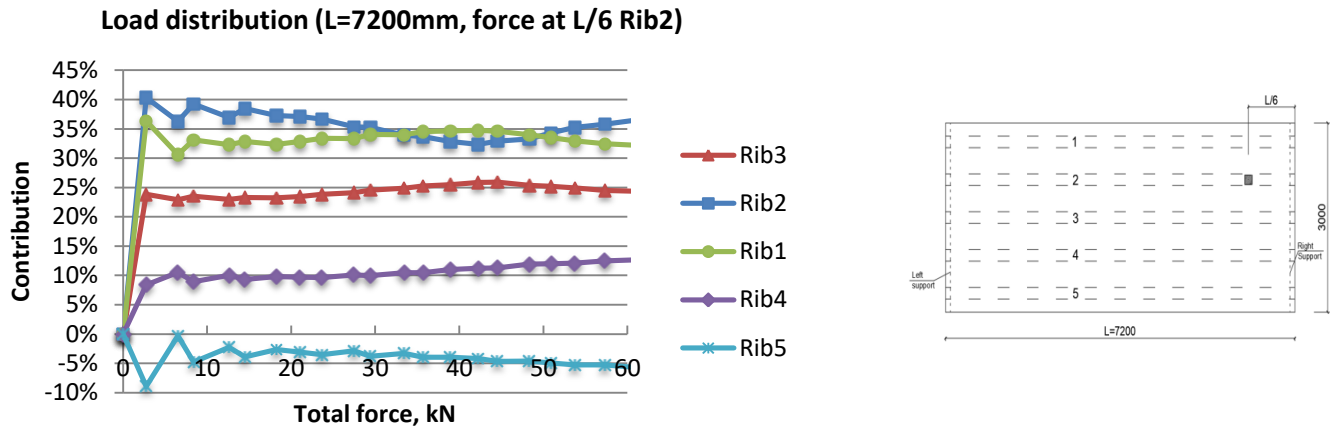


Figure 6.30 Distribution of concentrated load per rib (top figure) and reaction forces (bottom figure) in the composite slab L=7200mm with force on Rib 2 at L/6

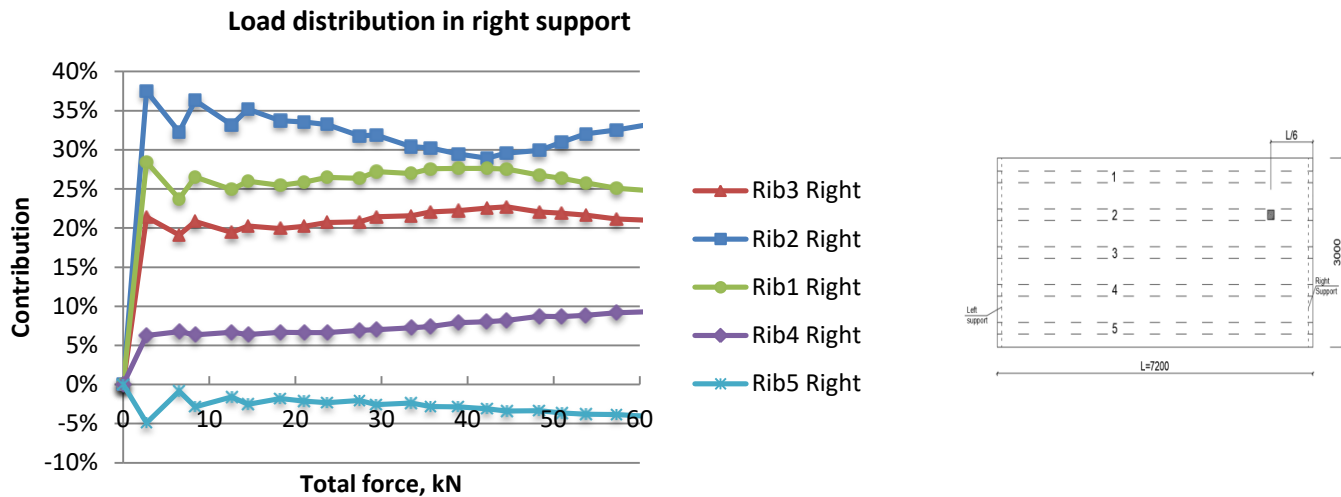


Figure 6.31 Distribution of concentrated load in the right support of each rib (L=7200mm with force on Rib 2 at L/6)

When the load is located on Rib 3 at the one-sixth of the span, the reaction force in Rib 3 varies from 39% to 33% in a range 15-60kN of the total load and is much higher in comparison to reaction forces in other ribs. Contributions of Rib 2 and Rib 1 are more or less constant in a range 15-60kN and equal 26% and 7% respectively (Figure 6.28). The reaction forces in the right support amount for 85% of the total load and the left support carries 15% of the total load. This proportion 85%-15% keeps unchanged through the whole analysis.

In a case when the load is placed on Rib 2 at the one-sixth of the span the reaction forces in Rib 1, Rib 3 and Rib 4 remain unaltered in a range 15-60kN. Rib 2 carries most of the load with average 37% of total load. In a range 15-60kN total load the reaction force in Rib 1 amounts for 34%, Rib 3 carries 24% and Rib 4 bears 11%. In a range 2-15kN the zigzag peaks in reaction force in Rib 2 and Rib 5 are noticeable; the first peak occurs when the force in Rib 2 linearly decreases from 40% to 36% and the force in Rib 5 changes from -9% to 0%. The asymmetric position of concentrated load results in uplift of the farthest corner of the slab and tensile reaction force in Rib 5. The sum of reaction forces in right supports of composite slab equals 84% of the total load; the proportion 84%-16% keeps constant.

6.5 Composite slab ComFlor210: change in cross-section properties

The change in the cross-section of composite slab ComFlor210 is induced by variation in thickness and effective area of profiled steel sheeting and diameter of the reinforcement in the rib:

- The thickness of profiled steel sheeting - 1.0mm (default value is 1.25mm).
- The diameter of rib reinforcement – 12mm and 25mm (default value is 20mm).
- The effective area of steel sheeting.

The other cross-sectional properties of composite slab correspond to the slab with 5.4 span; concentrated force 60kN is applied on middle Rib 3 at the half span length.

6.5.1 Variation of profile steel sheeting thickness

The composite slab ComFlor210 by default had the thickness of steel sheeting 1.25mm. It can be also produced with the thickness 1.0mm. In Figure 6.32 a comparison is made between the load-deflection response of composite slab with 1.25mm and 1.0mm thickness of steel sheeting.

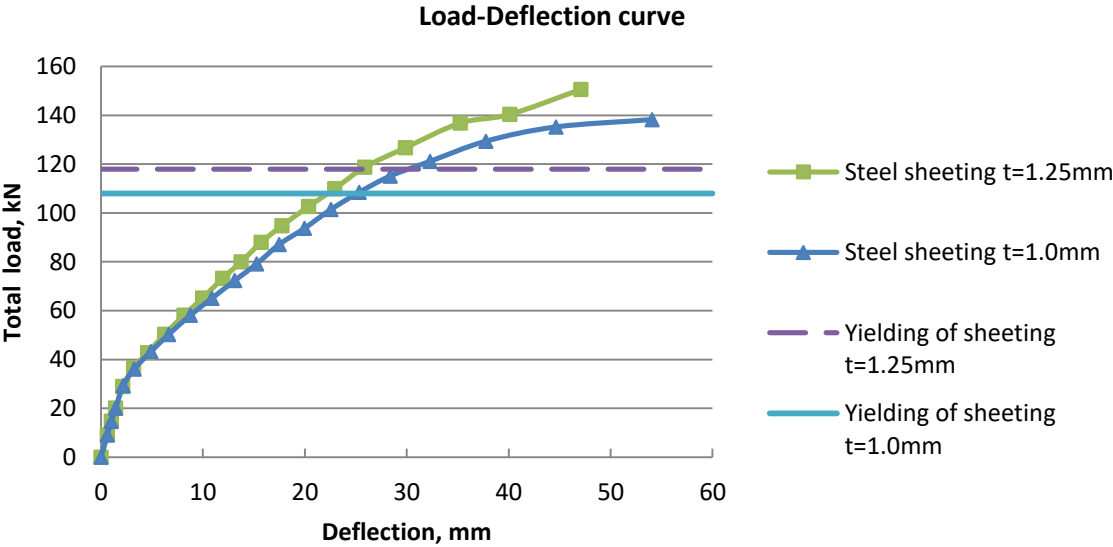


Figure 6.32 Load-deflection response of Rib 3 in composite slab ComFlor210 with steel sheeting thickness t=1.25mm and t=1.0mm

The load-deflection curves in Figure 6.32 are identical in a range 0-50kN meaning that the influence of steel sheeting thickness is insignificant for a slab in the elastic stage. With increasing the load, the response of a slab with 1.0mm thickness of steel sheeting becomes less stiff; additionally, the load, at which yielding of steel sheeting begins, decreases: steel sheeting with 1.0mm thickness yields at 108kN, while steel sheeting with 1.25mm thickness yields at approximately 118kN.

6.5.2 Variation of rib reinforcement

The composite slab ComFlor210 can be produced with a different cross-sectional area of rib reinforcement: diameter of steel rod can vary from 12mm to 25mm. The influence of rib reinforcement on composite slab behavior is revealed by examining slab with minimum and a

maximum diameter of rib reinforcement. Figure 6.33 displays the load-deflection response of composite slab ComFlor210 with 12mm, 20mm and 25mm diameter of rib reinforcement.

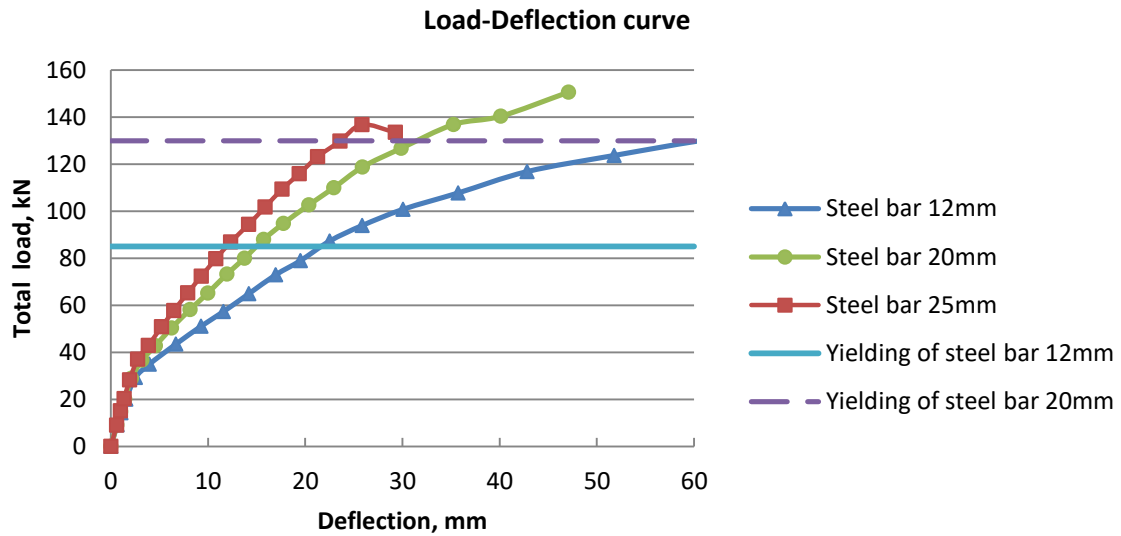


Figure 6.33 Load-deflection response of Rib 3 in composite slab ComFlor210 with a diameter of rib reinforcement 12mm, 20mm, and 25mm

From the figure above follows that with increasing the diameter of reinforcement in a rib the response of composite slab becomes stiffer. The load at which steel bar yields increases as well: steel bar 12mm yields at 85kN, while steel bar 20mm yields at approximately 130kN and yielding of steel bar 25mm does not occur even at maximum applied load 145kN.

6.5.3 Variation of the effective section of the steel sheeting

In the presented finite element model, the steel sheeting was modeled as a plain continuous element with constant thickness 1.25mm (see Section 1 in Table 6.2). In the engineering model, the steel sheeting was modeled as a combination of top and bottom flanges with different thicknesses (Section 2 in Table 6.2), and the effective area has been used in the followed calculations. It is of interest to check to what extent the presence and the size of the effective area of steel sheeting can influence the outcome of the finite element model.

Three configurations of the steel sheeting are compared:

- Section 1 – a flat continuous section with constant thickness 1.25mm and uniform yield stress (default in FEM).
- Section 2 – an effective area with the thickness of the top flange 1.25mm and the thickness of the bottom flange 2.5mm (default in engineering model), and uniform yield stress.
- Section 3 – an effective area with constant thickness 1.25mm and with varied yield stress: flat parts of the sheeting have a full yielding capacity ($f_y = 400\text{N/mm}^2$); the yielding capacity of the dimpled sheet (i.e. parts with indentations) is decreased by 50% ($0.5f_y = 200\text{N/mm}^2$). The folding reduces the yield stress of the sheeting due to the extra flexural deformations present in addition to the extensional deformations [9]. The 50% reduction in yield stress is an approximation; the exact value needs to be established by uniaxial tensile test on ComFlor210 sheeting.

Table 6.2 gives an overview of the geometry and properties of each section.

Table 6.2 Steel sheeting sections (per 600mm width)

	Section 1	Section 2	Section 3
Geometry			
Area A_{eff}, mm²	1210.2	559.25	1210.2
Yielding stress, N/mm²	$f_y = 400$	$f_y = 400$	$f_y = 400$ $0.5f_y = 200$
Remark on the section	Default in FEM. Uniform yield stress.	Default in the engineering model. Uniform yield stress.	Varied yield stress.

A comparison is made in Figure 6.34 between the load-deflection responses of the composite slab with different steel sheeting sections. From the figure follows that the responses of a composite slab with sections 1 and 3 are similar, while slab with section 2 is less stiff and less accurate in representing the slab behavior in a plastic part of the load-deflection curve. In the elastic stage (up to 60kN) all three sections can be used for determining the slab response because the difference between load-deflection curves is minor.

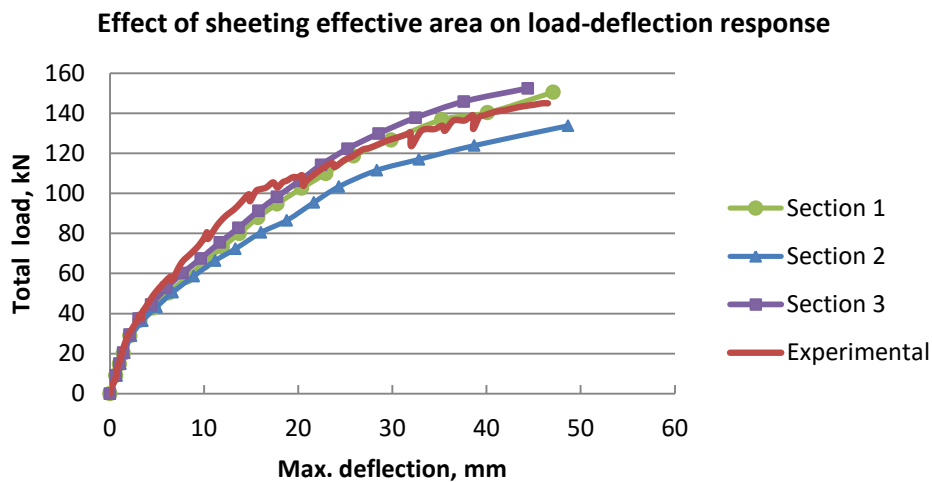


Figure 6.34 Load-deflection response of Rib3 with different sections of the steel sheeting

6.6 Conclusion on the parametric study of composite slab ComFlor210 with finite element analysis

The parametric study of composite slab ComFlor210 loaded with concentrated force 60kN was conducted with finite element model in Abaqus/CAE and included three slabs of different length: 3.2m, 5.4m, and 7.2m. The position of the concentrated force is varied as well: force was applied on the middle rib and adjacent to it rib at half of the span, quarter and one-sixth of the span. The distribution of the point load per rib was given in percentage % and force magnitude kN relative to the total load in §6.2-§6.4. Additionally, the results are illustrated in another way in Appendix G: the distribution per rib relative to the distance to the applied load.

In most of the cases, the load was carried by three middle ribs – loaded rib and two adjacent ribs, because the contribution of two outer ribs was less than 10% and, therefore, can be considered insignificant. Especially, this was evident in the shorter slab with 3.2m length in which the contribution of outer ribs was less than 5%. However, with increasing the slab length the reaction force in external ribs increases as well: for a slab with 7.2m span the contribution of these ribs needs to be taken into account because the outer ribs bear about 20% of total load together.

Another observation followed from the parametric study is that the loaded rib carries most of the applied load. When load travels towards the slab edge (distance between the load and support changes from $L_{span}/2$ to $L_{span}/6$), the reaction force in loaded rib increases significantly. Figure 6.35 gives an example of this effect in a case of a composite slab with length 3.6m and loaded middle rib, but the same can be said about a composite slab with 5.4m and 7.2m spans.

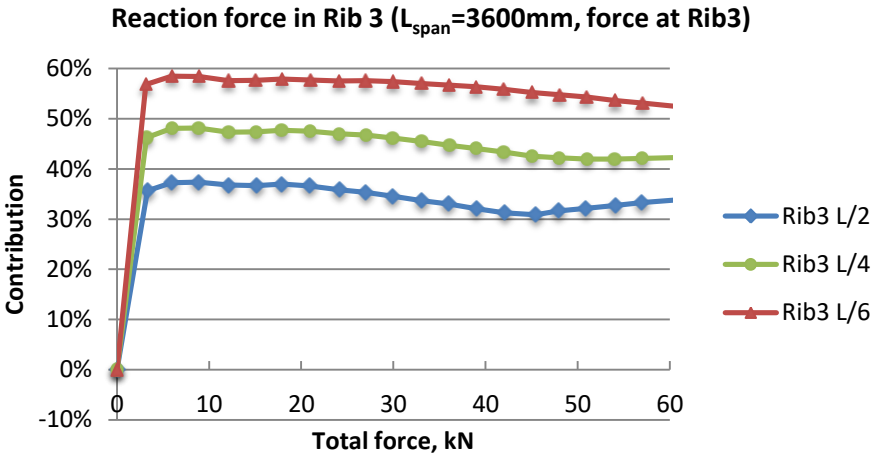


Figure 6.35 Reaction force distribution in the loaded Rib 3 in the composite slab with length 3.6m and different load location: at L/2, L/4, and L/6

This increase in reaction force in the middle rib is accompanied by the corresponding reduction in reaction force of external rib, see Figure 6.36. It can be concluded that the closer the concentrated force to the support, the higher the contribution of loaded rib and, therefore, lesser the spread of the load over slab width.

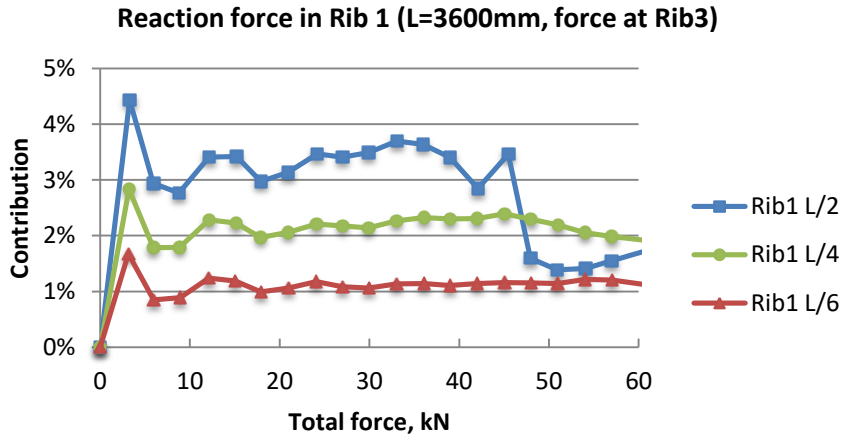


Figure 6.36 Reaction force distribution in the external Rib 1 in the composite slab with length 3.6m and different load location: at L/2, L/4, and L/6

It is of interest to see what happens with reaction force in one chosen rib, for instance, middle rib when the length of this rib is changed. Figure 6.37 shows that when the length of the slab increases, the contribution of the middle rib slightly decreases. This indicates that the load spreads more evenly over other ribs when the slab becomes longer.

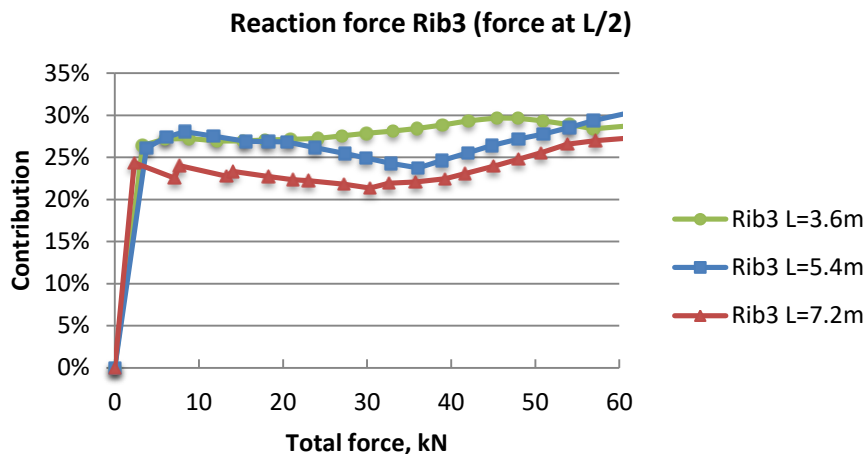


Figure 6.37 Reaction force distribution in the loaded Rib 3 in the composite slab with length 3.6m, 5.4m, 7.2m and load position at $L_{span}/2$

An observation was made during the parametric study regarding the slab performance in the serviceability state. For slabs with span 7.2m under a combination of dead load and concentrated force 60kN, the serviceability requirement - maximum deflection $L_{span}/250$ - was violated at a load lower 60kN. Table 6.3 and Table 6.4 show the maximum deflections reached in the finite element analysis of a composite slab 7.2m at the end of the loading when self-weight of a slab was activated in addition to a concentrated force. In practice, the positioning of the concentrated load on a longer slab must be treated with care depending on span length and load magnitude.

Table 6.3 Maximum deflection of composite slab 7.2m in FEA with a load on Rib 3

Slab length, mm	Load position, Rib 3	Max. deflection, mm	Limit, L/250, mm	Ratio
7200	L/2	37.51	28.8	1.30
	L/4	27.43		0.95
	L/6	20.64		0.72

Table 6.4 Maximum deflection of composite slab 7.2m in FEA with a load on Rib 2

Slab length, mm	Load position, Rib 2	Max. deflection, mm	Limit, L/250, mm	Ratio
7200	L/2	39.28	28.8	1.36
	L/4	28.55		0.99
	L/6	22.06		0.77

Another observation was made during the parametric study regarding the failure criterion of a composite slab: exceeding of the bending moment resistance of the rib. In order to calculate the acting moment, the following actions were taken into account: the dead load (3.05kN/m^2), live load (3.0kN/m^2) and concentrated force 60kN applied halfway the span on the middle rib. The corresponding coefficients were used to calculate the design load values: 1.35 for permanent action (self-weight) and 1.5 for variable free action (imposed loads). The results of this calculation are presented in Table 6.5. It can be noticed that the bending resistance of a rib is exceeded by 15% in a composite slab with 7.2m span; and thus, this slab cannot withstand the mentioned load combination. The detailed calculation of rib bending resistance is given in Appendix F.

Table 6.5 Bending moment resistance check for load combination dead load+live load+point load with point load placed halfway the span on Rib3

	Point load F, kN. nominal (design value)	Dead load, kN/mm2. nominal (design value)	Live load, N/mm2. nominal (design value)	Max. reaction force from point load, kN	Moment M_{ED} , kNm	Rib bending resistance M_{RD} , kNm	Unity check
Source	Dutch engineering		EN 1991.1.1	FEM	-	report §4.3.1	M_{ED}/M_{RD}
Slab $L_{span}=3.6\text{m}$	60 (90)	3.05 (4.12)	3.0 (4.5)	10.33	36.27	69.10	0.52
Slab $L_{span}=5.4\text{m}$				9.18	56.03		0.81
Slab $L_{span}=7.2\text{m}$				8.57	79.78		1.15

The parametric study of composite slab ComFlor210 loaded with concentrated force 145kN included a study on a slab with varied cross-sectional properties, namely, the diameter of rib reinforcement, thickness and effective area of the steel sheeting. The position of the concentrated force was at the middle rib at half of the span. The main conclusion on cross-sectional properties variation is that with increasing the area of rib reinforcement and the thickness of steel sheeting the composite slab exhibits stiffer behavior especially in the plastic part of the load-deflection curve. For the elastic part of the load-deflection curve, the variation in cross-sectional parameters causes a minor change in a slab response.

7 Conclusions and recommendations

7.1 Conclusions

The behavior of the simply-supported composite slab ComFlor210 under concentrated force placed on a rib at different locations was studied numerically and analytically. The followed conclusions are drawn based on the obtained results.

- *The engineering model can predict the deflection of the composite slab under concentrated load in a range 10-60kN with limited accuracy.*

The engineering model results of a composite slab 5.4m with one reinforcement mesh in the top deck with a load acting at the middle rib at a half span length exceeded the test results in average 2.8 times at 10kN load, and in 1.35 times at 60kN. The assumptions that modulus of elasticity of cracked concrete equals one-third of not cracked material can lead to an underestimation of rib bending stiffness at low load level.

- *The finite element model provides accurate results compared to the experimental results.*

The finite element model of a composite slab with 5.4m span shows good agreement with test results. The ratio of maximum deflections in FEM and test is 1.24 at a load 60kN and 1.01 at 145kN.

- *The structural performance of the composite slab under a concentrated load is mostly influenced by the bending stiffness of the rib.*

The parametric study on the engineering model reveals that the rib stiffness is the most influential parameter on the slab behavior. The stiffness of the rib can be affected by rib geometry and material (concrete grade, type of reinforcement). Reduction of the bending stiffness of a rib by 25% results in increased deflection of a loaded rib by 33%. Therefore, in order to change the structural behavior of the composite slab, it is advisable to influence the rib stiffness primarily.

- *For relatively short slabs (span 3.6m, 5.4m), the contribution of each rib expressed as a percentage in relation to the total load remains nearly constant in a loading range 5-60kN.*

In composite slabs with spans 3.6m and 5.4m, the contribution of each rib in all loading cases was regular in a range 5-60kN with slight fluctuations which can be considered insignificant. However, in the long composite slab (span 7.2m) the contribution of each rib showed abrupt change after concrete reached tensile strength. This change might be induced by the crack formation in a slab that causes significant redistribution of concentrated force at approximately 30kN.

- *The concentrated force is carried by three ribs (i.e. loaded rib and two adjacent ribs) in a loading range 5-60kN in relatively short slabs (span 3.6m, 5.4m).*

In a composite slab with span 3.6m and 5.4m, in all loading cases, the contribution of two external ribs was less than 10%, and, thus, can be considered negligible. The effective width over

which the concentrated load spreads is, then, the width of three ribs. However, with increasing the slab length, the reaction force in external ribs also increases: in a slab 7.2m the contribution of outer ribs needs to be taken into account because the outer ribs carry circa 20% of the total load together.

- *A larger percentage of the concentrated load in a loading range 5-60kN is transferred to the loaded rib when the load is placed closer to the support.*

The parametric study with finite element model revealed that the loaded rib bears most of the applied load. When load travels towards the slab edge (distance between the load and support changes from $L_{\text{span}}/2$ to $L_{\text{span}}/6$), the reaction force in loaded rib increases significantly. For example, the contribution of the loaded rib in the composite slab of 3.6m length is about 35% with load at $L_{\text{span}}/2$, and then the contribution of loaded rib becomes almost 60% with load at $L_{\text{span}}/6$.

- *The bending resistance of a rib is exceeded at a composite slab with span 7.2m under the design load combination “dead load, live load, and point load 60kN placed halfway the span”.*

The moment in a slab 7.2m under the combined action of dead load (3.05kN/m^2), live load (3.0kN/m^2) and concentrated force 60kN applied halfway the span exceeds the bending moment resistance of a rib by 15%.

- *The placement of the concentrated force on an external rib, which is unsupported along the long edge, might cause the excessive deflection that is higher than the serviceability limit $L_{\text{span}}/250$.*

In a normal stage, the deflection of the composite slab should not exceed $L_{\text{span}}/250$ [5]. In a composite slab with 5.4m span, the total deflection reaches this limit at approximately 58kN, when a concentrated load is placed at the middle of the external rib. The composite slab with longer span will reach the serviceability limit at a lower load. Therefore, the positioning of the concentrated load at external unsupported rib must be treated with care depending on span length and load magnitude, and it is better to be avoided.

- *The load combination “dead load and concentrated force 60kN” causes the excessive deflection of a composite slab with span 7.2m higher than the serviceability limit $L_{\text{span}}/250$ when a concentrated load is placed at the middle of a slab.*

7.2 Recommendations

The recommendation for further research in regard to the engineering model is:

- *Determination of rib bending stiffness and Young's modulus of cracked concrete for loading range 0-40kN.*

In a range 10-40kN load, the results obtained with the engineering model are different from the test. The assumption that modulus of elasticity of cracked concrete equals one-third of not cracked material, i.e. 10000MPa, and the implementation of the linear dependency between rib bending stiffness and the applied load do not produce satisfactory results. It is possible that if the dependency would be non-linear, the accuracy of the engineering model will increase. For example, the mean stiffness can be used instead of one-third of not cracked concrete. The procedure to determine the mean stiffness of the cracked reinforced structure is described in a paper written by Li [13].

The recommendations for further research in regard to the numerical model are:

- *Perform an analysis of the composite slab ComFlor210 with another type of boundary conditions numerically and in the laboratory.*

In this study, the composite slab was simply supported. In practice, this is rear the case, most of the composite floors are multiple-spanning. It is recommended to create a finite element model of a composite slab with two-way spans, or three-way spans in order to reflect the reality better.

- *Perform an analysis of the composite slab with the concentrated force placed between the ribs numerically and in the laboratory.*

In the study, the concentrated force was always placed on a rib. The resistance of the composite slab with a load acting on the top deck only is not known, and, thus, it can be a research question in the future.

8 References

- [1] A. Cholamhoseini, R. Gilbert, M. Bradford and Z. Chang, "Longitudinal shear stress and bond-slip relationships in composite concrete slabs.," *Engineering Structures*, no. 69, 37-48, 2014.
- [2] *Eurocode 4. Design of steel structures. Part 1-1: general rules for buildings*, Brussels: European Committee for Standardisation (CEN), 2004.
- [3] M. S. Dracht, *Horizontal distribution of concentrated loads in deep composite slabs: an analytical model validated FEM calculations and laboratory testing*, Delft, 2015.
- [4] M. Michalaki, *Distribution of Concentrated Loads on simply supported Deep Composite Slab ComFlor 210*, Delft: TNO, 2015.
- [5] *ComFlor® manual. Composite floor decking design and technical information*, Tata Steel UK Limited, 2017.
- [6] *Eurocode 1. Actions on structures. Part 1-1: general actions - densities, self-weight, imposed loads for buildings*, Brussels: European Committee for Standardisation (CEN), 2014.
- [7] H. Bode and T. Dauwel, "Gutachten zum Tragverhalten von COMFLOR210 - Verbunddecken, Tech. Rep.," Universität Kaiserslautern, Kaiserslautern, 1997.
- [8] J. Stark and R. Stark, "Vertical shear resistance of composite floors with ComFlor 60," Dutch Engineering, Zoeterwoude, 2012.
- [9] M. Veljkovic, *Behaviour and Resistance of Composite Slabs.*, Lulea: Lulea University of Technology, 1996.
- [10] S. Attarde, *Nonlinear finite element analysis of profiled steel deck composite slab system under monotonic loading*, Toronto: Ryerson University, 2014.
- [11] J. Blaauwendraad, *Plate analysis, theory and application. Volume I, Theory*, Delft: Delft University of Technology, 2006.
- [12] P. van Erp, *Horizontal shear resistance of ComFlor210*, Delft, 2017.
- [13] Y. Li, *Predicting of the Stiffness of Cracked Reinforced Concrete Structures*, Delft, 2010.
- [14] *ABAQUS/CAE Documentation, Version 6.12.*, Providence, RI: Dassault Systèmes Simulia Corp., 2012.

- [15] *Eurocode 2. Design of concrete structures. Part 1-1: general rules for buildings*, Brussels: European Committee for Standardisation (CEN), 2004.
- [16] B. Rabbat and H. Russel, "Friction Coefficient of Steel on Concrete or Grout," *Journal of Structural Engineering/ Volume 111 Issue 3*, 01 March 1985.
- [17] S. Hale, "Engineering Advantage," 6 06 2014. [Online]. Available: <https://caeai.com/blog/how-do-i-know-if-my-mesh-good-enough>.
- [18] B. Grzeszykowski, A. Golubisnka and M. L. Nieodspial, "Analiza numeryczna płyty stropu zespolonego stalowo-betonowego w sasiedztwie wezla podatnego," 2015.

A The effective area of profiled steel sheeting ComFlor210

The effective area of profiled steel sheeting ComFlor210 needs to be determined in order to calculate the bending stiffness of the composite slab.

The determination of this parameter is based on Van Erp [12] scientific work that includes several full-scale experiments of ComFlor210 in order to measure the effective area of steel deck using a large number of strain gauges during testing. The position of strain gauges on different specimens is given in Figure A. 1.

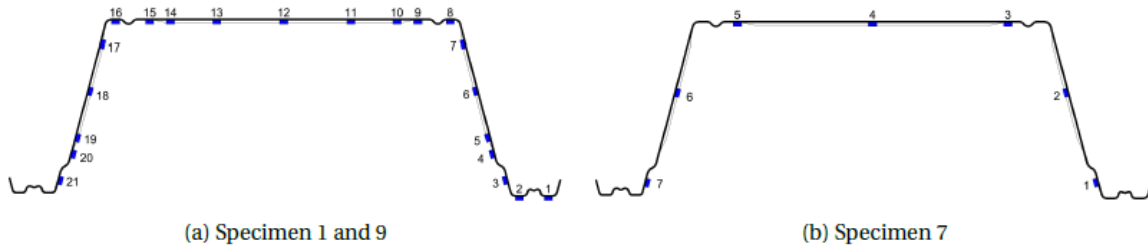


Figure A. 1 Location and numbering of strain gauges (Van Erp)

Specimen 1 and 9 had twenty-one strain gauges, and specimen 7 had only seven strain gauges. The calculated effective area per specimen was:

- specimen 1 – 556.3mm²,
- specimen 7 – 887.0mm²,
- specimen 9 – 562.2mm².

The average value of the effective area is used to define the bending stiffness of profiled steel sheeting. Because specimen 7 had a smaller amount of strain gauges, the corresponding value of the effective area is not added to the average value. Only specimen 1 and 7 contribute to the final result, see formula (A. 1).

$$A_{eff} = \frac{\sum A_{eff}}{2} = \frac{556.3 + 562.2}{2} = 559.25mm^2 \quad (\text{A. 1})$$

Now that the effective area is known, the geometry that corresponds to this value is shown in Figure A. 2. The thickness of the top flange is 1.25mm, the thickness of the bottom flange is 2.5mm.

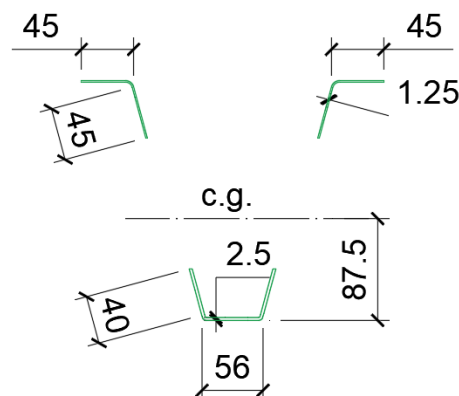


Figure A. 2 Effective area of ComFlor210

The center of gravity (c.g.) for the area presented in Figure A. 2 is located 87.5mm from the bottom.

B Engineering model parameters

B.1 Bending stiffness determination

The bending stiffness of the rib and the top deck is determined based on Steiner rule.

Rib bending stiffness (width 175mm) of no mesh, one mesh and two meshes slabs with uncracked concrete are given in [Table B. 1](#).

Rib bending stiffness (width 175mm) of no mesh, one mesh and two meshes slabs with cracked concrete in the rib is presented in [Table B. 2](#).

Rib bending stiffness (width 600mm) of no mesh, one mesh and two meshes slabs with uncracked concrete are given in [Table B.3](#).

Rib bending stiffness (width 600mm) of no mesh, one mesh and two meshes slabs with cracked concrete in the rib is presented in [Table B.4](#).

The bending stiffness of the top deck per 200mm length is given [Table B.5](#), [Table B.6](#) and [Table B.7](#).

B.2 Model in matrix notation

The rib model in matrix notation when the load is applied at the middle of a span, i.e. at $L_{rib}/2$, is given in Eq. (B. 1).

The rib model in matrix notation when the load is applied at quarter, i.e. $L_{rib}/4$ from right support, is given in Eq. (B. 2).

In equations (B. 1) and (B. 2) the values in resulting rightmost column can become zero if there is no distributive load q acting and only concentrated force F retains.

The transverse model in matrix notation for a composite slab with load at the central rib is given in Eq. B.3.

Table B. 1 Uncracked bending stiffness of rib with no mesh, 1 mesh, 2 meshes, and width 175mm

<i>Uncracked/no mesh</i>	<i>E</i>	<i>N/mm2</i>		<i>mm2</i>	<i>mm</i>				<i>mm4</i>	<i>mm</i>	<i>mm4</i>	<i>mm4</i>	<i>Nmm2</i>	
		<i>E</i>		<i>A</i>	<i>yc</i>	<i>y*EA</i>	<i>EA</i>		<i>I</i>	<i>z</i>	<i>A*z^2</i>	<i>I_{tot}</i>	<i>EI</i>	<i>%</i>
<i>Concrete top</i>	<i>E_c</i>	30000	<i>A_c</i>	12250	35	1.29E+10	3.68E+08		5.00E+06	90.51	1.00E+08	1.05E+08	3.16E+12	41.40
<i>Concrete rib</i>	<i>E_{rib}</i>	30000	<i>A_{c,rib}</i>	24255	157	1.14E+11	7.28E+08		8.13E+07	31.49	2.40E+07	1.05E+08	3.16E+12	41.37
<i>Steel sheeting</i>	<i>E_p</i>	210000	<i>A_p</i>	559.25	155	1.82E+10	1.17E+08		2.34E+06	29.49	4.86E+05	2.83E+06	5.94E+11	7.77
<i>Steel bar</i>	<i>E_s</i>	210000	<i>A_b</i>	314	230	1.52E+10	6.59E+07		7.85E+03	104.49	3.43E+06	3.44E+06	7.22E+11	9.45
						1.60E+11	1.28E+09							
											Total	2.17E+08	7.63E+12	100
Uncracked/1 mesh														
	<i>E</i>	<i>N/mm2</i>		<i>mm2</i>	<i>mm</i>				<i>I</i>	<i>z</i>	<i>A*z^2</i>	<i>I_{tot}</i>	<i>EI</i>	<i>%</i>
		<i>E</i>		<i>A</i>	<i>yc</i>	<i>y*EA</i>	<i>EA</i>		<i>I</i>	<i>z</i>	<i>A*z^2</i>	<i>I_{tot}</i>	<i>EI</i>	<i>%</i>
<i>Concrete top</i>	<i>E_c</i>	30000	<i>A_c</i>	12250	35	1.29E+10	3.68E+08		5.00E+06	88.91	9.68E+07	1.02E+08	3.06E+12	38.03
<i>Concrete rib</i>	<i>E_{rib}</i>	30000	<i>A_{c,rib}</i>	24255	157	1.14E+11	7.28E+08		8.13E+07	33.09	2.66E+07	1.08E+08	3.23E+12	40.25
<i>Steel sheeting</i>	<i>E_p</i>	210000	<i>A_p</i>	559.25	155	1.82E+10	1.17E+08		2.34E+06	31.09	5.40E+05	2.88E+06	6.05E+11	7.53
<i>Steel bar</i>	<i>E_s</i>	210000	<i>A_b</i>	314	230	1.52E+10	6.59E+07		7.85E+03	106.09	3.53E+06	3.54E+06	7.44E+11	9.26
<i>Reinforcement mesh, top</i>	<i>E_s</i>	210000	<i>A_{s1}</i>	100.53	27	5.70E+08	2.11E+07		9.45E+05	96.91	9.44E+05	1.89E+06	3.97E+11	4.94
						1.61E+11	1.30E+09					Total	2.18E+08	8.03E+12
						<i>z (n.a. from top)</i>	123.91							
Uncracked/2 meshes														
	<i>E</i>	<i>N/mm2</i>		<i>mm2</i>	<i>mm</i>				<i>I</i>	<i>z</i>	<i>A*z^2</i>	<i>I_{tot}</i>	<i>EI</i>	<i>%</i>
		<i>E</i>		<i>A</i>	<i>yc</i>	<i>y*EA</i>	<i>EA</i>		<i>I</i>	<i>z</i>	<i>A*z^2</i>	<i>I_{tot}</i>	<i>EI</i>	<i>%</i>
<i>Concrete top</i>	<i>E_c</i>	30000	<i>A_c</i>	12250	35	1.29E+10	3.68E+08		5.00E+06	87.83	9.45E+07	9.95E+07	2.98E+12	36.43
<i>Concrete rib</i>	<i>E_{rib}</i>	30000	<i>A_{c,rib}</i>	24255	157	1.14E+11	7.28E+08		8.13E+07	34.17	2.83E+07	1.10E+08	3.29E+12	40.13
<i>Steel sheeting</i>	<i>E_p</i>	210000	<i>A_p</i>	559.25	155	1.82E+10	1.17E+08		2.34E+06	32.17	5.79E+05	2.92E+06	6.13E+11	7.48
<i>Steel bar</i>	<i>E_s</i>	210000	<i>A_b</i>	314	230	1.52E+10	6.59E+07		7.85E+03	107.17	3.61E+06	3.61E+06	7.59E+11	9.26
<i>Reinforcement mesh, top</i>	<i>E_s</i>	210000	<i>A_{s1}</i>	100.53	27	5.70E+08	2.11E+07		9.24E+05	95.83	9.23E+05	1.85E+06	3.88E+11	4.73
<i>Reinforcement mesh, botom</i>	<i>E_s</i>	210000	<i>A_{s2}</i>	100.53	56	1.18E+09	2.11E+07		3.16E+05	66.83	4.49E+05	7.65E+05	1.61E+11	1.96
						1.62E+11	1.32E+09					Total	2.18E+08	8.19E+12
						<i>z (n.a. from top)</i>	122.83							

Table B. 2 Cracked bending stiffness of rib with no mesh, 1 mesh, 2 meshes and width 175mm

<i>Cracked/no mesh</i>	<i>E</i>	<i>N/mm2</i>		<i>mm2</i>	<i>mm</i>									
		<i>E</i>		<i>A</i>	<i>yc</i>	<i>y*EA</i>	<i>EA</i>		<i>I</i>	<i>z</i>	<i>A*z^2</i>	<i>Itot</i>	<i>EI</i>	<i>%</i>
<i>Concrete top</i>	<i>Ec</i>	30000	<i>Ac</i>	12250	35	1.29E+10	3.68E+08		5.00E+06	71.26	6.22E+07	6.72E+07	2.02E+12	38.52
<i>Concrete rib</i>	<i>Erib</i>	10000	<i>Ac,rib</i>	24255	157	3.81E+10	2.43E+08		8.13E+07	50.74	6.24E+07	1.44E+08	1.44E+12	27.45
<i>Steel sheeting</i>	<i>Ep</i>	210000	<i>Ap</i>	559.25	155	1.82E+10	1.17E+08		2.34E+06	48.74	1.33E+06	3.67E+06	7.70E+11	14.72
<i>Steel bar</i>	<i>Es</i>	210000	<i>Ab</i>	314	230	1.52E+10	6.59E+07		7.85E+03	123.74	4.81E+06	4.82E+06	1.01E+12	19.32
						8.43E+10	7.93E+08							
											Total	2.19E+08	5.23E+12	100
cracked/1 mesh														
	<i>E</i>	<i>N/mm2</i>		<i>mm2</i>	<i>mm</i>									
		<i>E</i>		<i>A</i>	<i>yc</i>	<i>y*EA</i>	<i>EA</i>		<i>I</i>	<i>z</i>	<i>A*z^2</i>	<i>Itot</i>	<i>EI</i>	<i>%</i>
<i>Concrete top</i>	<i>Ec</i>	30000	<i>Ac</i>	12250	35	1.29E+10	3.68E+08		5.00E+06	69.21	5.87E+07	6.37E+07	1.91E+12	34.80
<i>Concrete rib</i>	<i>Erib</i>	10000	<i>Ac,rib</i>	24255	157	3.81E+10	2.43E+08		8.13E+07	52.79	6.76E+07	1.49E+08	1.49E+12	27.11
<i>Steel sheeting</i>	<i>Ep</i>	210000	<i>Ap</i>	559.25	155	1.82E+10	1.17E+08		2.34E+06	50.79	1.44E+06	3.78E+06	7.94E+11	14.47
<i>Steel bar</i>		210000	<i>Ab</i>	314	230	1.52E+10	6.59E+07		7.85E+03	125.79	4.97E+06	4.98E+06	1.05E+12	19.04
<i>Reinforcement mesh, top</i>	<i>Es</i>	210000	<i>As1</i>	100.53	27	5.70E+08	2.11E+07		6.00E+05	77.21	5.99E+05	1.20E+06	2.52E+11	4.59
						8.49E+10	8.15E+08							
											Total	2.22E+08	5.49E+12	100
cracked/2 meshes														
	<i>E</i>	<i>N/mm2</i>		<i>mm2</i>	<i>mm</i>									
		<i>E</i>		<i>A</i>	<i>yc</i>	<i>y*EA</i>	<i>EA</i>		<i>I</i>	<i>z</i>	<i>A*z^2</i>	<i>Itot</i>	<i>EI</i>	<i>%</i>
<i>Concrete top</i>	<i>Ec</i>	30000	<i>Ac</i>	12250	35	1.29E+10	3.68E+08		5.00E+06	67.99	5.66E+07	6.16E+07	1.85E+12	33.02
<i>Concrete rib</i>	<i>Erib</i>	10000	<i>Ac,rib</i>	24255	157	3.81E+10	2.43E+08		8.13E+07	54.01	7.08E+07	1.52E+08	1.52E+12	27.14
<i>Steel sheeting</i>	<i>Ep</i>	210000	<i>Ap</i>	559.25	155	1.82E+10	1.17E+08		2.34E+06	52.01	1.51E+06	3.85E+06	8.09E+11	14.45
<i>Steel bar</i>		210000	<i>Ab</i>	314	230	1.52E+10	6.59E+07		7.85E+03	127.01	5.07E+06	5.07E+06	1.07E+12	19.02
<i>Reinforcement mesh, top</i>	<i>Es</i>	210000	<i>As1</i>	100.53	27	5.70E+08	2.11E+07		5.81E+05	75.99	5.81E+05	1.16E+06	2.44E+11	4.36
<i>Reinforcement mesh, botom</i>		210000	<i>As2</i>	100.53	56	1.18E+09	2.11E+07		3.16E+05	46.99	2.22E+05	5.38E+05	1.13E+11	2.02
						8.61E+10	8.36E+08							
											Total	2.24E+08	5.60E+12	100

Table B. 3 Uncracked bending stiffness of rib with no mesh, 1 mesh, 2 meshes, and width 600mm

<i>Uncracked/no mesh</i>		<i>N/mm2</i>		<i>mm2</i>	<i>mm</i>			<i>mm4</i>	<i>mm</i>	<i>mm4</i>	<i>mm4</i>	<i>Nmm2</i>	
		<i>E</i>		<i>A</i>	<i>yc</i>	<i>y*EA</i>	<i>EA</i>	<i>I</i>	<i>z</i>	<i>A*z^2</i>	<i>Itot</i>	<i>EI</i>	<i>%</i>
<i>Concrete top</i>	<i>Ec</i>	30000	<i>Ac</i>	42000	35	4.41E+10	1.26E+09	1.72E+07	53.30	1.19E+08	1.36E+08	4.09E+12	33.27
<i>Concrete rib</i>	<i>Erib</i>	30000	<i>Ac,rib</i>	24255	157	1.14E+11	7.28E+08	8.13E+07	68.70	1.14E+08	1.96E+08	5.87E+12	47.71
<i>Steel sheeting</i>	<i>Ep</i>	210000	<i>Ap</i>	559.25	155	1.82E+10	1.17E+08	2.34E+06	66.70	2.49E+06	4.83E+06	1.01E+12	8.24
<i>Steel bar</i>	<i>Es</i>	210000	<i>Ab</i>	314	230	1.52E+10	6.59E+07	7.85E+03	141.70	6.30E+06	6.31E+06	1.33E+12	10.77
						1.92E+11	2.17E+09						
										Total	3.43E+08	1.23E+13	100
Uncracked/1 mesh													
		<i>N/mm2</i>		<i>mm2</i>	<i>mm</i>			<i>I</i>	<i>z</i>	<i>A*z^2</i>	<i>Itot</i>	<i>EI</i>	<i>%</i>
<i>Concrete top</i>	<i>Ec</i>	30000	<i>Ac</i>	42000	35	4.41E+10	1.26E+09	1.72E+07	52.13	1.14E+08	1.31E+08	3.94E+12	31.23
<i>Concrete rib</i>	<i>Erib</i>	30000	<i>Ac,rib</i>	24255	157	1.14E+11	7.28E+08	8.13E+07	69.87	1.18E+08	2.00E+08	5.99E+12	47.48
<i>Steel sheeting</i>	<i>Ep</i>	210000	<i>Ap</i>	559.25	155	1.82E+10	1.17E+08	2.34E+06	67.87	2.58E+06	4.92E+06	1.03E+12	8.18
<i>Steel bar</i>		210000	<i>Ab</i>	314	230	1.52E+10	6.59E+07	7.85E+03	142.87	6.41E+06	6.42E+06	1.35E+12	10.68
<i>Reinforcement mesh, top</i>	<i>Es</i>	210000	<i>As1</i>	201.06	27	1.14E+09	4.22E+07	7.28E+05	60.13	7.27E+05	1.45E+06	3.06E+11	2.42
						1.93E+11	2.21E+09				Total	3.44E+08	1.26E+13
						<i>z (n.a. from top)</i>	87.13						
Uncracked/2 meshes													
		<i>N/mm2</i>		<i>mm2</i>	<i>mm</i>			<i>I</i>	<i>z</i>	<i>A*z^2</i>	<i>Itot</i>	<i>EI</i>	<i>%</i>
<i>Concrete top</i>	<i>Ec</i>	30000	<i>Ac</i>	42000	35	4.41E+10	1.26E+09	1.72E+07	51.55	1.12E+08	1.29E+08	3.86E+12	30.22
<i>Concrete rib</i>	<i>Erib</i>	30000	<i>Ac,rib</i>	24255	157	1.14E+11	7.28E+08	8.13E+07	70.45	1.20E+08	2.02E+08	6.05E+12	47.32
<i>Steel sheeting</i>	<i>Ep</i>	210000	<i>Ap</i>	559.25	155	1.82E+10	1.17E+08	2.34E+06	68.45	2.62E+06	4.96E+06	1.04E+12	8.15
<i>Steel bar</i>		210000	<i>Ab</i>	314	230	1.52E+10	6.59E+07	7.85E+03	143.45	6.46E+06	6.47E+06	1.36E+12	10.63
<i>Reinforcement mesh, top</i>	<i>Es</i>	210000	<i>As1</i>	201.06	27	1.14E+09	4.22E+07	7.14E+05	59.55	7.13E+05	1.43E+06	3.00E+11	2.34
<i>Reinforcement mesh, botom</i>		210000	<i>As2</i>	201.06	56	2.36E+09	4.22E+07	6.31E+05	30.55	1.88E+05	8.19E+05	1.72E+11	1.35
						1.95E+11	2.26E+09				Total	3.44E+08	1.28E+13
						<i>z (n.a. from top)</i>	86.55						

Table B. 4 Cracked bending stiffness of rib with no mesh, 1 mesh, 2 meshes, and width 600mm

<i>Cracked/no mesh</i>		<i>N/mm2</i>		<i>mm2</i>		<i>mm</i>							
		<i>E</i>		<i>A</i>	<i>yc</i>	<i>y*EA</i>	<i>EA</i>	<i>I</i>	<i>z</i>	<i>A*z^2</i>	<i>Itot</i>	<i>EI</i>	<i>%</i>
<i>Concrete top</i>	<i>Ec</i>	30000	<i>Ac</i>	42000	35	4.41E+10	1.26E+09	1.72E+07	33.54	4.72E+07	6.44E+07	1.93E+12	24.98
<i>Concrete rib</i>	<i>Erib</i>	10000	<i>Ac,rib</i>	24255	157	3.81E+10	2.43E+08	8.13E+07	88.46	1.90E+08	2.71E+08	2.71E+12	35.06
<i>Steel sheeting</i>	<i>Ep</i>	210000	<i>Ap</i>	559.25	155	1.82E+10	1.17E+08	2.34E+06	86.46	4.18E+06	6.52E+06	1.37E+12	17.71
<i>Steel bar</i>	<i>Es</i>	210000	<i>Ab</i>	314	230	1.52E+10	6.59E+07	7.85E+03	161.46	8.19E+06	8.19E+06	1.72E+12	22.25
						1.16E+11	1.69E+09						
										Total	3.50E+08	7.73E+12	100
cracked/1 mesh													
		<i>N/mm2</i>		<i>mm2</i>		<i>mm</i>							
		<i>E</i>		<i>A</i>	<i>yc</i>	<i>y*EA</i>	<i>EA</i>	<i>I</i>	<i>z</i>	<i>A*z^2</i>	<i>Itot</i>	<i>EI</i>	<i>%</i>
<i>Concrete top</i>	<i>Ec</i>	30000	<i>Ac</i>	42000	35	4.41E+10	1.26E+09	1.72E+07	32.52	4.44E+07	6.16E+07	1.85E+12	23.46
<i>Concrete rib</i>	<i>Erib</i>	10000	<i>Ac,rib</i>	24255	157	3.81E+10	2.43E+08	8.13E+07	89.48	1.94E+08	2.75E+08	2.75E+12	34.99
<i>Steel sheeting</i>	<i>Ep</i>	210000	<i>Ap</i>	559.25	155	1.82E+10	1.17E+08	2.34E+06	87.48	4.28E+06	6.62E+06	1.39E+12	17.66
<i>Steel bar</i>		210000	<i>Ab</i>	314	230	1.52E+10	6.59E+07	7.85E+03	162.48	8.29E+06	8.30E+06	1.74E+12	22.13
<i>Reinforcement mesh, top</i>	<i>Es</i>	210000	<i>As1</i>	201.06	27	1.14E+09	4.22E+07	3.31E+05	40.52	3.30E+05	6.61E+05	1.39E+11	1.76
						1.17E+11	1.73E+09						
										Total	3.53E+08	7.87E+12	100
cracked/2 meshes													
		<i>N/mm2</i>		<i>mm2</i>		<i>mm</i>							
		<i>E</i>		<i>A</i>	<i>yc</i>	<i>y*EA</i>	<i>EA</i>	<i>I</i>	<i>z</i>	<i>A*z^2</i>	<i>Itot</i>	<i>EI</i>	<i>%</i>
<i>Concrete top</i>	<i>Ec</i>	30000	<i>Ac</i>	42000	35	4.41E+10	1.26E+09	1.72E+07	32.25	4.37E+07	6.08E+07	1.82E+12	22.78
<i>Concrete rib</i>	<i>Erib</i>	10000	<i>Ac,rib</i>	24255	157	3.81E+10	2.43E+08	8.13E+07	89.75	1.95E+08	2.77E+08	2.77E+12	34.54
<i>Steel sheeting</i>	<i>Ep</i>	210000	<i>Ap</i>	559.25	155	1.82E+10	1.17E+08	2.34E+06	87.75	4.31E+06	6.65E+06	1.40E+12	17.43
<i>Steel bar</i>		210000	<i>Ab</i>	314	230	1.52E+10	6.59E+07	7.85E+03	162.75	8.32E+06	8.33E+06	1.75E+12	21.83
<i>Reinforcement mesh, top</i>	<i>Es</i>	210000	<i>As1</i>	201.06	27	1.14E+09	4.22E+07	3.27E+05	40.25	3.26E+05	6.52E+05	1.37E+11	1.71
<i>Reinforcement mesh, botom</i>		210000	<i>As2</i>	201.06	56	2.36E+09	4.22E+07	6.31E+05	11.25	2.54E+04	6.57E+05	1.38E+11	1.72
						1.19E+11	1.77E+09						
										Total	3.54E+08	8.01E+12	100

Table B. 5 Positive and negative bending stiffness of the top deck with no mesh per 200mm width

EI+	Positive bending moment		yc from top	r	Isteiner	I	Summ I	EI	%
	E	Area							
Concrete	30000	1476	3.69	25.86	9.87E+05	6.70E+03	9.94E+05	2.98E+10	36.71
Cracked concrete	10000	12524	38.69	9.14	1.05E+06	4.09E+06	5.14E+06	5.14E+10	63.29
									100
							EI+	8.12E+10	

EI-	Negative bending moment		yc from bottom	r	Isteiner	I	Summ I	EI	%
	E	Area							
Concrete	30000	1476	63.36	25.86	9.87E+05	6.70E+03	9.94E+05	2.98E+10	36.71
Cracked concrete	10000	12524	28.36	9.14	1.05E+06	4.09E+06	5.14E+06	5.14E+10	63.29
									100
							EI-	8.12E+10	

Table B. 6 Positive and negative bending stiffness of top deck with one mesh per 200mm width

EI+	Positive bending moment		yc from top	r	Isteiner	I	Summ I	EI	%
	E	Area							
Concrete	30000	1476	3.69	25.05	9.26E+05	6.70E+03	9.33E+05	2.80E+10	33.77
Cracked concrete	10000	12524	38.69	9.95	1.24E+06	4.09E+06	5.33E+06	5.33E+10	64.35
Top reinforcement	210000	67.02	19.00	9.74	6.36E+03	1.07E+03	7.43E+03	1.56E+09	1.88
									100
							EI+	8.29E+10	

EI-	Negative bending moment		yc from bottom	r	Isteiner	I	Summ I	EI	%
	E	Area							
Concrete	30000	1476	63.36	19.99	5.90E+05	6.70E+03	5.97E+05	1.79E+10	20.33
Cracked concrete	10000	12524	28.36	15.01	2.82E+06	4.09E+06	6.91E+06	6.91E+10	78.48
Top reinforcement	210000	67.02	51.00	7.64	3.91E+03	1.07E+03	4.98E+03	1.05E+09	1.19
									100
							EI-	8.81E+10	

Table B. 7 Positive and negative bending stiffness of the top deck with two meshes per 200mm width

<i>EI+</i>	<i>Positive bending moment</i>		<i>yc</i>	<i>r</i>	<i>Isteiner</i>	<i>I</i>	<i>Summ I</i>	<i>EI</i>	<i>%</i>
	<i>E</i>	<i>Area</i>	<i>from top</i>						
<i>Concrete</i>	30000	1476	3.69	26.99	1.08E+06	6.70E+03	1.08E+06	3.25E+10	34.97
<i>Cracked concrete</i>	10000	12524	38.69	8.01	8.04E+05	4.09E+06	4.90E+06	4.90E+10	52.75
<i>Top reinforcement</i>	210000	67.02	19	11.68	9.14E+03	1.07E+03	1.02E+04	2.15E+09	2.31
<i>Bottom reinforcement</i>	210000	67.02	56	25.32	4.30E+04	1.07E+03	4.40E+04	9.25E+09	9.96
							EI+	9.28E+10	100

<i>EI-</i>	<i>Negative bending moment</i>		<i>yc</i>	<i>r</i>	<i>Isteiner</i>	<i>I</i>	<i>Summ I</i>	<i>EI</i>	<i>%</i>
	<i>E</i>	<i>Area</i>	<i>from bottom</i>						
<i>Concrete</i>	30000	1476	63.36	26.57	1.04E+06	6.70E+03	1.05E+06	3.15E+10	34.24
<i>Cracked concrete</i>	10000	12524	28.36	8.43	8.90E+05	4.09E+06	4.98E+06	4.98E+10	54.23
<i>Top reinforcement</i>	210000	67.02	51	14.21	1.35E+04	1.07E+03	1.46E+04	3.07E+09	3.34
<i>Bottom reinforcement</i>	210000	67.02	14	22.79	3.48E+04	1.07E+03	3.59E+04	7.53E+09	8.20
							EI-	9.19E+10	100

Set of equations for rib model loaded at the center of the span (B. 1).

$$\begin{bmatrix}
 0 & 0 & 0 & \frac{1}{EI_{im}} & 0 & 0 & 0 & 0 & 0 & 0 & 0 & 0 & 0 & 0 & 0 & 0 \\
 0 & -1 & 0 & 0 & 0 & 0 & 0 & 0 & 0 & 0 & 0 & 0 & 0 & 0 & 0 & 0 \\
 0 & 0 & 0 & 0 & 0 & 0 & 0 & 0 & 0 & 0 & 0 & \frac{L^3}{6EI_{im}} & \frac{L^2}{2EI_{im}} & \frac{L}{EI_{im}} & \frac{1}{EI_{im}} & 0 \\
 0 & 0 & 0 & 0 & 0 & 0 & 0 & 0 & 0 & 0 & 0 & -L & -1 & 0 & 0 & 0 \\
 \frac{a^3}{6EI_{im}} & \frac{a^2}{2EI_{im}} & \frac{a}{EI_{im}} & \frac{1}{EI_{im}} & -\frac{a^3}{6EI_{cr}} & -\frac{a^2}{2EI_{cr}} & -\frac{a}{EI_{cr}} & -\frac{1}{EI_{cr}} & 0 & 0 & 0 & 0 & 0 & 0 & 0 & 0 \\
 -\frac{a^2}{2EI_{im}} & -\frac{a}{EI_{im}} & -\frac{1}{EI_{im}} & 0 & \frac{a^2}{2EI_{cr}} & \frac{a}{EI_{cr}} & \frac{1}{EI_{cr}} & 0 & 0 & 0 & 0 & 0 & 0 & 0 & 0 & 0 \\
 -a & -1 & 0 & 0 & a & 1 & 0 & 0 & 0 & 0 & 0 & 0 & 0 & 0 & 0 & 0 \\
 -1 & 0 & 0 & 0 & 1 & 0 & 0 & 0 & 0 & 0 & 0 & 0 & 0 & 0 & 0 & 0 \\
 0 & 0 & 0 & 0 & \frac{L^3}{48EI_{cr}} & \frac{L^2}{8EI_{cr}} & \frac{L}{2EI_{cr}} & \frac{1}{EI_{cr}} & -\frac{L^3}{48EI_{cr}} & -\frac{L^2}{8EI_{cr}} & -\frac{L}{2EI_{cr}} & -\frac{1}{EI_{cr}} & 0 & 0 & 0 & 0 \\
 0 & 0 & 0 & 0 & -\frac{L^2}{8EI_{cr}} & -\frac{L}{2EI_{cr}} & -\frac{1}{EI_{cr}} & 0 & \frac{L^2}{8EI_{cr}} & \frac{L}{2EI_{cr}} & \frac{1}{EI_{cr}} & 0 & 0 & 0 & 0 & 0 \\
 0 & 0 & 0 & 0 & -\frac{L}{2} & -1 & 0 & 0 & \frac{L}{2} & 1 & 0 & 0 & 0 & 0 & 0 & 0 \\
 0 & 0 & 0 & 0 & 1 & 0 & 0 & 0 & -1 & 0 & 0 & 0 & 0 & 0 & 0 & 0 \\
 0 & 0 & 0 & 0 & 0 & 0 & 0 & 0 & \frac{(-a+L)^3}{6EI_{cr}} & \frac{(-a+L)^2}{2EI_{cr}} & \frac{-a+L}{EI_{cr}} & \frac{1}{EI_{cr}} & -\frac{(-a+L)^3}{6EI_{im}} & -\frac{(-a+L)^2}{2EI_{im}} & -\frac{-a+L}{EI_{im}} & -\frac{1}{EI_{im}} \\
 0 & 0 & 0 & 0 & 0 & 0 & 0 & 0 & -\frac{(-a+L)^2}{2EI_{cr}} & -\frac{-a+L}{EI_{cr}} & -\frac{1}{EI_{cr}} & 0 & \frac{(-a+L)^2}{2EI_{im}} & \frac{-a+L}{EI_{im}} & \frac{1}{EI_{im}} & 0 \\
 0 & 0 & 0 & 0 & 0 & 0 & 0 & 0 & a-L & -1 & 0 & 0 & -a+L & 1 & 0 & 0 \\
 0 & 0 & 0 & 0 & 0 & 0 & 0 & 0 & -1 & 0 & 0 & 0 & 1 & 0 & 0 & 0
 \end{bmatrix}
 \times
 \begin{bmatrix}
 c1 \\
 c2 \\
 c3 \\
 c4 \\
 c5 \\
 c6 \\
 c7 \\
 c8 \\
 c9 \\
 c10 \\
 c11 \\
 c12 \\
 c13 \\
 c14 \\
 c15 \\
 c16
 \end{bmatrix}
 =
 \begin{bmatrix}
 0 \\
 0 \\
 -\frac{qL^4}{24EI_{im}} \\
 \frac{qL^2}{2} \\
 -\frac{qa^4}{24EI_{im}} + \frac{qa^4}{24EI_{cr}} \\
 \frac{qa^3}{6EI_{im}} - \frac{qa^3}{6EI_{cr}} \\
 0 \\
 0 \\
 0 \\
 0 \\
 0 \\
 0 \\
 -F \\
 -\frac{q(-a+L)^4}{24EI_{cr}} + \frac{q(-a+L)^4}{24EI_{im}} \\
 \frac{q(-a+L)^3}{6EI_{cr}} - \frac{q(-a+L)^3}{6EI_{im}} \\
 0 \\
 0
 \end{bmatrix}
 \tag{B. 1}$$

Set of equations for rib model loaded at the quarter of the span (B. 2).

$$\begin{bmatrix}
 0 & 0 & 0 & \frac{1}{EI_{im}} & 0 & 0 & 0 & 0 & 0 & 0 & 0 & 0 & 0 & 0 & 0 & 0 \\
 0 & -1 & 0 & 0 & 0 & 0 & 0 & 0 & 0 & 0 & 0 & 0 & 0 & 0 & 0 & 0 \\
 0 & 0 & 0 & 0 & 0 & 0 & 0 & 0 & 0 & 0 & 0 & \frac{L^3}{6EI_{im}} & \frac{L^2}{2EI_{im}} & \frac{L}{EI_{im}} & \frac{1}{EI_{im}} & 0 \\
 0 & 0 & 0 & 0 & 0 & 0 & 0 & 0 & 0 & 0 & 0 & -L & -1 & 0 & 0 & 0 \\
 \frac{a^3}{6EI_{im}} & \frac{a^2}{2EI_{im}} & \frac{a}{EI_{im}} & \frac{1}{EI_{im}} & -\frac{a^3}{6EI_{cr}} & -\frac{a^2}{2EI_{cr}} & -\frac{a}{EI_{cr}} & -\frac{1}{EI_{cr}} & 0 & 0 & 0 & 0 & 0 & 0 & 0 & 0 \\
 -\frac{a^2}{2EI_{im}} & -\frac{a}{EI_{im}} & -\frac{1}{EI_{im}} & 0 & \frac{a^2}{2EI_{cr}} & \frac{a}{EI_{cr}} & \frac{1}{EI_{cr}} & 0 & 0 & 0 & 0 & 0 & 0 & 0 & 0 & 0 \\
 -a & -1 & 0 & 0 & a & 1 & 0 & 0 & 0 & 0 & 0 & 0 & 0 & 0 & 0 & 0 \\
 -1 & 0 & 0 & 0 & 1 & 0 & 0 & 0 & 0 & 0 & 0 & 0 & 0 & 0 & 0 & 0 \\
 0 & 0 & 0 & 0 & \frac{9L^3}{128EI_{cr}} & \frac{9L^2}{32EI_{cr}} & \frac{3L}{4EI_{cr}} & \frac{1}{EI_{cr}} & -\frac{9L^3}{128EI_{cr}} & -\frac{9L^2}{32EI_{cr}} & -\frac{3L}{4EI_{cr}} & -\frac{1}{EI_{cr}} & 0 & 0 & 0 & 0 \\
 0 & 0 & 0 & 0 & -\frac{9L^2}{32EI_{cr}} & -\frac{3L}{4EI_{cr}} & -\frac{1}{EI_{cr}} & 0 & \frac{9L^2}{32EI_{cr}} & \frac{3L}{4EI_{cr}} & \frac{1}{EI_{cr}} & 0 & 0 & 0 & 0 & 0 \\
 0 & 0 & 0 & 0 & -\frac{3L}{4} & -1 & 0 & 0 & \frac{3L}{4} & 1 & 0 & 0 & 0 & 0 & 0 & 0 \\
 0 & 0 & 0 & 0 & 1 & 0 & 0 & 0 & -1 & 0 & 0 & 0 & 0 & 0 & 0 & 0 \\
 0 & 0 & 0 & 0 & 0 & 0 & 0 & 0 & \frac{(L-b)^3}{6EI_{cr}} & \frac{(L-b)^2}{2EI_{cr}} & \frac{L-b}{EI_{cr}} & \frac{1}{EI_{cr}} & -\frac{(L-b)^3}{6EI_{im}} & -\frac{(L-b)^2}{2EI_{im}} & -\frac{L-b}{EI_{im}} & -\frac{1}{EI_{im}} \\
 0 & 0 & 0 & 0 & 0 & 0 & 0 & 0 & -\frac{(L-b)^2}{2EI_{cr}} & -\frac{L-b}{EI_{cr}} & -\frac{1}{EI_{cr}} & 0 & \frac{(L-b)^2}{2EI_{im}} & \frac{L-b}{EI_{im}} & \frac{1}{EI_{im}} & 0 \\
 0 & 0 & 0 & 0 & 0 & 0 & 0 & 0 & -L+b & -1 & 0 & 0 & L-b & 1 & 0 & 0 \\
 0 & 0 & 0 & 0 & 0 & 0 & 0 & 0 & -1 & 0 & 0 & 0 & 1 & 0 & 0 & 0
 \end{bmatrix} \cdot \mathbf{x} = \begin{bmatrix}
 c1 \\
 c2 \\
 c3 \\
 c4 \\
 c5 \\
 c6 \\
 c7 \\
 c8 \\
 c9 \\
 c10 \\
 c11 \\
 c12 \\
 c13 \\
 c14 \\
 c15 \\
 c16
 \end{bmatrix} = \begin{bmatrix}
 0 \\
 0 \\
 -\frac{qL^4}{24EI_{im}} \\
 \frac{qL^2}{2} \\
 -\frac{qa^4}{24EI_{im}} + \frac{qa^4}{24EI_{cr}} \\
 \frac{qa^3}{6EI_{im}} - \frac{qa^3}{6EI_{cr}} \\
 0 \\
 0 \\
 0 \\
 0 \\
 0 \\
 0 \\
 0 \\
 -\frac{q(L-b)^4}{24EI_{cr}} + \frac{q(L-b)^4}{24EI_{im}} \\
 \frac{q(L-b)^3}{6EI_{cr}} - \frac{q(L-b)^3}{6EI_{im}} \\
 0 \\
 F
 \end{bmatrix} \quad (\text{B. 2})$$

Set of equations for slab model in width direction B.3.

C1
C2
C3
C4
S1
S2
S3
S4
S5
S6
S7
S8
D1
D2
D3
D4
D5
D6
D7
D8
B1
B2
B3
B4
B5
B6
B7
B8
G1
G2
G3
G4
G5
G6
G7
G8
H1
H2
H3
H4

=

$$\begin{aligned}
 & \frac{q(aI + 4LInt + a2)^2}{2} \\
 & aIq - \frac{kqal^4}{24EI} - \frac{EInegalq}{EI} \\
 & - \frac{kq(aI + 4LInt)^4}{24EIneg} \\
 & 2q(aI + 2LInt) - \frac{kq(aI + 2LInt)^4}{24EIpos} + F \\
 & - \frac{kq(aI + LInt)^4}{24EIpos} \\
 & - \frac{kq(aI + 3LInt)^4}{24EIneg} \\
 & \frac{qaI^2}{2} - \frac{EInegqal^2}{2EI} \\
 & - \frac{q(aI + LInt)^4}{24EIpos} + \frac{q(aI + LInt)^4}{24EIneg} \\
 & - \frac{q(aI + 3LInt)^4}{24EIneg} + \frac{q(aI + 3LInt)^4}{24EIpos} \\
 & - \frac{q(aI + 4LInt)^4}{24EIneg} + \frac{q(aI + 4LInt)^4}{24EI} \\
 & \frac{EInegq(aI + a_{nvt})^2}{2EI} - \frac{q(aI + a_{nvt})^2}{2} \\
 & - \frac{q(aI + a_{nvt})^4}{24EI} + \frac{q(aI + a_{nvt})^4}{24EIpos} \\
 & - \frac{q(aI + LInt + a_{nvt})^4}{24EIneg} + \frac{q(aI + LInt + a_{nvt})^4}{24EIpos} \\
 & - \frac{q(aI + 3LInt - a_{nvt})^4}{24EIpos} + \frac{q(aI + 3LInt - a_{nvt})^4}{24EIneg} \\
 & - \frac{q(aI + 4LInt - a_{nvt})^4}{24EIpos} + \frac{q(aI + 4LInt - a_{nvt})^4}{24EIneg} \\
 & \frac{q(aI + LInt)^3}{6EIpos} - \frac{q(aI + LInt)^3}{6EIneg} \\
 & \frac{q(aI + 3LInt)^3}{6EIneg} - \frac{q(aI + 3LInt)^3}{6EIpos} \\
 & \frac{q(aI + 4LInt)^3}{6EIneg} - \frac{q(aI + 4LInt)^3}{6EI} \\
 & \frac{q(aI + a_{nvt})^3}{6EI} - \frac{q(aI + a_{nvt})^3}{6EIpos} \\
 & \frac{q(aI + LInt + a_{nvt})^3}{6EIneg} - \frac{q(aI + LInt + a_{nvt})^3}{6EIpos} \\
 & \frac{q(aI + 3LInt - a_{nvt})^3}{6EIpos} - \frac{q(aI + 3LInt - a_{nvt})^3}{6EIneg} \\
 & \frac{q(aI + 4LInt - a_{nvt})^3}{6EIpos} - \frac{q(aI + 4LInt - a_{nvt})^3}{6EIneg} \\
 & \frac{EInegq(aI + a_{nvt})}{EI} - q(aI + a_{nvt}) \\
 & 0 \\
 & 0 \\
 & 0
 \end{aligned}$$

(B. 3)

C Damage parameters in concrete damaged plasticity model

Concrete damaged plasticity model (CDP) is a constitutive model for concrete in Abaqus. To determine the exact parameters of the CDP model several laboratory tests are necessary: uniaxial compression and tension, biaxial failure in the plane stress state and triaxial concrete test. These tests provide information about the shape of the potential flow surface and hardening and softening rule for concrete in tension and compression. However, it is not always possible to perform laboratory tests of concrete; therefore, the simplified approach needs to be established. The hardening and softening behavior of concrete can be specified with damaged parameters. According to scientific paper [18], the damaged parameters for concrete in compression and tension can be determined by relation (C. 1) and (C. 2),

$$d_c(\sigma_c) = \begin{cases} 0, & \text{for } \sigma_c \leq f_{cm} \\ 1 - \sigma_c/f_{cm}, & \text{for } \sigma_c > f_{cm} \end{cases} \quad (\text{C. 1})$$

$$d_t(\sigma_t) = \begin{cases} 0, & \text{for } \sigma_t \leq f_{ctm} \\ 1 - \sigma_t/f_{ctm}, & \text{for } \sigma_t > f_{ctm} \end{cases} \quad (\text{C. 2})$$

where d_c and d_t are damage parameters of concrete in compression and tension respectively, σ_c and σ_t are uniaxial compressive and tensile concrete stresses according to the defined stress-strain concrete curves, f_{cm} and f_{ctm} are mean values of concrete cylinder compressive strength and axial tensile strength respectively.

The stress-strain relations for non-linear concrete behavior in tension and compression under uniaxial loading are adopted from Eurocode 2 [15]. The compressive and tensile stress-strain curves for concrete C20/25 are shown in Figure C. 1. For the concrete grade C20/25 next values are specified in Eurocode 2:

- $f_{cm} = 28\text{MPa}$, $f_{ctm} = 2.2\text{MPa}$;
- $\varepsilon_{cu1} = 0.0035$, $E_{cm} = 30\text{GPa}$, $\nu = 0.15$.

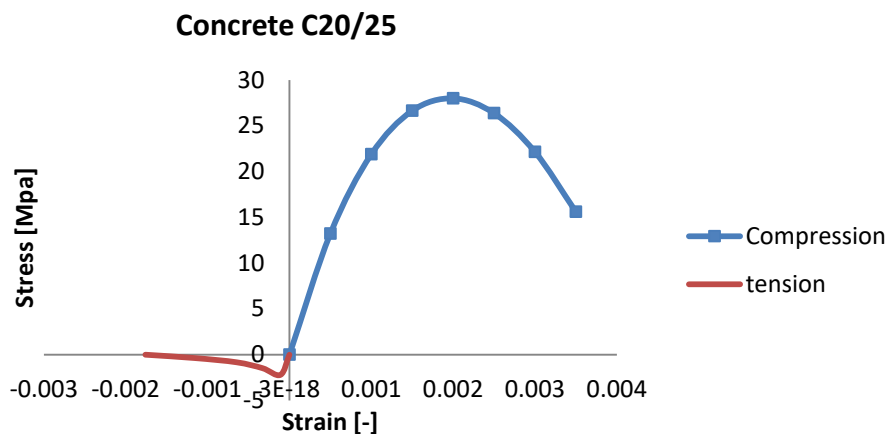


Figure C. 1 Compressive and tensile stress-strain curves for concrete C20/25

Now that the stress-strain curves for concrete in tension and compression are specified, the damage parameters can be computed using (C. 1) and (C. 2). The results are presented in Table C. 1 and Table C. 2.

Table C. 1 Concrete compression damage

Stress σ_c , MPa	Strain	Inelastic strain	Damage d_c
0.0	0.0	-	0.0
13.21	0.0	0.0	0.0
21.89	0.001	0.00027	0.0
26.64	0.0015	0.000612	0.0
28	0.002	0.001067	0.0
26.37	0.0025	0.001621	0.057861
22.14	0.003	0.002262	0.209030
15.60	0.0035	0.002980	0.442641

Table C. 2 Concrete tension damage

Stress σ_t , MPa	Strain	Inelastic strain	Damage d_t
0.0	0.0	-	0.0
2.20	0.00011	0.000037	0.0
1.467	0.00033	0.000281	0.333182
0.825	0.000646	0.000619	0.625000
0.367	0.001155	0.001143	0.833182
0.0	0.00176	0.001760	1.0

In Table C. 1 and Table C. 2 compressive and tensile stress values are presented together with corresponding values of total strain and inelastic (plastic) strain, and damage parameters. The effect of damage parameters on uniaxial compressive and tensile stress response is graphically shown in Figure C. 2 and Figure C. 3. One can notice that behavior of concrete C20/25 according to Eurocode 2 and concrete C20/25, which behavior is influenced by damaged plasticity, is identical on both graphs up to maximum stress point (ascending branches of stress-strain curves). This is expected because there is no damage present for concrete in the elastic zone according to the CDP model. On the contrary, the descending branches of stress-strain curves have a difference which is caused by damaged plasticity effect.

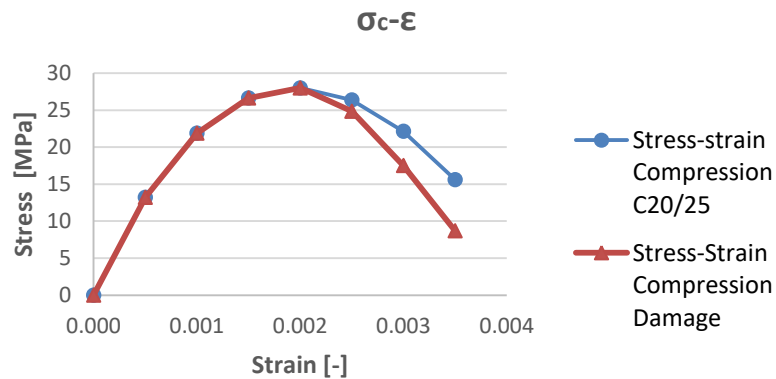


Figure C. 2 Uniaxial compressive stress response of concrete and damaged plasticity

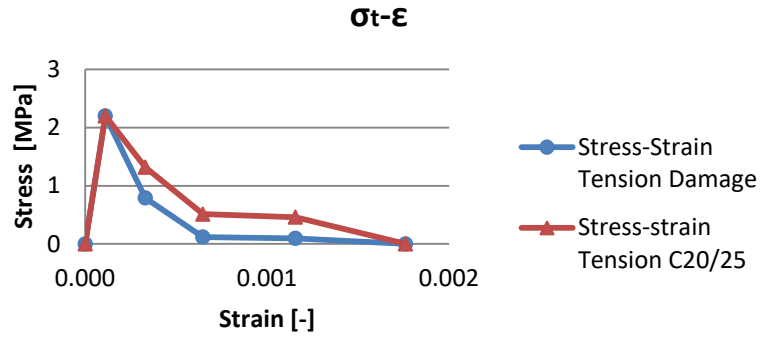


Figure C. 3 Uniaxial tensile stress response of concrete and damaged plasticity

The uniaxial stress response of concrete in tension and compression is characterized by elastic stiffness degradation when concrete is unloaded from any point on stress-strain curves beyond the maximum stress point. This is clearly can be seen on descending branches of stress-strain curves (see Figure C. 2 and Figure C. 3). Hence, the elastic stiffness degradation of concrete in tension and compression is taken into account in concrete damaged plasticity model by applying corresponding degradation parameters d_c and d_t . The representation of concrete behaviour is in some measure simplistic, however, it is enough to illustrate the main features of concrete response under uniaxial loading.

D Engineering model results

Hereby the detailed results of the engineering model are presented. The deflection and bending moment diagram of the composite slab with a different amount of reinforcement mesh in the top deck and width of the rib – $b_{rib}=600\text{mm}$ and $b_{rib}=175\text{mm}$ – are displayed for two load arrangements: concentrated load at the middle of the span and at the quarter of the span. These results display the influence of concentrated load only on the composite slab behavior, the self-weight of the composite slab is not included.

D.1 Load at the quarter of the span

The deflection and bending moment diagrams of composite slab ComFlor210 with one, two and no reinforcement mesh in the top deck under 10kN and 50kN concentrated force applied at the middle rib are shown in [FIGURE D. 1-FIGURE D. 10](#). The results of the engineering model with $b_{rib}=175\text{mm}$ are very different from test results; thus, only the results from the engineering model with $b_{rib}=600\text{mm}$ will be discussed below.

Composite slab with two, one and no reinforcement mesh in top deck under 10kN load shows more or less the same behavior: all five ribs deflect and, thus, participate in spreading the load. The resulting bending moment at 10kN is positive; this is a contradiction to the assumed earlier model of top deck clamped between the ribs. The possible explanation can be that in reality, the top deck behaves not as a clamped element between ribs but more like a continuous beam. However, the composite slab under 50kN has parts with the negative bending moment; the deflection shape is also different. The middle three ribs are affected the most with applied concentrated force; additionally, the uplift of free edges is observed. The comparison with experimental results (see § 4.5.2) shows that the difference in rib deflection between the engineering model and tests are acceptable but only for high load, i.e. 50kN. The conclusion can be drawn that the engineering model does not work adequately when a small load is applied; the possible reason might be the underestimation of rib bending stiffness.

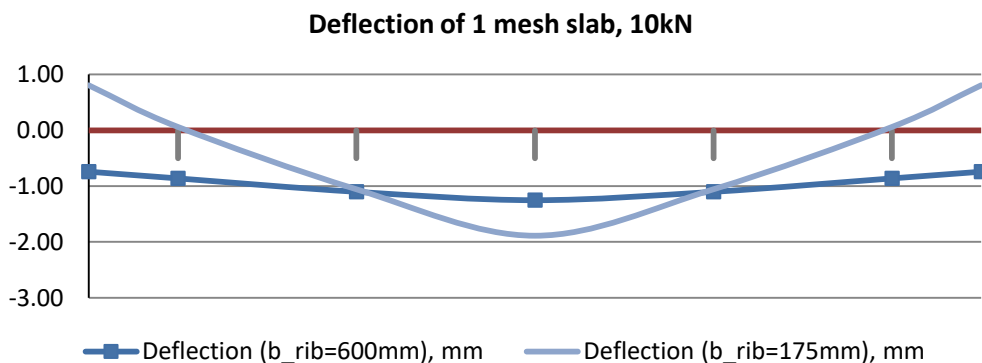


Figure D. 1 Deflection of one mesh slab under 10kN load resulting from the engineering model (vertical lines indicate rib position)

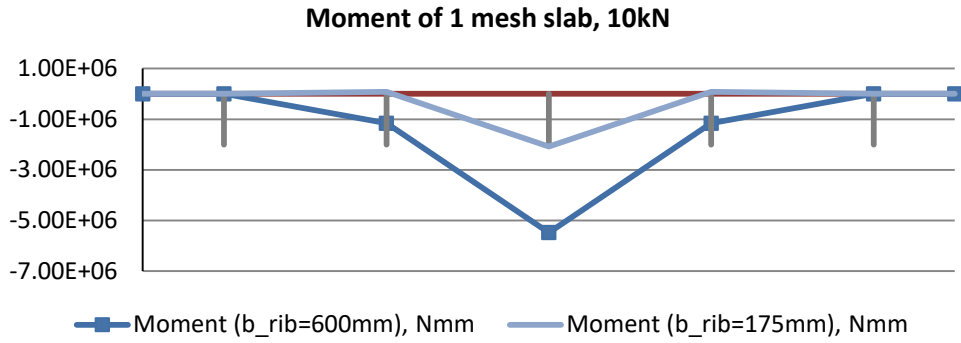


Figure D. 2 Bending moment diagram of one mesh slab under 10kN load resulting from the engineering model (vertical lines indicate rib position)

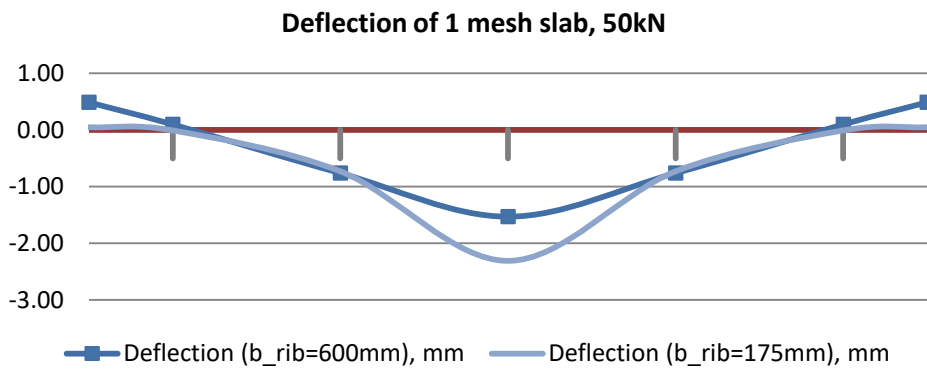


Figure D. 3 Deflection of one mesh slab under 50kN load resulting from the engineering model (vertical lines indicate rib position)

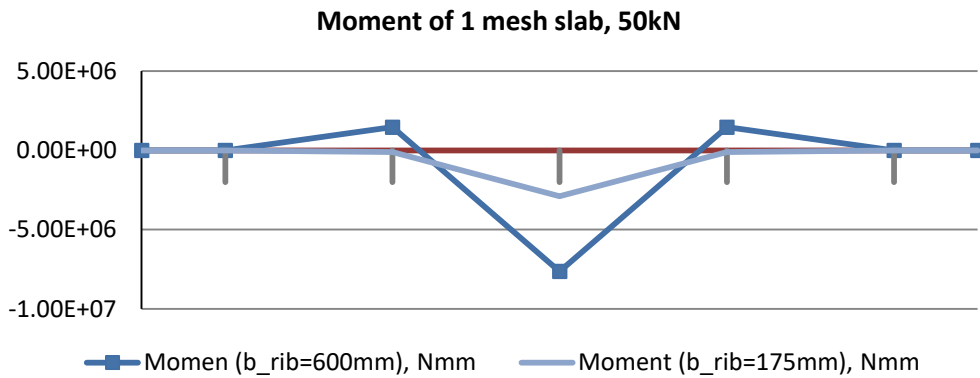


Figure D. 4 Bending moment diagram of one mesh slab under 50kN load resulting from the engineering model (vertical lines indicate rib position)

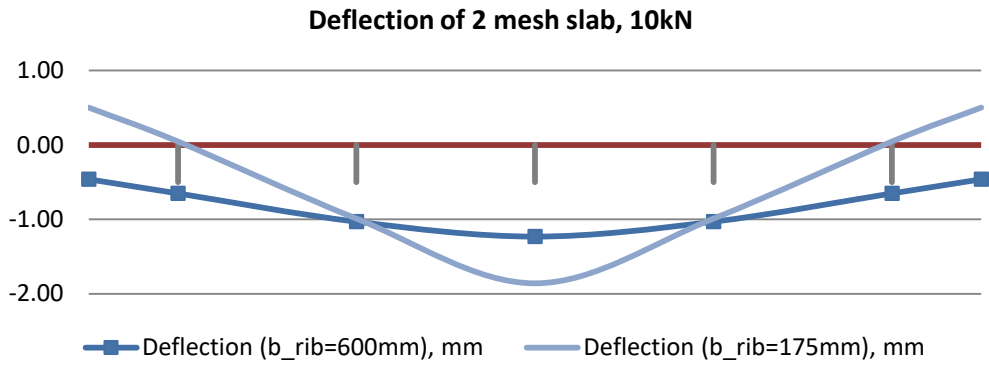


Figure D. 5 Deflection of two mesh slab under 10kN load resulting from the engineering model (vertical lines indicate rib position)

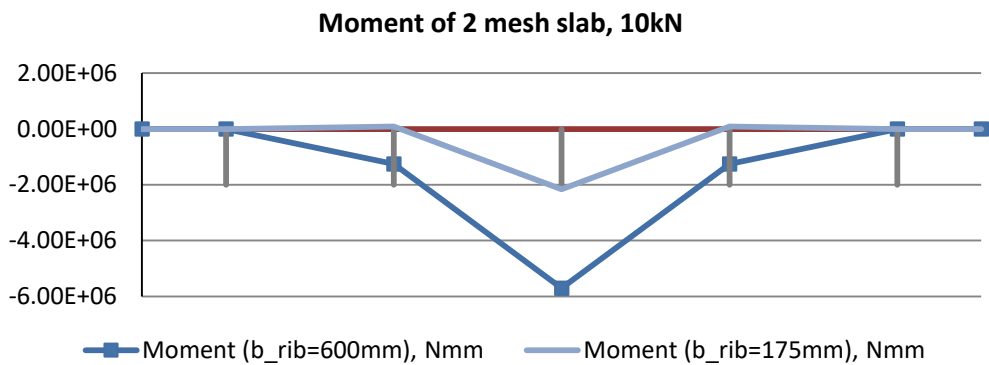


Figure D. 6 Bending moment diagram of two mesh slab under 10kN load resulting from the engineering model (vertical lines indicate rib position)

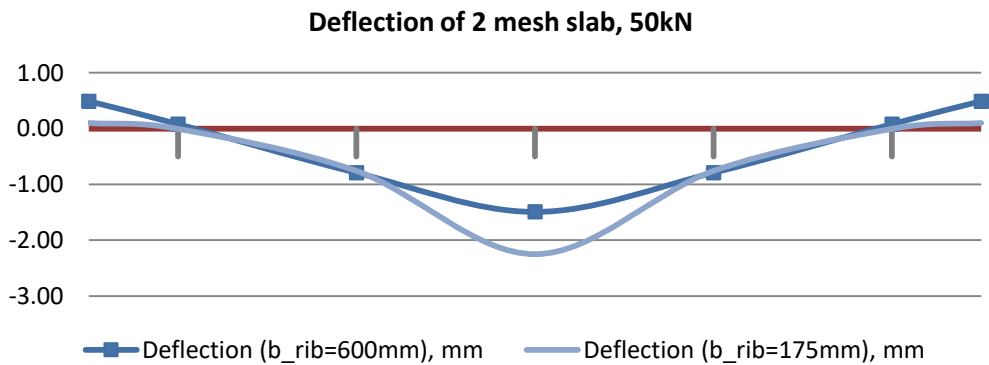


Figure D. 7 Deflection of two mesh slab under 50kN load resulting from the engineering model (vertical lines indicate rib position)

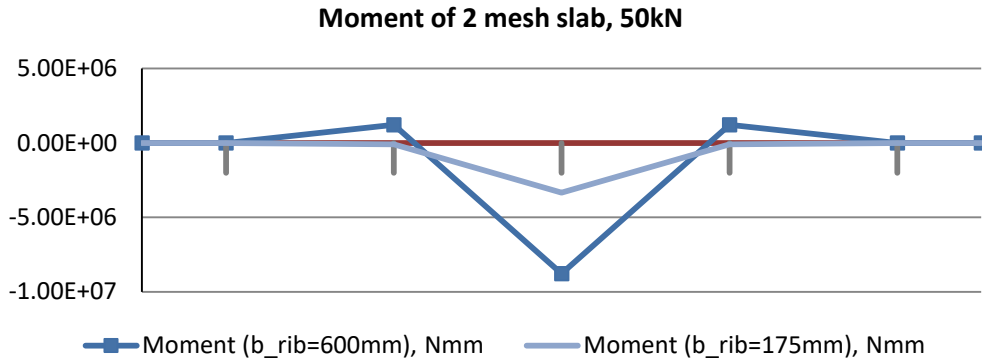


Figure D. 8 Bending moment diagram of two mesh slab under 50kN load resulting from the engineering model (vertical lines indicate rib position)

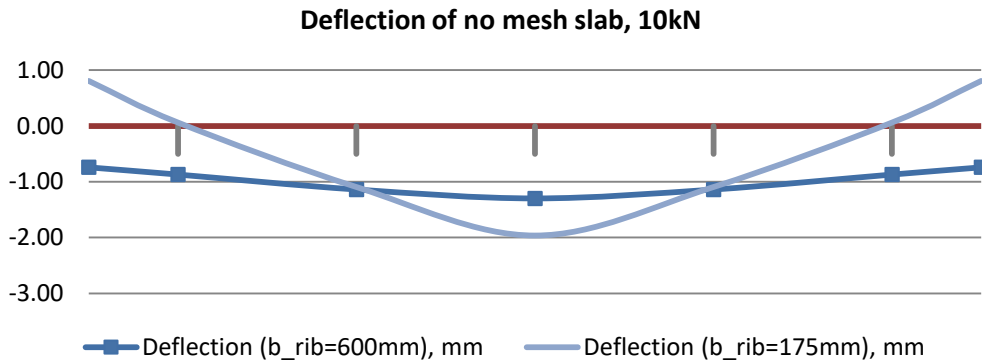


Figure D. 9 Deflection of no mesh slab under 10kN load resulting from the engineering model (vertical lines indicate rib position)

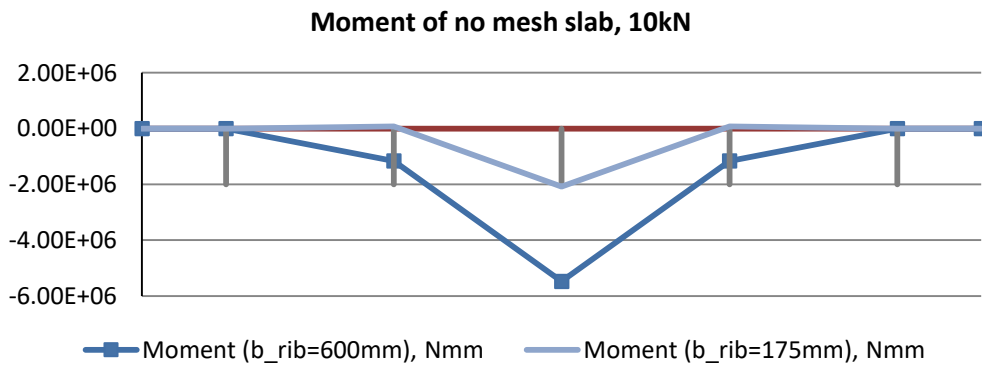


Figure D. 10 Bending moment diagram of no mesh slab under 10kN load resulting from the engineering model (vertical lines indicate rib position)

D.2 Load at the middle of the span

The deflection and bending moment diagrams of composite slab ComFlor210 with one, two and no reinforcement mesh in top deck under 10kN and 60kN concentrated force applied at the middle rib are shown in FIGURE D. 11-FIGURE D. 22. The results of the engineering model with $b_{rib}=175\text{mm}$ are very different from test results; therefore, only the results from the engineering model with $b_{rib}=600\text{mm}$ will be discussed below.

Composite slab with two, one and no reinforcement mesh in top deck under 10kN load behaves similarly: all five ribs deflect more or less evenly while spreading the load. Composite slabs under 60kN show that middle three ribs are influenced the most by concentrated force; the deflection of the middle rib is increased a lot compared to a slab under 10kN load. The uplift of free edges does not occur unlike in a case when the load was applied at a quarter of the span. Additionally, the resulting bending moment is positive in all cases; this is again dissension to the proposed model of top deck that is assumed to be clamped between the ribs. The comparison with experiment (see § 4.5.1) shows that the difference in rib deflection between engineering model and test results are reasonable but only for high load, i.e. 60kN. The conclusion can be drawn that the engineering model with a load in the middle of a span cannot deliver acceptable results when a load of small magnitude is applied; the possible reason might be the underestimation of rib bending stiffness.

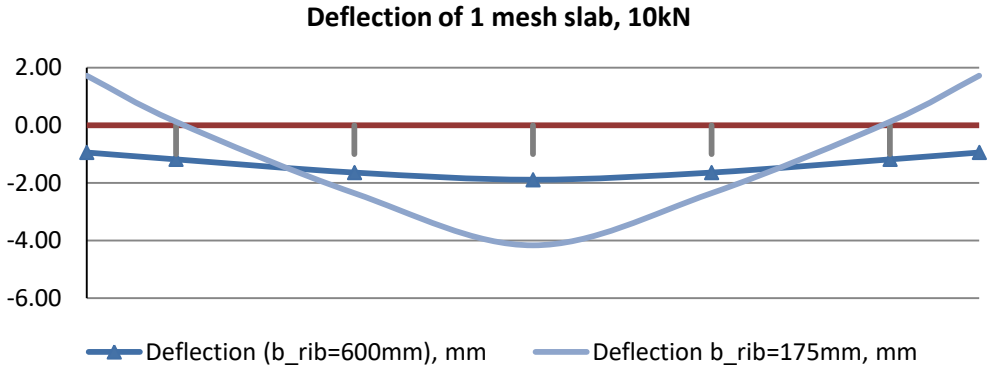


Figure D. 11 Deflection of one mesh slab under 10kN load resulting from the engineering model (vertical lines indicate rib position)

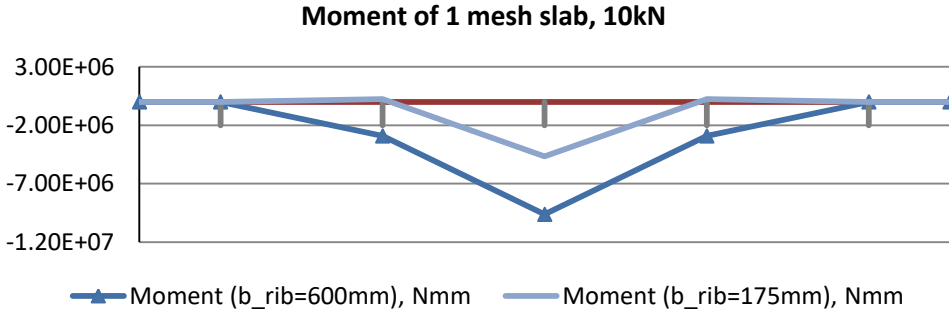


Figure D. 12 Bending moment diagram of one mesh slab under 10kN load resulting from the engineering model (vertical lines indicate rib position)

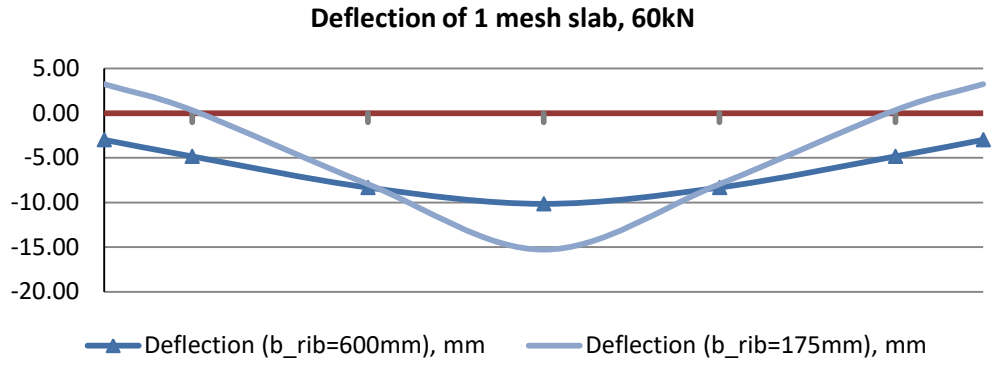


Figure D. 13 Deflection of one mesh slab under 60kN load resulting from the engineering model (vertical lines indicate rib position)

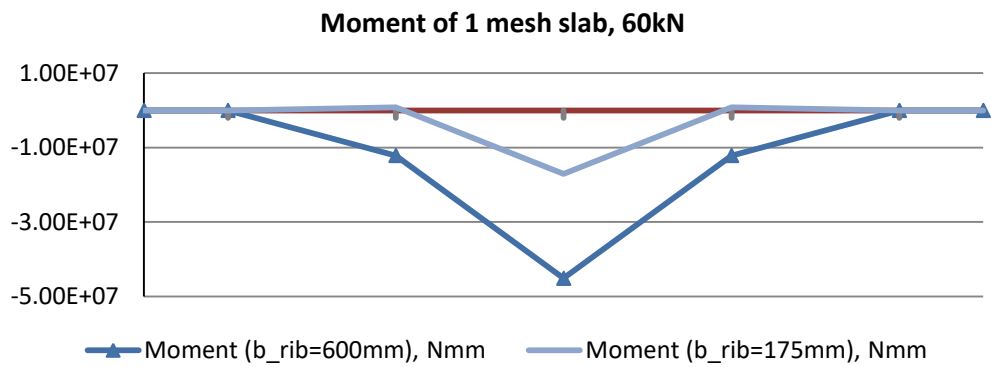


Figure D. 14 Bending moment diagram of one mesh slab under 60kN load resulting from the engineering model (vertical lines indicate rib position)

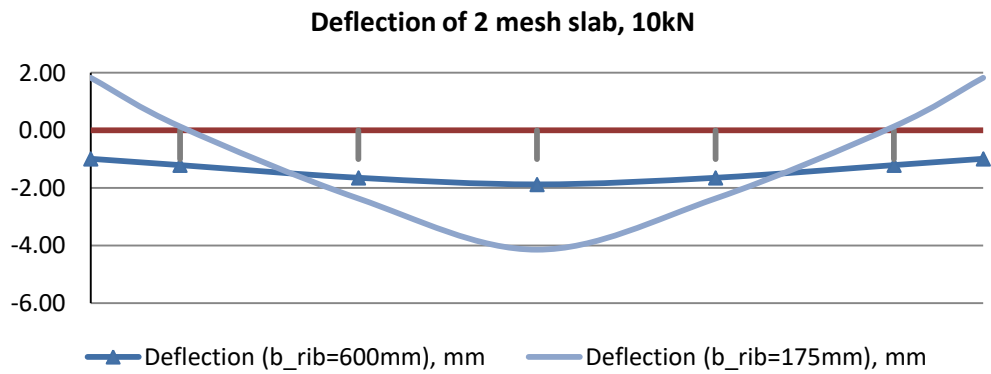


Figure D. 15 Deflection of two mesh slab under 10kN load resulting from the engineering model (vertical lines indicate rib position)

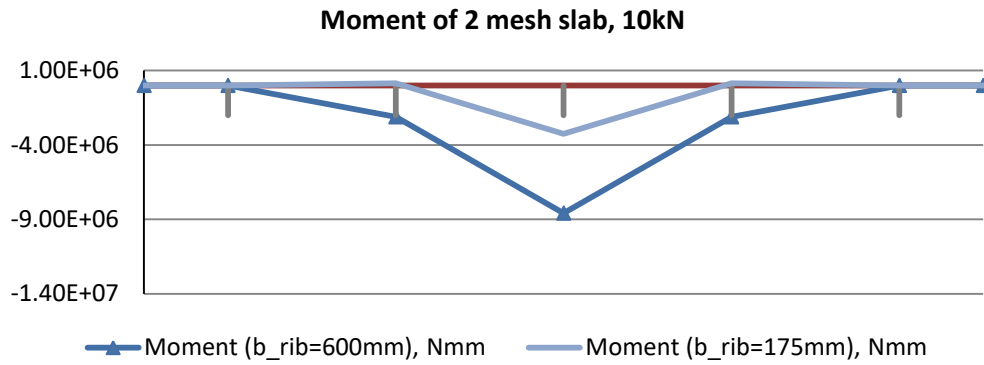


Figure D. 16 Bending moment diagram of two mesh slab under 10kN load resulting from the engineering model (vertical lines indicate rib position)

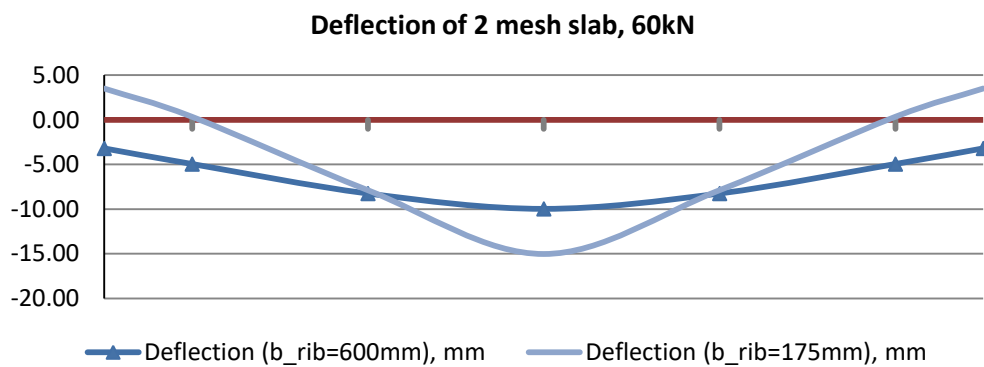


Figure D. 17 Deflection of two mesh slab under 60kN load resulting from the engineering model (vertical lines indicate rib position)

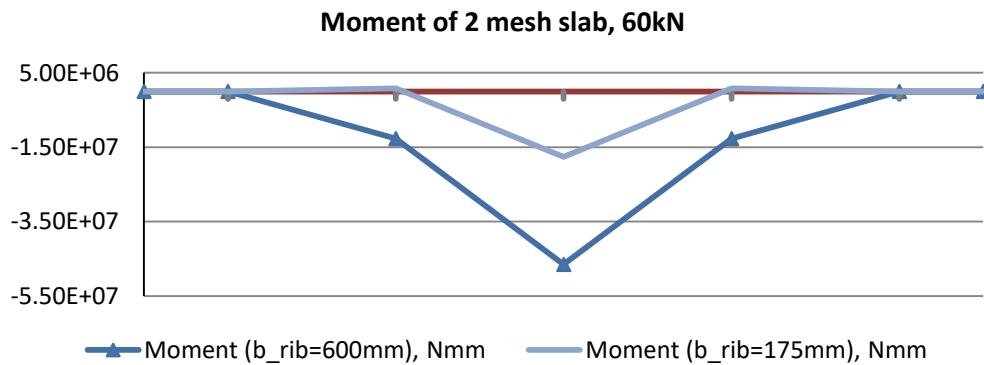


Figure D. 18 Bending moment diagram of two mesh slab under 60kN load resulting from the engineering model (vertical lines indicate rib position)

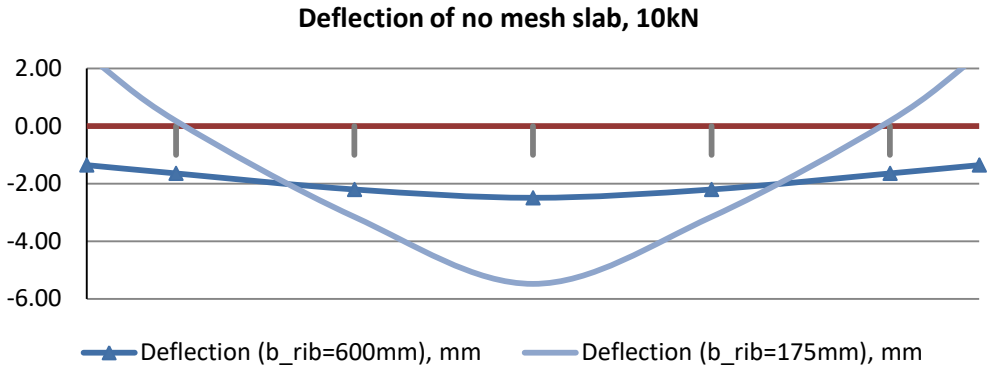


Figure D. 19 Deflection of no mesh slab under 10kN load resulting from the engineering model (vertical lines indicate rib position)

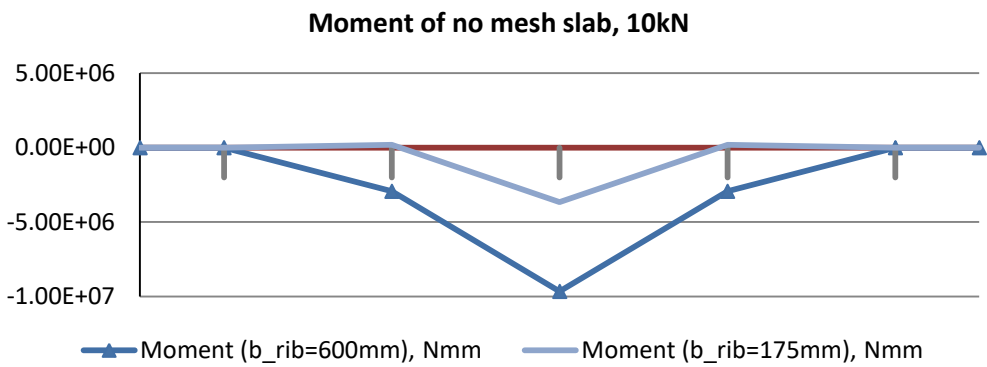


Figure D. 20 Bending moment diagram of no mesh slab under 10kN load resulting from the engineering model (vertical lines indicate rib position)

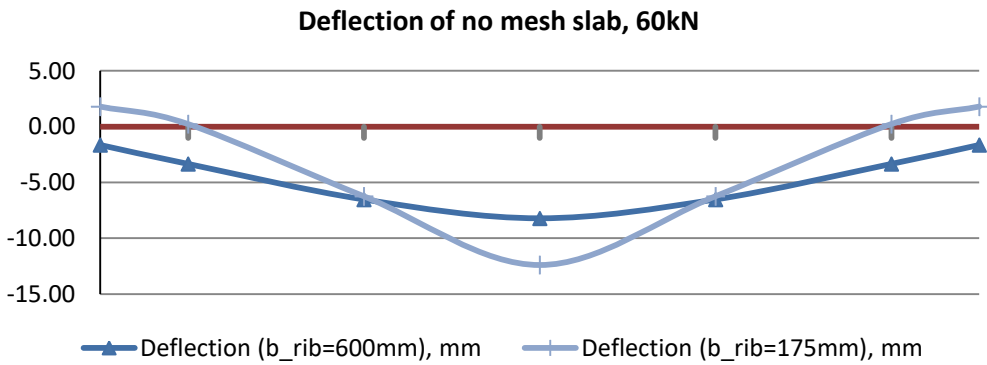


Figure D. 21 Deflection of no mesh slab under 60kN load resulting from the engineering model (vertical lines indicate rib position)

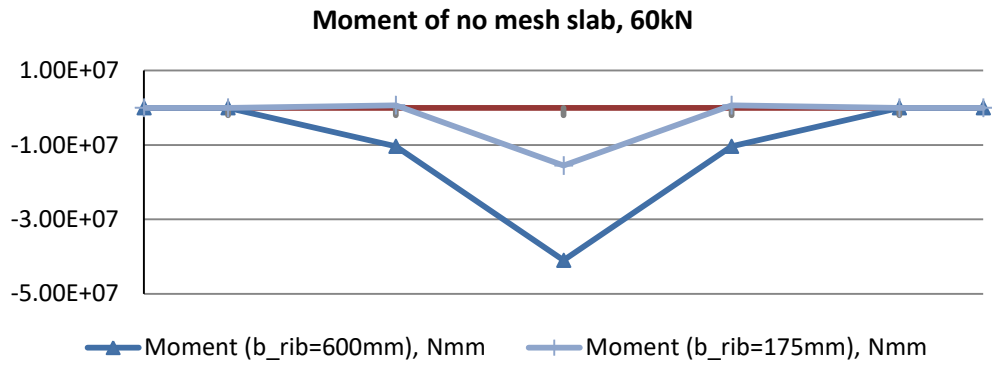


Figure D. 22 Bending moment diagram of no mesh slab under 60kN load resulting from the engineering model (vertical lines indicate rib position)

E Finite element model results

The detailed results of finite element analysis for a composite slab with length 3.6m, 5.4m and 7.2m are presented. The contour plots for deflection and stresses from finite element models are displayed for three load arrangements: concentrated load at the middle of the span, at the quarter of the span and at one-sixth of the span. The self-weight of the composite slab is not included in FEA.

E.1 Composite slab ComFlor210, $L_{span}=5.4m$

The displacement field U2 and Von Mises stress in the concrete of composite slab ComFlor210 with one reinforcement mesh in top deck under 60kN concentrated load applied at the middle Rib 3 and adjacent Rib 2 are shown in **Figure E. 1-Figure E. 12**.

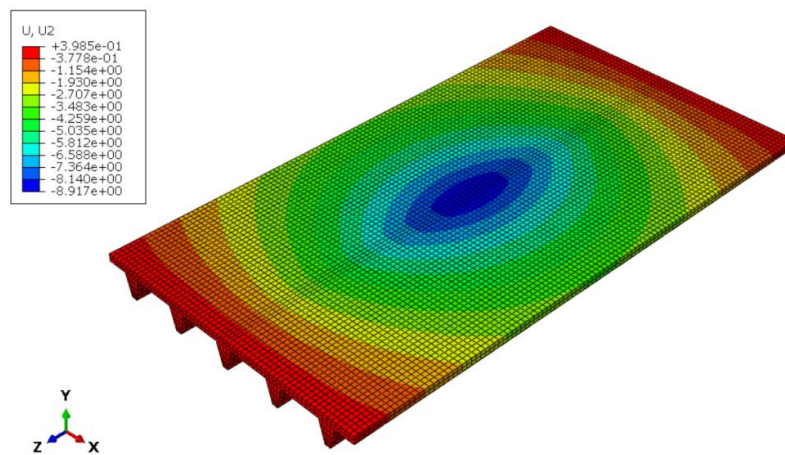


Figure E. 1 Displacement field U2 in composite slab 5.4m under concentrated force 60kN placed on Rib3 at $L_{span}/2$ in load-control FEA

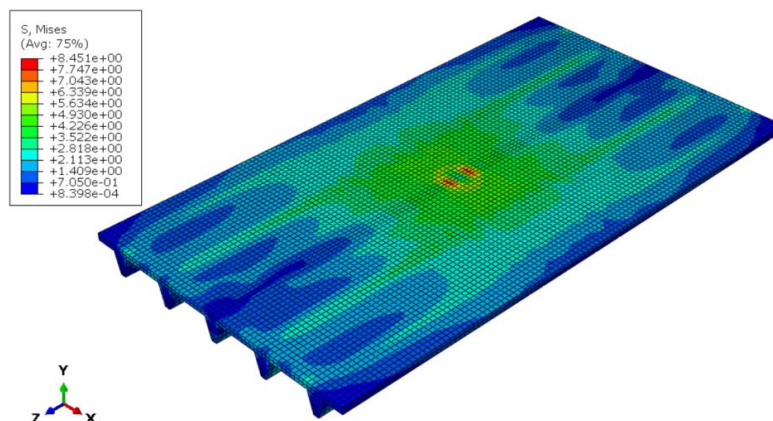


Figure E. 2 Von Mises stress distribution in concrete in composite slab 5.4m under concentrated force 60kN placed on Rib3 at $L_{span}/2$ at the end of the analysis

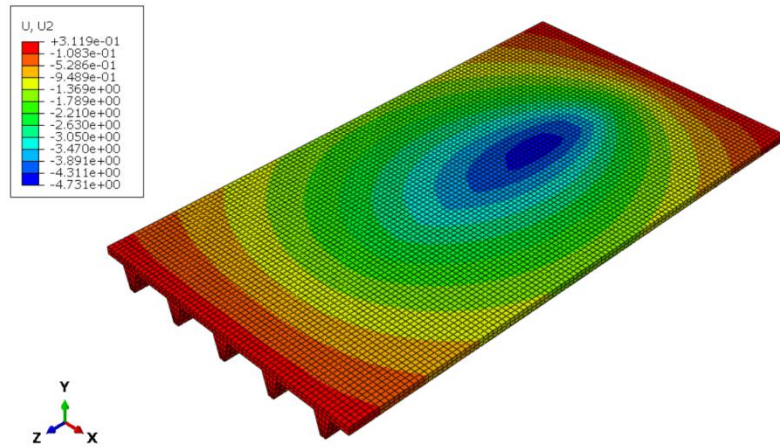


Figure E. 3 Displacement field U2 in composite slab 5.4m under concentrated force 60kN placed on Rib3 at $L_{span}/4$ in load-control FEA

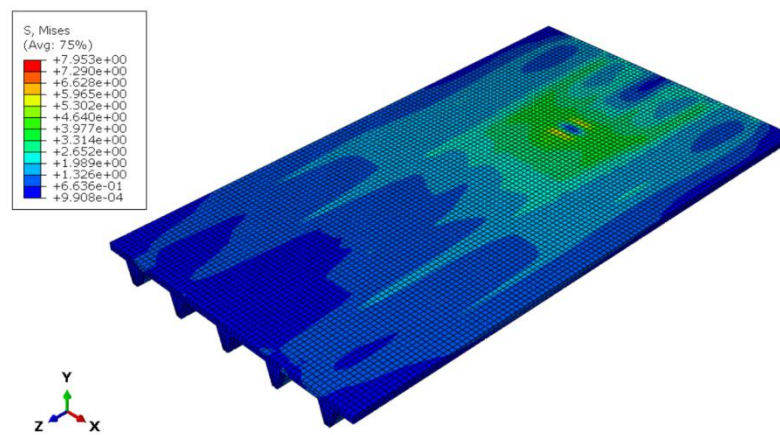


Figure E. 4 Von Mises stress distribution in concrete in composite slab 5.4m under concentrated force 60kN placed on Rib3 at $L_{span}/4$ at the end of the analysis

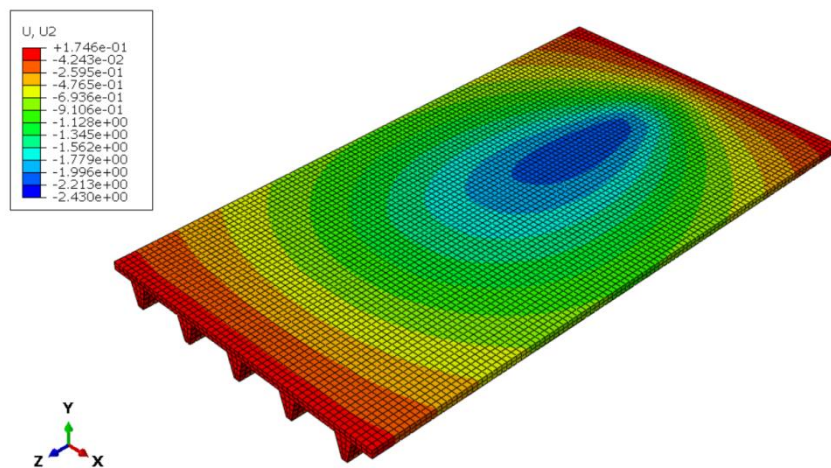


Figure E. 5 Displacement field U2 in composite slab 5.4m under concentrated force 60kN placed on Rib3 at $L_{span}/6$ in load-control FEA

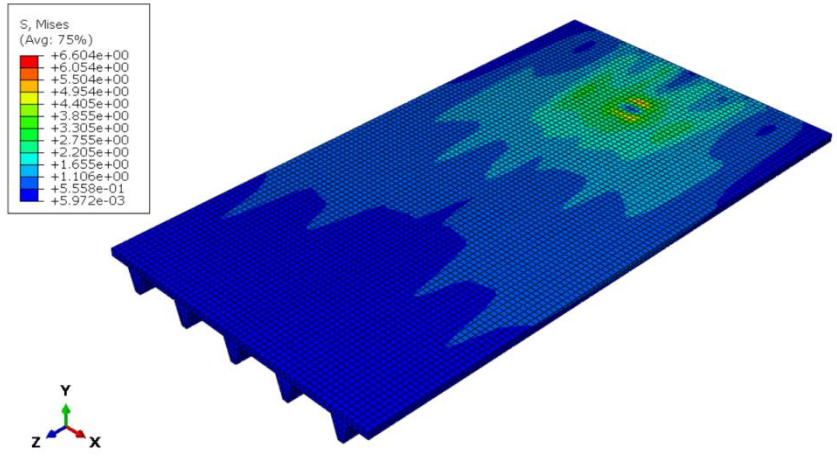


Figure E. 6 Von Mises stress distribution in concrete in composite slab 5.4m under concentrated force 60kN placed on Rib3 at $L_{span}/6$ at the end of the analysis

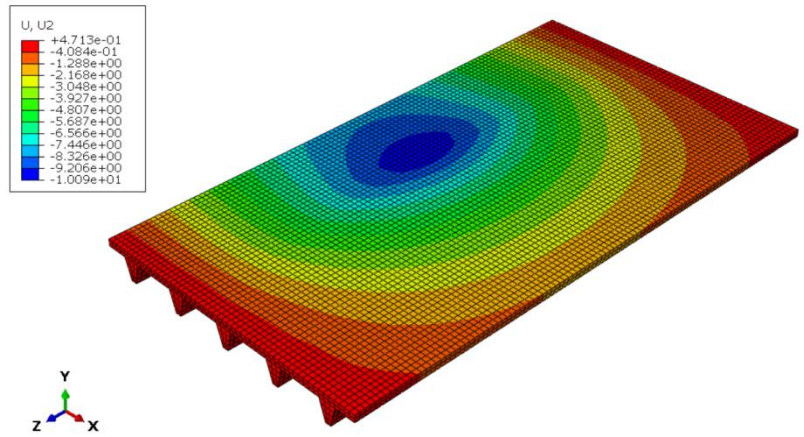


Figure E. 7 Displacement field U2 in composite slab 5.4m under concentrated force 60kN placed on Rib2 at $L_{span}/2$ in load-control FEA

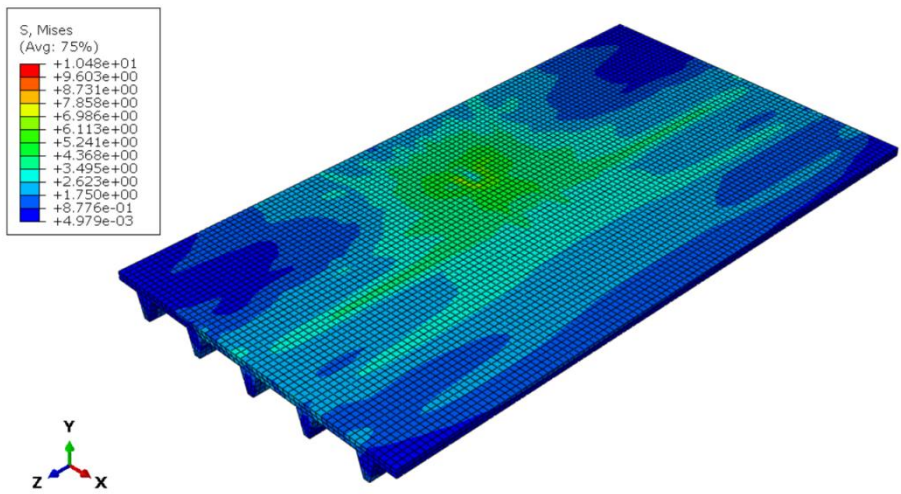


Figure E. 8 Von Mises stress distribution in concrete in composite slab 5.4m under concentrated force 60kN placed on Rib2 at $L_{span}/2$ at the end of the analysis

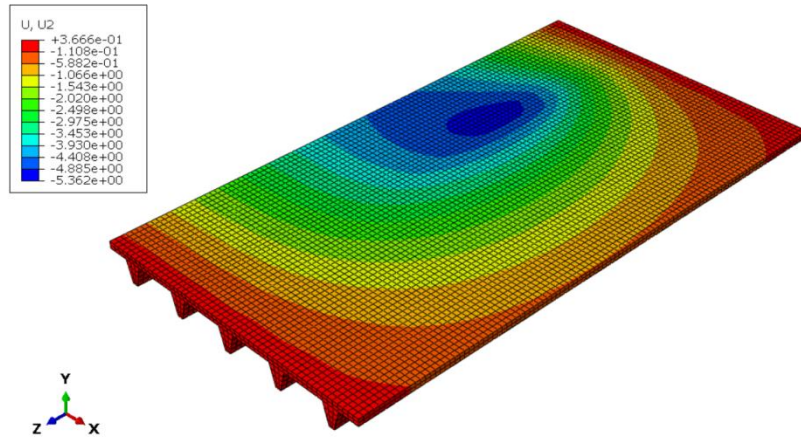


Figure E. 9 Displacement field U2 in composite slab 5.4m under concentrated force 60kN placed on Rib2 at $L_{span}/4$ in load-control FEA

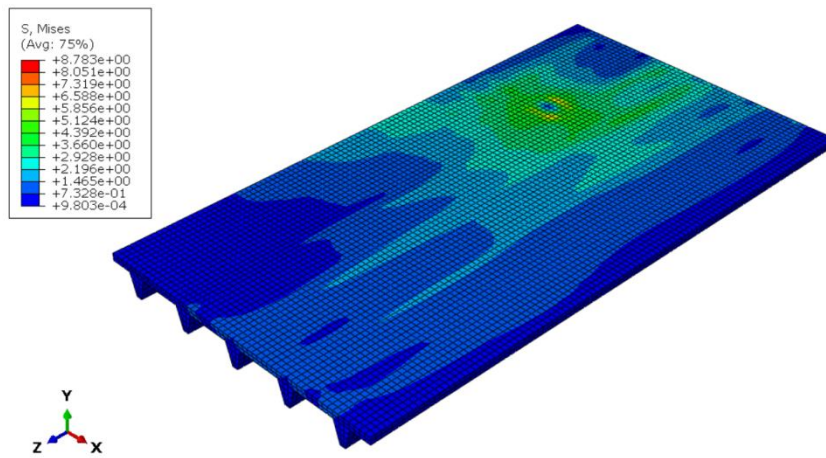


Figure E. 10 Von Mises stress distribution in concrete in composite slab 5.4m under concentrated force 60kN placed on Rib2 at $L_{span}/4$ at the end of the analysis

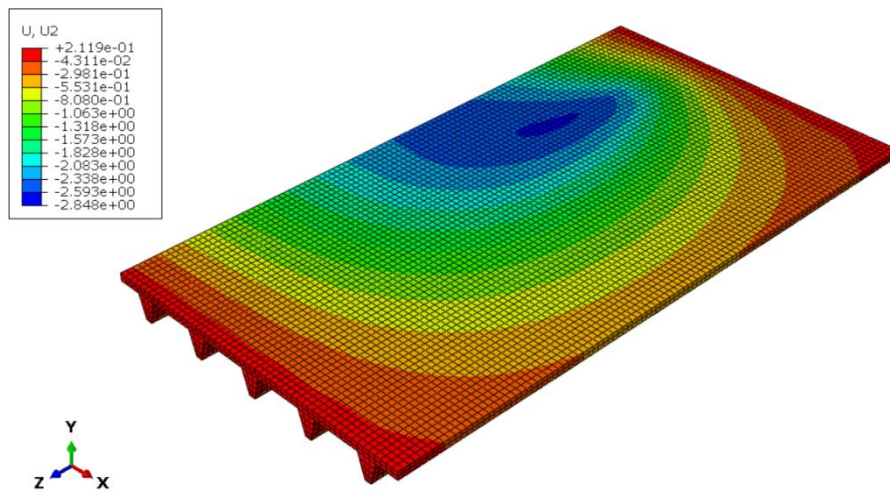


Figure E. 11 Displacement field U2 in composite slab 5.4m under concentrated force 60kN placed on Rib2 at $L_{span}/6$ in load-control FEA

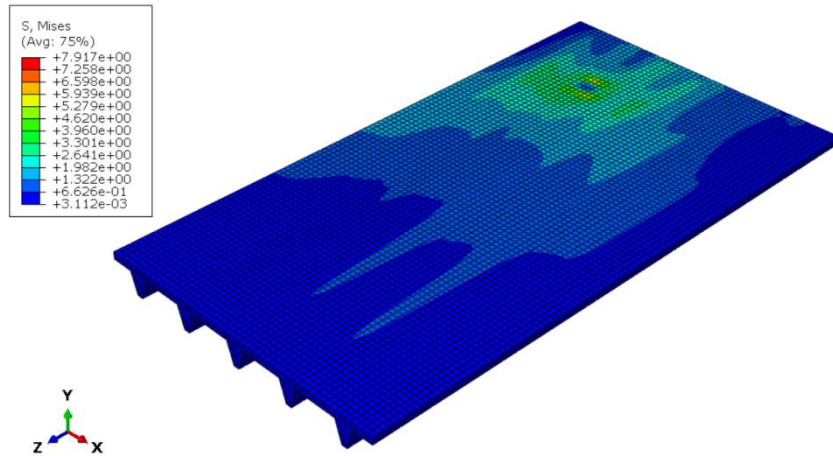


Figure E. 12 Von Mises stress distribution in concrete in composite slab 5.4m under concentrated force 60kN placed on Rib2 at $L_{span}/6$ at the end of the analysis

E.2 Composite slab ComFlor210, $L_{span}=3.6m$

The displacement field U2 and Von Mises stress in the concrete of composite slab ComFlor210 with one reinforcement mesh in top deck under 60kN concentrated load applied at the middle Rib 3 and adjacent Rib 2 are given in FIGURE E. 13-FIGURE E. 24.

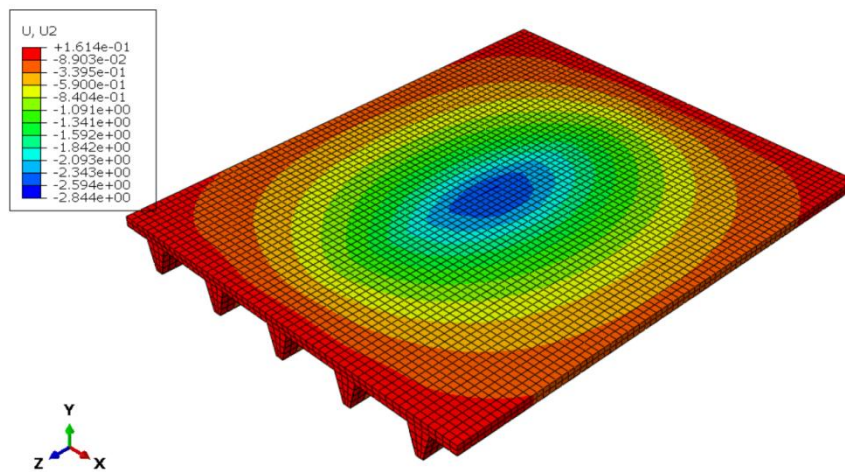


Figure E. 13 Displacement field U2 in composite slab 3.6m under concentrated force 60kN placed on Rib3 at $L_{span}/2$ in load-control FEA

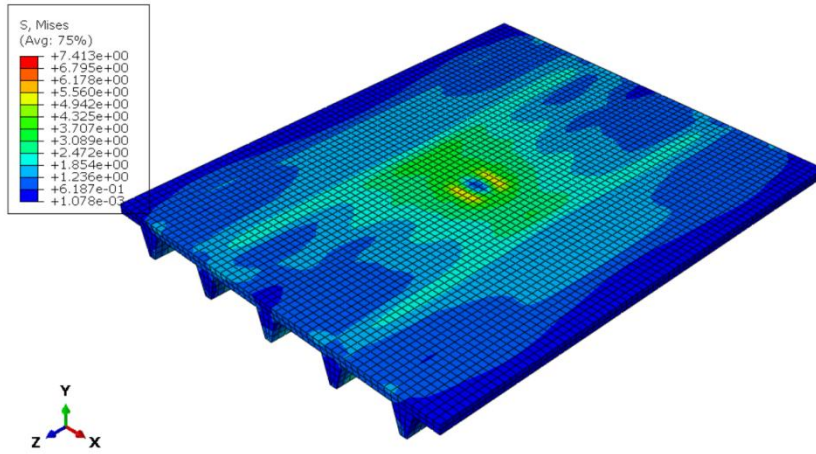


Figure E. 14 Von Mises stress distribution in concrete in composite slab 3.6m under concentrated force 60kN placed on Rib3 at $L_{span}/2$ at the end of the analysis

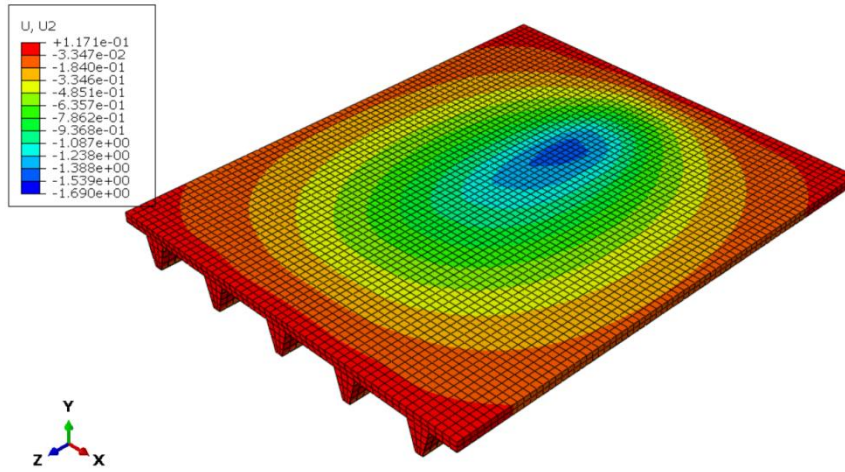


Figure E. 15 Displacement field U2 in composite slab 3.6m under concentrated force 60kN placed on Rib3 at $L_{span}/4$ in load-control FEA

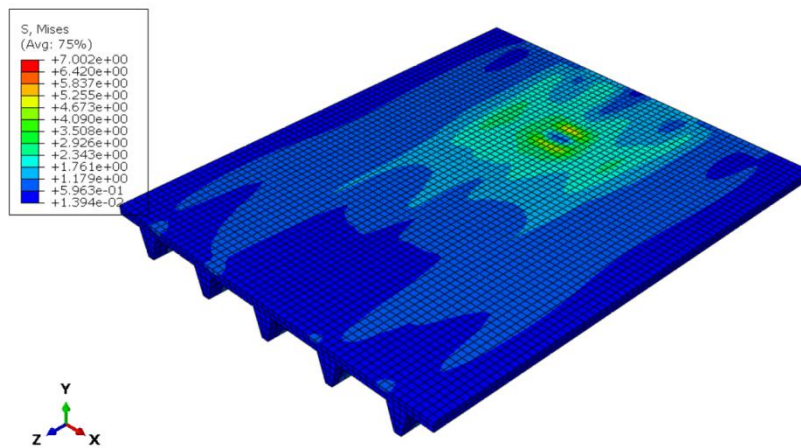


Figure E. 16 Von Mises stress distribution in concrete in composite slab 3.6m under concentrated force 60kN placed on Rib3 at $L_{span}/4$ at the end of the analysis

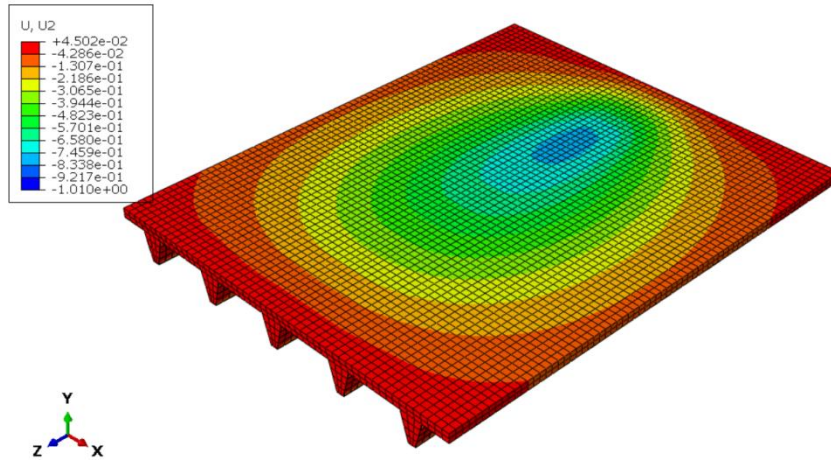


Figure E. 17 Displacement field U2 in composite slab 3.6m under concentrated force 60kN placed on Rib3 at $L_{span}/6$ in load-control FEA

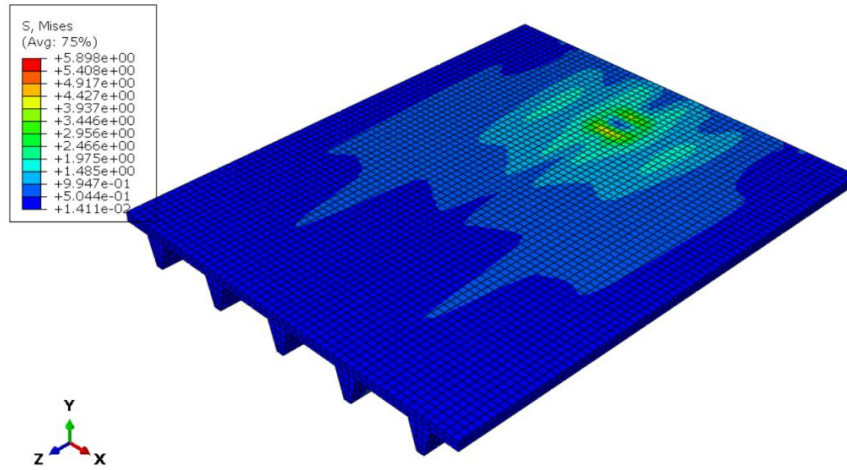


Figure E. 18 Von Mises stress distribution in concrete in composite slab 3.6m under concentrated force 60kN placed on Rib3 at $L_{span}/6$ at the end of the analysis

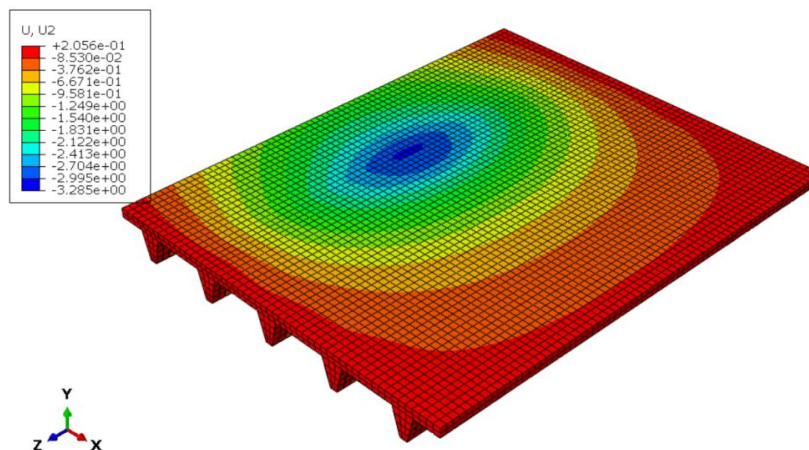


Figure E. 19 Displacement field U2 in composite slab 3.6m under concentrated force 60kN placed on Rib2 at $L_{span}/2$ in load-control FEA

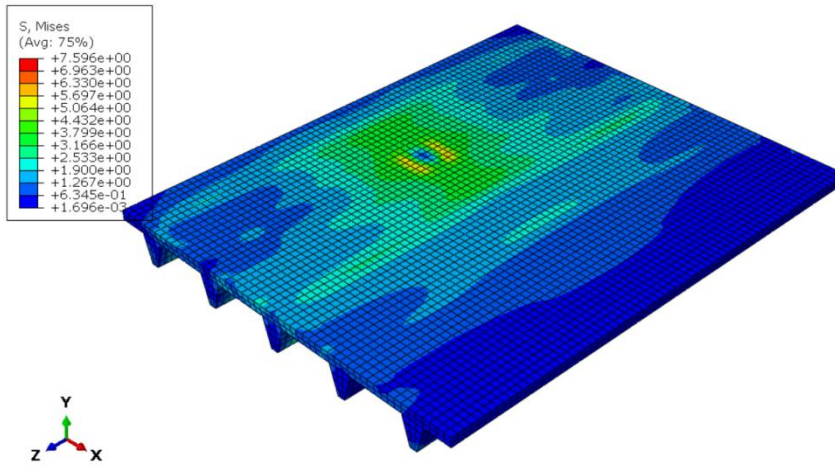


Figure E. 20 Von Mises stress distribution in concrete in composite slab 3.6m under concentrated force 60kN placed on Rib2 at $L_{span}/2$ at the end of the analysis

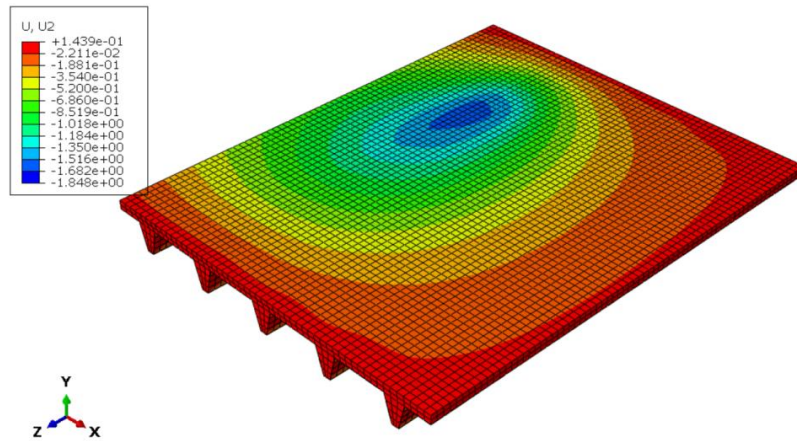


Figure E. 21 Displacement field U2 in composite slab 3.6m under concentrated force 60kN placed on Rib2 at $L_{span}/4$ in load-control FEA

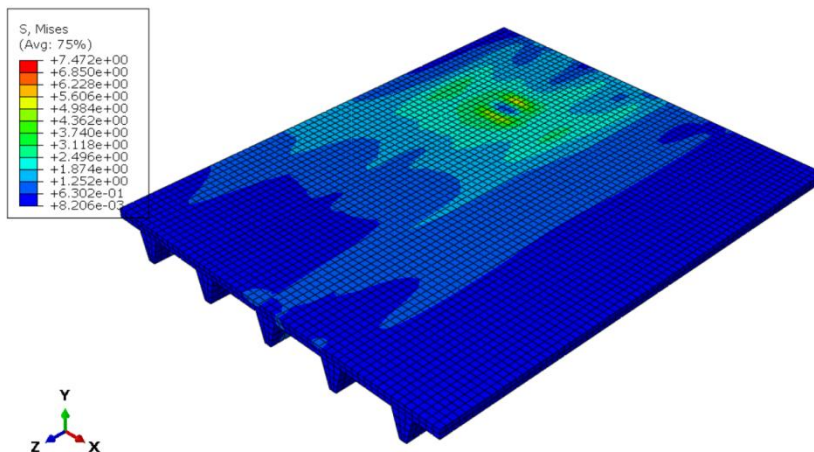


Figure E. 22 Von Mises stress distribution in concrete in composite slab 3.6m under concentrated force 60kN placed on Rib2 at $L_{span}/4$ at the end of the analysis

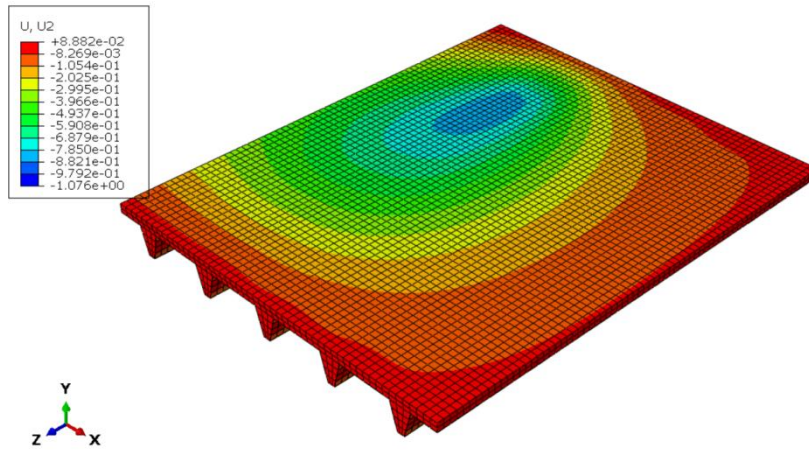


Figure E. 23 Displacement field U2 in composite slab 3.6m under concentrated force 60kN placed on Rib2 at $L_{span}/6$ in load-control FEA

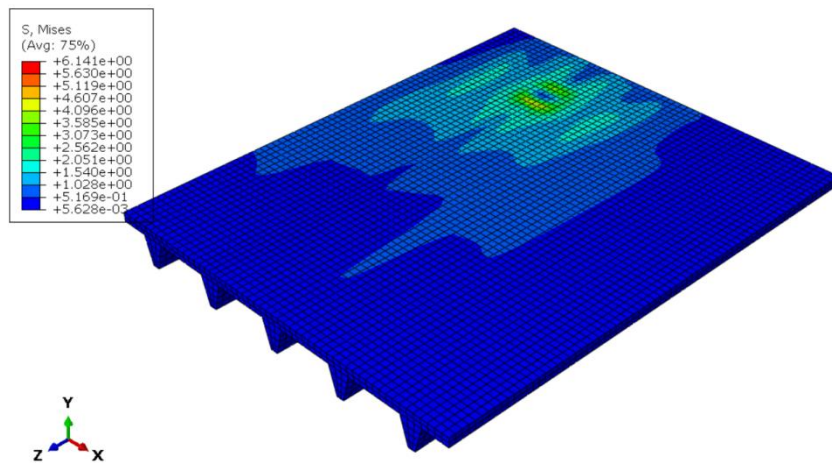


Figure E. 24 Von Mises stress distribution in concrete in composite slab 3.6m under concentrated force 60kN placed on Rib2 at $L_{span}/6$ at the end of the analysis

E.3 Composite slab ComFlor210, $L_{span}=7.2\text{m}$

The displacement field U2 and Von Mises stress in the concrete of composite slab ComFlor210 with one reinforcement mesh in top deck under 60kN concentrated load applied at the middle Rib 3 and adjacent Rib 2 are given in FIGURE E. 25-FIGURE E. 36.

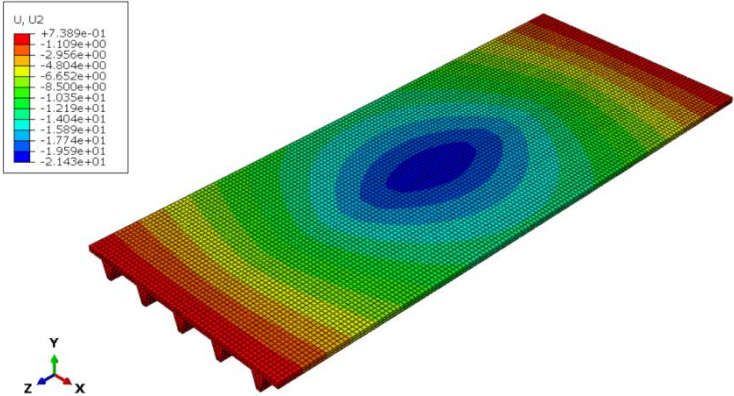


Figure E. 25 Displacement field U2 in composite slab 7.2m under concentrated force 60kN placed on Rib3 at $L_{span}/2$ in load-control FEA

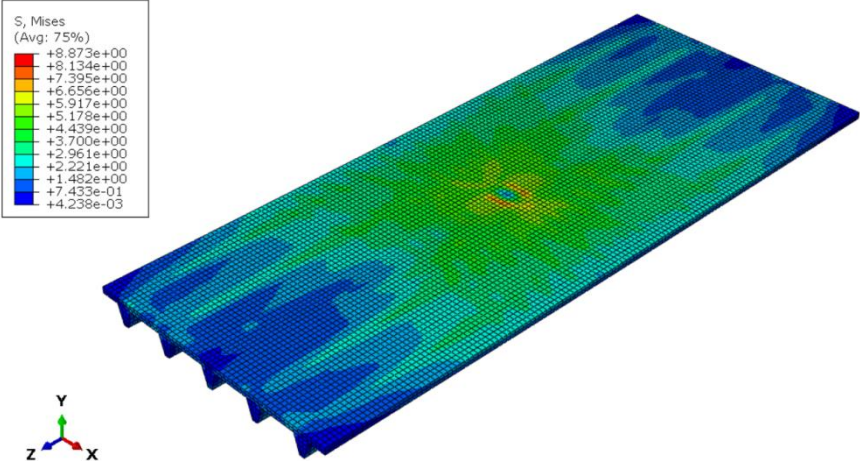


Figure E. 26 Von Mises stress distribution in concrete in composite slab 7.2m under concentrated force 60kN placed on Rib3 at $L_{span}/2$ at the end of the analysis

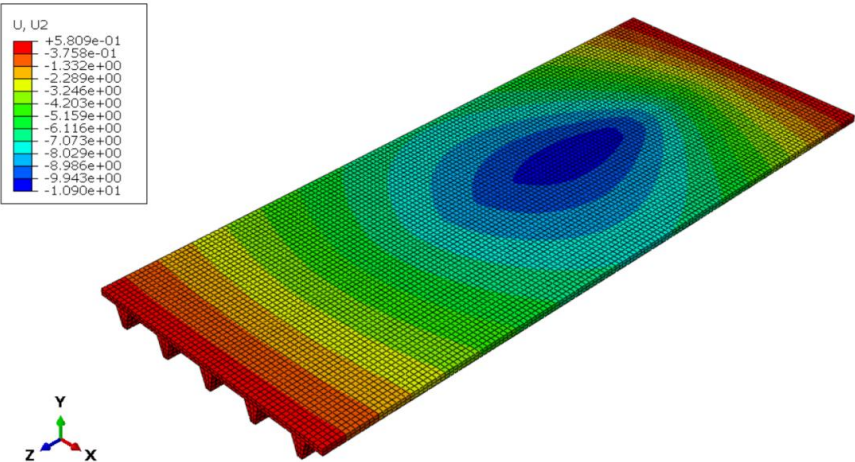


Figure E. 27 Displacement field U2 in composite slab 7.2m under concentrated force 60kN placed on Rib3 at $L_{span}/4$ in load-control FEA

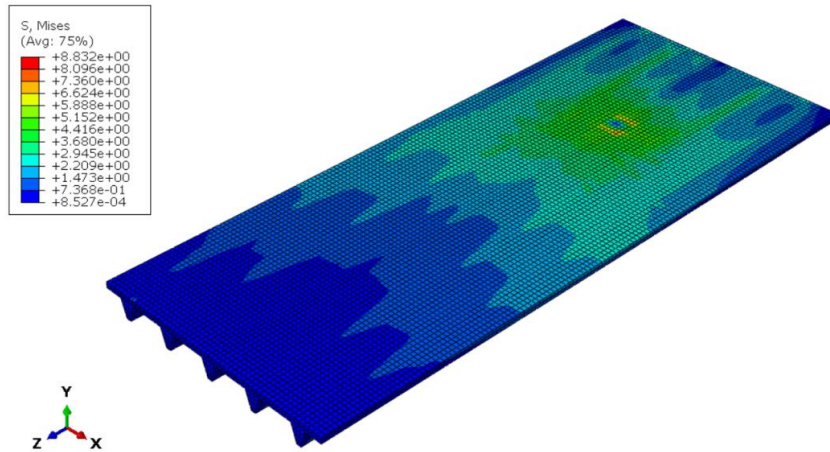


Figure E. 28 Von Mises stress distribution in concrete in composite slab 7.2m under concentrated force 60kN placed on Rib3 at $L_{span}/4$ at the end of the analysis

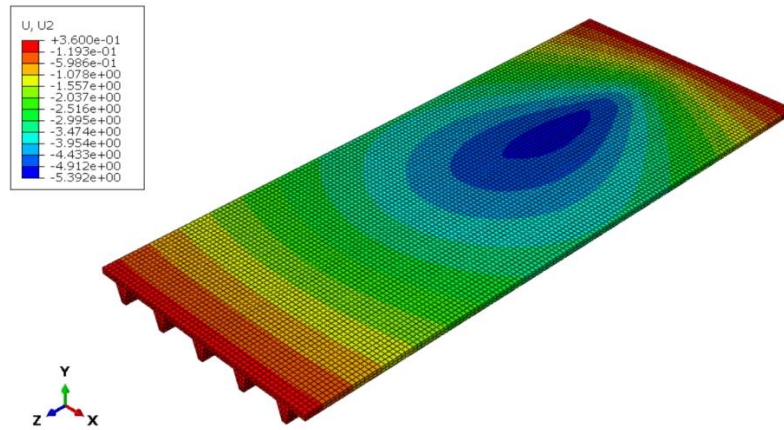


Figure E. 29 Displacement field U2 in composite slab 7.2m under concentrated force 60kN placed on Rib3 at $L_{span}/6$ in load-control FEA

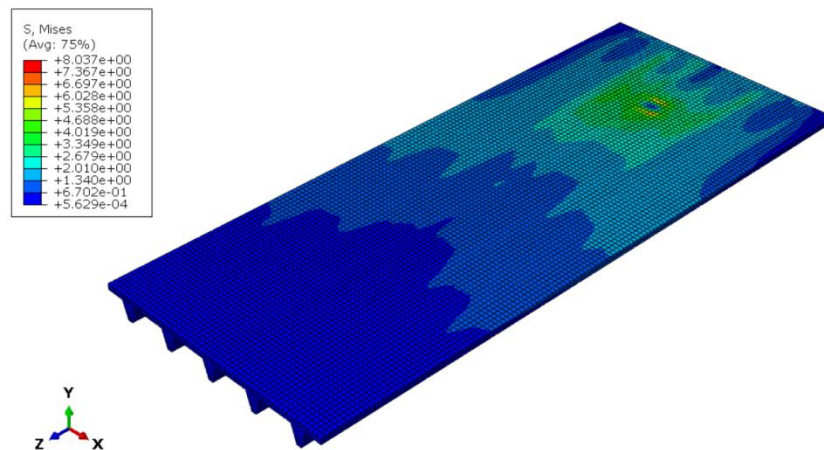


Figure E. 30 Von Mises stress distribution in concrete in composite slab 7.2m under concentrated force 60kN placed on Rib3 at $L_{span}/6$ at the end of the analysis

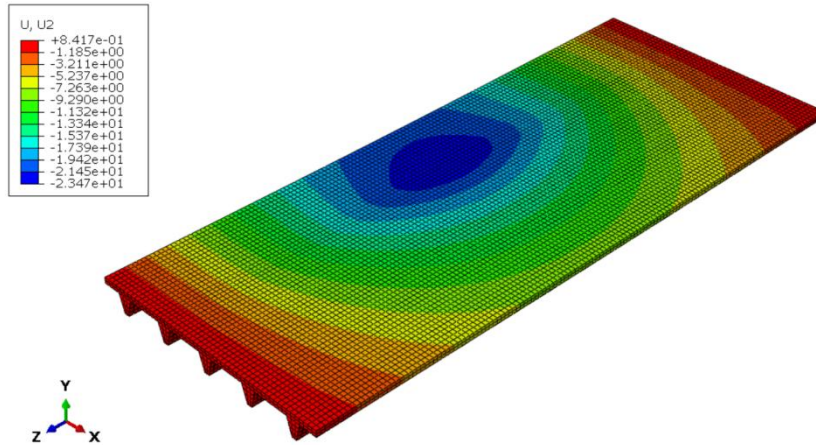


Figure E. 31 Displacement field U2 in composite slab 7.2m under concentrated force 60kN placed on Rib2 at $L_{span}/2$ in load-control FEA

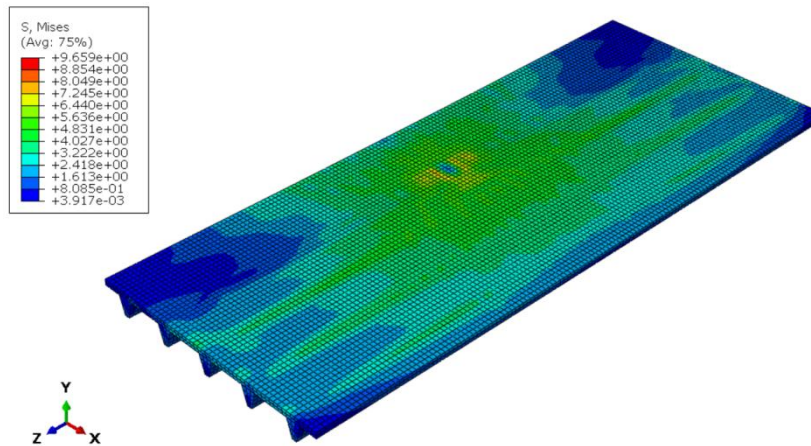


Figure E. 32 Von Mises stress distribution in concrete in composite slab 7.2m under concentrated force 60kN placed on Rib2 at $L_{span}/2$ at the end of the analysis

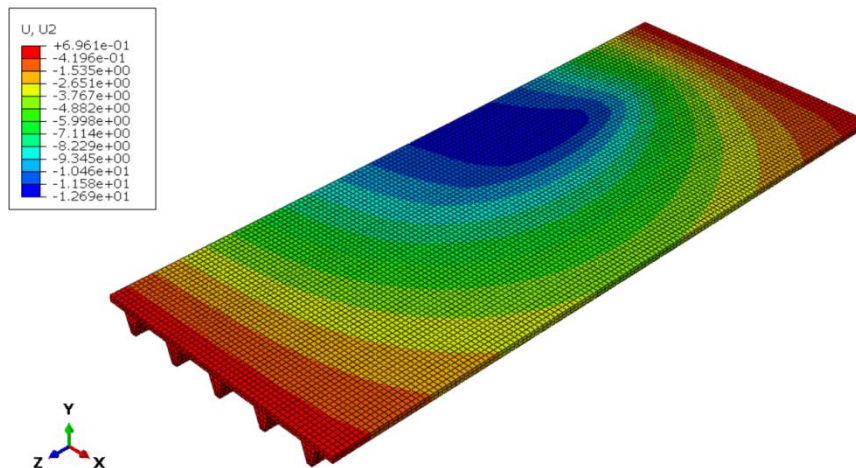


Figure E. 33 Displacement field U2 in composite slab 7.2m under concentrated force 60kN placed on Rib2 at $L_{span}/4$ in load-control FEA

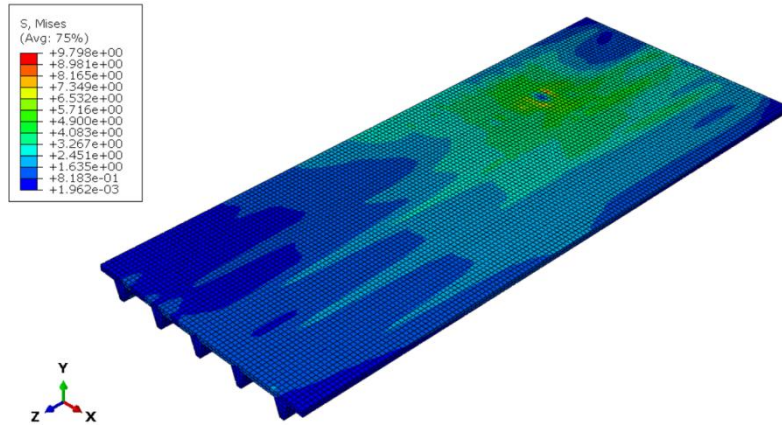


Figure E. 34 Von Mises stress distribution in concrete in composite slab 7.2m under concentrated force 60kN placed on Rib2 at $L_{span}/4$ at the end of the analysis

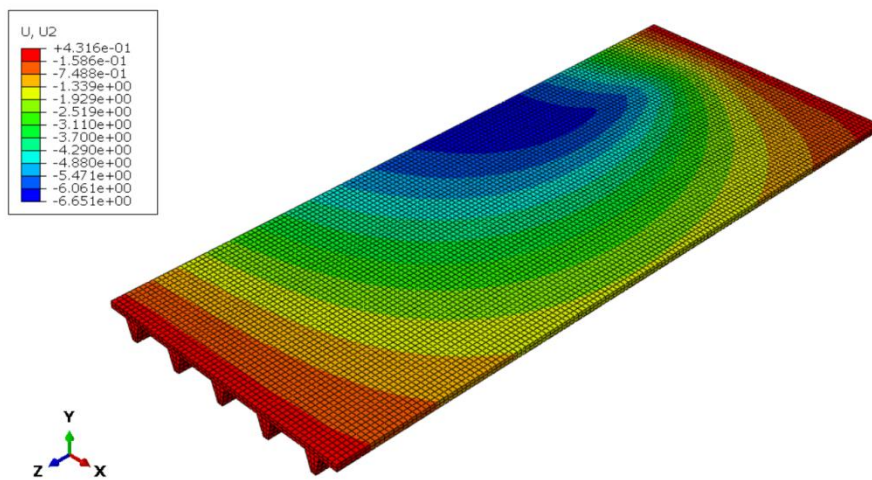


Figure E. 35 Displacement field U2 in composite slab 7.2m under concentrated force 60kN placed on Rib2 at $L_{span}/6$ in load-control FEA

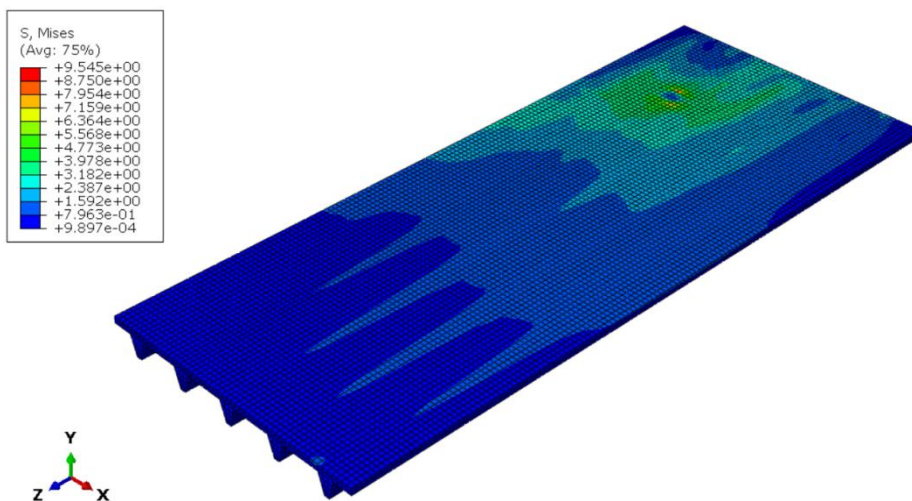


Figure E. 36 Von Mises stress distribution in concrete in composite slab 7.2m under concentrated force 60kN placed on Rib2 at $L_{span}/6$ at the end of the analysis

F Rib bending resistance verification

The bending resistance verification is performed for loaded rib Rib 3 and Rib 2 in a composite slab with 3.6m, 5.4m and 7.2m length. The design load combination includes self-weight of the slab, live load and concentrated force 60kN applied at $L_{span}/2$ and $L_{span}/4$.

Slab 3.6m

Slab 3.6m, point load at L/2 Rib 3	Dead load, q_d	Live load, q_v	Point load, F
<i>Area=3x3.6=10.8m²</i>	kN/m²	kN/m²	kN
Nominal value	3.05	3.00	60.00
Design value	4.12	4.50	90.00
	Rf from dead load	Rf from live load	Rf from point load
Rib reaction force R_f, kN	4.45	4.86	15.50
	<i>(DesignxArea/10)</i>	<i>(DesignxArea/10)</i>	<i>(1.5*Rf_from FEA)</i>
	Moments		
Moment from reaction force, kNm	8.00	8.75	27.89
<i>Total moment from reaction force, kNm</i>			44.64
Moment from the distributed load, kNm	-4.00	-4.37	
Resulting maximum moment M_{ed}, kNm			36.27
Rib resistance M_{rd}, kNm			69.10
Unity check M_{ed}/M_{rd}			0.52
			Passed

Slab 3.6m, point load at L/2 Rib 2	Dead load, q_d	Live load, q_v	Point load, F
<i>Area=3x3.6=10.8m²</i>	kN/m²	kN/m²	kN
Nominal value	3.05	3.00	60.00
Design value	4.12	4.50	90.00
	Rf from dead load	Rf from live load	Rf from point load
Rib reaction force R_f, kN	4.45	4.86	17.04
	<i>(DesignxArea/10)</i>	<i>(DesignxArea/10)</i>	<i>(1.5*Rf_from FEA)</i>
	Moments		
Moment from reaction force, kNm	8.00	8.75	30.67
<i>Total moment from reaction force, kNm</i>			47.42
Moment from the distributed load, kNm	-4.00	-4.37	
Resulting maximum moment M_{ed}, kNm			39.05
Rib resistance M_{rd}, kNm			69.10
Unity check M_{ed}/M_{rd}			0.57
			Passed

Slab 3.6m

Slab 3.6m, point load at L/4 Rib 3	Dead load, q_d	Live load, q_v	Point load, F
<i>Area=3x3.6=10.8m²</i>	kN/m²	kN/m²	kN
Nominal value	3.05	3.00	60.00
Design value	4.12	4.50	90.00
	Rf from dead load	Rf from live load	Rf from point load
Rib reaction force R_f, kN	4.45	4.86	32.55
	<i>(DesignxArea/10)</i>	<i>(DesignxArea/10)</i>	<i>(1.5*Rf_from FEA)</i>
	Moments		
Moment from reaction force, kNm	4.00	4.37	29.30
<i>Total moment from reaction force, kNm</i>			37.67
Moment from distributed load, kNm	-1.00	-1.09	
Resulting maximum moment M_{ed}, kNm			35.58
Rib resistance M_{rd}, kNm			69.10
Unity check M_{ed}/M_{rd}			0.51
			Passed

Slab 3.6m, point load at L/4 Rib 2	Dead load, q_d	Live load, q_v	Point load, F
<i>Area=3x3.6=10.8m²</i>	kN/m²	kN/m²	kN
Nominal value	3.05	3.00	60.00
Design value	4.12	4.50	90.00
	Rf from dead load	Rf from live load	Rf from point load
Rib reaction force R_f, kN	4.45	4.86	33.38
	<i>(DesignxArea/10)</i>	<i>(DesignxArea/10)</i>	<i>(1.5*Rf_from FEA)</i>
	Moments		
Moment from reaction force, kNm	4.00	4.37	30.04
<i>Total moment from reaction force, kNm</i>			38.41
Moment from distributed load, kNm	-1.00	-1.09	
Resulting maximum moment M_{ed}, kNm			36.32
Rib resistance M_{rd}, kNm			69.10
Unity check M_{ed}/M_{rd}			0.53
			Passed

Slab 5.4m

Slab 5.4m, point load at L/2 Rib 3	Dead load, q_d	Live load, q_v	Point load, F
<i>Area=3x5.4=16.2m²</i>	kN/m²	kN/m²	kN
Nominal value	3.05	3.00	60.00
Design value	4.12	4.50	90.00
	Rf from dead load	Rf from live load	Rf from point load
Rib reaction force R_f, kN	6.67	7.29	13.77
	<i>(DesignxArea/10)</i>	<i>(DesignxArea/10)</i>	<i>(1.5*Rf_from FEA)</i>
	Moments		
Moment from reaction force, kNm	18.01	19.68	37.18
<i>Total moment from reaction force, kNm</i>			74.87
Moment from distributed load, kNm	-9.00	-9.84	
Resulting maximum moment M_{ed}, kNm			56.03
Rib resistance M_{rd}, kNm			69.10
Unity check M_{ed}/M_{rd}			0.81
			Passed

Slab 5.4m, point load at L/2 Rib 2	Dead load, q_d	Live load, q_v	Point load, F
<i>Area=3x5.4=16.2m²</i>	kN/m²	kN/m²	kN
Nominal value	3.05	3.00	60.00
Design value	4.12	4.50	90.00
	Rf from dead load	Rf from live load	Rf from point load
Rib reaction force R_f, kN	6.67	7.29	13.05
	<i>(DesignxArea/10)</i>	<i>(DesignxArea/10)</i>	<i>(1.5*Rf_from FEA)</i>
	Moments		
Moment from reaction force, kNm	18.01	19.68	35.24
<i>Total moment from reaction force, kNm</i>			72.93
Moment from distributed load, kNm	-9.00	-9.84	
Resulting maximum moment M_{ed}, kNm			54.08
Rib resistance M_{rd}, kNm			69.10
Unity check M_{ed}/M_{rd}			0.78
			Passed

Slab 5.4m

Slab 5.4m, point load at L/4 Rib 3	Dead load, q_d	Live load, q_v	Point load, F
<i>Area=3x5.4=16.2m²</i>	kN/m²	kN/m²	kN
Nominal value	3.05	3.00	60.00
Design value	4.12	4.50	90.00
	Rf from dead load	Rf from live load	Rf from point load
Rib reaction force R_f, kN	6.67	7.29	27.30
	<i>(DesignxArea/10)</i>	<i>(DesignxArea/10)</i>	<i>(1.5*Rf_from FEA)</i>
	Moments		
Moment from reaction force, kNm	9.00	9.84	36.86
<i>Total moment from reaction force, kNm</i>			55.70
Moment from distributed load, kNm	-2.25	-2.46	
Resulting maximum moment M_{ed}, kNm			50.99
Rib resistance M_{rd}, kNm			69.10
Unity check M_{ed}/M_{rd}			0.74
			Passed

Slab 5.4m, point load at L/4 Rib 2	Dead load, q_d	Live load, q_v	Point load, F
<i>Area=3x5.4=16.2m²</i>	kN/m²	kN/m²	kN
Nominal value	3.05	3.00	60.00
Design value	4.12	4.50	90.00
	Rf from dead load	Rf from live load	Rf from point load
Rib reaction force R_f, kN	6.67	7.29	26.78
	<i>(DesignxArea/10)</i>	<i>(DesignxArea/10)</i>	<i>(1.5*Rf_from FEA)</i>
	Moments		
Moment from reaction force, kNm	9.00	9.84	36.15
<i>Total moment from reaction force, kNm</i>			54.99
Moment from distributed load, kNm	-2.25	-2.46	
Resulting maximum moment M_{ed}, kNm			50.28
Rib resistance M_{rd}, kNm			69.10
Unity check M_{ed}/M_{rd}			0.73
			Passed

Slab 7.2m

Slab 7.2m, point load at L/2 Rib 3	Dead load, q_d	Live load, q_v	Point load, F
<i>Area=3x7.2=21.6m²</i>	kN/m²	kN/m²	kN
Nominal value	3.05	3.00	60.00
Design value	4.12	4.50	90.00
	Rf from dead load	Rf from live load	Rf from point load
Rib reaction force R_f, kN	8.89	9.72	12.86
	<i>(DesignxArea/10)</i>	<i>(DesignxArea/10)</i>	<i>(1.5*Rf_from FEA)</i>
	Moments		
Moment from reaction force, kNm	32.02	34.99	46.28
<i>Total moment from reaction force, kNm</i>			113.29
Moment from distributed load, kNm	-16.01	-17.50	
Resulting maximum moment M_{ed}, kNm			79.78
Rib resistance M_{rd}, kNm			69.10
Unity check M_{ed}/M_{rd}			1.15
			Not passed

Slab 7.2m, point load at L/2 Rib 2	Dead load, q_d	Live load, q_v	Point load, F
<i>Area=3x7.2=21.6m²</i>	kN/m²	kN/m²	kN
Nominal value	3.05	3.00	60.00
Design value	4.12	4.50	90.00
	Rf from dead load	Rf from live load	Rf from point load
Rib reaction force R_f, kN	8.89	9.72	11.18
	<i>(DesignxArea/10)</i>	<i>(DesignxArea/10)</i>	<i>(1.5*Rf_from FEA)</i>
	Moments		
Moment from reaction force, kNm	32.02	34.99	40.23
<i>Total moment from reaction force, kNm</i>			107.24
Moment from distributed load, kNm	-16.01	-17.50	
Resulting maximum moment M_{ed}, kNm			73.73
Rib resistance M_{rd}, kNm			69.10
Unity check M_{ed}/M_{rd}			1.07
			Not passed

Slab7.2m

Slab 7.2m, point load at L/4 Rib 3	Dead load, q_d	Live load, q_v	Point load, F
<i>Area=3x7.2=21.6m²</i>	kN/m²	kN/m²	kN
Nominal value	3.05	3.00	60.00
Design value	4.12	4.50	90.00
	Rf from dead load	Rf from live load	Rf from point load
Rib reaction force Rf, kN	8.89	9.72	22.70
	<i>(DesignxArea/10)</i>	<i>(DesignxArea/10)</i>	<i>(1.5*Rf_from FEA)</i>
	Moments		
Moment from reaction force, kNm	16.01	17.50	40.85
<i>Total moment from reaction force, kNm</i>			74.36
Moment from the distributed load, kNm	-4.00	-4.37	
Resulting maximum moment Med, kNm			65.98
Rib resistance Mrd, kNm			69.10
Unity check Med/Mrd			0.95
			Passed

Slab 7.2m, point load at L/4 Rib 2	Dead load, q_d	Live load, q_v	Point load, F
<i>Area=3x7.2=21.6m²</i>	kN/m²	kN/m²	kN
Nominal value	3.05	3.00	60.00
Design value	4.12	4.50	90.00
	Rf from dead load	Rf from live load	Rf from point load
Rib reaction force Rf, kN	8.89	9.72	23.67
	<i>(DesignxArea/10)</i>	<i>(DesignxArea/10)</i>	<i>(1.5*Rf_from FEA)</i>
	Moments		
Moment from reaction force, kNm	16.01	17.50	42.61
<i>Total moment from reaction force, kNm</i>			76.11
Moment from the distributed load, kNm	-4.00	-4.37	
Resulting maximum moment Med, kNm			67.73
Rib resistance Mrd, kNm			69.10
Unity check Med/Mrd			0.98
			Passed

G

Distribution of the point load relative to the distance to the applied load

The distribution of the concentrated forces 10kN and 60kN per rib in relation to the relative distance to the applied load, i.e. distance to the load from a rib divided by span length, is given below for composite slab with 3.6m, 5.4m, and 7.2m length.

The points on x-axis (relative distances) are:

- 0.166 (load at 1/6 of the span);
- 0.25 (load at 1/4 of the span);
- 0.5 (load at 1/2 of the span).

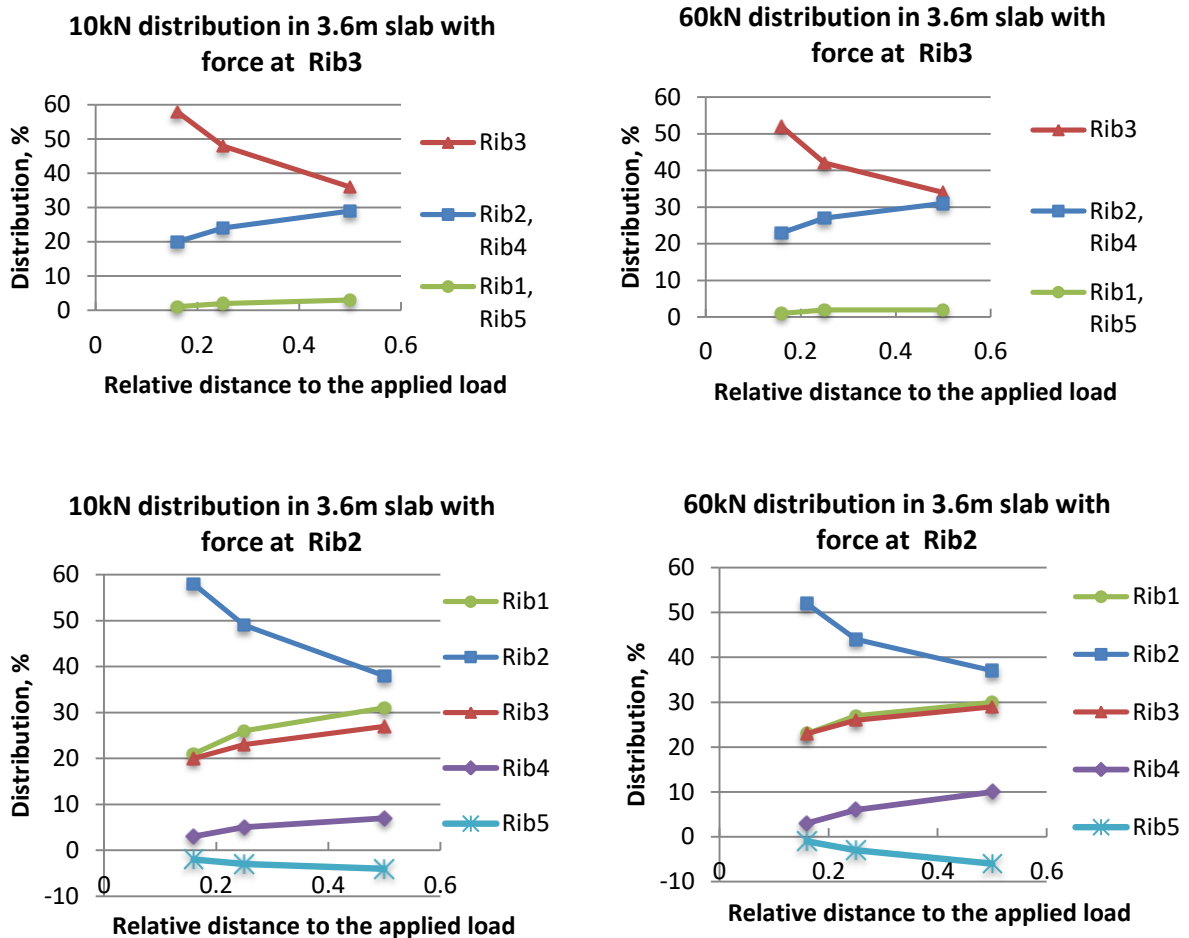
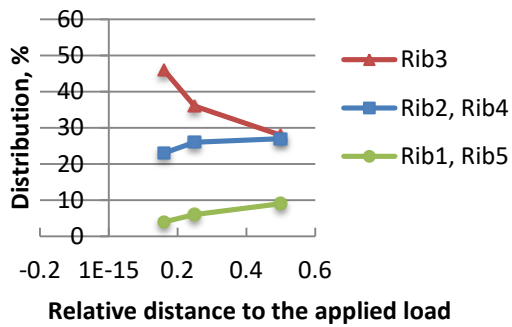
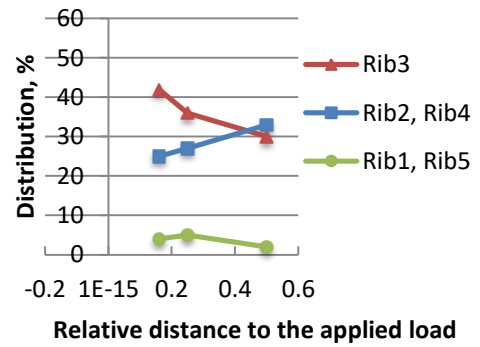


Figure G. 1 Distribution of 10kN and 60kN per rib in composite slab 3.6m relative to the distance to the applied load

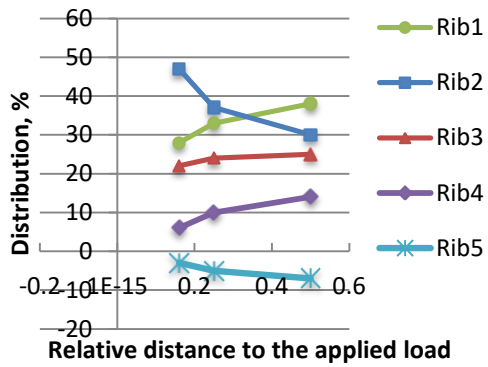
10kN distribution in 5.4m slab with force at Rib3



60kN distribution in 5.4m slab with force at Rib3



10kN distribution in 5.4m slab with force at Rib2



60kN distribution in 5.4m slab with force at Rib2

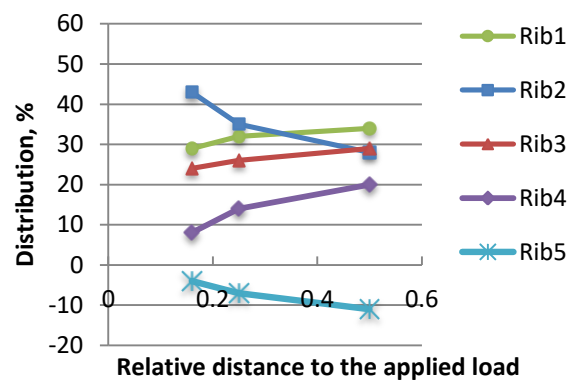
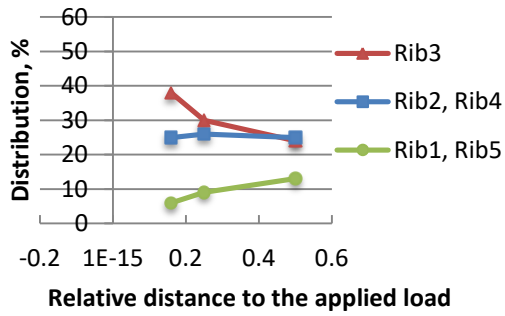
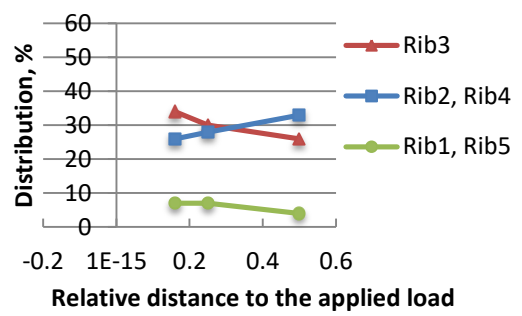


Figure G. 2 Distribution of 10kN and 60kN per rib in composite slab 5.4m relative to the distance to the applied load

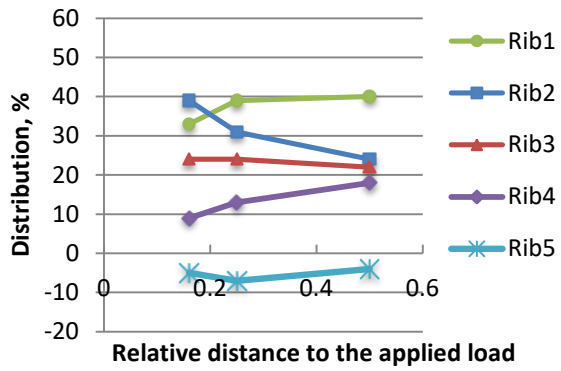
10kN distribution in 7.2m slab with force at Rib3



60kN distribution in 7.2m slab with force at Rib3



10kN distribution in 7.2m slab with force at Rib2



60kN distribution in 7.2m slab with force at Rib2

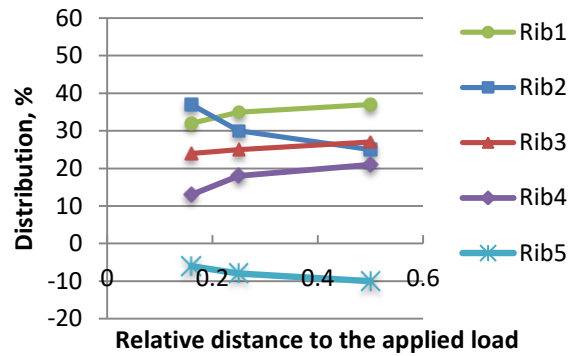


Figure G. 3 Distribution of 10kN and 60kN per rib in composite slab 7.2m relative to the distance to the applied load